The Effect of Chronic and Acute Temperature Stress on Two Populations of Threespine Stickleback (*Gasterosteus aculeatus*)

By

BRYN BO LEVITAN
DISSERTATION

Submitted in partial satisfaction of the requirements for the degree of

DOCTOR OF PHILOSOPHY

in

Ecology

in the

OFFICE OF GRADUATE STUDIES

of the

UNIVERSITY OF CALIFORNIA

DAVIS

Approved:

Dietmar Kültz, Chair

Gary N. Cherr

Nann Fangue

Committee in Charge

2021

ACKNOWLEDGMENTS

There are so many people who have helped me to conceive, plan, execute, and finish this dissertation and who have given me the strength to see it through to completion. To those both named and unnamed below, thank you.

Thank you to my major professor, Dr. Dietmar Kültz for your guidance during each step of this process. You gave me a lot of freedom with my research, but your advice and contributions run throughout these chapters. Thank you also to the rest of my dissertation committee, Dr. Gary Cherr and Dr. Nann Fangue, for your patience, understanding, and suggestions. I would like to thank my qualifying exam committee, Dr. Nann Fangue, Dr. Steven Morgan, Dr. Peter Moyle, Dr. Anne Todgham, and Dr. Peter Wainwright, for your questions, conversations, and insights. I am deeply grateful for Holly Hatfield Rogai, Elizabeth Sturdy, and JoAnna Lewis for your kindness, patience, professionalism, and the care that you put into your work. I would also like to extend a very heartfelt thank you to Dr. Janet Foley and Dr. Ellen Hartigan-O'Connor.

Many thanks to my lab mates for their support, help, and friendships through lab meetings, freezer dissections, survey and collection camping trips, conferences, game nights, and delicious meals. Thank you for making the Kueltz Lab such an enjoyable community over these past years. I am most grateful for the contributions and hard work of the various interns and volunteers who helped care for my research populations and helped with my projects. I would like to offer special thanks to our lab manager, Leah MacNiven. Your presence in the lab has made all our work and lives so much better. Thank you for your support and ideas, your constant willingness to help, and for listening and being there when things did not quite go as planned.

I would like to extend my sincere thanks to those who helped guide me towards research and graduate school, Dr. Scott Frey, Noah Marchal, and Dr. Minjie Wu. Thank you for being wonderful mentors, all-around good people, and for supporting me throughout my time in graduate school.

To my friends and teammates, I am beyond grateful for your wisdom and maturity, for taking me out of my comfort zone but helping me get through each challenge, for sharing tears of joy and pain with me, and for the many deep and meaningful conversations. You have all carried me more than you can know. Thank you for the acceptance and love that has given me the strength to step into myself. You helped pick me back up after every setback and walked with me every step of the way.

To Boba, thank you for being there every day with me throughout the pandemic, for keeping me grounded in the present and keeping me on my toes, for loving me no matter what, and gently (or not so gently) reminding me to take a break, eat, and sleep when I got caught up in my dissertation.

To my parents, thank you for all the love, advice, and support that you have given me throughout my time in graduate school. I could not have crossed the finish line without you. Your encouragement has gotten me through more than I could have imagined overcoming in my time at Davis. I am very grateful that you have given me the freedom and ability to pursue many passions throughout my life and for instilling in me the importance of education. I dedicate this dissertation to you.

## TABLE OF CONTENTS

**ABSTRACT**

Temperature stress will continue to be a major challenge for all organisms over the next century. Ectotherms in estuarine habitats are particularly susceptible to changes in temperature. Given genetic differences among populations, it is important to understand the variation in molecular changes during acclimation to and recovery from various types of temperature challenge. Threespine sticklebacks (*Gasterosteus aculeatus*) represent an ideal model organism to examine such questions given their phenotypic diversity and distribution throughout coastal and inland waterways of the northern hemisphere. This dissertation utilized metabolic assays in the gill and white muscle tissue, body indices and measurements, thermal tolerances, and bottom-up proteomic analysis of the liver to investigate the molecular impacts of both acute and chronic temperature stress on first generation, lab-reared progeny from two Northern California threespine stickleback populations. Both temperature and population dependent differences were apparent throughout the experiments, demonstrating unique signatures and functional variation in response to various types of temperature challenge. Analyses of individual protein abundance changes highlighted key regulatory proteins such as HSP40-B1b in acute temperature stress, while functional enrichment analyses provided insight on broader, network-level changes. This work shows that advances in proteomics can help elucidate important bioindicators, proteomic signatures, strategies, and mechanism used to overcome environmental challenge, and ultimately how molecular phenotypes contribute to evolutionary processes.

## INTRODUCTION

Temperature has profound effects on all living organisms, but especially so for poikilothermic ectotherms, whose body temperatures rise and fall with fluctuating environmental temperatures. Throughout the next century, heat waves are expected to increase in frequency, intensity, and duration (IPCC, 2014). Temperature challenge disrupts internal processes necessary for survival, growth, and reproduction, impacting biogeographic range, biodiversity, and ecosystem functioning (Loarie et al., 2009; Menge & Olson, 1990; Seebacher, 2005; Zinn et al., 2010). Given genetic differences and specific adaptations to various environments, it will become increasingly important to understand the molecular underpinnings of organismal responses to thermal stress and the unique responses of different populations (Crawford et al., 1999; Genner et al., 2004).

This dissertation focuses on two populations of threespine stickleback (*Gasterosteus aculeatus*), an extremely phenotypically diverse species of fish found in marine, brackish, and freshwater habitats throughout the Northern Hemisphere (Bell & Foster, 1994). These two populations were located within 35 miles of one another in Northern California and represent two estuarine habitats, river and lagoon, that are highly susceptible to climate change due to their shallower depths and limited interaction with the cooler waters of the ocean (Scanes et al., 2020). Fish from these populations were externally fertilized in the laboratory and first-generation progeny were reared under identical conditions.

Chapter one characterizes the two populations of threespine sticklebacks. Both acute and chronic thermal tolerance limits were tested, and various body indices, measurements, and metabolic assays of the gill and white muscle tissue were conducted to examine the effects of both warm and cold chronic acclimation. These tissues were chosen because the gill represents an organ that directly interfaces with the external environment and, besides serving locomotive

purposes, white muscle tissue acts as a storage reservoir that can be utilized as an energy source (Jürss & Bastrop, 1995; Weber & Zwingelstein, 1995; Wilson & Poe, 1974).

Chapter two utilizes liquid chromatography tandem-mass spectrometry (LCMS2) to examine changes to the liver proteome following chronic acclimation to either warm or cold temperatures. The liver provides a good overall representation of the condition of a fish and plays a vital role in a wide array of physiological processes such as the homeostasis and metabolism of lipids, glucose, and amino acids, and detoxification (Liu et al., 2016; Trefts et al., 2017). Data-dependent acquisition (DDA) data from samples representing the different temperature stress experiments were used to create a raw MS2 spectral library for the liver (Doerr, 2015; Fernández-Costa et al., 2020; Kültz et al., 2013). Multiple quality control filtering steps were then applied to create a data-independent acquisition (DIA) assay library that was used in combination with DIA-LCMS2 data for precise identification and quantification of protein changes (Li et al., 2018). Functional enrichment analyses were also conducted to aid in identifying larger networks and domains that were significantly enriched (Szklarczyk et al., 2019).

Chapter three examines changes to the liver proteome in the two populations after a two-hour acute heat stress either six or 24 hours into the recovery process using DIA-LCMS2 (Kültz et al., 2013; Li et al., 2018). The DIA assay library created in chapter two was used to identify and quantify the same set of proteins in the liver proteome after acute heat stress. Functional enrichment analyses were conducted on both the entire liver proteome set and on significantly higher or lower proteins six hours into the recovery process (Szklarczyk et al., 2019). Kyoto Encyclopedia of Genes and Genomes (KEGG) pathways were also mapped from significantly different proteins six hours after acute heat stress (Kanehisa & Sato, 2020). Overall, this

dissertation represents a comprehensive analysis of the effects of various types of temperature stress, chronic and acute, warm and cold, and various timepoints on the physiology and biochemistry of *G. aculeatus*, in particular the liver proteome. It contributes new knowledge to better understand the molecular underpinnings and functional variation of acclimation to and/or recovery from temperature stress.

References

Bell, M. A., & Foster, S. A. (Eds.). (1994). *The evolutionary biology of the threespine stickleback*. Oxford University Press.

Crawford, D. L., Pierce, V. A., & Segal, J. A. (1999). Evolutionary Physiology of Closely Related Taxa: Analyses of Enzyme Expression. *American Zoologist*, *39*(2), 389–400.

Doerr, A. (2015). DIA mass spectrometry. *Nature Methods*, *12*(1), 35–35. https://doi.org/10.1038/nmeth.3234

Fernández-Costa, C., Martínez-Bartolomé, S., McClatchy, D. B., Saviola, A. J., Yu, N.-K., & Yates, J. R. (2020). Impact of the Identification Strategy on the Reproducibility of the DDA and DIA Results. *Journal of Proteome Research*, *19*(8), 3153–3161. https://doi.org/10.1021/acs.jproteome.0c00153

Genner, M. J., Sims, D. W., Wearmouth, V. J., Southall, E. J., Southward, A. J., Henderson, P. A., & Hawkins, S. J. (2004). Regional climatic warming drives long–term community changes of British marine fish. *Proceedings of the Royal Society of London. Series B: Biological Sciences*, *271*(1539), 655–661. https://doi.org/10.1098/rspb.2003.2651

IPCC. (2014). *Climate Change 2014: Synthesis Report. Contribution of Working Groups I, II and III to the Fifth Assessment Report of the Intergovernmental Panel on Climate*

*Change* (p. 151). Intergovernmental Panel on Climate Change. https://www.ipcc.ch/site/assets/uploads/2018/02/SYR_AR5_FINAL_full.pdf

Jürss, K., & Bastrop, R. (1995). Chapter 7 Amino acid metabolism in fish. In T. P. Mommsen & P. Hochachka (Eds.), *Biochemistry and Molecular Biology of Fishes* (Vol. 4, pp. 159–189). Elsevier. https://doi.org/10.1016/S1873-0140(06)80010-X

Kanehisa, M., & Sato, Y. (2020). KEGG Mapper for inferring cellular functions from protein sequences. *Protein Science: A Publication of the Protein Society*, *29*(1), 28–35. https://doi.org/10.1002/pro.3711

Kültz, D., Li, J., Gardell, A., & Sacchi, R. (2013). Quantitative molecular phenotyping of gill remodeling in a cichlid fish responding to salinity stress. *Molecular & Cellular Proteomics: MCP*, *12*(12), 3962–3975. https://doi.org/10.1074/mcp.M113.029827

Li, J., Levitan, B., Gomez-Jimenez, S., & Kültz, D. (2018). Development of a Gill Assay Library for Ecological Proteomics of Threespine Sticklebacks (Gasterosteus aculeatus). *Molecular & Cellular Proteomics*, *17*(11), 2146–2163. https://doi.org/10.1074/mcp.RA118.000973

Liu, B., Xu, P., Brown, P. B., Xie, J., Ge, X., Miao, L., Zhou, Q., Ren, M., & Pan, L. (2016). The effect of hyperthermia on liver histology, oxidative stress and disease resistance of the Wuchang bream, Megalobrama amblycephala. *Fish & Shellfish Immunology*, *52*, 317–324. https://doi.org/10.1016/j.fsi.2016.03.018

Loarie, S. R., Duffy, P. B., Hamilton, H., Asner, G. P., Field, C. B., & Ackerly, D. D. (2009). The velocity of climate change. *Nature*, *462*(7276), 1052–1055. https://doi.org/10.1038/nature08649

Menge, B. A., & Olson, A. M. (1990). Role of scale and environmental factors in regulation of community structure. *Trends in Ecology & Evolution*, *5*(2), 52–57. https://doi.org/10.1016/0169-5347(90)90048-I

Scanes, E., Scanes, P. R., & Ross, P. M. (2020). Climate change rapidly warms and acidifies Australian estuaries. *Nature Communications*, *11*(1), 1803. https://doi.org/10.1038/s41467-020-15550-z

Seebacher, F. (2005). A review of thermoregulation and physiological performance in reptiles: What is the role of phenotypic flexibility? *Journal of Comparative Physiology B*, *175*(7), 453–461. https://doi.org/10.1007/s00360-005-0010-6

Szklarczyk, D., Gable, A. L., Lyon, D., Junge, A., Wyder, S., Huerta-Cepas, J., Simonovic, M., Doncheva, N. T., Morris, J. H., Bork, P., Jensen, L. J., & Mering, C. von. (2019). STRING v11: Protein-protein association networks with increased coverage, supporting functional discovery in genome-wide experimental datasets. *Nucleic Acids Research*, *47*(D1), D607–D613. https://doi.org/10.1093/nar/gky1131

Trefts, E., Gannon, M., & Wasserman, D. H. (2017). The liver. *Current Biology*, *27*(21), R1147–R1151. https://doi.org/10.1016/j.cub.2017.09.019

Weber, J.-M., & Zwingelstein, G. (1995). Chapter 2 Circulatory substrate fluxes and their regulation. In T. P. Mommsen & P. Hochachka (Eds.), *Biochemistry and Molecular Biology of Fishes* (Vol. 4, pp. 15–32). Elsevier. https://doi.org/10.1016/S1873-0140(06)80005-6

Wilson, R. P., & Poe, W. E. (1974). Nitrogen metabolism in channel catfish, Ictalurus punctatus—III. Relative pool sizes of free amino acids and related compounds in various

tissues of the catfish. *Comparative Biochemistry and Physiology Part B: Comparative Biochemistry*, *48*(4), 545–556. https://doi.org/10.1016/0305-0491(74)90134-5

Zinn, K. E., Tunc-Ozdemir, M., & Harper, J. F. (2010). Temperature stress and plant sexual reproduction: Uncovering the weakest links. *Journal of Experimental Botany*, *61*(7), 1959–1968. https://doi.org/10.1093/jxb/erq053

## CHAPTER 1

## Thermal tolerances and metabolic responses to chronic temperature stress in different morphotypes of threespine sticklebacks (*Gasterosteus aculeatus*)


## ABSTRACT

A riverine (Klamath, KL) and lacustrine (Big Lagoon, BL) population of threespine sticklebacks (*Gasterosteus aculeatus*) from Northern California were compared regarding their ability to cope with thermal stress. The KL population represented a fully plated morphotype while the BL population was low-plated. Thermal tolerance tests and a three-week chronic temperature acclimation at either 7°C, 15°C, or 25°C was performed on F1 fish raised under identical conditions. Critical thermal maxima (CTMax) were 31.4 ± 0.3°C (KL) and 31.5 ± 0.2°C (BL) and chronic lethal maxima (CLMax) were 29.0 ± 0.5°C (KL) and 29.0 ± 0.6°C (BL). KL fish grew significantly larger, had a smaller hepatosomatic index (HSI) and lower glucose levels in the gill than BL fish. Both populations experienced significant reduction of liver and male gonad weights, smaller HSI, and a decreased condition factor (K) at high temperature (25°C). These thermal effects on fish conditioning were accompanied by metabolic changes in white muscle. In this tissue, glutamine levels decreased at 7°C, glutamine:glutamate ratio was significantly different across all three temperatures, and glucose and lactate levels were lowered at 25°C compared to control (15°C). Gill glutamine levels differed significantly among all three temperatures and the glutamine:glutamate ratio was significantly lower at 7°C. We conclude that, when reared under identical conditions, thermal tolerances were nearly identical, thermal stress affects gill and white muscle metabolism similarly in both populations (except for gill glucose

levels), and that the susceptibility to thermal stress is similar in both morphotypes despite their major morphological differences.

## RESEARCH HIGHLIGHTS

Two populations of threespine stickleback had similar thermal tolerances. Both populations experienced similar changes in glutamine/glutamate metabolism in the gill and white muscle after chronic temperature stress but differed in glucose metabolism.

## GRAPHICAL ABSTRACT

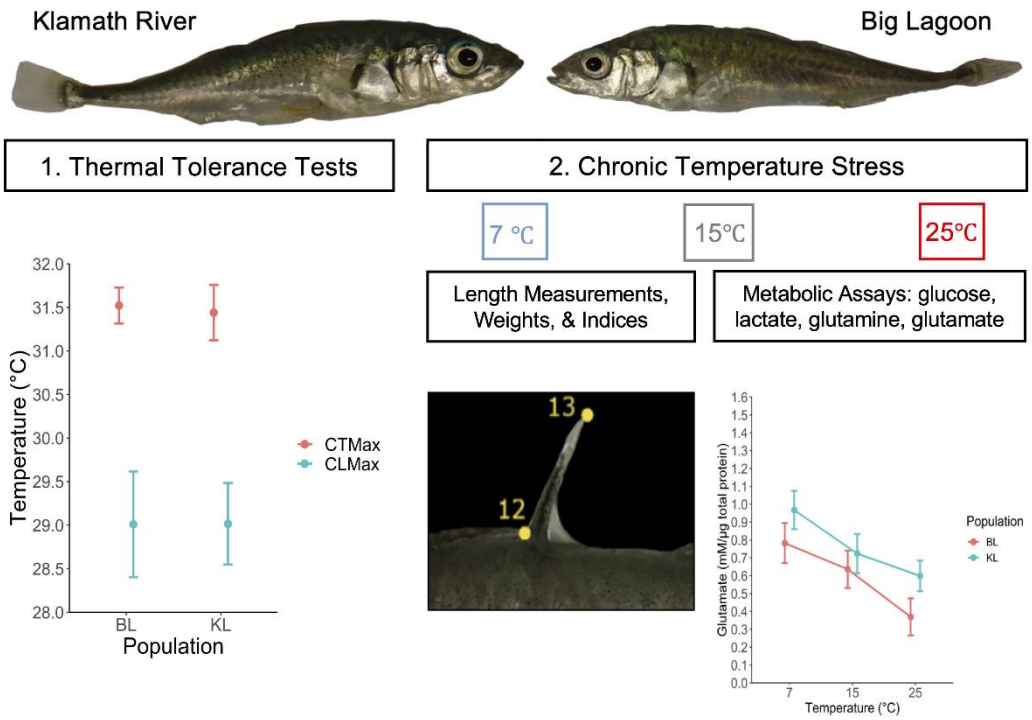

## INTRODUCTION

Temperature represents one of the main abiotic factors affecting the growth and metabolism of ectotherms on an individual level as well as dictating the general abundance and distribution of species. Acclimation to higher temperatures increases the metabolic demand necessary to maintain homeostasis, with subsequent increases in carbohydrate, lipid, and protein metabolism as energy sources to fuel the increase in basal metabolic rate (Baris et al., 2016; Dalvi et al., 2017). On the other hand, acclimation to lower temperatures slows down chemical reactions and organisms must work to actively increase their basal metabolic rates as a way of overcoming these slower enzymatic reactions (Baris et al., 2016). Metabolic rates are influenced by genetic factors, although more so in endotherms than ectotherms (Pettersen et al., 2018). There is, however, evidence that the effect of thermal sensitivity on growth rate has evolved quickly in ectotherms, and genetic differences in sticklebacks have been shown to influence growth and feeding rates as well as the thermal sensitivity of growth rates (Angilletta et al., 2002; Guderley & Leroy, 2001). Temperature challenge can induce both endocrine and metabolic changes in fish which leads to the mobilization of energy stores and cessation of growth (Bonga, 1997; Pottinger et al., 2002). Genetic differences also impact stress responses, even in a species that is tolerant to a wide variety of environmental conditions and with high levels of phenotypic plasticity (Schulte, 2014).

Threespine sticklebacks represent a well-studied euryhaline teleost species displaying tremendous phenotypic diversity among its numerous populations across the Northern Hemisphere. Included in this diversity is a broad range of morphological differences, including variation in lateral plate number. Seven different phenotypic traits, including lateral plate count and pelvic spine robustness, arise from specific gene mutations that contribute to variation

identified in threespine sticklebacks (Peichel & Marques, 2017). Sticklebacks are frequently used in evolutionary biology to understand how different genotypes and phenotypes lead to adaptation to different environments (Peichel & Marques, 2017). Given that sticklebacks are highly variable, readily available in the wild, and easy to capture and rear in the lab, they represent an ideal species to help understand the intersection of genetics or epigenetics and thermal history on the effects of thermal stress. Using two distinct populations representing different morphotypes but reared under identical laboratory conditions permits determining if population differences play a significant role, or if the response to chronic temperature stress remains relatively conserved across these morphotypes.

Thermal tolerance tests include the determination of the critical thermal maximum (CTMax), which was first introduced by Cowles and Bogert (1944) and is comparable across a wide array of species (Lutterschmidt & Hutchison, 1997). It involves a rapid and set increase in temperature (0.3-1ºC) and a sublethal endpoint such as onset of spasms or loss of equilibrium/loss of righting response (Beitinger & Lutterschmidt, 2011). Another common method for assessing the temperature tolerance of organisms, the chronic lethal method (CLM), determines the chronic lethal max (CLMax). In this thermal tolerance test, the temperature is typically increased by 1ºC/day, with the endpoint being death (Beitinger & Lutterschmidt, 2011).

In addition to affecting the function and survival of whole organisms, thermal stress is evident at the biochemical level prior to the manifestation of visible phenotypes in intact fish (Bonga, 1997; Sylvester, 1972). However, the role and importance of glucose metabolism in fish remains somewhat unclear (Polakof et al., 2012). Fish tend to have lower blood glucose levels and turnover rates than other vertebrates (Bever et al., 1981; Lin et al., 1978) and certain fish species appear to be glucose intolerant (Moon, 2001; Palmer & Ryman, 1972). Nevertheless,

glucose metabolism in fish plays an important role during a variety of challenges, including environmental challenges such as temperature stress (Barton & Schreck, 1987; Connors et al., 1978; Polakof et al., 2012; Vijayan & Moon, 1994). Glucose cannot readily pass through the cell membrane and for most fish species the concentration of cotransporters supporting its uptake by cells is low in many tissues (Moon & Foster, 1995). However, it has been demonstrated in rainbow trout that gill and blood glucose levels are at equilibrium suggesting that, at least in some species, glucose is readily transported between these compartments (Mommsen, 1984). Glucose and glycogen content in cells can also be regulated through other pathways, e.g. gluconeogenesis using precursors such as lactate, amino acids, glycerol, and fructose (Moon, 1988).

In fish, elevated levels of lactate occur after exercise, but can also be induced by stress (Vijayan et al., 1997; Vijayan & Moon, 1994; Weber & Zwingelstein, 1995). Most blood lactate is oxidized regardless of the activity level of the fish, with the remaining lactate not utilized by the liver being taken up by muscle to replenish glycogen levels (Milligan & Girard, 1993). Anaerobic metabolism depletes glycogen and causes lactate to build up in white muscle after substantial burst-like activity. However, there is also evidence, that unlike in mammals, fish retain most lactate within the muscle tissues and lactate is released from white muscle very slowly (Turner et al., 1983; Weber & Zwingelstein, 1995).

Besides glucose and lactate, glutamine and glutamate play a central role in cell energy metabolism, function, and maintenance. They are the most abundant amino acids, both extracellularly and intracellularly (Newsholme et al., 2003). These two amino acids are present in significant proportion in both free and protein-bound form in fish and act as extremely versatile metabolic fuels for a variety of tissues, including skeletal muscle, kidneys, liver, and

intestine (Li et al., 2020). Glutamine can also play a protective role during stress by helping to inhibit oxidative damage and apoptosis resulting from hydroxyl radicals and by improving antioxidant function (Li et al., 2013; Liu et al., 2015). Fish can also detoxify high levels of ammonia by converting it to glutamine in brain, liver, and muscle tissues and both glutamine and glutamate can be easily transported via the circulatory system (Wicks & Randall, 2002).

The four metabolites outlined above have often been measured in blood but not as frequently in peripheral tissues, where less is known about their regulation during stress. Given the differences between fish and other vertebrates, and even differences among fish species, it is important to examine individual tissues to fully understand the effect of temperature stress on fish metabolism and physiology.

In this study these metabolite levels were examined in two tissues, the gill and white muscle. The fish gill facilitates oxygen, carbon dioxide and water exchange and is active in ion transport (Piiper, 1982). The gill represents a tissue that interfaces with the external environment directly (Weber & Zwingelstein, 1995). Glucose appears to follow a concentration gradient into the gill and is not replenished from glycogen within the cell, whereas lactate can both be actively taken up as well as produced within the gill and is not released back into the blood stream, even after high levels accumulate (Mommsen, 1984).

In contrast to the externally interfacing gill, skeletal muscle represents an internal tissue used for storage and locomotion (Weber & Zwingelstein, 1995). This tissue represents a large free amino acid pool that can be utilized as an energy source (Jürss & Bastrop, 1995; Wilson & Poe, 1974). The axial muscles of threespine sticklebacks are predominantly composed of white muscle fibers with no red muscle fibers and some intermediate, or pink fibers, occurring along

the lateral line (Ellerby, 2011; Kronnie et al., 1983). Mitochondria are still present in white muscle, just at much lower levels than in red muscle (Pathi et al., 2012).

The present study compared two populations of threespine sticklebacks from Northern California, representing two different morphotypes, with regard to their specific morphometric characteristics and indices, temperature effects on organismal tolerance (critical thermal and chronic lethal maximum), and thermal regulation of select metabolites (glutamine, glutamate, glucose, lactate) in the gill and white muscle after exposure to either chronic warm or cold stress. This study examined if genetic or epigenetic differences that give rise to the different morphotypes of threespine sticklebacks influence tolerance to thermal stress and metabolism in both gill and white muscle tissues to better understand how temperature stress impacts functioning of a tissue that 1) directly interfaces with the external environment (gill) and 2) is internal and serves as a storage reservoir (white muscle).

## MATERIALS AND METHODS

All experimental work was approved by and conducted in accordance with UC Davis Institutional Animal Care and Use Committee (IACUC) rules and regulations (IACUC number 18010, AAALAC number 127 A3433-01).

### Breeding of wild-caught fish to create F1 progeny

Fish were collected from Klamath river (salinity: 0 g/kg; temperature: 13.2 °C) in Klamath, CA, and Big lagoon (salinity: 8.3 g/kg; temperature: 14.8 °C) in Trinidad, CA in the fall of 2016. Fish were fed a rotating diet of frozen blood worms, daphnia, and mysis shrimp (Cobalt Aquatics) with 25% water changes three times a week and 12hr light/12hr dark cycle. Fish were kept at 2-3

g/kg salinity and ambient temperatures (16-18 °C). To induce breeding, water temperature was raised to 20°C using a 50W submersible aquarium heater and the light/dark cycle was changed to 16h light/8h dark cycle.

Big lagoon (BL) and Klamath river (KL) wild-caught sticklebacks were externally fertilized and hatched in late winter and early spring of 2017. Fertilized embryos took from 8-10 days to hatch at ambient temperature (16-18°C). For BL, 591 fertilized embryos hatched and had an 84% survival rate one month later. The average number of viable hatchlings per clutch was 53. For KL, 627 fertilized embryos hatched and had a 99% survival rate one month later. The average number of viable hatchlings per clutch was 57.

**Hatchling care**

Hatchlings were kept in 10-gallon freestanding tanks at 0 g/kg and 18°C with Azoo Oxygen Plus Bio-Filter 6's attached to air hoses for biological filtration and to increase dissolved oxygen levels. Tanks were cleaned daily to remove waste and leftover food. Hatchlings were fed live baby bring shrimp (San Francisco Bay Brand or E-Z Egg) once or twice a day ad libitum. After hatchlings were large enough to be moved (~3 months), they were transferred to 30-gallon tanks and transitioned over to frozen brine shrimp larvae (Hikari) and progressively to daphnia, mysis shrimp, and blood worms (Cobalt Aquatics).

**Range finding experiments**

***Critical Thermal Maxima***

F1 Big lagoon and Klamath fish were acclimated for three weeks at 15°C and 9 g/kg. The critical thermal maxima (CTMax) were determined for both the BL and KL populations. The

experimental chamber consisted of a 10-gallon tank with a 240 gph aquarium circulation pump (Hydor) at the bottom to circulate water. The temperature of the water in the tank was controlled by a refrigerated/heated 6L circulating bath (PolyScience, 9106A11B) with ethylene glycol solution (PolyScience, cat. 060320) circulating through an attached metal coil that could be submersed in the tank. Ten quart-sized jars were placed on a raised plastic shelf so the pump and metal heating/cooling coil could sit below the jars. Each jar was filled with 400 mL of 9 g/kg water and was individually aerated by an air hose connected to a 10 μL pipette tip with the end cut off. This setup ensured bubbles were small enough to still maintain a clear visual of the fish. Each jar also contained a digital pocket thermometer (General, cat. DPT392FC) to track thermal ramping rate for each individual jar. A temperature ramping rate of 0.3°C per minute was used starting from 15°C. Final CTMax temperature readings were obtained with a 550A YSI instrument. CTMax experiments were conducted in two rounds on separate days. Fish were given an hour to acclimate to the individual jars in the experimental set up. Five fish from each population were run for each round and the positioning of the fish was rotated between the rounds (i.e. Klamath fish were run from the front jars in the first experiment and from the back jars in the second experiment). Loss of equilibrium (LOE) was used as the experimental endpoint. For both populations, loss of equilibrium was specified as cessation of movement and rigid extension of the pectoral fins outward at a perpendicular angle from the side of body. Opercula were often flared out away from the side of the head. Fish exhibiting loss of equilibrium were gently nudged with the temperature probe until no response occurred. Temperature was then immediately recorded, and fish were placed in individually marked recovery containers back at 15°C. After the fish were visually respiring and/or swimming, wet mass and standard length was recorded. Fish were allowed to recover for 24 hours and only

survivors were included in the final CTMax calculation to ensure consistency of the non-lethal end point (i.e. that the CTMax temperature was not exceeded). All ten KL fish survived, and nine BL fish survived the recovery period.

### *Chronic lethal maximum*

The chronic lethal maximum (CLMax) was determined for both the BL and KL populations. Twenty fish from each population were pre-acclimated for three weeks at 15°C and 9g/kg. The set up was similar to that described above for CTMax but using a 300-gallon stock tank as the water bath and 200-watt heaters to increase the temperature 1°C/day. Fish were fed ad libitum once per day after which any excess food and waste was removed. Death was used as the endpoint, and deceased fish were recorded daily prior to temperature increase. Standard length (cm) was recorded for each fish as they were removed.

## Temperature stress experiments

### *Chronic acclimation experiments*

First generation (F1) sticklebacks from BL (N=30) and KL (N=30) were pre-acclimated for three weeks at 15°C and 9 g/kg (plasma-isosmotic conditions that minimize energy expenditure for osmoregulation) prior to experimentation. Fish were fed ad libitum once per day during the pre-acclimation and experimental phases after which excess food and waste was removed. The temperature was either increased or decreased from 15°C by 2°C/day up to 25°C for the chronic warm and down to 7°C for the chronic cold acclimation, after which fish were held for 21 days at the respective temperatures. Ten fish from each population were randomly assigned to each experimental group: 25°C (warm), 15°C (control), 7°C (cold). As with the range finding

experiments, a water bath method was used with pumps and air stones to circulate the water. Heating to 25°C was achieved using 200-watt electric heaters and cooling to 7°C was done using a refrigerated/heated 6L circulating bath (PolyScience, 9106A11B). Controls were kept at 15°C but handled in the same manner as the 25°C and 7°C groups. Fish were held at the final temperatures (25°C warm; 7°C cold) for a total of three weeks. Because the temperature change was 10°C overall for warm and 8°C overall for cold, the 7°C acclimation group was dissected a day earlier than the 25°C acclimation group. Half of the controls were dissected each day to account for any differences between the two days, and the dissections occurred under the same conditions and at the same time of day. Dissection order was alternated among the different conditions and between the two populations. Wet weight, standard length, and lateral plate count were recorded prior to dissection. Fish were sexed upon dissection. Tissues were extracted and individually flash frozen in liquid nitrogen. There was no mortality during this experiment.

***Morphometric measurements – chronic acclimation experiment***

Standard length was measured prior to dissection. Longest dorsal spine, anterior dorsal spine, and 2$^{nd}$ dorsal spine length were measured during the dissections for the gill and white muscle tissue. All other length measurements were taken using Image J (NIH) from photographs recorded prior to sacrifice at the conclusion of the acclimation experiment. Length measurements were taken as depicted in Figure 1.1.

***Body conditioning measurements***

Wet weight, hepatosomatic index (HSI), gonadosomatic index (GSI), and condition factor (K) were determined for fish acclimated chronically to different temperatures. Wet weight was

measured prior to sacrifice. Liver weight and gonad weight were measured post dissection. Condition factor (K) was calculated as K = weight (g) x 100/total length $(cm)^3$ as per Moyle & Cech (2004). Hepatosomatic Index was measured as (liver weight/wet weight)*100. Gonadosomatic Index was measured as (gonad weight/wet weight)*100.

**Metabolite assays**

Glucose, lactate, and glutamine/glutamate bioluminescent metabolite assays were performed on gill and white muscle tissue (Promega). Previously flash frozen white muscle tissue was finely sliced and chopped with a scalpel into one mm pieces. Previously flash frozen gill tissue was gently scraped off the larger filaments with the edge of a scalpel. Individual tissues were then weighed and transferred to 10 x 75 mm glass culture tubes (VWR Scientific Products, cat. 47729-568) filled with 1.125 mL of an 8:1 ratio of homogenization buffer (50 mM Tris, pH 7.5) and inactivation solution II (0.6N HCl). Tissues were homogenized with a tissue-tearor (BioSpec Products, Inc., cat. 985370-07) for 30 seconds at full speed and then 0.125 mL of tris solution II (600 mM, pH 8.5) was added. All tissues were prepared using the protocol for the glutamine/glutamate assay, as this procedure required the most precise pH range of the three protocols and was compatible with the other protocols. The tissue-tearor was operated for 5 seconds in deionized water (DI) water and cleaned between samples. The homogenate was pipetted into 2 mL pre-labeled tubes and stored overnight in a -30 °C freezer. Two µL was pipetted into a 96-well plate in duplicate for a 660 nm protein assay (Thermo Scientific™, cat. 22660) to determine relative protein abundance among samples and account for differences in sample weights. The following day, samples were thawed and assayed for all four metabolites in opaque 96-well plates containing appropriate standards.

***Glutamine/glutamate***

Glutamine/Glutamate-Glo™ assay kits were used to determine glutamine and glutamate concentrations (Promega, cat. J8021). For the glutamine/glutamate opaque 96-well plate, 12.5 µL of glutaminase buffer was added to every other column of the microplate to test for glutamate only. Glutaminase enzyme solution was added to every other column of the plate to test for the sum of glutamine and glutamate, as glutaminase was used to convert glutamine to glutamate. Glutamine values could then be obtained by subtracting glutamate only levels from the total glutamate levels (which included conversion of glutamine to glutamate). Glutamate standards were added in duplicate at the following concentrations: 0 mM, 0.78 mM, 1.56 mM, 3.13 mM, 6.25 mM, 12.5 mM, 25, mM, and 50 mM. The 0 mM well served as a negative control containing 12.5 µL of a buffer comprised of an 8:1:1 ratio of 50 mM Tris, pH 7.5, 0.6N HCL, and 600mM Tris, pH 8.5, respectively. Samples were added in duplicate to columns containing both glutaminase buffer and glutaminase enzyme solution (4 wells total per sample). The plate was mixed for 60 seconds at 1600 rpm using a Fisher Scientific™ microplate advanced vortex mixer and incubated for 30 minutes at room temperature. Glutamate detection reagent (25 µL) was added to each well, mixed for 60 seconds with a lid at 1350 rpm and incubated for 60 minutes. Glutamine and glutamate luminescence readings were detected using a GloMax® navigator microplate luminometer (Promega).

***Glucose***

Glucose-Glo™ assay kits were used to determine glutamine and glutamate concentrations (Promega, cat. J6021). For the glucose 96-well plate, 12.5 µL of glucose detection reagent was

added to each well and 12.5 µL of glucose standards were added in duplicate at the following concentrations: 0 mM, 0.78 mM, 1.56 mM, 3.13 mM, 6.25 mM, 12.5 mM, 25, mM, and 50 mM. The 0 mM well served as a negative control containing 12.5 µL of a buffer comprised of an 8:1:1 ratio of 50 mM Tris, pH 7.5, 0.6N HCL, and 600mM Tris, pH 8.5, respectively. Samples were added in duplicate, and the plate was mixed with a lid for 60 seconds at 1600 rpm using a Fisher Scientific™ microplate advanced vortex mixer. The microplate was then incubated for 60 minutes at room temperature. Glucose luminescence readings were detected using a GloMax® navigator microplate luminometer (Promega).

***Lactate***

Lactate-Glo™ assay kits were used to determine glutamine and glutamate concentrations (Promega, cat. J5021). For the lactate 96-well plate, 12.5 µL of lactate detection reagent was added to each well and 12.5 µL of lactate standards were added in duplicate at the following concentrations: 0 mM, 0.78 mM, 1.56 mM, 3.13 mM, 6.25 mM, 12.5 mM, 25, mM, 50 mM, 100 mM, and 200 mM. The 0 mM well served as a negative control containing 12.5 µL of a buffer comprised of an 8:1:1 ratio of 50 mM Tris, pH 7.5, 0.6N HCL, and 600mM Tris, pH 8.5, respectively. Samples were added in duplicate, and the plate was mixed with a lid for 60 seconds at 1600 rpm using a Fisher Scientific™ microplate advanced vortex mixer. The microplate was then incubated for 60 minutes at room temperature. Lactate luminescence readings were detected using a GloMax® navigator microplate luminometer (Promega).

**Statistical analysis**

Two-way analysis of variance (ANOVA) was used to investigate differences between the two populations (KL and BL) and temperature treatments (7 °C, 15 °C, 25°C). Significant findings were followed up with Tukey's post-hoc tests. Data sets were tested for normality (Shapiro-Wilk test) and homogeneity of variance (Brown-Forsythe test). For data violating assumptions of normality, the non-parametric Kruskal-Wallis test was run, with significant findings evaluated further using Fisher's least significant difference (LSD) post hoc tests. For unbalanced ANOVAs, the reverse order of the independent variables was also run to confirm results. A Welch one way test was used for the body depth data as they violated assumptions of homogeneity of variance. Values of $p < 0.05$ were considered significant for all test results and all data are reported as mean ± standard error of the mean (SE). All statistical analysis was conducted using R statistical software v3.6.1 (R Core Team, 2019) and graphs were created using ggplot2 (Wickham, 2016). The car package v3 was used for the Brown-Forsythe test (Fox & Weisberg, 2019) and the agricolae package v1.3.1 was used for Kruskal-Wallis and Fisher's LSD post hoc test (de Mendiburu & Yaseen, 2019).

## RESULTS

### Critical thermal maxima do not differ between BL and KL populations

As shown in Figure 1.2, CTMax for KL (N=10) was 31.4 ± 0.3°C and 31.5 ± 0.2°C for BL (N=9). CTMax was not significantly different between the two populations (Kruskal-Wallis: chi-squared = 0.041887, df = 1, p-value = 0.8378). Since only ten fish could be analyzed in the CTMax chamber at a time, five fish from each population were analyzed in two different rounds. No significant differences in CTMax were observed between the two rounds (BL Kruskal-Wallis: chi-squared = 1.8, df = 2, p-value = 0.407; KL Kruskal-Wallis: chi-squared = 4, df = 4,

p-value = 0.406). The average wet weight of specimens used for CTMax was 1.19 ± 0.07 g for BL and 1.07 ± 0.06 g for KL. Standard Length was 4.603 ± 0.083 cm for BL and 4.528 ± 0.103 cm for KL. There was no significant difference for either wet weight (Welch's Two Sample t-test: t = 1.268, df = 16.181, p-value = 0.2227) or standard length between the two populations (Welch's Two Sample t-test: t = 0.563, df = 16.59, p-value = 0.5807). A Spearman's correlation was used to examine the relationship of weight and standard length to CTMax. The correlations of both wet weight ($r_s$=0.2582, p = 0.2857) and standard length ($r_s$=0.3544, p = 0.1365) to CTMax were weak.

**Chronic lethal maxima are identical for BL and KL populations**

As shown in Figure 1.2, CLMax for KL (N=20) was 29.0 ± 0.5°C and for BL threespine sticklebacks (N=20) was 29.0 ± 0.6°C. There was no significant difference in CLMax between the two populations (Kruskal-Wallis: chi-squared = 0.68433, df = 1, p-value = 0.4081). Standard Length was 4.673 ± 0.072 cm for BL and 4.509 ± 0.067 cm for KL. There was no significant difference in standard length between the two populations (Welch's Two Sample t-test: t = 1.6714, df = 37.729, p-value = 0.1029). A Spearman's correlation was run to examine the relationship between standard length and CLMax ($r_s$=0.2187, p = 0.1752), which showed a weak correlation.

**Morphometric parameters are population-specific but not influenced by chronic temperature acclimation**

All two-way ANOVAs were balanced except for longest pelvic spine and anterior dorsal spine as some of the specimens had broken spines and measurements were thus not taken for

those particular spines. For unbalanced ANOVAs, the reverse order of the independent variables was also run to confirm results, but only the first set of results is included in Table 1.1. Table 1.1 lists degrees of freedom (df), mean squares (MS), F-value, and exact p-value for all the two-way ANOVAs and Welch one-way test (minus MS), and chi-squared ($\chi^2$), df, and p-value for Kruskal-Wallis tests. There were no significant interaction effects for any of the two-way ANOVAs. Body depth was run using a Welch one-way test. Orbit diameter, plate count (L/R), gonad weight (females), liver weight, and GSI (females) were run with Kruskal-Wallis tests, and all other measures were analyzed with a two-way ANOVA.

As can be seen in Table 1.1 and Figure 1.3, there were numerous significant differences between the KL and BL populations with regards to morphometric parameters. Standard length (SL), total length (TL), snout length, head length, body depth, longest pelvic spine, and 2$^{nd}$ dorsal spine were all longer in KL than BL. Orbit diameter was also significantly larger in the KL population than the BL population. The number of lateral plates on both the left and right sides were significantly greater in the KL than the BL population with KL having on average 22 plates and BL having 7. The Klamath population represented a predominantly fully plated population with some partial plated morphs, while the Big lagoon population was overwhelmingly a low plated morphotype. As shown in Table 1.1, temperature had no significant effect on any of the morphometric measurements.

**Body conditioning indices are altered by chronic thermal acclimation**

For gonad weight and GSI, males and females were separated for analysis given the large disparity in gonad size between the two sexes. As shown in Table 1.1, HSI was significantly different by population, with BL having a larger HSI than KL. However, chronic temperature

acclimation significantly changed body conditioning in both populations. Liver weight, HSI, condition factor (K), and gonad weight for males was significantly different among the different temperatures (Figure 1.4). Liver weight and gonad weight in males was significantly lower in the 25°C group compared to the 7°C group. For HSI, the 25°C group was significantly lower than the control group (15°C). K in the 25°C group was significantly lower than both the control (15°C) and 7°C group. There were no significant interaction effects. Specific values from the ANOVAs for HSI, K and gonad weight for males and Kruskal-Wallis tests for liver weight, gonad weight in females, and GSI in females can be found in Table 1.1.

**White muscle metabolites are altered by chronic temperature acclimation**

There were no significant differences between the two populations for the metabolites in the white muscle tissue, and no interaction effects (Table 1.2). Exact values (df, MS, F-values, p-values) from the statistical analysis can be found in Table 1.2. However, temperature acclimation did significantly alter the levels of these metabolites. As shown in Figure 1.5, glutamate levels were significantly lower in white muscle tissue in the 25°C group compared to the 7°C group. Glucose and lactate levels were both significantly lower in the 25°C group compared to the 15°C control group (Figure 1.6). Glutamine levels were significantly lower in the 7°C group than either the 15°C or 25°C groups. The glutamine/glutamate ratio was significantly different across all three temperature conditions.

**Gill glutamine and glucose are altered by chronic temperature acclimation**

Glutamine values for each acclimation temperature were significantly different from those at all other temperatures (Figure 1.5). Population-specific metabolite differences were also observed.

Glucose levels were significantly higher in BL than KL (Figure 1.6). There were no significant differences in glutamate levels or lactate levels. For lactate, of the 60 samples run, only 2 KL samples and 16 BL samples yielded results for analysis. The glutamine/glutamate ratio was significantly smaller in the 7ºC group than either the 15ºC or 25ºC group.

## DISCUSSION

### BL and KL populations have the same upper thermal tolerance limits

The CTMax findings in this study (Figure 1.2) are very much in line with existing literature, showing threespine sticklebacks having a CTMax of approximately 30-32 °C (Barrett et al., 2011; Dammark et al., 2018; Metzger et al., 2016). CTMax was within 0.1 °C between the two populations, and CLMax was identical between the two populations, suggesting that environmental factors (rearing temperatures and other conditions) were more important contributors to thermal limits than underlying genetic differences in the populations (i.e. morphotype). These findings are also in alignment with the literature, which has demonstrated that thermal history of the organism, in particular the last temperature experienced, is probably the most important parameter influencing thermal tolerance (Beitinger et al., 2000; Beitinger & Lutterschmidt, 2011; Lutterschmidt & Hutchison, 1997). Although few studies have examined both CTMax and CLMax, one study examining four genetic lines of largemouth bass consistently found higher CTMax than CLMax values, resulting in differences of 1.8, 2.5, 2.6, and 3.6 °C (Fields et al., 1987). Our findings of CTMax at 2.4 and 2.5 degrees higher than CLMax are in good agreement with these results. Another study demonstrated that threespine sticklebacks consistently had the highest upper lethal temperatures at 12 g/kg, compared to the other two salinities tested, regardless of acclimation salinity or temperature. This result suggests

that testing thermal tolerance at salinities that are approximately isosmotic to blood confers slightly higher thermal tolerances as fish can minimize the extent of energy exerted for osmoregulating (Jordan & Garside, 1972). Therefore, the salinity for both acclimation and thermal testing in this study was chosen at 9 g/kg. This salinity is equal to the approximate osmolality of extracellular fluids (300 mosmol/kg) maintained in teleosts, which are osmoregulators (Kültz, 2015), and supports achieving the highest thermal limits.

**The morphotype of BL and KL populations indicates significant genetic divergence**

Overall, KL represents a predominantly fully plated, or *trachurus*, morphotype (with some intermediate-partial, or *semiarmatus* morphs), while BL represented a low plated, or *leiurus*, morphotype. KL was significantly longer, deeper, and weighed more than BL and had longer spines for all three spines (longest pelvic, anterior dorsal, 2$^{nd}$ dorsal) measured (two significantly different). There were also significant differences in head morphology, with KL having a significantly longer head, snout, and orbit diameter. These attributes are typical of a marine phenotype versus a freshwater phenotype (Bell, 2001; Bell & Foster, 1994; Howes et al., 2017). Anadromous and marine populations tend to be fully plated and freshwater populations often consist of low plated morphs (Wootton, 1984). Longer spines could also be indicative of a bigger threat of predation by gape limited fish or birds for KL over BL (Morris et al., 1956; Webster et al., 2011). However, since BL had an average of 7 plates per side (as opposed to fewer plates), this suggests BL also historically faced predation by fish (Hagen & Gilbertson, 1972).

**Temperature affects body condition more than genetic population differences**

Unlike morphometric parameters, the two populations did not differ much in body conditioning indices. Only HSI was significantly smaller in KL than BL, however, most of the differences in weights and indices were due to temperature effects rather than population differences. Perhaps the slightly larger sizes of the KL over the BL population required a greater basal metabolic rate under the various temperature conditions and thus required a greater utilization of stored energy from the liver. After chronic thermal acclimation, HSI was significantly smaller in the 25°C group versus control (15°C) and liver weight was significantly smaller in the 25°C group than the 7°C group. HSI is a good indicator of total glycogen (Chellappa et al., 1995), suggesting greater utilization of this stored energy source by fish in the 25°C group. Condition factor was significantly lower in the 25°C group than the 7°C group or control group. There were also several insignificant trends where liver weight, gonad weight/GSI in males, and wet weight decreased as temperature increased. Wet weight and condition factor are good predictors of energy reserves in threespine sticklebacks year-round (Chellappa et al., 1995), further suggesting the 25°C group experienced a higher metabolic demand that could not keep pace with energy input and resulted in a heavy utilization of energy reserves. Other studies have also found a decrease in body mass or condition during warm acclimations, despite ample amounts of food, in threespine sticklebacks (Guderley et al., 1994; Vézina & Guderley, 1991), zebrafish (Vergauwen et al., 2010), sea urchin (Delorme & Sewell, 2016) and emerald rockcod (Enzor et al., 2017). Male gonad weight was also significantly smaller in the 25°C group compared to the 7°C group. Male sticklebacks invest a significant amount of energy in gonad development prior to the breeding season in the form of glycogen and lipid utilization (Huntingford et al., 2001). The chronic acclimation experiments were conducted in August, which would be at the end of the typical breeding season (Wootton, 1984), but increased temperatures can also induce

reproductive behaviors in sticklebacks (Sokołowska & Kulczykowska, 2009). However, the fact that both male gonad weight and male GSI decreased along with overall wet weight and condition factor suggests that a decrease in overall condition of the fish was not due to investing energy in reproduction, which could otherwise be a confounding factor. Similarly to our study, threespine sticklebacks from Verneuil-en-Halatte (France) exposed to 21°C for 90 days experienced a decrease in lipid, protein content, and weight (Hani et al., 2018).

**Effects of temperature acclimation on energy metabolites**

Metabolite concentrations after chronic warm temperature stress have been examined in a variety of other aquatic organisms with varying results. In Senegalese sole (*Solea senegalensis*) exposed to 26°C for 21 days, plasma glucose, lactate, and glutamate concentrations increased (Costas et al., 2012). Increases in plasma lactate concentrations for that study were attributed to a higher metabolic activity. In silver catfish (*Rhamdia quelen*) exposed to 31°C for 21 days, plasma glucose increased, white muscle glucose increased, and white muscle lactate decreased (Lermen et al., 2004). Our study similarly showed a decrease in white muscle lactate, but also showed a decrease in white muscle glucose, adding further support to the species-specific nature of glucose metabolism. Sea cucumber (*Apostichopus japonicus*) exposed to 25°C for 7 days had increased glucose and glutamine and decreased glutamate concentrations in their muscle tissue (Shao et al., 2015). In contrast to this study on an echinoderm, our study found no significant differences between 25°C vs. 15°C acclimated fish for white muscle glutamine and glutamate although glutamine decreased significantly at 7°C.

In our study, both white muscle glucose and lactate concentrations were significantly reduced in the 25°C group relative to the control group (15°C), glutamate was significantly

reduced relative to the 7°C group, and glutamine was significantly higher in the 7°C group compared to the 15°C and 25°C group. Lactate, glutamate, and to some degree glutamine can all be used as substrates for gluconeogenesis, which might be one explanation for their decreased concentrations in the 25°C group. Furthermore, glutamate can be combined with NH3 via glutamine synthetase and then transported out of the cell (Newsholme et al., 2003). A study of catfish (*Clarias batrachus*), demonstrated that glutamate supported a higher rate of gluconeogenesis in perfused liver cells than either lactate or pyruvate, and that other amino acids such as alanine, glutamine, ornithine, serine, proline and glycine can also be used as substrates for gluconeogenesis (Goswami et al., 2004).

It is well established that basal metabolic rate increases with warm acclimation (Brett, 1964; Clarke & Fraser, 2004; Gillooly et al., 2001). Accordingly, plasma glucose concentrations have been shown to increase linearly with temperature (Costas et al., 2012), and an increase in plasma glucose concentration usually coincides with an increase in muscle glucose uptake (Wasserman et al., 2011). However, in our study, muscle glucose significantly decreased in the warm-acclimated versus control group, along with a decrease in lactate. Combined with the decline in body conditioning discussed above, it appears that food intake was not keeping pace with metabolic demand. Besides an initial utilization of liver glycogen and possibly some muscle glycogen, it is believed that lipids are utilized early on during periods of starvation, and that proteins are only mobilized after these other resources have been depleted (Costas et al., 2012; Lermen et al., 2004; Morata et al., 1982; Navarro & Gutiérrez, 1995). A study applying warm acclimation for 6 weeks at 20°C in threespine sticklebacks found that the majority of the decline in body conditioning was due to a diminishment of the axial musculature (Vézina & Guderley, 1991). It is possible that the fish in our study were likewise catabolizing white muscle protein as

an energy source. They looked visibly emaciated compared to control and 7°C groups even though they had been offered food ad libitum. White muscle breakdown occurs when blood glucose and lactate levels have declined (Navarro & Gutiérrez, 1995), as was mirrored by the decline in white muscle glucose and lactate in our study suggesting that feeding rate does not keep pace with increased metabolic demand during high temperature stress.

White muscle represents the largest free amino acid (FAA) pool by percent distribution (Jürss & Bastrop, 1995; Wilson & Poe, 1974). In our study, glutamine was significantly altered by temperature in both tissues examined. In white muscle for the cold group, glutamine was significantly lower in the 7°C group than both the control and 25°C groups. In the gill, glutamine was significantly different in all three groups with glutamine increasing with increasing temperature and vice versa. Our study clearly demonstrates an effect of chronic temperature stress, either cold or warm, on glutamine-glutamate metabolism. However, the effect of temperature is tissue-specific, and one should be careful in generalizing metabolic effects across different tissues. Clearly, gills metabolize glutamine differently than white muscle, e.g. by conversion to ammonia and excretion of ionic and non-ionic forms of ammonia (Evans et al., 2005).

Although most of the metabolic differences were associated with temperature, the glucose concentration in gills was significantly higher in BL than KL, demonstrating population differences to identical temperature stress within a species. KL fish only elevated gill glucose levels to BL levels under the 25°C condition while they were lower than BL levels at 7°C and 15°C. While BL fish kept relatively stable gill glucose levels with a slight decrease as temperature increases, KL fish increased glucose levels only under the warm acclimation condition. One study with sticklebacks from different habitats found variation in carbohydrate

metabolism depending on factors such as salinity, temperature, and food consumption (Churova et al., 2018). These findings highlight that differences within a species can be varied and highly dependent on circumstances, or perhaps in this case, genetic/epigenetic differences between morphotypes.

## Conclusions

In summary, our study demonstrates significant changes to glutamine, glutamate, lactate, and glucose metabolism after 21 days of chronic warm or cold acclimation in threespine sticklebacks. While morphometric parameters differed between populations but were unaffected by temperature, body conditioning and key energy metabolite levels in white muscle and gill tissues were similarly affected by chronic temperature stress in both populations. However, population differences in glucose levels highlight that some key metabolic differences do exist, and that these differences may be temperature dependent. Overall body conditioning decreased in both warm acclimated populations while it increased in both cold acclimated populations. This study also confirms existing temperature limits for this species, provides further evidence for the importance of temperature history over genetic differences in morphotype or population in the determination of upper temperature limits, and provides an approximate difference of 2.5 °C between CTMax and CLMax in this species, with CTMax being the higher value. Based on these data, we conclude that threespine stickleback populations representing different morphotypes are similarly susceptible to thermal stress.

ACKNOWLEDGMENTS

Part of this work was funded by NSF grant IOS-1656371.

**REFERENCES**


Angilletta, M. J., Niewiarowski, P. H., & Navas, C. A. (2002). The evolution of thermal physiology in ectotherms. *Journal of Thermal Biology*, *27*(4), 249–268. https://doi.org/10.1016/S0306-4565(01)00094-8

Baris, T. Z., Crawford, D. L., & Oleksiak, M. F. (2016). Acclimation and acute temperature effects on population differences in oxidative phosphorylation. *American Journal of Physiology - Regulatory, Integrative and Comparative Physiology*, *310*(2), R185–R196. https://doi.org/10.1152/ajpregu.00421.2015

Barrett, R. D. H., Paccard, A., Healy, T. M., Bergek, S., Schulte, P. M., Schluter, D., & Rogers, S. M. (2011). Rapid evolution of cold tolerance in stickleback. *Proceedings of the Royal Society B: Biological Sciences*, *278*(1703), 233–238. https://doi.org/10.1098/rspb.2010.0923

Barton, B. A., & Schreck, C. B. (1987). Metabolic Cost of Acute Physical Stress in Juvenile Steelhead. *Transactions of the American Fisheries Society*, *116*(2), 257–263. https://doi.org/10.1577/1548-8659(1987)116<257:MCOAPS>2.0.CO;2

Beitinger, T. L., Bennett, W. A., & McCauley, R. W. (2000). Temperature Tolerances of North American Freshwater Fishes Exposed to Dynamic Changes in Temperature. *Environmental Biology of Fishes*, *58*(3), 237–275. https://doi.org/10.1023/A:1007676325825

Beitinger, T. L., & Lutterschmidt, W. I. (2011). Temperature | Measures of Thermal Tolerance. In A. P. Farrell (Ed.), *Encyclopedia of Fish Physiology* (pp. 1695–1702). Academic Press. https://doi.org/10.1016/B978-0-12-374553-8.00200-8

Bell, M. A. (2001). Lateral plate evolution in the threespine stickleback: Getting nowhere fast. *Genetica*, *112*, 445–461. https://doi.org/10.1023/A:1013326024547

Bell, M. A., & Foster, S. A. (Eds.). (1994). *The evolutionary biology of the threespine stickleback*. Oxford University Press.

Bever, K., Chenoweth, M., & Dunn, A. (1981). Amino acid gluconeogenesis and glucose turnover in kelp bass (Paralabrax sp.). *American Journal of Physiology-Regulatory, Integrative and Comparative Physiology*, *240*(3), R246–R252. https://doi.org/10.1152/ajpregu.1981.240.3.R246

Bonga, S. E. W. (1997). The stress response in fish. *Physiological Reviews*, *77*(3), 591–625. https://doi.org/10.1152/physrev.1997.77.3.591

Brett, J. R. (1964). The Respiratory Metabolism and Swimming Performance of Young Sockeye Salmon. *Journal of the Fisheries Research Board of Canada*, *21*(5), 1183–1226. https://doi.org/10.1139/f64-103

Chellappa, S., Huntingford, F. A., Strang, R. H. C., & Thomson, R. Y. (1995). Condition factor and hepatosomatic index as estimates of energy status in male three-spined stickleback. *Journal of Fish Biology*, *47*(5), 775–787. https://doi.org/10.1111/j.1095-8649.1995.tb06002.x

Churova, M. V., Shulgina, N. S., & Nemova, N. N. (2018). Activity of the Enzymes of the Energy and Carbohydrate Metabolism in the Organs of the Three-Spined Stickleback Gasterosteus aculeatus from Different Biotopes of the White Sea. *Doklady Biological Sciences*, *482*(1), 185–187. https://doi.org/10.1134/S0012496618050010

Clarke, A., & Fraser, K. P. P. (2004). Why does metabolism scale with temperature? *Functional Ecology*, *18*(2), 243–251. https://doi.org/10.1111/j.0269-8463.2004.00841.x

Connors, T. J., Schneider, M. J., Genoway, R. G., & Barraclough, S. A. (1978). Effect of acclimation temperature on plasma levels of glucose and lactate in rainbow trout, Salmo

gairdneri. *Journal of Experimental Zoology*, *206*(3), 443–449. https://doi.org/10.1002/jez.1402060313

Costas, B., Aragão, C., Ruiz-Jarabo, I., Vargas-Chacoff, L., Arjona, F. J., Mancera, J. M., Dinis, M. T., & Conceição, L. E. C. (2012). Different environmental temperatures affect amino acid metabolism in the eurytherm teleost Senegalese sole (Solea senegalensis Kaup, 1858) as indicated by changes in plasma metabolites. *Amino Acids*, *43*(1), 327–335. https://doi.org/10.1007/s00726-011-1082-0

Cowles, R. B., & Bogert, C. M. (1944). A preliminary study of the thermal requirements of desert reptiles. *Bulletin of the American Museum of Natural History*, *83*, 261–296.

Dalvi, R. S., Das, T., Debnath, D., Yengkokpam, S., Baruah, K., Tiwari, L. R., & Pal, A. K. (2017). Metabolic and cellular stress responses of catfish, Horabagrus brachysoma (Günther) acclimated to increasing temperatures. *Journal of Thermal Biology*, *65*, 32–40. https://doi.org/10.1016/j.jtherbio.2017.02.003

Dammark, K. B., Ferchaud, A.-L., Hansen, M. M., & Sørensen, J. G. (2018). Heat tolerance and gene expression responses to heat stress in threespine sticklebacks from ecologically divergent environments. *Journal of Thermal Biology*, *75*, 88–96. https://doi.org/10.1016/j.jtherbio.2018.06.003

de Mendiburu, F., & Yaseen, M. (2019). *agricolae: Statistical Procedures for Agricultural Research* (R package version 1.3.1) [Computer software]. https://cran.r-project.org/package=agricolae

Delorme, N. J., & Sewell, M. A. (2016). Effects of warm acclimation on physiology and gonad development in the sea urchin Evechinus chloroticus. *Comparative Biochemistry and*

*Physiology Part A: Molecular & Integrative Physiology*, *198*, 33–40. https://doi.org/10.1016/j.cbpa.2016.03.020

Ellerby, D. J. (2011). Buoyancy, locomotion, and movement in fishes | Undulatory swimming. In *Encyclopedia of Fish Physiology* (pp. 547–554). Elsevier. https://doi.org/10.1016/B978-0-12-374553-8.00222-7

Enzor, L. A., Hunter, E. M., & Place, S. P. (2017). The effects of elevated temperature and ocean acidification on the metabolic pathways of notothenioid fish. *Conservation Physiology*, *5*(1), cox019. https://doi.org/10.1093/conphys/cox019

Evans, D. H., Piermarini, P. M., & Choe, K. P. (2005). The multifunctional fish gill: Dominant site of gas exchange, osmoregulation, acid-base regulation, and excretion of nitrogenous waste. *Physiol Rev*, *85*(1), 97–177. https://doi.org/10.1152/physrev.00050.2003

Fields, R., Lowe, S. S., Kaminski, C., Whitt, G. S., & Philipp, D. P. (1987). Critical and Chronic Thermal Maxima of Northern and Florida Largemouth Bass and Their Reciprocal F1 and F2 Hybrids. *Transactions of the American Fisheries Society*, *116*(6), 856–863. https://doi.org/10.1577/1548-8659(1987)116<856:CACTMO>2.0.CO;2

Fox, J., & Weisberg, S. (2019). *An R Companion to Applied Regression* (Third edition) [Computer software]. Sage. https://socialsciences.mcmaster.ca/jfox/Books/Companion/

Gillooly, J. F., Brown, J. H., West, G. B., Savage, V. M., & Charnov, E. L. (2001). Effects of Size and Temperature on Metabolic Rate. *Science*, *293*(5538), 2248–2251. https://doi.org/10.1126/science.1061967

Goswami, C., Datta, S., Biswas, K., & Saha, N. (2004). Cell volume changes affect gluconeogenesis in the perfused liver of the catfish Clarias batrachus. *Journal of Biosciences*, *29*(3), 337–347. https://doi.org/10.1007/BF02702616

Guderley, H., & Leroy, P. H. (2001). Family origin and the response of threespine stickleback, Gasterosteus aculeatus, to thermal acclimation. *Journal of Comparative Physiology B*, *171*(2), 91–101. https://doi.org/10.1007/s003600000162

Guderley, Helga, Lavoie, B. A., & Dubois, N. (1994). The interaction among age, thermal acclimation and growth rate in determining muscle metabolic capacities and tissue masses in the threespine stickleback, Gasterosteus aculeatus. *Fish Physiology and Biochemistry*, *13*(5), 419–431. https://doi.org/10.1007/BF00003421

Hagen, D. W., & Gilbertson, L. G. (1972). Geographic variation and environmental selection in Gasterosteus aculeatus L. in the Pacific Northwest, America. *Evolution*, *26*(1), 32–51. https://doi.org/10.1111/j.1558-5646.1972.tb00172.x

Hani, Y. M. I., Turies, C., Palluel, O., Delahaut, L., Gaillet, V., Bado-nilles, A., Porcher, J.-M., Geffard, A., & Dedourge-geffard, O. (2018). Effects of chronic exposure to cadmium and temperature, alone or combined, on the threespine stickleback (Gasterosteus aculeatus): Interest of digestive enzymes as biomarkers. *Aquatic Toxicology*, *199*, 252–262. https://doi.org/10.1016/j.aquatox.2018.04.006

Howes, T. R., Summers, B. R., & Kingsley, D. M. (2017). Dorsal spine evolution in threespine sticklebacks via a splicing change in MSX2A. *BMC Biology*, *15*(1), 115. https://doi.org/10.1186/s12915-017-0456-5

Huntingford, F. A., Chellappa, S., Taylor, A. C., & Strang, R. H. C. (2001). Energy reserves and reproductive investment in male three-spined sticklebacks, Gasterosteus aculeatus. *Ecology of Freshwater Fish*, *10*(2), 111–117. https://doi.org/10.1034/j.1600-0633.2001.100206.x

Jordan, C. M., & Garside, E. T. (1972). Upper lethal temperatures of threespine stickleback, *Gasterosteus aculeatus* (L.), in relation to thermal and osmotic acclimation, ambient salinity, and size. *Canadian Journal of Zoology*, *50*(11), 1405–1411. https://doi.org/10.1139/z72-189

Jürss, K., & Bastrop, R. (1995). Chapter 7 Amino acid metabolism in fish. In T.P. Mommsen & P. Hochachka (Eds.), *Biochemistry and Molecular Biology of Fishes* (Vol. 4, pp. 159–189). Elsevier. https://doi.org/10.1016/S1873-0140(06)80010-X

Kronnie, G. te, Tatarczuch, L., Raamsdonk, W., & Kilarski, W. (1983). Muscle fibre types in the myotome of stickleback, Gasterosteus aculeatus L.; a histochemical, immunohistochemical and ultrastructural study. *Journal of Fish Biology*, *22*(3), 303–316. https://doi.org/10.1111/j.1095-8649.1983.tb04754.x

Kültz, D. (2015). Physiological mechanisms used by fish to cope with salinity stress. *Journal of Experimental Biology*, *218*(12), 1907–1914. https://doi.org/10.1242/jeb.118695

Lermen, C. L., Lappe, R., Crestani, M., Vieira, V. P., Gioda, C. R., Schetinger, M. R. C., Baldisserotto, B., Moraes, G., & Morsch, V. M. (2004). Effect of different temperature regimes on metabolic and blood parameters of silver catfish Rhamdia quelen. *Aquaculture*, *239*(1), 497–507. https://doi.org/10.1016/j.aquaculture.2004.06.021

Li, H.-T., Feng, L., Jiang, W.-D., Liu, Y., Jiang, J., Li, S.-H., & Zhou, X.-Q. (2013). Oxidative stress parameters and anti-apoptotic response to hydroxyl radicals in fish erythrocytes: Protective effects of glutamine, alanine, citrulline and proline. *Aquatic Toxicology*, *126*, 169–179. https://doi.org/10.1016/j.aquatox.2012.11.005

Li, X., Zheng, S., & Wu, G. (2020). Nutrition and metabolism of glutamate and glutamine in fish. *Amino Acids*, *52*(5), 671–691. https://doi.org/10.1007/s00726-020-02851-2

Lin, H., Romsos, D. R., Tack, P. I., & Leveille, G. A. (1978). Determination of glucose utilization in coho salmon [Oncorhynchus kisutch (Walbaum)] with (6-3H)- and (U-14C)-glucose. *Comparative Biochemistry and Physiology*, *59A*(2), 189–193.

Liu, J., Mai, K., Xu, W., Zhang, Y., Zhou, H., & Ai, Q. (2015). Effects of dietary glutamine on survival, growth performance, activities of digestive enzyme, antioxidant status and hypoxia stress resistance of half-smooth tongue sole (Cynoglossus semilaevis Günther) post larvae. *Aquaculture*, *446*, 48–56. https://doi.org/10.1016/j.aquaculture.2015.04.012

Lutterschmidt, W. I., & Hutchison, V. H. (1997). The critical thermal maximum: History and critique. *Canadian Journal of Zoology*, *75*(10), 1561–1574. https://doi.org/10.1139/z97-783

Metzger, D. C. H., Healy, T. M., & Schulte, P. M. (2016). Conserved effects of salinity acclimation on thermal tolerance and hsp70 expression in divergent populations of threespine stickleback (Gasterosteus aculeatus). *Journal of Comparative Physiology B, 186*(7), 879–889. https://doi.org/10.1007/s00360-016-0998-9

Milligan, C. L., & Girard, S. S. (1993). Lactate Metabolism in Rainbow Trout. *Journal of Experimental Biology*, *180*(1), 175–193. https://doi.org/10.1242/jeb.180.1.175

Mommsen, Thomas P. (1984). Biochemical characterization of the rainbow trout gill. *Journal of Comparative Physiology B*, *154*(2), 191–198. https://doi.org/10.1007/BF00684145

Moon, T. W. (1988). Adaptation, constraint, and the function of the gluconeogenic pathway. *Canadian Journal of Zoology*, *66*(5), 1059–1068. https://doi.org/10.1139/z88-156

Moon, T. W. (2001). Glucose intolerance in teleost fish: Fact or fiction? *Comparative Biochemistry and Physiology Part B: Biochemistry and Molecular Biology*, *129*(2), 243–249. https://doi.org/10.1016/S1096-4959(01)00316-5

Moon, T. W., & Foster, G. D. (1995). Chapter 4 Tissue carbohydrate metabolism, gluconeogenesis and hormonal and environmental influences. In *Biochemistry and Molecular Biology of Fishes* (Vol. 4, pp. 65–100). Elsevier. https://doi.org/10.1016/S1873-0140(06)80007-X

Morata, P., Vargas, A. M., Sánchez-medina, F., Garcia, M., Cardenete, G., & Zamora, S. (1982). Evolution of gluconeogenic enzyme activities during starvation in liver and kidney of the rainbow trout (Salmo gairdneri). *Comparative Biochemistry and Physiology Part B: Comparative Biochemistry*, *71*(1), 65–70. https://doi.org/10.1016/0305-0491(82)90176-6

Morris, D., Tinbergen, N., & Hoogland, R. (1956). The Spines of Sticklebacks (Gasterosteus and Pygosteus) as Means of Defence Against Predators (Perca and Esox). *Behaviour*, *10*(1), 205–236. https://doi.org/10.1163/156853956X00156

Moyle, P. B., & Cech Jr., J. (2004). *Fishes: An introduction to ichtyology* (5th ed.). Prentice Hall.

Navarro, I., & Gutiérrez, J. (1995). Chapter 17 Fasting and starvation. In *Biochemistry and Molecular Biology of Fishes* (Vol. 4, pp. 393–434). Elsevier. https://doi.org/10.1016/S1873-0140(06)80020-2

Newsholme, P., Procopio, J., Lima, M. M. R., Pithon-Curi, T. C., & Curi, R. (2003). Glutamine and glutamate—Their central role in cell metabolism and function. *Cell Biochemistry and Function*, *21*(1), 1–9. https://doi.org/10.1002/cbf.1003

Palmer, T. N., & Ryman, B. E. (1972). Studies on oral glucose intolerance in fish. *Journal of Fish Biology*, *4*(2), 311–319. https://doi.org/10.1111/j.1095-8649.1972.tb05680.x

Pathi, B., Kinsey, S. T., Howdeshell, M. E., Priester, C., McNeill, R. S., & Locke, B. R. (2012). The formation and functional consequences of heterogeneous mitochondrial distributions

in skeletal muscle. *The Journal of Experimental Biology*, *215*(11), 1871–1883. https://doi.org/10.1242/jeb.067207

Peichel, C. L., & Marques, D. A. (2017). The genetic and molecular architecture of phenotypic diversity in sticklebacks. *Philosophical Transactions of the Royal Society B: Biological Sciences*, *372*(1713), 20150486. https://doi.org/10.1098/rstb.2015.0486

Pettersen, A. K., Marshall, D. J., & White, C. R. (2018). Understanding variation in metabolic rate. *Journal of Experimental Biology*, *221*(1), jeb166876. https://doi.org/10.1242/jeb.166876

Piiper, J. (1982). Respiratory gas exchange at lungs, gills and tissues: Mechanisms and adjustments. *The Journal of Experimental Biology*, *100*, 5–22.

Polakof, S., Panserat, S., Soengas, J. L., & Moon, T. W. (2012). Glucose metabolism in fish: A review. *Journal of Comparative Physiology B, 182*(8), 1015–1045. https://doi.org/10.1007/s00360-012-0658-7

Pottinger, T. G., Carrick, T. R., & Yeomans, W. E. (2002). The three-spined stickleback as an environmental sentinel: Effects of stressors on whole-body physiological indices. *Journal of Fish Biology*, *61*(1), 207–229. https://doi.org/10.1111/j.1095-8649.2002.tb01747.x

R Core Team. (2019). *R: A language and environment for statistical computing.* R Foundation for Statistical Computing. https://www.R-project.org/

Schulte, P. M. (2014). What is environmental stress? Insights from fish living in a variable environment. *The Journal of Experimental Biology*, *217*(Pt 1), 23–34. https://doi.org/10.1242/jeb.089722

Shao, Y., Li, C., Chen, X., Zhang, P., Li, Y., Li, T., & Jiang, J. (2015). Metabolomic responses of sea cucumber Apostichopus japonicus to thermal stresses. *Aquaculture*, *435*, 390–397. https://doi.org/10.1016/j.aquaculture.2014.10.023

Sokołowska, E., & Kulczykowska, E. (2009). Environmental influence on maturation and dominance relationships in the three-spined stickleback (Gasterosteus aculeatus L.): Temperature competes with photoperiod for primacy. *Oceanological and Hydrobiological Studies*, *38*(4), 31–48. https://doi.org/10.2478/v10009-009-0042-4

Sylvester, J. R. (1972). Possible effects of thermal effluents on fish: A review. *Environmental Pollution (1970)*, *3*(3), 205–215. https://doi.org/10.1016/0013-9327(72)90004-3

Turner, J. D., Wood, C. M., & Clark, D. (1983). Lactate and Proton Dynamics in the Rainbow Trout (Salmo Gairdneri). *Journal of Experimental Biology*, *104*(1), 247–268.

Vergauwen, L., Benoot, D., Blust, R., & Knapen, D. (2010). Long-term warm or cold acclimation elicits a specific transcriptional response and affects energy metabolism in zebrafish. *Comparative Biochemistry and Physiology Part A: Molecular & Integrative Physiology*, *157*(2), 149–157. https://doi.org/10.1016/j.cbpa.2010.06.160

Vézina, D., & Guderley, H. (1991). Anatomic and enzymatic responses of the three-spined stickleback, Gasterosteus aculeatus to thermal acclimation and acclimatization. *Journal of Experimental Zoology*, *258*(3), 277–287. https://doi.org/10.1002/jez.1402580302

Vijayan, M. M., & Moon, T. W. (1994). The stress response and the plasma disappearance of corticosteroid and glucose in a marine teleost, the sea raven. *Canadian Journal of Zoology*, *72*(3), 379–386. https://doi.org/10.1139/z94-054

Vijayan, Mathilakath M., Pereira, C., Grau, E. G., & Iwama, G. K. (1997). Metabolic Responses Associated with Confinement Stress in Tilapia: The Role of Cortisol. *Comparative*

*Biochemistry and Physiology Part C: Pharmacology, Toxicology and Endocrinology*, *116*(1), 89–95. https://doi.org/10.1016/S0742-8413(96)00124-7

Wasserman, D. H., Kang, L., Ayala, J. E., Fueger, P. T., & Lee-Young, R. S. (2011). The physiological regulation of glucose flux into muscle in vivo. *The Journal of Experimental Biology*, *214*(2), 254–262. https://doi.org/10.1242/jeb.048041

Weber, J.-M., & Zwingelstein, G. (1995). Chapter 2 Circulatory substrate fluxes and their regulation. In T.P. Mommsen & P. Hochachka (Eds.), *Biochemistry and Molecular Biology of Fishes* (Vol. 4, pp. 15–32). Elsevier. https://doi.org/10.1016/S1873-0140(06)80005-6

Webster, M. M., Atton, N., Hart, P. J. B., & Ward, A. J. W. (2011). Habitat-Specific Morphological Variation among Threespine Sticklebacks (Gasterosteus aculeatus) within a Drainage Basin. *PLoS ONE*, *6*(6), e21060. https://doi.org/10.1371/journal.pone.0021060

Wickham, H. (2016). *ggplot2: Elegant Graphics for Data Analysis*. Springer-Verlag New York. https://ggplot2.tidyverse.org

Wicks, B. J., & Randall, D. J. (2002). The effect of sub-lethal ammonia exposure on fed and unfed rainbow trout: The role of glutamine in regulation of ammonia. *Comparative Biochemistry and Physiology Part A: Molecular & Integrative Physiology*, *132*(2), 275–285. https://doi.org/10.1016/S1095-6433(02)00034-X

Wilson, R. P., & Poe, W. E. (1974). Nitrogen metabolism in channel catfish, Ictalurus punctatus—III. Relative pool sizes of free amino acids and related compounds in various tissues of the catfish. *Comparative Biochemistry and Physiology Part B: Comparative Biochemistry*, *48*(4), 545–556. https://doi.org/10.1016/0305-0491(74)90134-5

Wootton, R. J. (1984). *A Functional Biology of Sticklebacks*. Croom Helm.

https://www.springer.com/gp/book/9781461585152

## TABLES AND FIGURES

**Table 1.1.** Mean, standard error (SE), and number of biological replicates (N) by population and temperature for all morphometric measurements, weights, and indices. Statistical results are also shown for two-way ANOVAs (df = degrees of freedom, MS = mean square, F-value, p-value), Welch one-way test (F-value, p-value), and Kruskal-Wallis tests ($\chi 2$ = chi-squared, p-value). Tests were run using two-way ANOVA unless otherwise demarcated in the footnotes. Values with different superscript letters within the temperature comparison rows (7ºC, 15ºC, 25ºC) are significantly different from the adjacent temperature values within that column.

| Population | | Standard Length (cm)* | Total Length (cm)* | [l]Body depth (cm)* | Caudal Peduncle depth (cm) | Caudal fin length (cm) | Snout length (cm)* | Head length (cm)* | [t]Orbit diameter (cm)* | Longest pelvic spine (cm)* | Anterior dorsal spine (cm) | 2nd dorsal spine (cm)* | [t]Plates - Left side* | [t]Plates - Right side* | [t]Gonad weight (mg) - females | Gonad weight (mg) - males* | [t]Liver weight (mg)* | Wet weight (g) | Hepatosomatic Index (HSI)* | [t]Gonada-somatic Index (GSI) - females | Gonadas-omatic Index (GSI) - males | Condition Factor (K)* |
|---|---|---|---|---|---|---|---|---|---|---|---|---|---|---|---|---|---|---|---|---|---|---|
| **Klamath** | **Mean** | 4.335 | 4.987 | 0.921 | 0.162 | 0.605 | 0.337 | 1.215 | 0.383 | 0.528 | 0.305 | 0.400 | 21.6 | 21.5 | 23.90526 | 4.4 | 17.6 | 0.808 | 2.16 | 3.049 | 0.560 | 0.64 |
| | **SE** | 0.070 | 0.079 | 0.015 | 0.004 | 0.012 | 0.011 | 0.022 | 0.005 | 0.013 | 0.012 | 0.012 | 1.8 | 1.8 | 2.833059 | 0.579184 | 1.2 | 0.04 | 0.09 | 0.432 | 0.086 | 0.01 |
| | **N** | 30 | 30 | 30 | 30 | 30 | 30 | 30 | 30 | 30 | 29 | 30 | 30 | 30 | 19 | 11 | 30 | 30 | 30 | 19 | 11 | 30 |
| **Big Lagoon** | **Mean** | 4.072 | 4.730 | 0.877 | 0.154 | 0.615 | 0.296 | 1.122 | 0.335 | 0.470 | 0.281 | 0.365 | 6.8 | 6.6 | 26.985 | 4.8 | 19.2 | 0.714 | 2.61 | 3.747 | 0.600 | 0.67 |
| | **SE** | 0.067 | 0.074 | 0.015 | 0.004 | 0.010 | 0.011 | 0.020 | 0.004 | 0.014 | 0.014 | 0.009 | 0.2 | 0.3 | 5.23216 | 0.702191 | 1.8 | 0.03 | 0.14 | 0.617 | 0.073 | 0.02 |
| | **N** | 30 | 30 | 30 | 30 | 30 | 30 | 30 | 30 | 29 | 28 | 30 | 30 | 30 | 20 | 10 | 30 | 30 | 30 | 20 | 10 | 30 |
| **Temperature** | | | | | | | | | | | | | | | | | | | | | | |
| **7 °C** | **Mean** | 4.221 | 4.891 | 0.922 | 0.162 | 0.619 | 0.327 | 1.175 | 0.350 | 0.500 | 0.306 | 0.396 | 13.6 | 13.4 | 31.07273 | 5.8[a] | 21.0[a] | 0.83 | 2.53[ab] | 3.690 | 0.730 | 0.70[a] |
| | **SE** | 0.088 | 0.099 | 0.018 | 0.005 | 0.013 | 0.013 | 0.030 | 0.007 | 0.018 | 0.013 | 0.015 | 2.2 | 2.2 | 5.298595 | 0.560285 | 1.5 | 0.04 | 0.12 | 0.645 | 0.088 | 0.01 |
| | **N** | 20 | 20 | 20 | 20 | 20 | 20 | 20 | 20 | 20 | 19 | 20 | 20 | 20 | 11 | 9 | 20 | 20 | 20 | 11 | 9 | 20 |
| **15 °C** | **Mean** | 4.120 | 4.768 | 0.899 | 0.161 | 0.600 | 0.303 | 1.158 | 0.369 | 0.482 | 0.274 | 0.366 | 17.0 | 17.0 | 23.16429 | 4.3[ab] | 19.9[ab] | 0.76 | 2.56[a] | 3.061 | 0.480 | 0.69[a] |
| | **SE** | 0.096 | 0.108 | 0.023 | 0.005 | 0.016 | 0.018 | 0.032 | 0.008 | 0.020 | 0.015 | 0.013 | 2.5 | 2.5 | 6.174173 | 0.835364 | 2.3 | 0.05 | 0.18 | 0.735 | 0.055 | 0.02 |
| | **N** | 20 | 20 | 20 | 20 | 20 | 20 | 20 | 20 | 19 | 19 | 20 | 20 | 20 | 14 | 6 | 20 | 20 | 20 | 14 | 6 | 20 |
| **25 °C** | **Mean** | 4.269 | 4.916 | 0.877 | 0.150 | 0.610 | 0.320 | 1.172 | 0.359 | 0.516 | 0.300 | 0.385 | 12.1 | 11.9 | 23.41429 | 2.7[b] | 14.4[b] | 0.69 | 2.07[b] | 3.530 | 0.420 | 0.57[b] |
| | **SE** | 0.079 | 0.086 | 0.014 | 0.004 | 0.012 | 0.010 | 0.022 | 0.008 | 0.017 | 0.018 | 0.013 | 2.1 | 2.1 | 3.876541 | 0.474342 | 1.2 | 0.04 | 0.13 | 0.602 | 0.094 | 0.01 |
| | **N** | 20 | 20 | 20 | 20 | 20 | 20 | 20 | 20 | 20 | 19 | 20 | 20 | 20 | 14 | 6 | 20 | 20 | 20 | 14 | 6 | 20 |
| **Population** | **df** | 1 | 1 | 1 | 1 | 1 | 1 | 1 | 1 | 1 | 1 | 1 | 1 | 1 | 1 | 1 | 1 | 1 | 1 | 1 | 1 | 1 |
| | **MS** | 1.034 | 0.996 | | 0.001 | 0.001 | 0.025 | 0.129 | | 0.049 | 0.008 | 0.019 | | | | 0.841 | | 0.133 | 3.077 | | 0.008 | 0.008 |
| | **F-value** | 7.406 | 5.594 | 4.239 | 2.221 | 0.410 | 6.895 | 9.387 | | 8.859 | 1.796 | 5.320 | | | | 0.349 | | 3.630 | 8.155 | | 0.134 | 1.609 |
| | **$\chi^2$** | | | | | | | | 28.027 | | | | 26.302 | 30.700 | 0.178 | | 0.060 | | | 0.664 | | |
| | **p-value** | 0.009* | 0.022* | 0.044* | 0.142 | 0.525 | 0.011* | 0.003* | 1.2E-07* | 0.004* | 0.186 | 0.025* | 2.92E-07* | 3.01E-08* | 0.673 | 0.564 | 0.807 | 0.062 | 0.006* | 0.415 | 0.720 | 0.210 |
| **Temperature** | **df** | 2 | 2 | 2 | 2 | 2 | 2 | 2 | 2 | 2 | 2 | 2 | 2 | 2 | 2 | 2 | 2 | 2 | 2 | 2 | 2 | 2 |
| | **MS** | 0.115 | 0.124 | | 0.001 | 0.002 | 0.003 | 0.002 | | 0.006 | 0.005 | 0.004 | | | | 15.248 | | 0.102 | 1.497 | | 0.191 | 0.104 |
| | **F-value** | 0.825 | 0.699 | 1.924 | 2.303 | 0.526 | 0.898 | 0.117 | | 1.085 | 1.071 | 1.277 | | | | 6.327 | | 2.782 | 3.966 | | 3.254 | 21.080 |
| | **$\chi^2$** | | | | | | | | 2.746 | | | | 0.776 | 1.220 | 2.525 | | 8.916 | | | 2.221 | | |
| | **p-value** | 0.444 | 0.502 | 0.161 | 0.110 | 0.594 | 0.414 | 0.890 | 0.253 | 0.345 | 0.350 | 0.287 | 0.678 | 0.543 | 0.283 | 0.011* | 0.012* | 0.071 | 0.025* | 0.329 | 0.069 | 1.71E-07* |
| **Population: Temperature** | **df** | 2 | 2 | | 2 | 2 | 2 | 2 | | 2 | 2 | 2 | | | | 2 | | 2 | 2 | | 2 | 2 |
| | **MS** | 0.128 | 0.181 | | 0.000 | 0.008 | 0.004 | 0.018 | | 0.005 | 0.004 | 0.002 | | | | 7.296 | | 0.043 | 0.150 | | 0.014 | 0.002 |
| | **F-value** | 0.914 | 1.015 | | 0.606 | 2.391 | 1.051 | 1.328 | | 0.822 | 0.867 | 0.710 | | | | 3.028 | | 1.179 | 0.398 | | 0.235 | 0.455 |
| | **p-value** | 0.407 | 0.369 | | 0.549 | 0.101 | 0.357 | 0.274 | | 0.445 | 0.427 | 0.496 | | | | 0.081 | | 0.316 | 0.673 | | 0.794 | 0.637 |
| **Residuals** | **df** | 54 | 54 | | 54 | 54 | 54 | 54 | | 53 | 51 | 54 | | | | 14 | | 54 | 54 | | 14 | 54 |
| | **MS** | 0.140 | 0.178 | | 0.000 | 0.003 | 0.004 | 0.014 | | 0.006 | 0.004 | 0.004 | | | | 2.410 | | 0.037 | 0.377 | | 0.059 | 0.005 |

* = signficant difference ($p < 0.05$); [l] = Welch one-way test; [t] = Kruskal-Wallis statistics

**Table 1.2.** Mean, standard error (SE), and number of biological replicates (N) by population and temperature for glutamine, glutamate, glutamine/glutamate ratio, glucose, and lactate in white muscle and gill. Statistical results are also shown for two-way ANOVAs (df = degrees of freedom, MS = mean square, F-value, p-value) and Kruskal-Wallis tests ($\chi^2$ = chi-squared, p-value). Values with different superscript letters within the temperature comparison rows (7ºC, 15ºC, 25ºC) are significantly different from the adjacent temperature values within that column.

| | | White Muscle | | | | | Gill | | | | |
|---|---|---|---|---|---|---|---|---|---|---|---|
| **Population** | | **glutamine (mM/µg total protein)*** | **glutamate (mM/µg total protein)*** | **glutamine/ glutamate ratio*** | **glucose (mM/µg total protein)*** | **lactate (mM/µg total protein)*** | **glutamine (mM/µg total protein)*** | **glutamate (mM/µg total protein)** | **glutamine/ glutamate ratio*** | **glucose* (mM/µg total protein)** | **lactate (mM/µg total protein)** |
| **Klamath** | **Mean** | 1.005 | 0.763 | 1.317 | 0.995 | 6.562 | 1.132 | 2.058 | 0.550 | 0.404 | 1.385 |
| | **SE** | 0.022 | 0.012 | 0.158 | 0.017 | 0.107 | 0.201 | 0.277 | 0.056 | 0.105 | 0.016 |
| | **N** | 30 | 30 | 30 | 30 | 30 | 29 | 29 | 29 | 30 | 2 |
| **Big Lagoon** | **Mean** | 0.903 | 0.596 | 1.516 | 0.973 | 8.017 | 1.178 | 2.145 | 0.549 | 0.827 | 1.688 |
| | **SE** | 0.018 | 0.012 | 0.203 | 0.016 | 0.124 | 0.278 | 0.295 | 0.052 | 0.137 | 0.558 |
| | **N** | 30 | 30 | 30 | 30 | 30 | 30 | 30 | 30 | 30 | 16 |
| **Temperature** | | | | | | | | | | | |
| **7 °C** | **Mean** | $0.561^{a}$ | $0.875^{a}$ | $0.641^{a}$ | $1.057^{ab}$ | $6.783^{ab}$ | $0.487^{a}$ | 1.886 | $0.258^{a}$ | 0.558 | 2.707 |
| | **SE** | 0.018 | 0.017 | 0.069 | 0.028 | 0.124 | 0.052 | 0.298 | 0.031 | 0.143 | 1.326 |
| | **N** | 20 | 20 | 20 | 20 | 20 | 19 | 19 | 19 | 20 | 6 |
| **15 °C** | **Mean** | $1.223^{b}$ | $0.680^{ab}$ | $1.799^{b}$ | $1.138^{a}$ | $9.163^{a}$ | $0.971^{b}$ | 1.783 | $0.545^{b}$ | 0.499 | 1.308 |
| | **SE** | 0.032 | 0.017 | 0.133 | 0.024 | 0.204 | 0.189 | 0.322 | 0.062 | 0.169 | 0.433 |
| | **N** | 20 | 20 | 20 | 20 | 20 | 20 | 20 | 20 | 20 | 7 |
| **25 °C** | **Mean** | $1.078^{b}$ | $0.484^{b}$ | $2.228^{c}$ | $0.757^{b}$ | $5.922^{b}$ | $1.974^{c}$ | 2.626 | $0.752^{b}$ | 0.790 | 0.878 |
| | **SE** | 0.030 | 0.016 | 0.194 | 0.018 | 0.156 | 0.406 | 0.398 | 0.057 | 0.153 | 0.429 |
| | **N** | 20 | 20 | 20 | 20 | 20 | 20 | 20 | 20 | 20 | 5 |
| **Population** | **df** | 1 | 1 | 1 | 1 | 1 | 1 | 1 | 1 | 1 | 1 |
| | **MS** | | 0.420 | | 0.007 | 31.760 | | | | | |
| | **F-value** | | 3.877 | | 0.029 | 2.969 | | | | | |
| | $\chi^2$ | 0.197 | | 1.617 | | | 0.406 | 0.074 | 0.386 | 11.765 | 0.493 |
| | **p-value** | 0.657 | 0.054 | 0.204 | 0.866 | 0.091 | 0.524 | 0.785 | 0.534 | 0.001* | 0.482 |
| **Temperature** | **df** | 2 | 2 | 2 | 2 | 2 | 2 | 2 | 2 | 2 | 2 |
| | **MS** | | 0.764 | | 0.806 | 56.390 | | | | | |
| | **F-value** | | 7.056 | | 3.385 | 5.271 | | | | | |
| | $\chi^2$ | 14.847 | | 39.075 | | | 17.533 | 2.903 | 28.954 | 3.206 | 1.777 |
| | **p-value** | 5.97E-04* | 0.002* | 3.27E-09* | 0.041* | 0.008* | 1.56E-04* | 0.234 | 5.16E-07* | 0.201 | 0.411 |
| **Population: Temperature** | **df** | | 2 | | 2 | 2 | | | | | |
| | **MS** | | 0.026 | | 0.031 | 4.370 | | | | | |
| | **F-value** | | 0.244 | | 0.129 | 0.409 | | | | | |
| | **p-value** | | 0.785 | | 0.879 | 0.666 | | | | | |
| **Residuals** | **df** | | 54 | | 54 | 54 | | | | | |
| | **MS** | | 0.108 | | 0.238 | 10.700 | | | | | |

* = signficant difference (p <0.05)

**Figure 1.1.** Length measurements were taken as depicted: total length: from point 1 to point 11, standard length: 2 to 10, snout length: 2 to 3, head length: 2 to 5, length of orbit: 3 to 4, body depth: 6 to 7, depth of caudal peduncle: 8 to 9, length of caudal fin: 10 to 11. Spines, including longest pelvic spine, anterior dorsal spine and 2nd dorsal spine were measured as depicted from 12 to 13, in a straight line from where the spine meets the body to the tip of the spine.

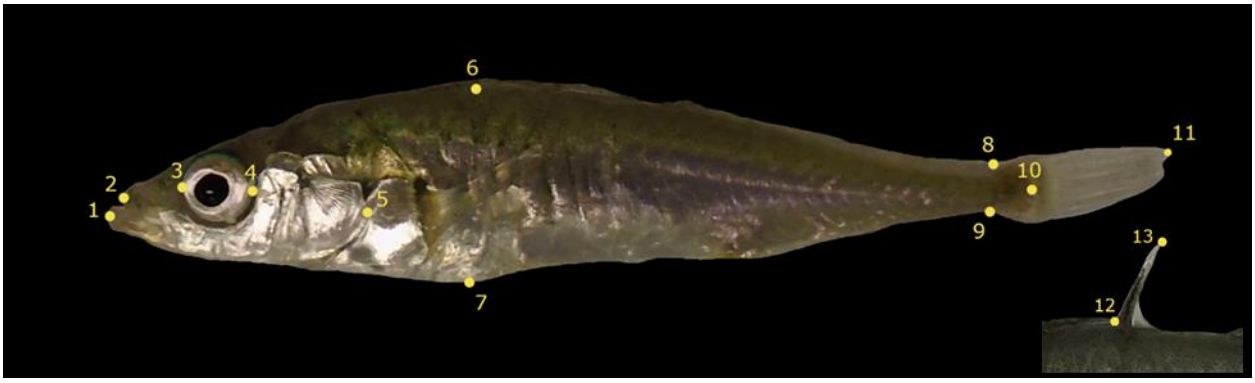

**Figure 1.2.** Plot of both CTMax and CLMax for both Big lagoon (BL) and Klamath river (KL) populations with standard error bars.

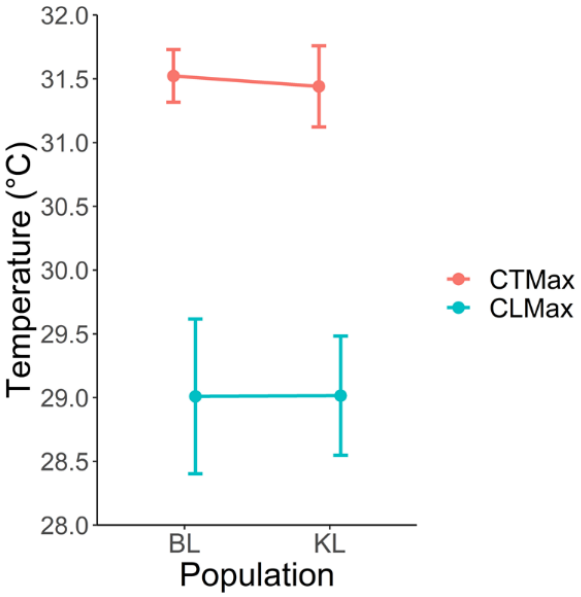

**Figure 1.3.** Significantly different lengths between Big lagoon (BL) and Klamath river (KL) populations with standard error bars. p-values are annotated with asterisks above the measurements as follows: * < 0.05, ** < 0.01, *** < 0.001, ***** < 0.0001. All lengths are depicted in cm on the y-axis and measurements are listed along the x-axis. KL had significantly longer snout length, head length, orbit diameter, 2nd dorsal spine length, longest pelvic spine, standard length, and total length than the BL population.

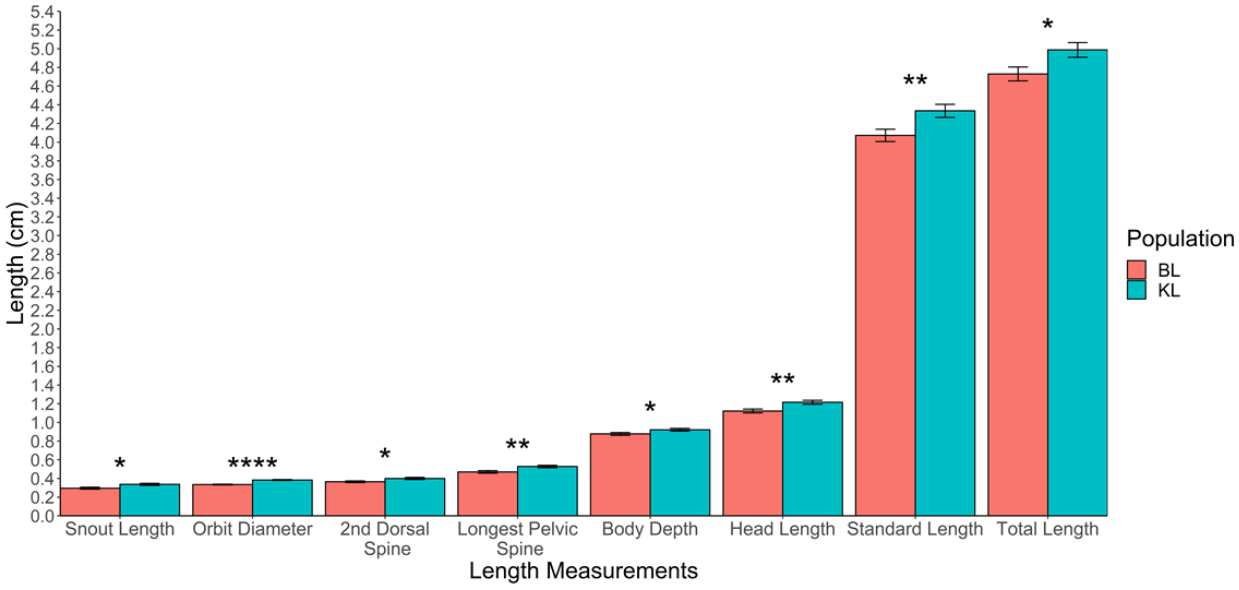

**Figure 1.4.** a) Liver weight, b) hepatosomatic index (HSI), c) condition factor (K), and d) gonad weight for males are graphed by population (BL and KL) and temperature (7°C, 15°C, 25°C) with standard error bars.

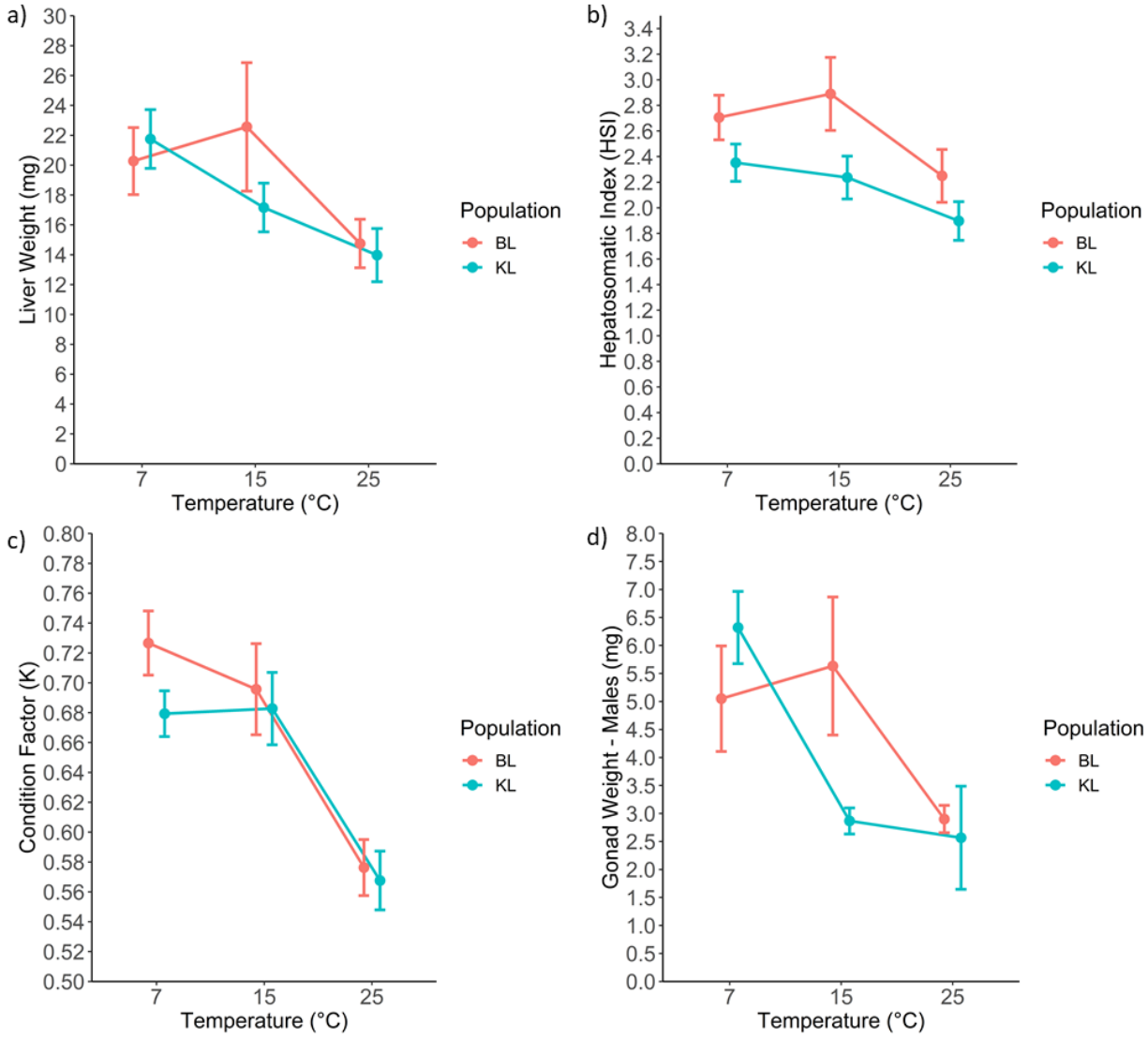

**Figure 1.5.** White muscle tissue concentrations (mM/µg total protein) of a) glutamine, c) glutamate and e) glutamine/glutamate ratio are graphed by population (BL and KL) and temperature (7°C, 15°C, 25°C) with standard error bars. Gill tissue concentrations of b) glutamine, d) glutamate and f) glutamine/glutamate ratio are graphed by population (BL and KL) and temperature (7°C, 15°C, 25°C) with standard error bars.

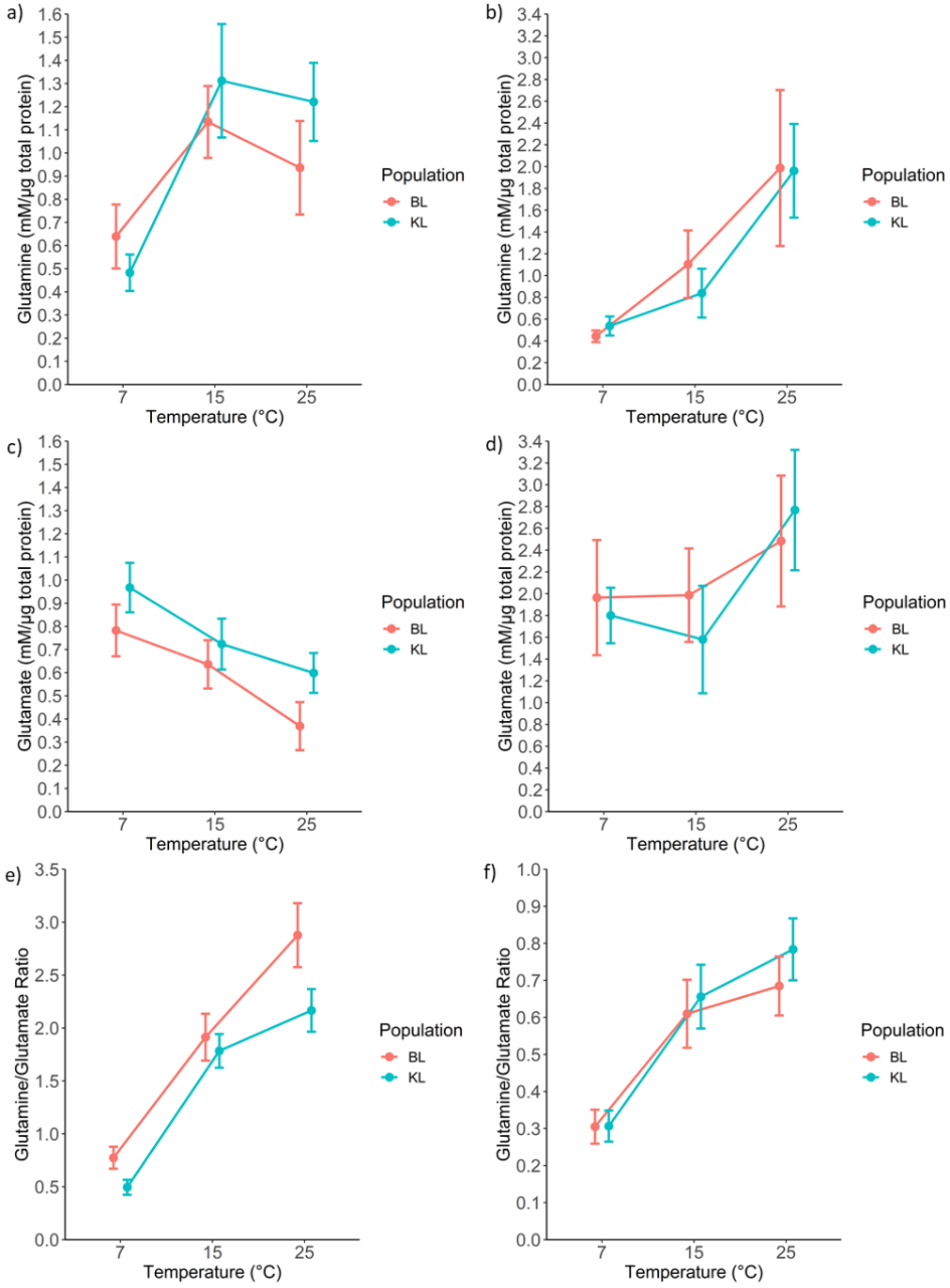

**Figure 1.6.** White muscle tissue concentrations (mM/µg total protein) of a) glucose and c) lactate are graphed by population (BL and KL) and temperature (7°C, 15°C, 25°C) with standard error bars. b) Gill tissue concentrations of glucose are graphed by population (BL and KL) and temperature (7°C, 15°C, 25°C) with standard error bars. d) Gill tissue lactate concentration with both populations combined (as only two out of thirty gill samples for KL had a measurable amount of lactate) by temperature (7°C, 15°C, 25°C) with standard error bars.

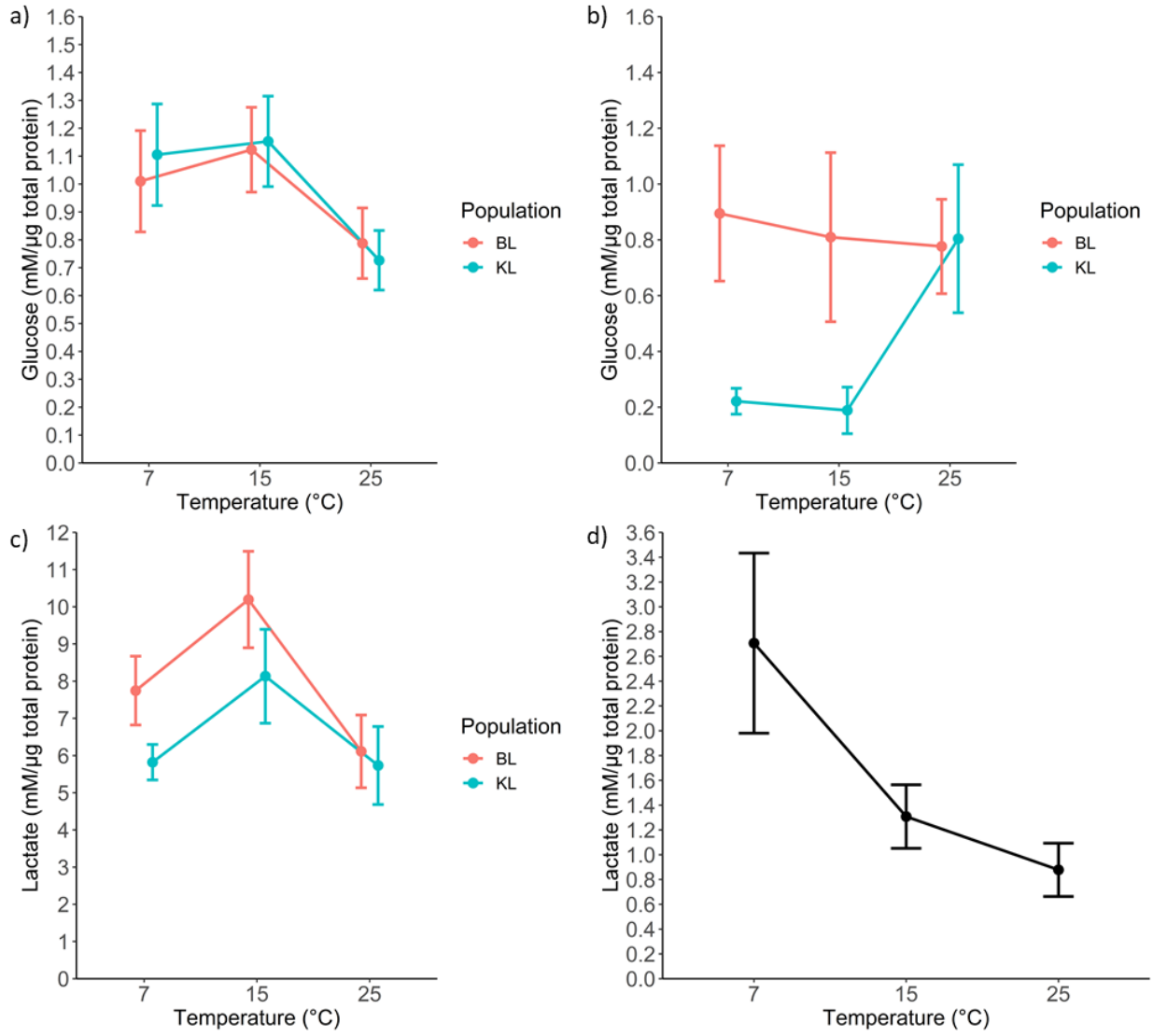

## CHAPTER 2

## Assessment of chronic temperature stress on the liver proteome of two threespine stickleback (*Gasterosteus aculeatus*) populations using a novel DIA assay library


## ABSTRACT

A data-independent acquisition (DIA) assay library was generated for the liver of threespine sticklebacks to evaluate alterations in protein abundance and functional enrichment of molecular pathways following either a chronic warm (25°C) or cold (7°C) three-week temperature challenge in two estuarine populations. The DIA assay library was created from a data-dependent acquisition (DDA) based raw spectral library that was filtered to remove low quality or ambiguous peptides. Functional enrichment analyses using STRING aided in identifying larger networks and domains that were significantly enriched in the different groups by examining both the entire liver proteome and only significantly elevated or depleted proteins from the various comparisons. These systems level analyses reveal the unique liver proteomic signatures of two populations of threespine sticklebacks acclimated to chronic temperature stress. The Big lagoon population (BL) had a stronger response to both temperature stresses than the Klamath river population (KL). At 7°C, BL showed alterations in protein homeostasis that likely fueled a higher demand for energy, but both populations successfully acclimated to this temperature. The warm acclimation induced major increases in proteins involved in chromatin structure, including a variety of histones, and transcription, while there were decreases in proteins related to translation and fatty acid metabolism. Functional enrichment analyses of the entire liver proteome uncovered differences in glycolysis and carbohydrate metabolism between the two populations and between the cold acclimated and control groups. We conclude that the

synchronous regulatory patterns of many proteins observed in the liver of threespine sticklebacks provide much more comprehensive insight into population-specific responses to thermal stress than the use of less specific pre-determined biomarkers.

## INTRODUCTION

Temperature is one of the most important abiotic factors that profoundly affects molecular, cellular, and organismal processes including directly fitness-related traits such as reproduction, development, and survival (Loarie et al., 2009; Menge & Olson, 1990; Seebacher, 2005; Zinn et al., 2010). Fish, along with reptiles, amphibians, and invertebrates, are mostly ectothermic, thus temperature exerts more control than any other abiotic factor on internal processes (Beitinger & Fitzpatrick, 1979). It is projected that global temperatures will continue to rise throughout the 21$^{st}$ century along with the duration, intensity, and spatial extent of heat waves (IPCC, 2014). Temperature (thermal stress) is likely to be a driver of natural selection (Seebacher, 2005) and different species, or different populations within a species, are adapted to their unique environmental conditions such that proteins function best at temperatures that match their habitats (Crawford et al., 1999). Coastal ecosystem biodiversity and ecosystem functioning and services have already been impacted by intensified heatwaves, acidification, sea level rise and changes in oxygen and salinity levels (IPCC, 2019). In marine and estuary environments, increases in air and water temperatures change biogeographic patterns (Nicolas et al., 2011; Somero, 2011), and populations from different parts of a species' biogeographic range handle these temperature changes differently (Genner et al., 2004). Because external temperatures dictate internal temperatures for ectotherms, behavioral modifications are used to a large extent to control their body temperatures, but such means depend on an accessible temperature gradient.

Estuaries are especially susceptible to warming, with lagoons and rivers facing the highest levels or warming due to shallower depths and limited exchange with the ocean, which limits opportunities for behavioral modifications (Scanes et al., 2020). Since most fish do not actively regulate temperature via internal mechanisms, temperature is of vital importance for basic physiological functions, and certain habitats, such as estuaries, present greater challenges for escape or migration. One major question of significance given the predictions about climate change is how organisms living across different environmental conditions will respond to increased environmental challenge. Do different populations employ different mechanisms and pathways to regulate internal conditions?

Many species have been used as model organisms for examining thermal stress responses, however, the threespine stickleback (*Gasterosteus aculeatus*) represents an ideal candidate for numerous reasons. Threespine sticklebacks are widely distributed throughout the northern hemisphere, representing many phenotypically diverse populations along both a longitudinal (North America, Europe, Asia) and latitudinal (Mexico to Alaska) gradient (Bell & Foster, 1994). These euryhaline fish inhabit freshwater, brackish water, and coastal marine habitat, including habitats most susceptible to warming from climate change such as lagoons and rivers (Scanes et al., 2020). In addition, the genome sequence and a high-quality annotated reference proteome are available for this species. Furthermore, these fish are abundant, easy to capture, survive captivity well, and have relatively short life cycles.

Proteomics is a powerful tool for examining the effects of environmental conditions on organisms. Proteomics arose in the 1980s and was originally developed to allow for the study of the proteome, which represents all the proteins that are expressed by a genome (López, 2007; Wilkins et al., 1996). Data dependent acquisition (DDA) is a proteomics method for selecting the

highest abundance precursor ions in MS1 spectra to fragment for MS2 acquisition, thus producing tandem (MS/MS) mass spectra that are then matched to a database for identification (Doerr, 2015; Fernández-Costa et al., 2020). Because the most abundant precursor ions are chosen, this is a stochastic method and there can be differences in spectra matched from one run to another, even on the same sample (Pappireddi et al., 2019). To overcome this stochasticity, data independent acquisition (DIA) is a more recent method that fragments all precursor ions within a specified m/z window (Fernández-Costa et al., 2020). This method allows for precise and reproducible identification and quantification of peptides, including lower abundance precursor ions, and greatly increases the number of proteins that can be reproducibly quantified (Li et al., 2018). Protein abundance, synthesis, degradation, protein-protein interactions, location in subcellular compartments, and post-translational modifications such as phosphorylation, glycosylation, acetylation, and methylation can all be examined using proteomics (Biron et al., 2006; Karr, 2008; Tomanek, 2010). Since natural selection ultimately acts on phenotypes, proteins represent a more direct readout of what is being selected for than either the genome or the transcriptome (Diz et al., 2012). Additionally the correlation between the abundance of transcripts and the corresponding proteins is often highly nonlinear (Anderson & Seilhamer, 1997; Diz et al., 2012; Feder & Walser, 2005). Proteomics studies help elucidate which transcript changes are resulting in changes at the protein level. Furthermore, co-expression patterns of proteins can be used to identify which molecular pathways are up- or down-regulated under a given stressor (Tomanek, 2010). Proteomic analysis of chronic exposure from the laboratory or the field is still sparse (Tomanek, 2014), even though proteomic signatures to environmental stress exposures provide deep insight into the evolution of organisms to changing environments (Silvestre et al., 2012).

In this study, the liver proteomes of two populations of threespine sticklebacks were compared after exposure to either chronic warm or cold stress to understand the proteins and pathways utilized to overcome temperature stress. The liver provides a good representation of the general condition of a fish as it plays a vital role in critical physiological processes such as homeostasis and metabolism of lipids, glucose, and amino acids, detoxification, and immune system function (Liu et al., 2016; Trefts et al., 2017). Warm exposure increases metabolic rates, stimulates physiological and behavioral processes, and requires maintenance to counteract protein denaturation, DNA mutations, oxidative damage and cell death, all of which require more energy to sustain at the expense of growth, reproduction, and immunity (Alfonso et al., 2020). Cold exposure decreases metabolic rates, alters lipid homeostasis and metabolism, and increases protein degradation, while oxidative stress, altered protein homeostasis, and large metabolic changes are shared responses to temperature stress regardless of directionality (Qian & Xue, 2016; Tomanek, 2014). However, there are few proteomics experiments examining chronic acclimation to temperature challenge in fish (Silvestre et al., 2012; Tomanek, 2014). This study examined differences in the protein abundance and functional enrichments in the liver proteome of threespine stickleback populations from two estuarine habitats (lagoon and river) after a three-week chronic acclimation to either 7°C (cold) or 25°C (warm) to characterize population-specific proteomic signatures of chronic temperature stress.

## MATERIALS AND METHODS

### Temperature acclimation of fish

Experimental work was approved by and conducted according to UC Davis Institutional Animal Care and Use Committee (IACUC) rules and regulations (IACUC number 18010, AAALAC

number 127 A3433-01). Fish were collected from two populations in Northern California (Big Lagoon, BL and Klamath River, KL) as previously described (Chapter 1). Wild-caught BL and KL fish were bred by external fertilization to create F1 progeny and the chronic acclimation of F1 fish to 7°C, 15°C (control), and 25°C was performed for three weeks as detailed in Chapter 1 and illustrated in Figure 2.1.

**Sample preparation**

Protein extraction and trypsin digestion were performed as previously documented (Kültz et al., 2013) but with the following modifications detailed below. The liver tissues were crushed using a steel-handle Teflon pestle inside of a 2 mL low retention microcentrifuge tube (LR-MCF) that was dipped in liquid nitrogen. Proteins were reduced with a 150mM dithiothreitol (DDT) stock solution to achieve a final concentration of 10 mM and incubated at 37°C for 30 minutes. Proteins were alkylated with a 450 mM iodoacetamide (IAA) stock solution to a final concentration of 30 mM and incubated in the dark at room temperature for 30 minutes. Proteins were precipitated with an ice-cold solution of 10% trichloroacetic acid (TCA), 0.15% DTT, 90% acetone (5x volume), incubated at -30°C for 30 minutes to precipitate proteins and dissolve contaminants and then centrifuged for 5 minutes at 19,000 g at 4°C. The precipitated pellet was then washed once with an ice-cold solution of 0.15% (weight/volume) DDT in acetone and centrifuged for 5 minutes at 19,000 g at 4°C. The protein pellet was dissolved in a solution of UT buffer (7 m urea/2 M thiourea/0.2% DTT, 6x the volume of the original tissue weight), incubated at room temperature on a rotator for 30 minutes to maximize protein dissolving, centrifuged for 5 minutes at 19,000 g, and the supernatant was removed and transferred to a clean 0.5 mL LR-MCF tube. A 660 nm protein assay (Thermo-Pierce, cat. 22660) compatible with diluted UT

buffer was completed in duplicate for each sample. Based on the average protein concentration, 1M ammonium bicarbonate (Ambic) buffer (pH 8.5) and LCMS water were added to dilute samples to 150 ng/100 µL total protein concentration and 100 mM Ambic. Immobilized trypsin beads (Promega, cat. V9012) were added at a 1:30 ratio relative to the total protein and samples were incubated at 35°C for 16 hours on a rotator. The immobilized trypsin was pelleted via centrifugation at 19,000 g for five minutes at 4°C and the supernatant was carefully removed and transferred to a clean LR-MCF tube. Samples were dried by speed vacuum (Thermo-Savant, ISS-110) until just dry, resuspended in 0.1% formic acid (FA), transferred to maximum recovery glass vials (Waters, cat. 186000384C), and stored at 4°C prior to sample injection in the mass spectrometer.

Tryptic peptides (2 µl, 150 ng/µl) were trapped for 1 minute at 15 µL/min on a Symmetry trap column (Waters, cat. 186003514) and separated on a 1.7 µm particle size BEH C18 column (250mm x 75µm, Waters, cat. 186003545) after injection using a nanoAcquity sample manager (Waters, Milford, MA) via reversed-phase liquid chromatography with a nanoAcquity binary solvent manager (Waters). Peptide elution occurred over a linear acetonitrile gradient (3-35%) for 140 minutes directly into a UHR-qTOF mass spectrometer (Impact II, Bruker) using a pico-emitter tip (New Objective FS360–20-10-D-20, Woburn, MA). Samples were run in batches using Hystar 4.1 (Bruker). A 68 fmol BSA peptide mix was run a minimum of once per week to serve as a control monitor baseline instrument performance.

**Data-dependent acquisition (DDA)**

Peak lists were generated using DataAnalysis 4.4 (Bruker Daltonics) from DDA raw data and imported into PEAKS X (Bioinformatics Solutions Inc., Waterloo, Canada). Peptide spectrum

matches were identified using the following three database search engines: PEAKS X, Mascot (Matrix Science), and X!Tandem Alanine (The Global Proteome Machine Organization). Unambiguous assignment of peptides to unique proteins was made using the *G. aculeatus* proteome database downloaded from UniprotKB on July 14, 2019. The proteome database included 27,249 *G. aculeatus* proteins plus the same number of randomly scrambled decoys and 282 common contaminants (human keratins, porcine trypsin, etc.). Cleavage specificity for trypsin was C-terminus of either Lys or Arg except when followed by Pro, and up to two missed cleavages were the allowed. In the first search round, the following PTMs were allowed: Cys carbamido-methylation, Met oxidation, Protein N-terminal acetylation, and Pro oxidation. Second round PEAKS-PTM searches included all 313 variable PTMs contained in the PEAKS database, with a maximum of two PTMs per peptide allowed. Precursor mass tolerance limits were 20 ppm and fragment ion mass tolerance limits were 0.03 Da. All DDA data are available at ProteomeXchange (PXD024617).

**Construction of raw spectral library and DIA assay library**

Peptide-to-peptide spectrum matches and annotations from the DDA data were exported from PEAKS X in pepxml format and compiled into a raw liver spectral library for *G. aculeatus* in Skyline 20.0 (Pino et al., 2017). The target list of proteins went through multiple filtering steps as detailed in the first results section (see below). The final DIA assay library and all relevant metadata are available at Panorama Public (https://panoramaweb.org/bbl02.url).

**Data-independent acquisition (DIA)**

Samples were run a second time to acquire DIA data. Liquid chromatography conditions were identical to those used for DDA data acquisition, but only MS2 spectra were acquired. The mass range was 390-1015 m/z with a scan rate of 25 Hz in 2.5 second intervals and an isolation width of 10 m/z (1 m/z overlap).

**Statistical analysis and figure generation**

Heat maps were generated using Genesis 1.8.1 (Thallinger Lab, Graz University of Technology). Functional enrichment networks were analyzed and created in STRING 11.0. STRING settings were set as follows: Network edges were set to confidence (line thickness indicates strength of data support), all active interaction sources were included (text mining, experiments, databases, co-expression, neighborhood, gene fusion, and co-occurrence), the minimum required interaction score was medium confidence (0.400). Volcano, mass error, retention time, and q-value plots were generated in Skyline 20.1.0.76 (MacCoss Lab, University of Washington). Skyline 20.0 was used for quantitative analyses and visualization of DIA data, and slight variations in retention time across runs were corrected using 14 manually selected iRT standards (Pino et al., 2017). mProphet was used in Skyline to train models that optimized selection of correct peaks (Pino et al., 2017; Reiter et al., 2011). The mass accuracy was set at 20 ppm for transitions. For group comparisons, the normalization method employed was equalize medians, the confidence level was 95% at the protein level, the summary method was Tukey's median polish, and the q-value cutoff was 0.05.

**Functional enrichment analysis**

Functional enrichment analysis was conducted with STRING 11.0 (Szklarczyk et al., 2019). For the four overall comparisons (KL vs. BL, 15°C vs. 7°C, 15°C vs. 25°C, and 7°C vs. 25°C) the STRING "proteins with values/ranks" search function was used, with fold change serving as the rank used for the search. This list included the entire protein set with the corresponding fold changes based on the particular comparison for the liver tissue after both automated and manual curation of the assay library. For smaller comparisons (all others), the STRING "multiple proteins" search function was used for significantly up- or down-regulated groups of proteins from that comparison. For all comparisons functional enrichments were considered significant for FDR<0.01. Functional enrichments in STRING networks, Uniprot keywords, PFAM protein domains, INTERPRO protein domains and features, and SMART protein domains were populated from these comparisons.

## RESULTS

### Generation of the spectral library and DIA assay library

A raw MS2 spectral library was created from the DDA data from 22 samples from both KL and BL populations that were chosen to represent chronic (three weeks) warm (25°C) and cold (7°C) exposure, acute (two hour) warm (28°C) exposure at six and 24 hours post temperature stress and at both elevated (22°C) and control (15°C) recovery temperatures, and acute (2hr) cold stress (4°C) for just the KL population to represent a diverse and representative array of proteins present in stickleback livers after temperature challenge. The assay library includes representatives of both fully plated and low plated morphotypes, as well as representatives from two different types of estuarine habitat, river mouth and lagoon. The DDA search results of these samples were consolidated from three different search engines with PEAKS Studio and used for

the creation of the MSMS spectral library which initially contained 5,768 proteins, 87,898 peptides, 99,762 precursors and 448,077 transitions.

The spectral library was assembled and then subjected to various quality control measures which greatly reduced the number of transitions, peptides, precursors, and proteins included in the final assay library (Figure 2.2) and will be detailed below. The point of the filtering steps was to reduce low quality peptides and to reduce any ambiguous or redundant peptides that might conflate quantitative peptide analysis. DIA data for all 60 chronic temperature stress samples were inputted into the spectral library to create the final assay library for this experiment. The number of proteotypic peptides, or peptides unique to a particular protein, are shown in Figure 2.2e. There were 1714 proteins, 7209 peptides, 8212 precursors, and 40,493 transitions at the end of all the filtering steps. The average number of peptides per protein was 4.2, and the average number of precursors per peptide was 4.8. The vast majority (7627) of the precursors in the assay library were represented by five transitions, with 558 precursors represented by four transitions and nine precursors represented by three transitions. 2+ was the most common precursor charge (5244 precursors), then 3+ (2161 precursors), 4+ (399 precursors), and finally 1+ (350 precursors). The five most common transitions were: y6+ (5044), y7+ (4741), y5+ (4611), y+8 (3984), and y+4 (3765). Any proteins that were significantly different between the populations or any treatments were then manually validated, and the absolute final count after all automated filtration and manual validation steps was: 1708 proteins, 7086 peptides, 7928 precursors, and 39,081 transitions. Mass error, retention time reproducibility, and the q-value distributions after the final mProphet model training and peak reintegration serve as quality control validation and are visualized in Figure 2.3. This assay

library can be used in the future to systematically study protein abundance for a variety of temperature stress experiments with *G. aculeatus*.

## Population comparisons

### *Overall population comparison (KL vs. BL)*

Only a single protein (Figure 2.4a, Supplemental Table 2.1) was significantly different between the two populations (all three temperature groups collapsed for each population) and met the fold change threshold (FC > 2). BL had significantly more abundant levels of stromal cell-derived factor 2-like 1 (G3NI26, 2.1-fold difference, adjusted p-value = 6.31E-5). There were eight additional proteins significantly higher (adjusted p-value < 0.05) in BL (ribosomal protein L12, heterogeneous nuclear ribonucleoprotein A1a, sorbitol dehydrogenase, thioredoxin, alpha-2-macroglobulin-like 1, heat shock cognate 70, single-stranded DNA binding protein 1, and fibrillarin) and one protein significantly higher in KL (an uncharacterized protein; G3NAC1) that did not surpass the minimum fold change cut off (FC > 2).

STRING functional enrichment analysis, which was based on fold changes of proteins across the entire liver assay library proteome, identified seven STRING network clusters that were significantly (FDR < 0.01) enriched in BL (Supplemental Table 2.2). These seven STRING network clusters fell under two main groupings, both of which were elevated in BL (BL > KL), 1) glycolysis and carbohydrate metabolism and 2) AMP-binding and aldehyde dehydrogenase domain. Two representative STRING network clusters are visually depicted in Figure 2.4b-c, with the corresponding protein list, description, FC, and adjusted-p values in Supplemental Tables 2.3 and 2.4. Additional functional enrichments (Supplemental Table 2.2) that were lower in BL (KL > BL) included the following Uniprot, INTERPRO, PFAM, and SMART protein

domains and keywords: winged helix-like DNA-binding domain superfamily, histone H1, and histone H5. Additional Uniprot, INTERPRO, PFAM, and SMART protein domains that were elevated in BL (BL > KL) included oxidoreductase, and NAD(P)-binding domain superfamily.

***Comparison of populations to cold acclimation (KL7 vs. BL7)***

There were 35 proteins that were higher in abundance in BL at 7°C and three that were higher in abundance in KL passing both the fold change (FC > 2) and significance thresholds (adjusted $p < 0.05$) (Supplemental Table 2.1). A volcano plot for the proteins in this comparison are shown in Supplemental Figure 2.1a and significantly different proteins are visualized in a heat map in Supplemental Figure 2.2a. Functionally enriched STRING network clusters (Supplemental Table 2.2) for proteins more abundant in BL7 than KL7 included: low-density lipoprotein (LDL) receptor class A repeat, terpenoid cyclases/protein prenyltransferase alpha-alpha toroid, LDLR class B repeat, lipid transport protein, apolipoprotein A/E, lipoprotein N-terminal Domain, AMP-binding, conserved site, aldehyde dehydrogenase domain, amidohydrolase family, and purine metabolism. Additional functional enrichments for the proteins higher in abundance in BL7 (Supplemental Table 2.2) included Uniprot keyword oxidoreductase, PFAM, SMART, and INTERPRO domain alpha-2-macroglobulin family, and the additional INTERPRO domain 6-phosphogluconate dehydrogenase.

Proteins higher in abundance in KL included COX assembly mitochondrial protein, tubulin-specific chaperone A, and peptidyl-prolyl cis-trans isomerase. No functional enrichments were found from just these three proteins.

***Comparison of populations at the control temperature and to warm acclimation (KL15 vs. BL15 and KL25 vs. BL25)***

There were no significant differences between the two populations at the control temperature (KL15 vs. BL15) or at the warm temperature (KL25 vs. BL25).

**Temperature comparisons**

***Overall effects of cold acclimation (15°C vs. 7°C)***

No proteins were both significantly different and had a fold change greater than two for 15°C vs. 7°C (Figure 2.5a). L-threonine dehydrogenase was the one protein that was significantly lower in 7°C (adjusted p-value = 0.0004) and alpha-mannosidase was the one protein that was significantly higher in 15°C (adjusted p-value = 0.001), but these proteins did not meet the fold change cut off. There were nine significantly (FDR < 0.01) functionally enriched STRING network clusters (Supplemental Table 2.2) for 15°C vs. 7°C. Those lower at 7°C included glycolysis, L-lactate/malate dehydrogenase, tetrahydrofolate dehydrogenase/cyclohydrolase, pyridoxal phosphate-dependent transferase domain 1, carbohydrate metabolism, enolase, and NAD(P)-binding domain. Those elevated at 7°C included ribosome biogenesis, and DEAD/DEAH box helicase. Three of the main STRING network clusters that were significantly functionally enriched, one involving glycolysis and carbohydrate metabolism, a second involving ribosome biogenesis and DEAD/DEAH box helicase, and the last involving pyridoxal phosphate-dependent transferase domain 1 and NAD(P)-binding domain are visually represented in Figure 2.5b-d, with the corresponding protein list, description, FC, and adjusted-p values in Supplemental Tables 2.5-2.7. Additional functional enrichments (15°C > 7°C) included Uniprot keyword glycolysis and pyridoxal phosphate.

***Population-specific effects of cold acclimation (KL15 vs. KL7 and BL15 vs. BL7)***

There were not any significant differences between KL15 and KL7. For BL15 vs. BL7, one protein, alpha-mannosidase, was lower in BL7 and met both significance (adjusted p-value=0.042) and fold change (FC=2.5) requirements (Supplemental Table 2.1). One additional protein, nucleolar protein interacting with the FHA domain of MKI67 was significantly higher in abundance in BL7 but did not meet the fold change cut off.

***Overall effects of warm acclimation (15°C vs. 25°C)***

A total of 35 proteins were significantly different and had a fold change of at least two that were higher in abundance at 25°C and 51 proteins were significantly different with at least a fold change of two that were lower in abundance at 25°C (Figure 2.6a-b, Supplemental Table 2.1). An additional 44 proteins were significantly higher at 25°C but did not meet the fold change cut off and 108 additional proteins that were significantly lower at 25°C but did not meet the fold change cut off. There were ten functionally enriched STRING network clusters (Supplemental Table 2.2) falling into three main groupings: 1) core histones H2A/H2B/H3/H4 (elevated at 25°C), 2) ribosomal proteins, including S18, L37, and S30 and translational protein SH3-like (depleted at 25°C), and 3) acyltransferase ChoActase/COT/CPT, and SCP2 sterol-binding domain (depleted at 25°C). Three of the main functionally enriched (FDR < 0.01) STRING network clusters representing each of the three main groupings are visually represented in Figure 2.6d-f, with the corresponding protein list, description, FC, and adjusted-p values in Supplemental Tables 2.8-2.10. Additional functional enrichments elevated at 25°C included Uniprot keywords chromosome and DNA-binding, and PFAM, INTERPRO, and SMART

protein domains histone H1 and H5 family, and winged helix-like DNA-binding domain superfamily. Additional functional enrichments depleted at 25°C included ribosomal protein S5 domain and thiolase-like.

***Population-specific effects of warm acclimation***

*KL15 vs. KL25*

For KL15 vs. KL25 there were five proteins significantly higher in abundance in KL25 (heterogeneous nuclear ribonucleoprotein D, ATP synthase, H+ transporting, mitochondrial Fo complex, subunit F6, OCIA domain containing 1, and two uncharacterized proteins) and five proteins significantly lower in abundance in KL25 (Leukocyte cell-derived chemotaxin 2 like, phytanoyl-CoA 2-hydroxylase, peptidylprolyl isomerase, mitochondrial ribosomal protein S16, and ribonuclease T2) that met the fold change cut off (FC > 2) (Supplemental Table 2.1). There was one additional protein significantly higher for KL25 (heat shock protein family [HSP40] member B1b) and lower for KL25 (adenylate kinase 2, mitochondrial) that did not meet the fold change cut off. There were no functional enrichments found from these proteins. A volcano plot for the proteins in this comparison are shown in Supplemental Figure 2.1b and significantly different proteins are visualized in a heat map in Supplemental Figure 2.2b.

*BL15 vs. BL25*

For BL15 vs. BL25 there were 17 proteins significantly higher in abundance in BL25 and 51 proteins lower in abundance in BL25 that met the fold change cut off (FC>2) (Supplemental Table 2.1). A volcano plot for the proteins in this comparison are shown in Supplemental Figure 2.1c and significantly different proteins are visualized in a heat map in Supplemental Figure

2.2c. Functional enrichments (Supplemental Table 2.2) in proteins significantly higher in BL25 included STRING network clusters core histone H2A/H2B/H3/H4, Uniprot keyword chromosome, PFAM protein domain linker histone H1 and H5 family, INTERPRO Protein domains and features histone H5 and linker histone H1/H5, domain H15, and SMART protein domains histone families 1 and 5. Functional enrichments (Supplemental Table 2.2) that were significantly lower in BL25 (BL15 > BL25) included seven STRING network clusters pertaining to ribosomal protein and protein biosynthesis, several proteinase inhibitors, peptidase S1A, coagulation factors VII/IX/X/C/Z, cystatin, cathepsin D, fibrinogen, and PAN domain. Additional functional enrichments that were depleted in BL25 (BL15 > BL25) included Uniprot keyword RNA-binding and the following PFAM protein domains: RNA recognition motif. (a.k.a. RRM, RBD, or RNP domain), ubiquitin family, various elongation factors, cystatin domain, cyclophilin type peptidyl-prolyl cis-trans isomerase/CLD, and ubiquitin-2 like Rad60 SUMO-like. Finally, there were 17 functionally depleted (BL15 > BL25) INTERPRO protein domains and features pertaining to RNA recognition motif, nucleotide-binding, RNA-binding, multiple different elongation factors, ubiquitin, cystatin, thiolase-like, cyclophilin-type peptidyl-prolyl cis-trans isomerase, ribosomal protein S5, and transcription factor GTP-binding.

*Overlap of significant proteins between the two individual population comparisons of warm acclimation (KL15 vs. KL25 versus BL15 vs. BL25)*

There were seven proteins that overlapped in being significantly higher or lower in abundance between the KL15 vs. KL25 and BL15 vs. BL25 comparisons (Figure 2.6c). Proteins that were higher in abundance at 25°C for both population comparisons included: 1) Heterogeneous nuclear ribonucleoprotein, 2) ATP synthase, H+ transporting, mitochondrial Fo complex, subunit

F6, and 3) OCIA domain containing 1. Proteins that were lower in abundance at 25°C for both population comparisons included: 1) Leukocyte cell-derived chemotaxin 2 like, 2) Phytanoyl-CoA 2-hydroxylase, 3) Peptidylprolyl isomerase, and 4) Ribonuclease T2. There were no significant functional enrichments from these seven proteins.

***Overall differences between cold and warm acclimation (7°C vs. 25°C)***

A total of 77 proteins were significantly higher in abundance at 25°C and 72 proteins that were significantly higher in abundance at 7°C that met the fold change cut off of at least two (Figure 2.7, Supplemental Table 2.1). Additionally, there were 73 more proteins that were significantly more abundant in 25 and 79 more proteins that were significantly more abundant in 7, but that did not meet the fold change cut off. Results are similar to the comparison of the cold and warm comparisons to the control temperature (15°C), so networks are not depicted, but functionally enriched STRING network clusters (Supplementary Table 2.2) included five pertaining to core histones H2A/H2B/H3/H4 (25°C > 7°C), and one network cluster for ribosomal protein and ribosomal protein L37/S30 (7°C > 25°C). Functionally enriched UniProt keywords elevated at 25°C included chromosome, DNA-binding, and nucleosome core, while RNA-binding was lower at 25°C. Significantly enriched PFAM, INTERPRO, and SMART domains elevated at 25°C included linker histone H1 and H5 family, histone fold, and histones H2A/H2B/H3. Significant PFAM, INTERPRO, and SMART domains that were depleted at 25°C included RNA binding domain, RNA recognition motif, elongation factor G, nucleotide-binding alpha-beta plait domain superfamily, thiolase-like, and ribosomal protein S5.

***Population-specific differences between cold and warm acclimation***

*KL7 vs. KL25*

For KL7 vs. KL25, there were 49 proteins significantly higher in abundance in KL25 and 29 proteins significantly higher in abundance in KL7 that met the fold change cut off (FC > 2) (Supplemental Table 2.1). A volcano plot for the proteins in this comparison are shown in Supplemental Figure 2.1d and significantly different proteins are visualized in a heat map in Supplemental Figure 2.2d. Functional enrichments for the 49 proteins higher in abundance in KL25 included the following STRING network clusters (Supplementary Table 2.2): glycolysis, enolase, phosphoglycerate mutase 1, carbohydrate metabolism, calponin repeat, caldesmon, annexin A2 and A11, FAD dependent oxidoreductase, D-isomer specific 2-hydroxyacid dehydrogenase, catalytic domain, and core histones H2A/H2B/H3/H4. Functionally enriched UniProt keywords elevated in KL25 included chromosome and nucleosome core. Additional functional enrichments (KL25 > KL15) for PFAM, INTERPRO, and SMART protein domains included core histones H2A/H2B/H3/H4, enolase, TIM barrel domain, and tropomyosin.

Functional enrichments (Supplemental Table 2.2) for the 29 proteins significantly higher in abundance in KL7 included STRING network clusters involved with ribosomal proteins, RNA recognition motif domains, and mRNA processing, translation protein SH3-like domain superfamily, and protein biosynthesis. Additional functional domains and keywords that were depleted in KL7 (KL15 > KL7) pertained to RNA-binding, RNA recognition motif nucleotide-binding alpha-beta plait domain superfamily.

*BL7 vs. BL25*

For BL7 vs. BL25, there were 82 proteins significantly higher in abundance in BL25 and 96 proteins significantly higher in abundance in BL7 that met the fold change cut off (FC > 2)

(Supplemental Table 2.1). A volcano plot for the proteins in this comparison are shown in Supplemental Figure 2.1e and significantly different proteins are visualized in a heat map in Supplemental Figure 2.2e. Functional enrichments (Supplemental Table 2.2) for the 82 proteins higher in abundance in BL25 included STRING network clusters pertaining to core histones H2A/H2B/H3/H4 and H5, HMG box A DNA-binding domain, calponin repeat, and caldesmon. Functionally enriched Uniprot keywords in BL25 included: chromosome, DNA-binding, nucleosome core, and the nucleus. Additional functionally enriched PFAM, INTERPRO, and SMART protein domains elevated in BL25 involved linker histone H1 and H5 histone H2A, Histone H5, and winged helix-like DNA-binding domain superfamily.

Functional enrichments (Supplemental Table 2.2) for the 96 proteins higher in abundance in BL7 (BL7 > BL25) included the following STRING network clusters: ribosomal protein, protein biosynthesis, heterogeneous nuclear ribonucleoprotein C, HnRNP-L/PTB, HSP70 protein, DnaJ C terminal domain, hnRNP A0, RNA recognition motif translation protein SH3-like domain superfamily, fatty acid hydroxylase, sterol biosynthesis, and mRNA processing. Uniprot Keywords that were depleted in BL25 included: RNA-binding, cytoplasm, cytoskeleton, nucleotide-binding, protein biosynthesis, sterol biosynthesis, microtubule, lipid metabolism, lipid biosynthesis, ATP-binding, and tricarboxylic acid cycle. Numerous elongation factors, RNA recognition motif, tubulin/FtsZ family, GTPase, nucleotide-binding alpha-beta plait domain superfamily, RNA-binding domain superfamily, tubulin, ribosomal proteins, transcription factor, translation protein beta-barrel domain superfamily, K homology domain, and thiolase-like proteins were functionally depleted in BL25 (BL7 > BL25).

*Overlap of significant proteins between the two individual population comparisons of cold vs. warm acclimation (KL7 vs. KL25 versus BL7 vs. BL25)*

There were 28 proteins (Figure 2.7c) that overlapped in being significantly higher or lower in abundance between the KL15 vs. KL25 and BL15 vs. BL25 comparisons (17 proteins higher at the 25°C temperature, 11 proteins lower at the 25°C temperature). Functional enrichments (Supplemental Table 2.2) for these 28 overlapping significant proteins included calponin repeat, and caldesmon, annexin A2, and annexin A11, and core histone H2A/H2B/H3/H4, and histone H4. Additional function enrichments included: Uniprot Keywords included chromosome, PFAM protein domains C-terminus of histone H2A, INTERPRO protein domains and features histone H2A, histone H2A, C-terminal domain, and histone H2A conserved site, and SMART protein domains histone 2A and calponin homology domain.

## DISCUSSION

### Proteins involved in protein homeostasis fuel higher metabolic need in BL sticklebacks

As a population, BL had a higher number of elevated proteins over KL and had more significantly different proteins for each within population temperature comparison than KL. Despite having a small number of significantly different proteins in population-to-population comparisons, there were clearly differences in how the two populations handled chronic temperature stress. The network analyses helped elucidate some of these differences and the chronic cold temperature challenge yielded the most differences between the two populations, both of which will be discussed in more detail below.

Regardless of temperature, all but one of the proteins that were significantly different between the populations were higher in abundance in the BL population. Many of these proteins

are either directly or peripherally involved in maintaining protein homeostasis. Stromal cell-derived factor 2-like 1 (SDF2L1) is localized in the endoplasmic reticulum (ER) and in mice, it has been suggested to increase the amount of time available for misfolded proteins to regain their correct conformation and that it acts as a regulator in the ER stress response (Sasako et al., 2019; Tiwari et al., 2013). The constitutively expressed molecular chaperone heat shock cognate 70 (hsc70) is involved in a range of protein homeostasis functions such as de novo protein folding, protein translocation, protein assembly and disassembly, regulation of protein activity, protection from proteolysis, and coordinating with other smaller molecular chaperones (Rosenzweig et al., 2019; Zügel & Kaufmann, 1999). Thioredoxin is a ubiquitous antioxidant found in all cell types and organisms (Pacitti et al., 2014). Alpha-2-macroglobulin-like 1 is involved in the immune response through the complement and coagulation cascades and was elevated in grass carp (*Ctenopharyngodon idellus*) after 48 hour exposure to high temperature (Yang et al., 2016). 60S ribosomal protein L12 is at the core of translation and catalyzes the formation of peptide bonds (Lafontaine & Tollervey, 2001), heterogeneous nuclear ribonucleoprotein A1a is involved in mRNA splicing and stability as well as overall regulation of translation (Geuens et al., 2016), fibrillarin is a component of a nucleolar ribonucleoprotein involved in rRNA processing (Newton et al., 2003), and single-stranded DNA binding protein 1 is integral for processes such as DNA replication and repair (Wold, 1997). Overall, these elevated proteins in BL represent proteins that aid in protein folding or refolding, reactive oxygen species (ROS) scavenging, immune response, transcription, and translation. Increases in these processes signify a significant response and would contribute to a higher metabolic demand. Sorbitol dehydrogenase was significantly higher in abundance in BL over KL and from the network analysis, glycolysis and carbohydrate

metabolism were functionally enriched with proteins aligning to this network being elevated in BL over KL.

The main difference between the two populations occurred under the cold temperature stress condition, again, with BL having a vast majority of the significantly elevated proteins, or conversely, with KL having significantly lower abundance of many proteins. Molecular chaperones heat shock cognate 70 and heat shock 60 protein 1 were elevated in BL7 as were the previously described proteins stromal cell-derived factor 2-like 1 and single-stranded DNA protein 1. Two aldehyde dehydrogenase (ALDH) proteins from family 8 and 2 were also higher in BL7 and ALDH was found to be functionally enriched as well. These proteins are oxidative stress proteins and aldehyde dehydrogenase was similarly elevated after cold acclimation in the mussel *Mytilus trossulus* (Fields et al., 2012). Aspartate aminotransferase (ALT) and alanine-glyoxylate aminotransferase 2 were both more abundant in BL7 and play a role in glutamate metabolism (Sookoian & Pirola, 2012). Both of these proteins also serve as biomarkers for liver damage (Huang et al., 2006), as can alpha-2-macroglobulin, which was both functionally enriched and significantly elevated at the individual protein level and may explain the increase in the ROS-scavenging ALDH proteins. Both alpha and beta chain tubulin proteins and one tubulin-specific chaperone were significantly elevated in BL7 over KL7. Cold acclimated gilthead seabream (*Sparus aurata*) also had elevated levels of tubulin, which comprise the microtubule network forming the cytoskeleton and are thought to play a role in the cellular stress response, although the exact mechanism is unknown (Ibarz et al., 2010; Parker et al., 2014). Additionally, in a study examining two mussel congeners, the warm-adapted congener had increased abundances of tubulin after cold acclimation (Fields et al., 2012). Glycerol-3-phosphate dehydrogenase (GPDH) was one of the proteins significantly elevated in BL7 over KL7. GPDH

activity increased at low temperatures in rainbow smelt (Driedzic et al., 2006; Liebscher et al., 2006) and snow trout (Barat et al., 2012) and resulted in an increase in glycerol, which can act as an antifreeze. From the functional enrichment analysis, 6-phosphogluconate dehydrogenase (6PGD) was identified twice from the INTERPRO database. 6PGD is a part of the pentose phosphate pathway (PPP) and produces NADPH which can reduce ROS via the glutathione system, so 6PGD can be considered an antioxidant enzyme (Budak et al., 2014). Transaldolase is another elevated protein that is part of the pentose phosphate pathway (Samland & Sprenger, 2009). In zebrafish, cold resistance is conferred through lipid catabolism and autophagy (Lu et al., 2019). In the BL7 group, autophagy-related protein 3 was in higher abundance along with various proteins involved with lipid metabolism, such as GPDH, 3-hydroxyisobutyrate dehydrogenase, and lipid transport (apolipoprotein Ea). The autophagy-related protein 3 and lysosomal enzyme N-acetylglucosamine-6-sulfatase suggest the increased need in the BL7 group to degrade damaged molecules, which is consistent with an increase in ROS related damage. Aconitate hydratase catalyzes the isomerization of citrate to isocitrate in the citric acid cycle and is sensitive to ROS (Matasova & Popova, 2008). There are clear differences between the two populations, with BL exhibiting higher abundances of proteins involved in carbohydrate, amino acid, and lipid metabolism, as well as an increase in antioxidant proteins and molecular chaperones, possibly to deal with the increased ROS produced via the higher metabolic demand.

Overall, there could be several reasons for these population differences. The BL population might have a more uniform response among individuals in the population thus leading to more significant differences, while the KL population may have greater within-population variation in how individuals deal with temperature stress. Alternatively, BL might have more energy available to devote to processes that demand higher metabolic rates or simply

be able to alter metabolic flux more easily. A third possibility is that the KL population was able to achieve a state of homeostasis faster than the BL population and that after three weeks, more of the protein concentrations had returned to baseline levels in KL than BL, which was still mounting a response to the chronic stress. KL and BL might also be employing different strategies, one that requires more upkeep and energy versus one that does not mount as much of a response but has a lower energetic cost.

**Both populations re-establish liver proteome homeostasis during chronic cold acclimation**

Despite differences at 7°C between the two populations, there were no significant effects of cold acclimation on individual proteins irrespective of whether the populations were combined or analyzed within population. Tolerance limit tests for the KL and BL populations were only conducted on upper limits (see Chapter 1) due to logistical constraints, but for marine populations, the lower limit is around 4°C and for freshwater populations it is around 1°C (Barrett et al., 2011). However, even in freshwater lakes farther north in British Columbia, 4°C is the mean monthly temperature for winter months (Barrett et al., 2011). Functional enrichments pertaining to glycolysis, ribosome biogenesis, and RNA metabolism (DEAD/DEAH box helicase) hint at some differences between 15°C and 7°C, but for the most part, it appears that the populations were able to re-establish homeostasis after the initial temperature shock at 7°C. This is likely a temperature that both populations would experience in the wild. Given that water has the highest density at 4°C, it would be unrealistic to expose these populations to conditions at much lower than 4°C. Whether a cold-acclimation to 4°C results in a different response than cold-acclimation to 7°C remains to be explored in future studies.

**Chronic warm acclimation increases chromatin regulation and transcriptional control while reducing translation and fatty acid metabolism proteins**

The majority of proteins that are significantly increased at 25°C over the control temperature pertain to histones and proteins that regulate transcription or chromatin structure. Host cell factor C1a has been linked to cell proliferation, gluconeogenesis promotion, and regulation of transcription (Minocha et al., 2019). Two ribonucleoproteins were higher in abundance, including SAP domain containing ribonucleoprotein and heterogeneous nuclear ribonucleoprotein D, which was elevated at 25°C for the overall temperature and population-specific comparisons and serves as a transcriptional repressor (Zieger et al., 2011). Serpine1 mRNA binding protein 1b is involved in mRNA stability (Heaton et al., 2001; Mari et al., 2015). Ataxin 2-like protein is a component of stress granules in mammals, but is evolutionarily conserved across eukaryotes (Jiménez-López & Guzmán, 2014), and responds to a variety of stressors via mRNA regulation with links to mRNA degradation (Kaehler et al., 2012). One study on carp found that the expression of four H2A variants were enriched during the summer, and that a ubiquitylated variant regulated chromatin structure (Simonet et al., 2013). Another study also demonstrated large changes in nucleolar structure and the expression of ribosomal genes with acclimatization to seasonal changes in carp liver (Pinto et al., 2005). Besides numerous histone proteins with significantly higher abundance at 25°C, functional enrichment of networks involving core histones (including 11 proteins that were significantly more abundant in 25°C) as well as functional enrichment of chromosome and DNA binding point to a key role of chromatin regulation for warm acclimation. It is likely that there is epigenetic regulation occurring in various histones to both alter the chromatin structure and regulate transcription and translation to acclimate to the increased temperature. Future studies should examine the specific

types of post-translational modifications (PTMs) associated with these elevated proteins. PTMs are easily identified in mass spectrometry-based proteomics but identifying and quantifying them was outside the scope of this study.

There were some additional proteins of note that were higher in abundance at 25°C than 15°C beyond histones, and others involved in chromatin structure and transcription. Paxillin is a molecular scaffold or adaptor protein that regulates cellular responses to changes in the environment (Brown & Turner, 2004), and may be linked to other structural related proteins that were higher in abundance at 25°C such as tropomyosin 1 and calponin to increase cytoskeletal stability. Peptide-methionine (R)-S-oxide reductase can be considered an antioxidant and converts methionine sulfoxide back to the amino acid methionine, one of the easiest amino acids to oxidize (Weissbach et al., 2002). Two isoforms of Tpd52 like protein 2b were also elevated at 25°C. Tpd52 associates with lipid droplets and likely signifies changes in lipid storage (Chen et al., 2016).

Functional enrichment analysis for proteins that were lower in abundance at 25°C, centered around ribosomal and thiolase like proteins, suggesting a decrease in translation (including significantly reduced proteins mitochondrial ribosomal proteins S16, L41, L24, L14, S18A, and L27; Supplemental Table 2.10) and alteration in fatty acid metabolism (including significantly lower abundance proteins: fatty acid synthase, acetyl-CoA acetyltransferase 2, and sterol carrier protein 2a). Phytanoyl-CoA 2-hydroxylase, another protein involved in fatty acid metabolism, is involved in the oxidation of 3-methyl branched fatty acids (Foulon et al., 2003). There were also three elongation factors (eukaryotic translation elongation factor 2b, elongation factor like GTPase1, and eukaryotic translation elongation factor 2a) and two splicing factors (serine/arginine-rich splicing factor 4 and serine/arginine-rich splicing factor 2b) that were less

abundant at 25°C, adding more evidence of a decrease in translation. Leukocyte cell-derived chemotaxin 2-like protein was lower in abundance in the overall comparison and for both population comparisons. Leukocyte cell-derived chemotaxin (LECT2) modulates immune function and inflammatory pathways and serum levels are indicative of liver fat content (Kikuchi et al., 2020). Chronic stress can divert energy away from the immune system (Alfonso et al., 2020), and the lower levels of this protein could also indicate a depletion of liver fat content that would likewise explain a decrease in various proteins linked to fatty acid metabolism.

There were many more significantly different proteins in the population-specific comparisons that support the above conclusions regarding the overall warm-acclimation effect. Many additional proteins that were higher in abundance in the BL population clustered into the same functional categories as those discussed above for overall differences, i.e. histone and chromatin structure, and transcription. Proteins that were significantly elevated at 25°C only in the BL population (BL25 > BL15) include centromere protein V, SUB 1 homolog, transcriptional regulator 1, and pleckstrin homology domain containing, family A member 6 (PLEKHA6). The overexpression of centromere protein V can lead to hypercondensation of certain types of heterochromatin (Tadeu et al., 2008). SUB 1 homolog, transcriptional regulator b is inducible by oxidative stress and protects DNA from oxidative damage when it is exposed or partially unwound (Yu et al., 2016).

Functions of the proteins that were significantly lower in abundance only in BL fish acclimated to 25°C (BL15 > BL25) also reflected functional categories that were decreased at 25°C overall in both populations. From the functional enrichment analysis, ribosomal proteins were again significantly depleted in BL25. Beyond just ribosomal proteins, there were also individual proteins with significantly lower abundance at BL25 that are involved more generally

in protein biosynthesis (eukaryotic translation elongation factor 2b, RNA binding protein S1 serine-rich domain, nascent polypeptide associated complex subunit alpha, ribosomal protein L37, eukaryotic translation initiation factor 3 subunit G, and eukaryotic translation elongation factor 1 beta 2). Two peptidylprolyl isomerase proteins were also lower in abundance. These proteins help with folding newly synthesized proteins, but also play a role in the immune system, cell cycle control, and transcriptional regulation (Shaw, 2002). Two lysosomal proteins (legumain and acid phosphatase 2, lysosomal) were likewise lower in abundance in BL25. Filamin B is an actin-binding cytoskeletal protein, but also binds RNA and decreased transcript levels of Filamin B have resulted in lower apoptosis, and a downregulation of immune and inflammatory related genes (Ma et al., 2020), which is consistent with some of the functions discussed above. Besides the common proteins involved in lipid metabolism that were significantly lower in abundance in both populations as mentioned above (sterol carrier protein 2a, phytanoyl-CoA 2-hydroxylase, fatty acid synthase), an additional lipid metabolism protein (lipase) was significantly reduced in the BL population. Lipase is involved in triglyceride regulation (Chatterjee & Sparks, 2011). Another protein of note that was only significantly reduced at 25°C in BL fish (BL15 > BL25) was thioredoxin domain containing 17, which is involved in cellular redox homeostasis (Liyanage et al., 2019).

**Key functional enrichment differences between cold and warm acclimation**

The 7°C vs. 25°C comparison yielded results similar to those already discussed in the 7°C vs. 15°C and 15°C vs. 25°C comparisons, but with a much higher number of significant differences. There were significant functional enrichments of proteins associated with histones, chromosomes, DNA-binding, and the nucleosome core that were elevated at 25°C, and

ribosomal proteins, RNA-binding, elongation factors, and RNA recognition motifs that were elevated at 7°C, suggesting increased protection of DNA from damage and increased regulation over transcription at higher temperatures and an increase in translation at colder temperatures perhaps to combat slower reactions rates.

**Proteome signatures provide comprehensive insight into mechanisms of environmental acclimation**

While individual proteins can serve as good bioindicators for injury, disease, or other conditions, proteomic signatures, which encompass the patterns of multiple proteins of interest, have the potential to give specific insight into the physiological state or condition of an organism (da Costa et al., 2015). With enough data sets, the repeated paired expression patterns of a wide range of proteins could potentially give more context and specificity to the type and degree of a particular stressor. While this data is derived from only two populations from one species, it provides a very detailed snapshot of the molecular phenotypes of these organisms and can identify the strategies and mechanism utilized to overcome a change in the environment. Proteins often have numerous roles, so connecting overall changes in protein abundance helps disentangle the particular pathways that are activated or suppressed and to identify new networks and connections.

DATA ACCESSIBILITY

All proteomics data and metadata are accessible at the following repositories: ProteomeXchange (ID=PXD024617) for all DDA data and Panorama Public (https://panoramaweb.org/bbl02.url) for the DIA assay library and all DIA data.

ACKNOWLEDGMENTS

Part of this work was funded by NSF grant IOS-1656371.

## REFERENCES


Alfonso, S., Gesto, M., & Sadoul, B. (2020). Temperature increase and its effects on fish stress physiology in the context of global warming. *Journal of Fish Biology*, *2020*, 1–13. https://doi.org/10.1111/jfb.14599

Anderson, L., & Seilhamer, J. (1997). A comparison of selected mRNA and protein abundances in human liver. *ELECTROPHORESIS*, *18*(3–4), 533–537. https://doi.org/10.1002/elps.1150180333

Barat, A., Goel, C., Tyagi, A., Ali, S., & Sahoo, P. K. (2012). Molecular cloning and expression profile of snow trout GPDH gene in response to abiotic stress. *Molecular Biology Reports*, *39*(12), 10843–10849. https://doi.org/10.1007/s11033-012-1980-6

Barrett, R. D. H., Paccard, A., Healy, T. M., Bergek, S., Schulte, P. M., Schluter, D., & Rogers, S. M. (2011). Rapid evolution of cold tolerance in stickleback. *Proceedings of the Royal Society B: Biological Sciences*, *278*(1703), 233–238. https://doi.org/10.1098/rspb.2010.0923

Beitinger, T. L., & Fitzpatrick, L. C. (1979). Physiological and Ecological Correlates of Preferred Temperature in Fish. *American Zoologist*, *19*(1), 319–329. https://doi.org/10.1093/icb/19.1.319

Bell, M. A., & Foster, S. A. (Eds.). (1994). *The evolutionary biology of the threespine stickleback*. Oxford University Press.

Biron, D. G., Loxdale, H. D., Ponton, F., Moura, H., Marché, L., Brugidou, C., & Thomas, F. (2006). Population proteomics: An emerging discipline to study metapopulation ecology. *PROTEOMICS*, *6*(6), 1712–1715. https://doi.org/10.1002/pmic.200500423

Brown, M. C., & Turner, C. E. (2004). Paxillin: Adapting to Change. *Physiological Reviews*, *84*(4), 1315–1339. https://doi.org/10.1152/physrev.00002.2004

Budak, H., Ceylan, H., Kocpinar, E. F., Gonul, N., & Erdogan, O. (2014). Expression of Glucose-6-Phosphate Dehydrogenase and 6-Phosphogluconate Dehydrogenase in Oxidative Stress Induced by Long-Term Iron Toxicity in Rat Liver. *Journal of Biochemical and Molecular Toxicology*, *28*(5), 217–223. https://doi.org/10.1002/jbt.21556

Chatterjee, C., & Sparks, D. L. (2011). Hepatic Lipase, High Density Lipoproteins, and Hypertriglyceridemia. *The American Journal of Pathology*, *178*(4), 1429–1433. https://doi.org/10.1016/j.ajpath.2010.12.050

Chen, Y., Frost, S., & Byrne, J. A. (2016). Dropping in on the lipid droplet- tumor protein D52 (TPD52) as a new regulator and resident protein. *Adipocyte*, *5*(3), 326–332. https://doi.org/10.1080/21623945.2016.1148835

Crawford, D. L., Pierce, V. A., & Segal, J. A. (1999). Evolutionary Physiology of Closely Related Taxa: Analyses of Enzyme Expression. *American Zoologist*, *39*(2), 389–400.

da Costa, J. P., Carvalhais, V., Ferreira, R., Amado, F., Vilanova, M., Cerca, N., & Vitorino, R. (2015). Proteome signatures—How are they obtained and what do they teach us? *Applied Microbiology and Biotechnology*, *99*(18), 7417–7431. https://doi.org/10.1007/s00253-015-6795-7

Diz, A. P., Martínez-Fernández, M., & Rolán-Alvarez, E. (2012). Proteomics in evolutionary ecology: Linking the genotype with the phenotype. *Molecular Ecology*, *21*(5), 1060–1080. https://doi.org/10.1111/j.1365-294X.2011.05426.x

Doerr, A. (2015). DIA mass spectrometry. *Nature Methods*, *12*(1), 35–35. https://doi.org/10.1038/nmeth.3234

Driedzic, W. R., Clow, K. A., Short, C. E., & Ewart, K. V. (2006). Glycerol production in rainbow smelt (Osmerus mordax) may be triggered by low temperature alone and is associated with the activation of glycerol-3-phosphate dehydrogenase and glycerol-3-phosphatase. *Journal of Experimental Biology*, *209*(6), 1016–1023. https://doi.org/10.1242/jeb.02086

Feder, M. E., & Walser, J.-C. (2005). The biological limitations of transcriptomics in elucidating stress and stress responses. *Journal of Evolutionary Biology*, *18*(4), 901–910. https://doi.org/10.1111/j.1420-9101.2005.00921.x

Fernández-Costa, C., Martínez-Bartolomé, S., McClatchy, D. B., Saviola, A. J., Yu, N.-K., & Yates, J. R. (2020). Impact of the Identification Strategy on the Reproducibility of the DDA and DIA Results. *Journal of Proteome Research*, *19*(8), 3153–3161. https://doi.org/10.1021/acs.jproteome.0c00153

Fields, P. A., Zuzow, M. J., & Tomanek, L. (2012). Proteomic responses of blue mussel (Mytilus) congeners to temperature acclimation. *Journal of Experimental Biology*, *215*(7), 1106–1116. https://doi.org/10.1242/jeb.062273

Foulon, V., Asselberghs, S., Geens, W., Mannaerts, G. P., Casteels, M., & Van Veldhoven, P. P. (2003). Further studies on the substrate spectrum of phytanoyl-CoA hydroxylase: Implications for Refsum disease? *Journal of Lipid Research*, *44*(12), 2349–2355. https://doi.org/10.1194/jlr.M300230-JLR200

Genner, M. J., Sims, D. W., Wearmouth, V. J., Southall, E. J., Southward, A. J., Henderson, P. A., & Hawkins, S. J. (2004). Regional climatic warming drives long–term community changes of British marine fish. *Proceedings of the Royal Society of London. Series B: Biological Sciences*, *271*(1539), 655–661. https://doi.org/10.1098/rspb.2003.2651

Geuens, T., Bouhy, D., & Timmerman, V. (2016). The hnRNP family: Insights into their role in health and disease. *Human Genetics*, *135*, 851–867. https://doi.org/10.1007/s00439-016-1683-5

Heaton, J. H., Dlakic, W. M., Dlakic, M., & Gelehrter, T. D. (2001). Identification and cDNA Cloning of a Novel RNA-binding Protein That Interacts with the Cyclic Nucleotide-responsive Sequence in the Type-1 Plasminogen Activator Inhibitor mRNA. *Journal of Biological Chemistry*, *276*(5), 3341–3347. https://doi.org/10.1074/jbc.M006538200

Huang, X.-J., Choi, Y.-K., Im, H.-S., Yarimaga, O., Yoon, E., & Kim, H.-S. (2006). Aspartate Aminotransferase (AST/GOT) and Alanine Aminotransferase (ALT/GPT) Detection Techniques. *Sensors*, *6*(7), 756–782. https://doi.org/10.3390/s6070756

Ibarz, A., Martín-Pérez, M., Blasco, J., Bellido, D., Oliveira, E. de, & Fernández-Borràs, J. (2010). Gilthead sea bream liver proteome altered at low temperatures by oxidative stress. *PROTEOMICS*, *10*(5), 963–975. https://doi.org/10.1002/pmic.200900528

IPCC. (2014). *Climate Change 2014: Synthesis Report. Contribution of Working Groups I, II and III to the Fifth Assessment Report of the Intergovernmental Panel on Climate Change* (p. 151). Intergovernmental Panel on Climate Change. https://www.ipcc.ch/site/assets/uploads/2018/02/SYR_AR5_FINAL_full.pdf

IPCC. (2019). *Summary for Policymakers. In: IPCC Special Report on the Ocean and Cryosphere in a Changing Climate* (p. In press). Intergovernmental Panel on Climate Change. https://www.ipcc.ch/srocc/chapter/summary-for-policymakers/

Jiménez-López, D., & Guzmán, P. (2014). Insights into the evolution and domain structure of ataxin-2 proteins across eukaryotes. *BMC Research Notes*, *7*(1), 453. https://doi.org/10.1186/1756-0500-7-453

Kaehler, C., Isensee, J., Nonhoff, U., Terrey, M., Hucho, T., Lehrach, H., & Krobitsch, S. (2012). Ataxin-2-Like Is a Regulator of Stress Granules and Processing Bodies. *PLOS ONE*, *7*(11), e50134. https://doi.org/10.1371/journal.pone.0050134

Karr, T. L. (2008). Application of proteomics to ecology and population biology. *Heredity*, *100*(2), 200–206. https://doi.org/10.1038/sj.hdy.6801008

Kikuchi, A., Takayama, H., Tsugane, H., Shiba, K., Chikamoto, K., Yamamoto, T., Matsugo, S., Ishii, K., Misu, H., & Takamura, T. (2020). Plasma half-life and tissue distribution of leukocyte cell-derived chemotaxin 2 in mice. *Scientific Reports*, *10*(1), 13260. https://doi.org/10.1038/s41598-020-70192-x

Kültz, D., Li, J., Gardell, A., & Sacchi, R. (2013). Quantitative molecular phenotyping of gill remodeling in a cichlid fish responding to salinity stress. *Molecular & Cellular Proteomics: MCP*, *12*(12), 3962–3975. https://doi.org/10.1074/mcp.M113.029827

Lafontaine, D. L. J., & Tollervey, D. (2001). The function and synthesis of ribosomes. *Nature Reviews Molecular Cell Biology*, *2*(7), 514–520. https://doi.org/10.1038/35080045

Li, J., Levitan, B., Gomez-Jimenez, S., & Kültz, D. (2018). Development of a Gill Assay Library for Ecological Proteomics of Threespine Sticklebacks (Gasterosteus aculeatus). *Molecular & Cellular Proteomics*, *17*(11), 2146–2163. https://doi.org/10.1074/mcp.RA118.000973

Liebscher, R. S., Richards, R. C., Lewis, J. M., Short, C. E., Muise, D. M., Driedzic, W. R., & Ewart, K. V. (2006). Seasonal Freeze Resistance of Rainbow Smelt (Osmerus mordax) Is Generated by Differential Expression of Glycerol-3-Phosphate Dehydrogenase, Phosphoenolpyruvate Carboxykinase, and Antifreeze Protein Genes. *Physiological and Biochemical Zoology*, *79*(2), 411–423. https://doi.org/10.1086/499981

Liu, B., Xu, P., Brown, P. B., Xie, J., Ge, X., Miao, L., Zhou, Q., Ren, M., & Pan, L. (2016). The effect of hyperthermia on liver histology, oxidative stress and disease resistance of the Wuchang bream, Megalobrama amblycephala. *Fish & Shellfish Immunology*, *52*, 317–324. https://doi.org/10.1016/j.fsi.2016.03.018

Liyanage, D. S., Omeka, W. K. M., Yang, H., Godahewa, G. I., Kwon, H., Nam, B.-H., & Lee, J. (2019). Identification of thioredoxin domain-containing protein 17 from big-belly seahorse Hippocampus abdominalis: Molecular insights, immune responses, and functional characterization. *Fish & Shellfish Immunology*, *86*, 301–310. https://doi.org/10.1016/j.fsi.2018.11.040

Loarie, S. R., Duffy, P. B., Hamilton, H., Asner, G. P., Field, C. B., & Ackerly, D. D. (2009). The velocity of climate change. *Nature*, *462*(7276), 1052–1055. https://doi.org/10.1038/nature08649

López, J. L. (2007). Applications of proteomics in marine ecology. *Marine Ecology Progress Series*, *332*, 275–280. https://doi.org/10.3354/meps332275

Lu, D.-L., Ma, Q., Wang, J., Li, L.-Y., Han, S.-L., Limbu, S. M., Li, D.-L., Chen, L.-Q., Zhang, M.-L., & Du, Z.-Y. (2019). Fasting enhances cold resistance in fish through stimulating lipid catabolism and autophagy. *The Journal of Physiology*, *597*(6), 1585–1603. https://doi.org/10.1113/JP277091

Ma, H.-R., Cao, L., Wang, F., Cheng, C., Jiang, R., Zhou, H., Xie, Z., Wuermanbieke, S., & Qian, Z. (2020). Filamin B extensively regulates transcription and alternative splicing, and is associated with apoptosis in HeLa cells. *Oncology Reports*, *43*(5), 1536–1546. https://doi.org/10.3892/or.2020.7532

Mari, Y., West, G. M., Scharager-Tapia, C., Pascal, B. D., Garcia-Ordonez, R., & Griffin, P. R. (2015). SERBP1 is a component of the Liver Receptor Homolog-1 transcriptional complex. *Journal of Proteome Research*, *14*(11), 4571–4580. https://doi.org/10.1021/acs.jproteome.5b00379

Matasova, L. V., & Popova, T. N. (2008). Aconitate hydratase of mammals under oxidative stress. *Biochemistry (Moscow)*, *73*(9), 957–964. https://doi.org/10.1134/S0006297908090010

Menge, B. A., & Olson, A. M. (1990). Role of scale and environmental factors in regulation of community structure. *Trends in Ecology & Evolution*, *5*(2), 52–57. https://doi.org/10.1016/0169-5347(90)90048-I

Minocha, S., Villeneuve, D., Praz, V., Moret, C., Lopes, M., Pinatel, D., Rib, L., Guex, N., & Herr, W. (2019). Rapid Recapitulation of Nonalcoholic Steatohepatitis upon Loss of Host Cell Factor 1 Function in Mouse Hepatocytes. *Molecular and Cellular Biology*, *39*(5), e00405-18. https://doi.org/10.1128/MCB.00405-18

Newton, K., Petfalski, E., Tollervey, D., & Cáceres, J. F. (2003). Fibrillarin Is Essential for Early Development and Required for Accumulation of an Intron-Encoded Small Nucleolar RNA in the Mouse. *Molecular and Cellular Biology*, *23*(23), 8519–8527. https://doi.org/10.1128/MCB.23.23.8519-8527.2003

Nicolas, D., Chaalali, A., Drouineau, H., Lobry, J., Uriarte, A., Borja, A., & Boët, P. (2011). Impact of global warming on European tidal estuaries: Some evidence of northward migration of estuarine fish species. *Regional Environmental Change*, *11*(3), 639–649. https://doi.org/10.1007/s10113-010-0196-3

Pacitti, D., Wang, T., Martin, S. A. M., Sweetman, J., & Secombes, C. J. (2014). Insights into the fish thioredoxin system: Expression profile of thioredoxin and thioredoxin reductase in rainbow trout (Oncorhynchus mykiss) during infection and in vitro stimulation. *Developmental & Comparative Immunology*, *42*(2), 261–277. https://doi.org/10.1016/j.dci.2013.09.013

Pappireddi, N., Martin, L., & Wühr, M. (2019). A Review on Quantitative Multiplexed Proteomics. *ChemBioChem*, *20*(10), 1210–1224. https://doi.org/10.1002/cbic.201800650

Parker, A. L., Kavallaris, M., & McCarroll, J. A. (2014). Microtubules and Their Role in Cellular Stress in Cancer. *Frontiers in Oncology*, *4*, 153. https://doi.org/10.3389/fonc.2014.00153

Pino, L. K., Searle, B. C., Bollinger, J. G., Nunn, B., MacLean, B., & MacCoss, M. J. (2017). The Skyline ecosystem: Informatics for quantitative mass spectrometry proteomics. *Mass Spectrometry Reviews*, *39*(3), 229–244. https://doi.org/10.1002/mas.21540

Pinto, R., Ivaldi, C., Reyes, M., Doyen, C., Mietton, F., Mongelard, F., Alvarez, M., Molina, A., Dimitrov, S., Krauskopf, M., Vera, M. I., & Bouvet, P. (2005). Seasonal environmental changes regulate the expression of the histone variant macroH2A in an eurythermal fish. *FEBS Letters*, *579*(25), 5553–5558. https://doi.org/10.1016/j.febslet.2005.09.019

Qian, B., & Xue, L. (2016). Liver transcriptome sequencing and de novo annotation of the large yellow croaker (Larimichthy crocea) under heat and cold stress. *Marine Genomics*, *25*, 95–102. https://doi.org/10.1016/j.margen.2015.12.001

Reiter, L., Rinner, O., Picotti, P., Hüttenhain, R., Beck, M., Brusniak, M.-Y., Hengartner, M. O., & Aebersold, R. (2011). mProphet: Automated data processing and statistical validation for large-scale SRM experiments. *Nature Methods*, *8*(5), 430–435. https://doi.org/10.1038/nmeth.1584

Rosenzweig, R., Nillegoda, N. B., Mayer, M. P., & Bukau, B. (2019). The Hsp70 chaperone network. *Nature Reviews Molecular Cell Biology*, *20*(11), 665–680. https://doi.org/10.1038/s41580-019-0133-3

Samland, A. K., & Sprenger, G. A. (2009). Transaldolase: From biochemistry to human disease. *The International Journal of Biochemistry & Cell Biology*, *41*(7), 1482–1494. https://doi.org/10.1016/j.biocel.2009.02.001

Sasako, T., Ohsugi, M., Kubota, N., Itoh, S., Okazaki, Y., Terai, A., Kubota, T., Yamashita, S., Nakatsukasa, K., Kamura, T., Iwayama, K., Tokuyama, K., Kiyonari, H., Furuta, Y., Shibahara, J., Fukayama, M., Enooku, K., Okushin, K., Tsutsumi, T., … Ueki, K. (2019). Hepatic Sdf2l1 controls feeding-induced ER stress and regulates metabolism. *Nature Communications*, *10*(1), 947. https://doi.org/10.1038/s41467-019-08591-6

Scanes, E., Scanes, P. R., & Ross, P. M. (2020). Climate change rapidly warms and acidifies Australian estuaries. *Nature Communications*, *11*(1), 1803. https://doi.org/10.1038/s41467-020-15550-z

Seebacher, F. (2005). A review of thermoregulation and physiological performance in reptiles: What is the role of phenotypic flexibility? *Journal of Comparative Physiology B*, *175*(7), 453–461. https://doi.org/10.1007/s00360-005-0010-6

Shaw, P. E. (2002). Peptidyl-prolyl isomerases: A new twist to transcription. *EMBO Reports*, *3*(6), 521–526. https://doi.org/10.1093/embo-reports/kvf118

Silvestre, F., Gillardin, V., & Dorts, J. (2012). Proteomics to assess the role of phenotypic plasticity in aquatic organisms exposed to pollution and global warming. *Integrative and Comparative Biology*, *52*(5), 681–694. https://doi.org/10.1093/icb/ics087

Simonet, N. G., Reyes, M., Nardocci, G., Molina, A., & Alvarez, M. (2013). Epigenetic regulation of the ribosomal cistron seasonally modulates enrichment of H2A.Z and H2A.Zub in response to different environmental inputs in carp (Cyprinus carpio). *Epigenetics & Chromatin*, *6*, 22. https://doi.org/10.1186/1756-8935-6-22

Somero, G. N. (2011). The Physiology of Global Change: Linking Patterns to Mechanisms. *Annual Review of Marine Science*, *4*(1), 39–61. https://doi.org/10.1146/annurev-marine-120710-100935

Sookoian, S., & Pirola, C. J. (2012). Alanine and aspartate aminotransferase and glutamine-cycling pathway: Their roles in pathogenesis of metabolic syndrome. *World Journal of Gastroenterology : WJG*, *18*(29), 3775–3781. https://doi.org/10.3748/wjg.v18.i29.3775

Szklarczyk, D., Gable, A. L., Lyon, D., Junge, A., Wyder, S., Huerta-Cepas, J., Simonovic, M., Doncheva, N. T., Morris, J. H., Bork, P., Jensen, L. J., & Mering, C. von. (2019). STRING v11: Protein-protein association networks with increased coverage, supporting functional discovery in genome-wide experimental datasets. *Nucleic Acids Research*, *47*(D1), D607–D613. https://doi.org/10.1093/nar/gky1131

Tadeu, A. M. B., Ribeiro, S., Johnston, J., Goldberg, I., Gerloff, D., & Earnshaw, W. C. (2008). CENP-V is required for centromere organization, chromosome alignment and cytokinesis. *The EMBO Journal*, *27*(19), 2510–2522. https://doi.org/10.1038/emboj.2008.175

Tiwari, A., Schuiki, I., Zhang, L., Allister, E. M., Wheeler, M. B., & Volchuk, A. (2013). Stromal Cell-Derived Factor 2 Like-1 (SDF2L1) Associates with the Endoplasmic Reticulum-Associated Degradation (ERAD) Machinery and Retards the Degradation of

Mutant Proinsulin in Pancreatic β-Cells. *Journal of Cell Science*, *126*(9), 1962–1968. https://doi.org/10.1242/jcs.117374

Tomanek, L. (2010). Environmental Proteomics: Changes in the Proteome of Marine Organisms in Response to Environmental Stress, Pollutants, Infection, Symbiosis, and Development. *Annual Review of Marine Science*, *3*(1), 373–399. https://doi.org/10.1146/annurev-marine-120709-142729

Tomanek, L. (2014). Proteomics to study adaptations in marine organisms to environmental stress. *Journal of Proteomics*, *105*, 92–106. https://doi.org/10.1016/j.jprot.2014.04.009

Trefts, E., Gannon, M., & Wasserman, D. H. (2017). The liver. *Current Biology*, *27*(21), R1147–R1151. https://doi.org/10.1016/j.cub.2017.09.019

Weissbach, H., Etienne, F., Hoshi, T., Heinemann, S. H., Lowther, W. T., Matthews, B., St. John, G., Nathan, C., & Brot, N. (2002). Peptide Methionine Sulfoxide Reductase: Structure, Mechanism of Action, and Biological Function. *Archives of Biochemistry and Biophysics*, *397*(2), 172–178. https://doi.org/10.1006/abbi.2001.2664

Wilkins, M. R., Sanchez, J.-C., Gooley, A. A., Appel, R. D., Humphery-Smith, I., Hochstrasser, D. F., & Williams, K. L. (1996). Progress with Proteome Projects: Why all Proteins Expressed by a Genome Should be Identified and How To Do It. *Biotechnology and Genetic Engineering Reviews*, *13*(1), 19–50. https://doi.org/10.1080/02648725.1996.10647923

Wold, M. S. (1997). REPLICATION PROTEIN A: A Heterotrimeric, Single-Stranded DNA-Binding Protein Required for Eukaryotic DNA Metabolism. *Annual Review of Biochemistry*, *66*(1), 61–92. https://doi.org/10.1146/annurev.biochem.66.1.61

Yang, Y., Yu, H., Li, H., Wang, A., & Yu, H. (2016). Effect of high temperature on immune response of grass carp (Ctenopharyngodon idellus) by transcriptome analysis. *Fish & Shellfish Immunology, 58*, 89–95. https://doi.org/10.1016/j.fsi.2016.09.014

Yu, L., Ma, H., Ji, X., & Volkert, M. R. (2016). The Sub1 nuclear protein protects DNA from oxidative damage. *Molecular and Cellular Biochemistry*, *412*(1), 165–171. https://doi.org/10.1007/s11010-015-2621-x

Zieger, M. A., Gupta, M. P., & Wang, M. (2011). Proteomic analysis of endothelial cold-adaptation. *BMC Genomics*, *12*, 630. https://doi.org/10.1186/1471-2164-12-630

Zinn, K. E., Tunc-Ozdemir, M., & Harper, J. F. (2010). Temperature stress and plant sexual reproduction: Uncovering the weakest links. *Journal of Experimental Botany*, *61*(7), 1959–1968. https://doi.org/10.1093/jxb/erq053

Zügel, U., & Kaufmann, S. H. E. (1999). Role of Heat Shock Proteins in Protection from and Pathogenesis of Infectious Diseases. *Clinical Microbiology Reviews*, *12*(1), 19–39. https://doi.org/10.1128/CMR.12.1.19

## TABLES AND FIGURES

**Figure 2.1.** Sampling locations for two wild-caught populations of threespine sticklebacks from Northern California: Klamath river (coordinates: -124.071111, 41.545278) and Big lagoon (coordinates: -124.105994, 41.177013). Wild caught fish were externally fertilized and reared for at least one year under identical conditions in the laboratory, pre-acclimated for three weeks, and then exposed to a three-week chronic temperature stress experiment at either cold (7°C), control (15°C), or warm (25°C) conditions. Liver samples were analyzed by liquid chromatography tandem mass spectrometry (LCMS2) and data transformed into a DIA assay library used to quantify proteins and detect significant abundance differences and functional enrichment.

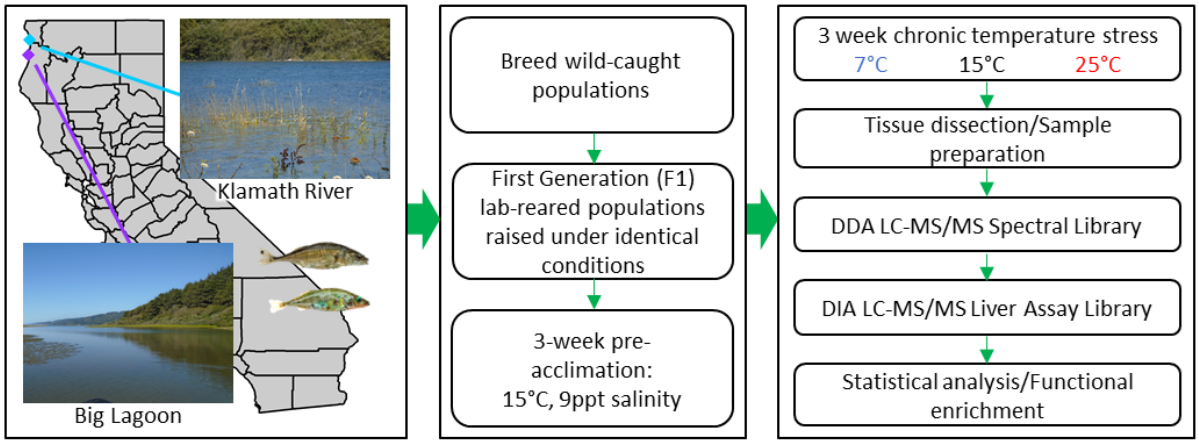

**Figure 2.2.** The numbers of a) proteins, b) peptides, c) precursors, and d) transitions are shown throughout the filtration steps used to finalize the liver DIA assay library (AL). e) depicts the number of unique peptides used for protein quantitation. All proteins were identified by at least two peptides, but for some proteins in the DIA assay library all but one unique peptide was filtered out during the quality control steps. f) represents the frequency of fragment ion types in the DIA assay library.

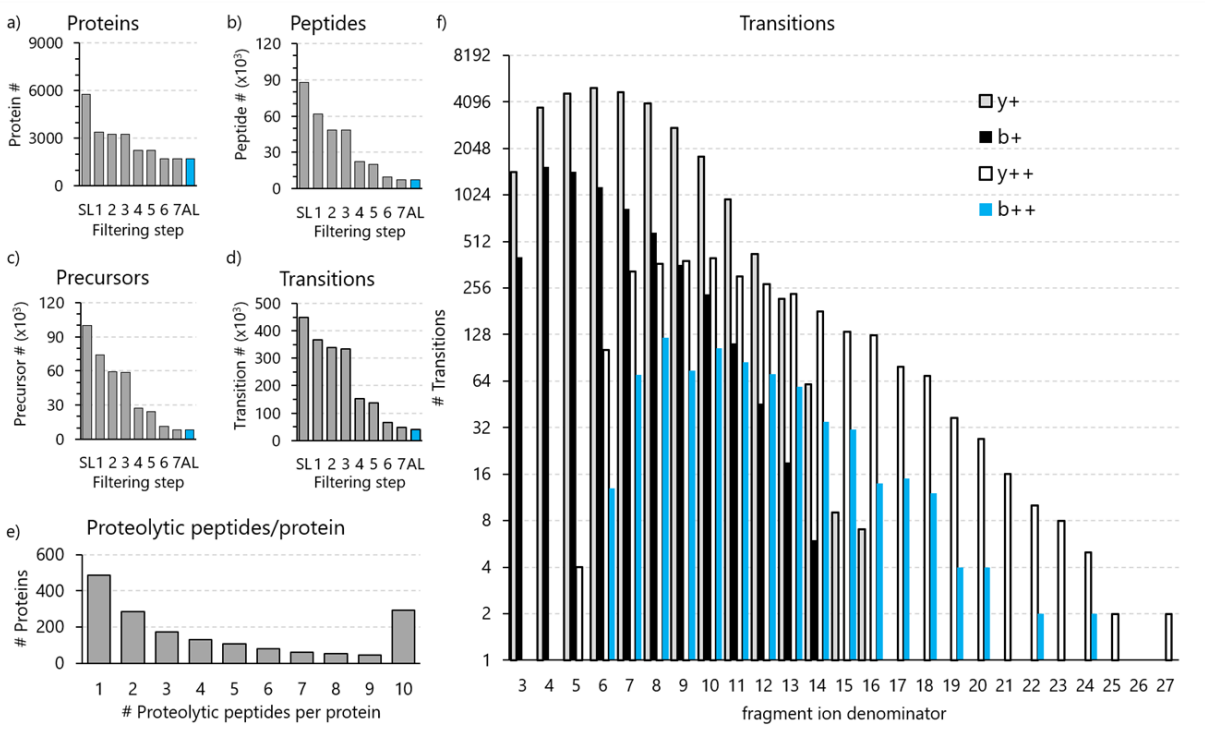

**Figure 2.3.** a) Mass error in parts per million (ppm) for all transitions present in the chronic temperature experiment liver assay library as a function of retention time (time of elution from the liquid chromatography column). b) Correlation between measured and predicted retention times. c) Q-values for all peaks of the target peptides in the DIA assay library.

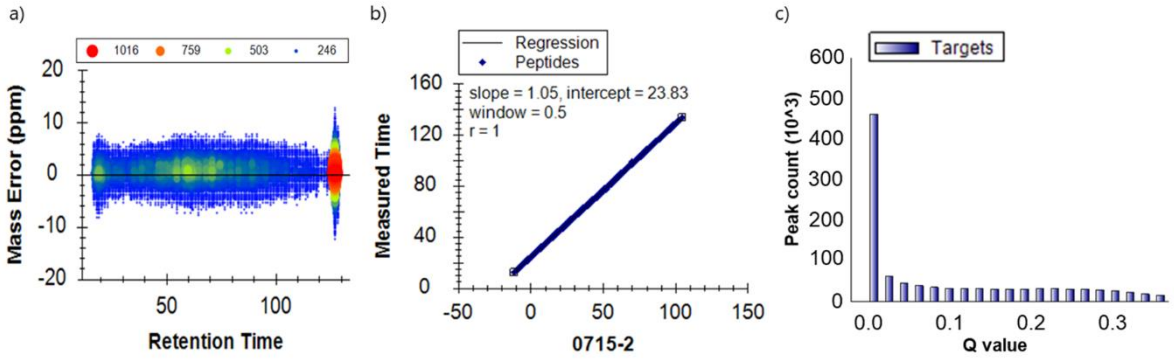

**Figure 2.4.** Comparison of liver proteomes in two stickleback populations (KL, N=30; all temperatures collapsed vs. BL, N=30; all temperatures collapsed). a) Volcano plot showing proteins as 1) red diamonds: significantly higher in abundance (FC > 2) and significantly different (adjusted p-value < 0.05), 2) blue diamonds: significantly lower in abundance (FC < 0.5) and significantly different, and 3) grey diamonds: did not meet cut off for both FC and significance requirements. b) & c) depict significantly (FDR < 0.01) functionally enriched STRING network clusters, with rings around nodes signifying proteins present in the liver DIA assay library. Rings are colored based on the fold change with red indicating the highest increase in BL relative to KL and blue indicating the highest decrease in BL relative to KL. b) STRING network cluster glycolysis and carbohydrate metabolism (CL:21363, functional enrichment FDR = $2.43E^{-7}$). The blue star identifies sorbitol dehydrogenase, which was significantly increased in BL over KL (FC = 1.88, adjusted p-value = 0.0037). c) STRING network cluster AMP-binding, conserved site, and aldehyde dehydrogenase domain (CL:22008, functional enrichment FDR = 0.00035).

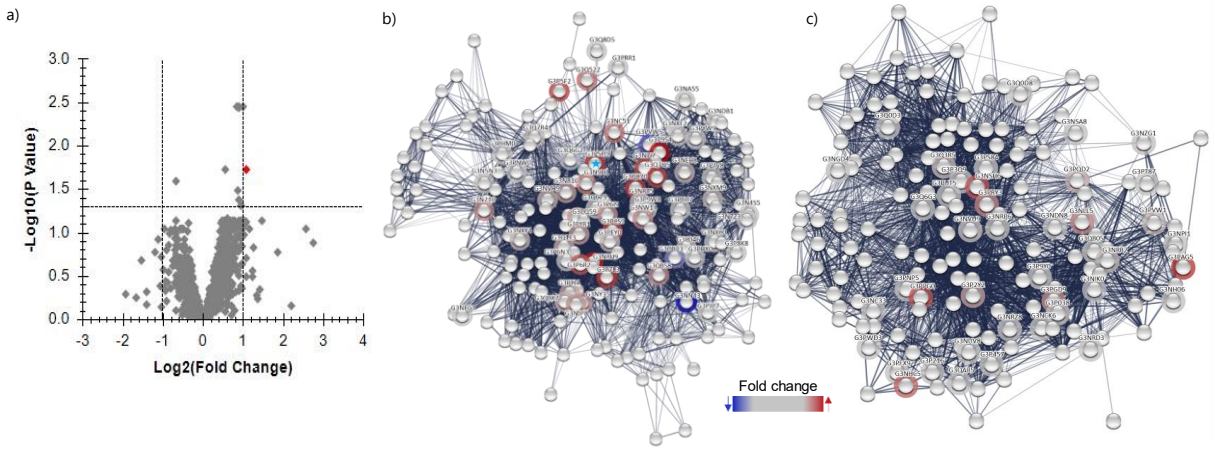

**Figure 2.5.** Overall effect of cold stress on the stickleback liver proteome (15°C, N=20; collapsed across both populations vs. 7°C, N=20; collapsed across both populations). a) Volcano plot with proteins depicted as all grey diamonds as none of them met the cut off for both FC (FC < 0.5 or FC > 2) and significance requirements (adjusted p-value < 0.05). b)-d) depict significantly (FDR < 0.01) functionally enriched STRING network clusters, with rings around nodes signifying proteins present in the liver DIA assay library. Rings are colored based on the fold change relative to all other proteins in the liver set, with red indicating the highest increase in 7°C relative to 15°C and blue indicating the maximal decrease in 7°C relative to 15°C. b) Enriched STRING network cluster glycolysis and carbohydrate metabolism (CL:21363, FDR = 0.0039). c) Enriched STRING network ribosome biogenesis and DEAD/DEAH box helicase (CL:16360, FDR = 0.0037). d) Enriched STRING network pyridoxal phosphate-dependent transferase domain 1 and NAD(P)-binding domain (CL:21790, FDR = 0.0054). The blue star identifies sorbitol dehydrogenase (FC = 1.79, adj. p = 0.001).

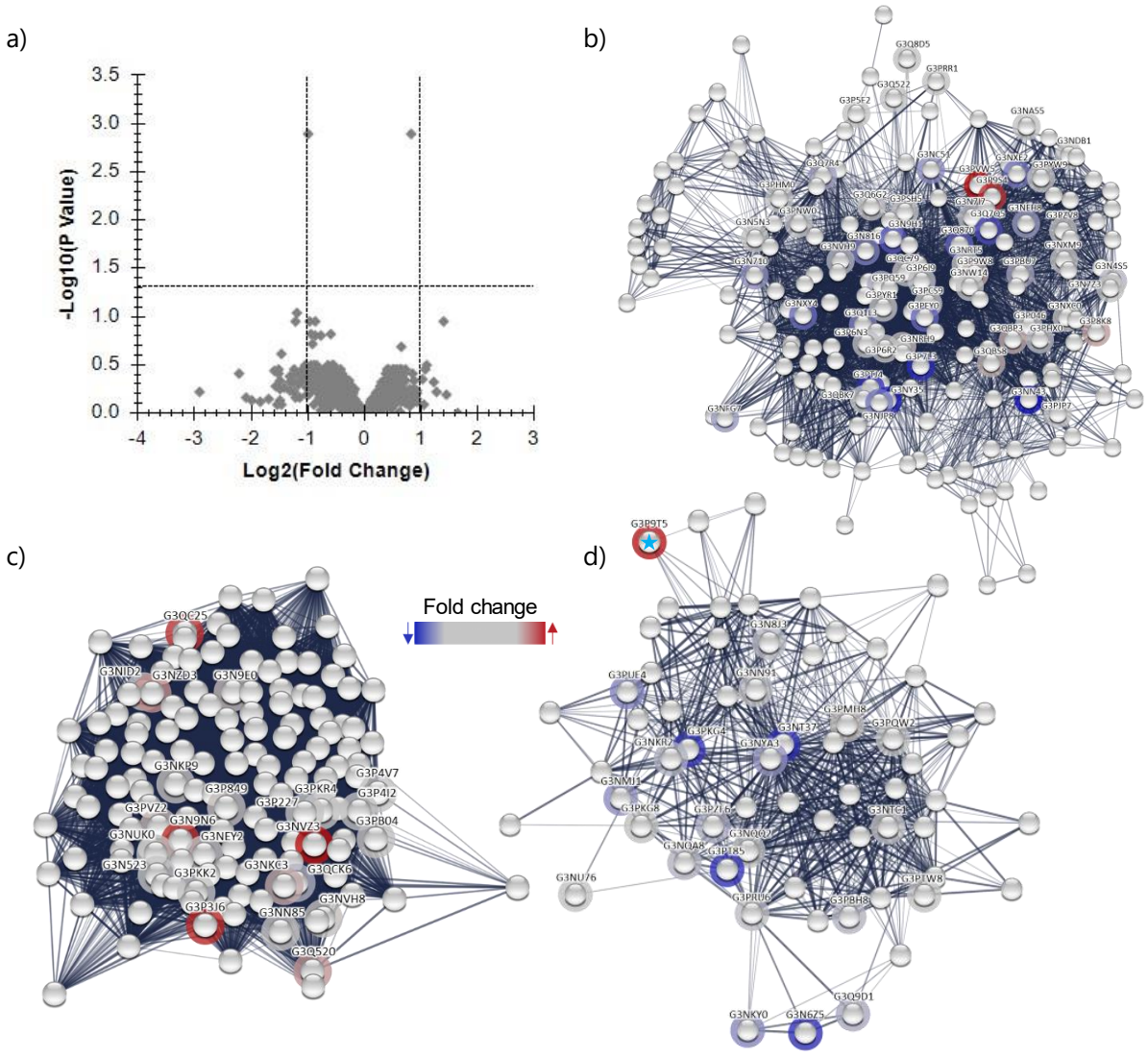

**Figure 2.6.** 15°C (N=20; collapsed across both populations) vs. 25°C (N=20; collapsed across both populations). a) Heat map depicting significantly (adjusted p-value < 0.05) up and down regulated proteins for all biological replicates. Yellow to red coloring represents proteins with a higher abundance, with red having the highest abundance. Dark blue to light blue represents proteins with a lower abundance, with light blue having the lowest abundance. b) Volcano plot showing proteins depicted as 1) red diamonds: significantly higher in abundance (FC > 2) and significantly different (adjusted p-value < 0.05), 2) blue diamonds: significantly lower in abundance (FC < 0.5) and significantly different, and 3) grey diamonds: did not meet cut off for both FC and significance requirements. c) Ven diagram depicting number of significantly different proteins between the KL15°C vs. KL25°C comparison and the BL15°C vs. BL25°C comparison. d)-f) depict significantly (FDR < 0.01) functionally enriched STRING network clusters, with rings around nodes signifying proteins present in the liver DIA assay library. Rings are colored based on the fold change relative to all other proteins in the liver set, with red indicating the highest increase in 25°C relative to 15°C and blue indicating the maximal decrease in 25°C relative to 15°C.  Blue stars indicate proteins that were significantly different in abundance between 15°C vs. 25°C d) Enriched STRING network cluster, core histone H2A/H2B/H3/H4, and histone H4 (CL:11311, FDR = 8.88e-9). e) Enriched STRING network cluster, acyltransferase choactase/COT/CPT, and SCP2 sterol-binding domain (CL:22217, FDR = 0.0027). f) Enriched STRING network cluster, ribosomal protein, and ribosomal protein S18 (CL:16051, FDR = 0.0023).

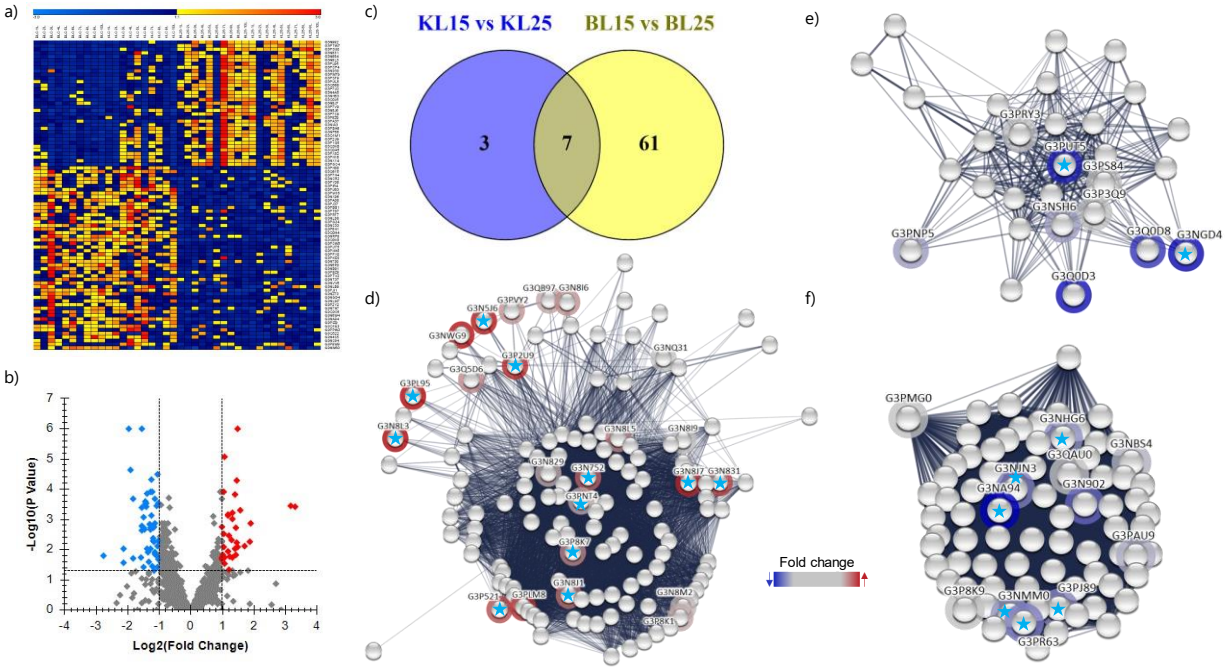

**Figure 2.7.** 7°C (N=20; collapsed across both populations) vs. 25°C (N=20; collapsed across both populations). a) Heat map depicting significantly (adjusted p-value < 0.05) up and down regulated proteins for all biological replicates. Yellow to red coloring represents proteins with a higher abundance, with red having the highest abundance. Dark blue to light blue represents proteins with a lower abundance, with light blue having the lowest abundance. b) Volcano plot showing proteins depicted as 1) red diamonds: significantly higher in abundance (FC > 2) and significantly different, 2) blue diamonds: significantly lower in abundance (FC < 0.5) and significantly different, and 3) grey diamonds: did not meet cut off for both FC and significance requirements. c) Ven diagram depicting number of significantly different proteins between the KL7°C vs. KL25°C comparison and the BL7°C vs. BL25°C comparison.

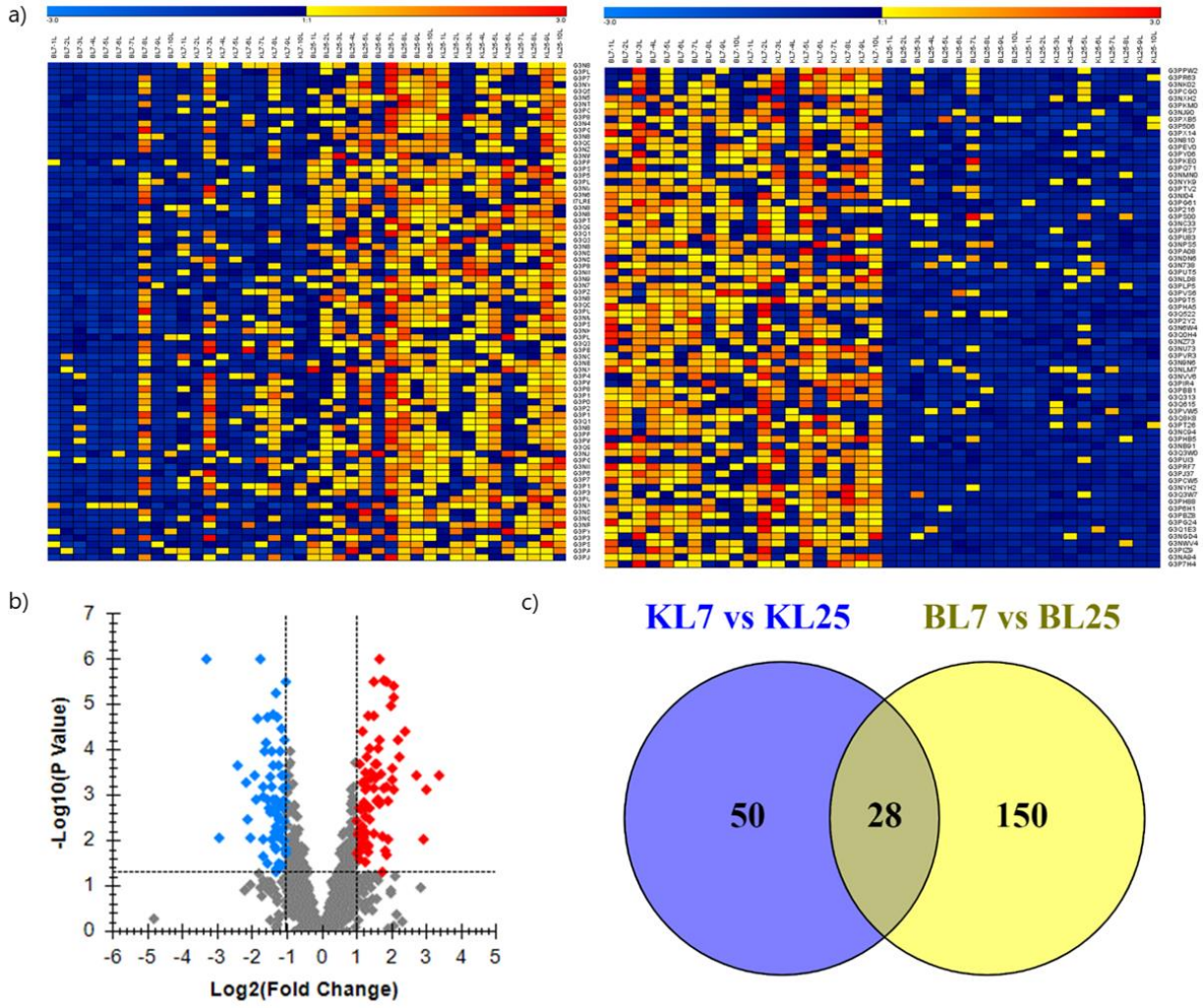

**Supplemental Table 2.1.** Skyline generated adjusted p-value and fold change with both Skyline and STRING descriptions for all the significantly higher or lower abundance proteins that also met fold change requirements (FC > 2 or < 0.5). The “Inverse Dn Fold Change” column takes -1/FC to make lower abundance values more intuitive. For example, for A vs. B, a fold change of 0.127 is 7.87 times lower in B than A (or 7.87 times higher in A than B). Direction of fold change can also be determined from the "Change" column, with "Up" having increased abundance in B relative to A and "Dn" having decreased abundance in B relative to A.

| Comparison | Change | Protein Accession | Skyline Description | STRING Description | Adjusted p-value | Fold Change | Inverse Dn Fold Change |
|---|---|---|---|---|---|---|---|
| KL v BL | Up | G3NI26 | Stromal cell-derived factor 2-like 1 | Stromal cell-derived factor 2-like 1 | 0.0189 | 2.1061 | |
| KL7 vs. BL7 | Up | G3PIG1 | Tubulin beta chain | #N/A | 0.0374 | 4.9889 | |
| KL7 vs. BL7 | Up | G3NT34 | Tubulin alpha chain | Tubulin alpha chain | 0.0374 | 4.3984 | |
| KL7 vs. BL7 | Up | G3NFC3 | Glycerol-3-phosphate dehydrogenase [NAD(+)] | Glycerol-3-phosphate dehydrogenase 1a | 0.0374 | 4.0207 | |
| KL7 vs. BL7 | Up | G3PTN7 | Aspartate aminotransferase | #N/A | 0.0374 | 4.0069 | |
| KL7 vs. BL7 | Up | G3PPG0 | Acyl-CoA dehydrogenase long chain | acyl-Coenzyme A dehydrogenase, long chain | 0.0374 | 3.7076 | |
| KL7 vs. BL7 | Up | G3P4B9 | Uncharacterized protein | Heterogeneous nuclear ribonucleoprotein A1a | 0.0374 | 3.4614 | |
| KL7 vs. BL7 | Up | G3NI26 | Stromal cell-derived factor 2-like 1 | Stromal cell-derived factor 2-like 1 | 0.0374 | 3.3577 | |
| KL7 vs. BL7 | Up | G3PAG5 | Aldehyde dehydrogenase 8 family, member A1 | Aldehyde dehydrogenase 8 family, member A1 | 0.0374 | 3.2750 | |
| KL7 vs. BL7 | Up | G3NJ86 | Aldehyde dehydrogenase 2 family member, tandem duplicate 2 | #N/A | 0.0486 | 3.1742 | |
| KL7 vs. BL7 | Up | G3NY15 | Niemann-Pick disease, type C2 | Niemann-Pick disease, type C2 | 0.0404 | 3.1200 | |
| KL7 vs. BL7 | Up | G3NXH8 | Heat shock cognate 70 | #N/A | 0.0374 | 3.0365 | |
| KL7 vs. BL7 | Up | G3PTA6 | AP-1 complex subunit gamma | Adaptor-related protein complex 1, gamma 1 subunit | 0.0374 | 2.9166 | |
| KL7 vs. BL7 | Up | G3PVW2 | Alanine--glyoxylate aminotransferase 2 | Alanine-glyoxylate aminotransferase 2; Belongs to the class-III pyridoxal-phosphate-dependent aminotransferase family | 0.0478 | 2.8759 | |
| KL7 vs. BL7 | Up | G3N710 | Alpha-1,4 glucan phosphorylase | Alpha-1,4 glucan phosphorylase | 0.0374 | 2.8195 | |
| KL7 vs. BL7 | Up | G3NKP4 | Zgc:103559 | Zgc:103559 | 0.0374 | 2.7272 | |
| KL7 vs. BL7 | Up | G3NFB8 | Uncharacterized protein | #N/A | 0.0478 | 2.6421 | |
| KL7 vs. BL7 | Up | G3P038 | 3-hydroxyisobutyrate dehydrogenase | 3-hydroxyisobutyrate dehydrogenase b | 0.0486 | 2.6381 | |
| KL7 vs. BL7 | Up | G3NGS3 | Uncharacterized protein | Apolipoprotein C-I like | 0.0374 | 2.5583 | |
| KL7 vs. BL7 | Up | G3NNM8 | Uncharacterized protein | Alpha-2-macroglobulin-like 1 | 0.0374 | 2.5498 | |
| KL7 vs. BL7 | Up | G3NCX8 | Apolipoprotein Ea | Apolipoprotein Ea | 0.0478 | 2.5000 | |
| KL7 vs. BL7 | Up | G3PZS2 | Ribosomal protein L12 | #N/A | 0.0374 | 2.4660 | |
| KL7 vs. BL7 | Up | G3Q9G8 | Single-stranded DNA binding protein 1 | Single-stranded DNA binding protein 1 | 0.0374 | 2.4360 | |
| KL7 vs. BL7 | Up | G3PYR1 | Transaldolase | Transaldolase | 0.0374 | 2.4299 | |
| KL7 vs. BL7 | Up | G3PRC7 | Autophagy-related protein 3 | #N/A | 0.0478 | 2.3675 | |
| KL7 vs. BL7 | Up | G3P140 | Tyrosine--tRNA ligase | Tyrosine--tRNA ligase; tyrosyl-tRNA synthetase | 0.0478 | 2.3329 | |
| KL7 vs. BL7 | Up | G3Q9H8 | N-acetylglucosamine-6-sulfatase | N-acetylglucosamine-6-sulfatase | 0.0478 | 2.2536 | |
| KL7 vs. BL7 | Up | G3NLM7 | Uncharacterized protein | Adaptor-related protein complex 2, mu 1 subunit | 0.0374 | 2.2501 | |
| KL7 vs. BL7 | Up | G3PPH3 | Karyopherin (importin) beta 1 | #N/A | 0.0280 | 2.2438 | |
| KL7 vs. BL7 | Up | G3PXC5 | Fibrinogen gamma chain | Fibrinogen, gamma polypeptide | 0.0374 | 2.2094 | |
| KL7 vs. BL7 | Up | G3P2N4 | Heat shock 60 protein 1 | #N/A | 0.0478 | 2.2063 | |
| KL7 vs. BL7 | Up | G3PFH7 | Uncharacterized protein (Fragment) | annotation not available | 0.0478 | 2.1657 | |
| KL7 vs. BL7 | Up | G3N8L1 | Uncharacterized protein | annotation not available | 0.0374 | 2.1609 | |
| KL7 vs. BL7 | Up | G3NMJ6 | Uncharacterized protein (Fragment) | #N/A | 0.0478 | 2.1091 | |
| KL7 vs. BL7 | Up | G3NXM9 | Aconitate hydratase, mitochondrial | Aconitate hydratase, mitochondrial; Aconitase 2, mitochondrial | 0.0374 | 2.0757 | |
| KL7 vs. BL7 | Up | G3P6A1 | Uncharacterized protein (Fragment) | annotation not available | 0.0404 | 2.0364 | |
| KL7 vs. BL7 | Dn | G3NSU1 | COX assembly mitochondrial protein | COX assembly mitochondrial protein 1 homolog (S. cerevisiae) | 0.0280 | 0.4135 | 2.4184 |
| KL7 vs. BL7 | Dn | G3PT75 | Tubulin-specific chaperone A | #N/A | 0.0478 | 0.4525 | 2.2099 |
| KL7 vs. BL7 | Dn | G3Q395 | Peptidyl-prolyl cis-trans isomerase | Peptidyl-prolyl cis-trans isomerase; Protein (peptidylprolyl cis/trans isomerase) NIMA-interacting, 4 (parvulin) | 0.0374 | 0.4705 | 2.1254 |
| BL15 vs. BL7 | Dn | G3N4S6 | Alpha-mannosidase | Alpha-mannosidase; Mannosidase, alpha, class 2B, member 1 | 0.0420 | 0.4044 | 2.4728 |
| 15 vs. 25 | Up | G3PL95 | Uncharacterized protein | Uncharacterized protein; Histone H1 like | 0.0004 | 9.9166 | |
| 15 vs. 25 | Up | G3N8L3 | Uncharacterized protein | Uncharacterized protein; Histone H1 like | 0.0004 | 9.0105 | |
| 15 vs. 25 | Up | G3Q568 | Uncharacterized protein | Uncharacterized protein; Caldesmon 1 like | 0.0014 | 3.7435 | |
| 15 vs. 25 | Up | G3P7V9 | Tpd52 like 2b | #N/A | 0.0055 | 3.6899 | |
| 15 vs. 25 | Up | G3P7C9 | Host cell factor C1a | Host cell factor C1b | 0.0077 | 3.3068 | |
| 15 vs. 25 | Up | G3PCP4 | SAP domain containing ribonucleoprotein | SAP domain containing ribonucleoprotein | 0.0005 | 3.0132 | |
| 15 vs. 25 | Up | G3P8Z9 | Tropomyosin 1 | Zgc:171719; Tropomyosin 1 (alpha) | 0.0087 | 2.8358 | |
| 15 vs. 25 | Up | G3N992 | Uncharacterized protein | ATP synthase, H+ transporting, mitochondrial Fo complex, subunit F6 | 0.0000 | 2.8294 | |
| 15 vs. 25 | Up | G3PSU0 | Heterogeneous nuclear ribonucleoprotein D | #N/A | 0.0001 | 2.7708 | |
| 15 vs. 25 | Up | G3N5J6 | Uncharacterized protein | Uncharacterized protein; Histone H1 like | 0.0061 | 2.7456 | |

| Comparison | Change | Protein Accession | Skyline Description | STRING Description | Adjusted p-value | Fold Change | Inverse Dn Fold Change |
|---|---|---|---|---|---|---|---|
| 15 vs. 25 | Up | G3Q1M1 | Uncharacterized protein | annotation not available | 0.0153 | 2.7261 | |
| 15 vs. 25 | Up | G3N4A5 | Calponin | Calponin | 0.0020 | 2.6932 | |
| 15 vs. 25 | Up | G3N654 | Uncharacterized protein | #N/A | 0.0002 | 2.6819 | |
| 15 vs. 25 | Up | G3NIA3 | Succinate dehydrogenase complex assembly factor 4 | Succinate dehydrogenase complex assembly factor 4; Chromosome 6 open reading frame 57 | 0.0098 | 2.6497 | |
| 15 vs. 25 | Up | G3Q3K8 | Eukaryotic translation initiation factor 4E binding protein 3, like | Eukaryotic translation initiation factor 4E binding protein 3, like | 0.0184 | 2.5277 | |
| 15 vs. 25 | Up | G3ND30 | Peptide-methionine (R)-S-oxide reductase | #N/A | 0.0006 | 2.5021 | |
| 15 vs. 25 | Up | G3PUL5 | SERPINE1 mRNA binding protein 1b | SERPINE1 mRNA binding protein 1 | 0.0010 | 2.4958 | |
| 15 vs. 25 | Up | G3N8J7 | Histone H2A | annotation not available | 0.0051 | 2.4494 | |
| 15 vs. 25 | Up | G3P2U9 | H1 histone family, member 0 | H1 histone family, member 0 | 0.0171 | 2.3601 | |
| 15 vs. 25 | Up | G3NX14 | Uncharacterized protein | Ataxin 2-like | 0.0468 | 2.3386 | |
| 15 vs. 25 | Up | G3Q0J5 | Uncharacterized protein (Fragment) | #N/A | 0.0035 | 2.3248 | |
| 15 vs. 25 | Up | G3PGC4 | Uncharacterized protein | Uncharacterized protein; Periaxin | 0.0484 | 2.3125 | |
| 15 vs. 25 | Up | G3PW79 | Endothelial differentiation-related factor 1 | Endothelial differentiation-related factor 1 | 0.0007 | 2.2797 | |
| 15 vs. 25 | Up | G3PSF9 | Tight junction protein 1a | Tight junction protein 1a; Belongs to the MAGUK family | 0.0008 | 2.2733 | |
| 15 vs. 25 | Up | G3PBA6 | Cysteine-rich protein 2 | annotation not available | 0.0116 | 2.2647 | |
| 15 vs. 25 | Up | G3PTW7 | Uncharacterized protein | OCIA domain containing 1 | 0.0000 | 2.1359 | |
| 15 vs. 25 | Up | G3Q0A5 | Si:ch211-217k17.7 | Si:ch211-217k17.7; Coiled-coil domain containing 86 | 0.0188 | 2.1285 | |
| 15 vs. 25 | Up | G3PH16 | Paxillin b | Paxillin | 0.0309 | 2.1080 | |
| 15 vs. 25 | Up | G3NH63 | Uncharacterized protein | Translational machinery associated 7 homolog (S. cerevisiae) | 0.0030 | 2.0799 | |
| 15 vs. 25 | Up | G3PA37 | Uncharacterized protein | Haptoglobin | 0.0087 | 2.0705 | |
| 15 vs. 25 | Up | G3N831 | Histone H2A | annotation not available | 0.0001 | 2.0630 | |
| 15 vs. 25 | Up | G3NP66 | Nucleoporin 153 | Nucleoporin 153 | 0.0153 | 2.0466 | |
| 15 vs. 25 | Up | G3P7U2 | Tpd52 like 2b | Tumor protein D52-like 2b | 0.0018 | 2.0155 | |
| 15 vs. 25 | Up | G3PX82 | RAN binding protein 3b | #N/A | 0.0218 | 2.0108 | |
| 15 vs. 25 | Up | G3P1Q8 | Coiled-coil domain containing 124 | Coiled-coil domain containing 124 | 0.0184 | 2.0041 | |
| 15 vs. 25 | Dn | G3NA94 | Mitochondrial ribosomal protein S16 | Mitochondrial ribosomal protein S16 | 0.0163 | 0.1471 | 6.7981 |
| 15 vs. 25 | Dn | G3N4S5 | Uncharacterized protein | Oxoglutarate (alpha-ketoglutarate) dehydrogenase b (lipoamide) | 0.0287 | 0.2292 | 4.3630 |
| 15 vs. 25 | Dn | G3NGD4 | Podocan | Podocan | 0.0098 | 0.2300 | 4.3478 |
| 15 vs. 25 | Dn | G3Q615 | Phytanoyl-CoA 2-hydroxylase | phytanoyl-CoA 2-hydroxylase | 0.0000 | 0.2601 | 3.8447 |
| 15 vs. 25 | Dn | G3P7H4 | Leukocyte cell-derived chemotaxin 2 like | #N/A | 0.0000 | 0.2661 | 3.7580 |
| 15 vs. 25 | Dn | G3Q1E3 | Uncharacterized protein | Ubiquitin-conjugating enzyme E2 variant 2 | 0.0203 | 0.2845 | 3.5149 |
| 15 vs. 25 | Dn | G3NX96 | Uncharacterized protein | annotation not available | 0.0002 | 0.2866 | 3.4892 |
| 15 vs. 25 | Dn | G3PIZ9 | TIA1 cytotoxic granule associated RNA binding protein | annotation not available | 0.0188 | 0.3354 | 2.9815 |
| 15 vs. 25 | Dn | G3PH88 | Peptidylprolyl isomerase | Peptidylprolyl isomerase; FK506 binding protein 3 | 0.0000 | 0.3410 | 2.9326 |
| 15 vs. 25 | Dn | G3PUT5 | Sterol carrier protein 2a | Sterol carrier protein 2a; Belongs to the thiolase family | 0.0017 | 0.3460 | 2.8902 |
| 15 vs. 25 | Dn | G3PBZ8 | Uncharacterized protein | #N/A | 0.0024 | 0.3467 | 2.8843 |
| 15 vs. 25 | Dn | G3NC33 | Fatty acid synthase | Fatty acid synthase | 0.0004 | 0.3468 | 2.8835 |
| 15 vs. 25 | Dn | G3P8W9 | Cardiac myosin light chain-1 | Cardiac myosin light chain-1 | 0.0392 | 0.3551 | 2.8161 |
| 15 vs. 25 | Dn | G3PPX0 | Dihydropyrimidine dehydrogenase [NADP(+)] | Dihydropyrimidine dehydrogenase [NADP(+)] | 0.0019 | 0.3565 | 2.8050 |
| 15 vs. 25 | Dn | G3Q0H4 | Phosphoethanolamine methyltransferase | #N/A | 0.0009 | 0.3587 | 2.7878 |
| 15 vs. 25 | Dn | G3NB91 | Acetylserotonin O-methyltransferase-like | #N/A | 0.0022 | 0.3674 | 2.7218 |
| 15 vs. 25 | Dn | G3PJ37 | ELAV-like protein | #N/A | 0.0003 | 0.3721 | 2.6874 |
| 15 vs. 25 | Dn | G3PRF7 | Eukaryotic translation elongation factor 2b | Eukaryotic translation elongation factor 2b | 0.0003 | 0.3729 | 2.6817 |
| 15 vs. 25 | Dn | G3PBB1 | RNA binding protein S1, serine-rich domain | RNA binding protein S1, serine-rich domain | 0.0003 | 0.3786 | 2.6413 |
| 15 vs. 25 | Dn | G3PG24 | Elongation factor like GTPase 1 | Elongation factor Tu GTP binding domain containing 1 | 0.0004 | 0.3798 | 2.6330 |
| 15 vs. 25 | Dn | G3NZ73 | Sulfurtransferase | #N/A | 0.0097 | 0.3830 | 2.6110 |
| 15 vs. 25 | Dn | G3PM16 | Acid phosphatase 2, lysosomal | #N/A | 0.0001 | 0.3835 | 2.6076 |
| 15 vs. 25 | Dn | G3P2Y2 | Acetyl-CoA acetyltransferase 2 | acetyl-CoA acetyltransferase 2; Belongs to the thiolase family | 0.0128 | 0.3904 | 2.5615 |
| 15 vs. 25 | Dn | G3Q522 | Aldo-keto reductase family 1, member B1 (aldose reductase) | Aldo-keto reductase family 1, member B1 (aldose reductase) | 0.0261 | 0.4027 | 2.4832 |
| 15 vs. 25 | Dn | G3Q8K8 | UHRF1 binding protein 1-like | UHRF1 (ICBP90) binding protein 1-like | 0.0015 | 0.4102 | 2.4378 |
| 15 vs. 25 | Dn | G3N6R0 | Acyl-coenzyme A oxidase | #N/A | 0.0022 | 0.4132 | 2.4201 |
| 15 vs. 25 | Dn | G3N738 | Peptidyl-prolyl cis-trans isomerase | Peptidyl-prolyl cis-trans isomerase | 0.0020 | 0.4141 | 2.4149 |
| 15 vs. 25 | Dn | G3NLM7 | Uncharacterized protein | Adaptor-related protein complex 2, mu 1 subunit; Belongs to the adaptor complexes medium subunit family | 0.0098 | 0.4150 | 2.4096 |
| 15 vs. 25 | Dn | G3PU83 | Ribonuclease T2 | Ribonuclease T2; Belongs to the RNase T2 family | 0.0001 | 0.4164 | 2.4015 |
| 15 vs. 25 | Dn | G3P6H1 | Lipase | Lipase, gastric; Belongs to the AB hydrolase superfamily. Lipase family | 0.0008 | 0.4209 | 2.3759 |
| 15 vs. 25 | Dn | G3PY06 | Peptidylprolyl isomerase | #N/A | 0.0001 | 0.4261 | 2.3469 |
| 15 vs. 25 | Dn | G3PCW5 | Fras1 related extracellular matrix protein 2b | Fras1 related extracellular matrix protein 2b | 0.0017 | 0.4277 | 2.3381 |
| 15 vs. 25 | Dn | G3NC94 | Uncharacterized protein | poly(rC) binding protein 3 | 0.0369 | 0.4301 | 2.3250 |

| Comparison | Change | Protein Accession | Skyline Description | STRING Description | Adjusted p-value | Fold Change | Inverse Dn Fold Change |
|---|---|---|---|---|---|---|---|
| 15 vs. 25 | Dn | G3PIR4 | Ubiquilin 4 | annotation not available | 0.0001 | 0.4349 | 2.2994 |
| 15 vs. 25 | Dn | G3NT37 | Serine hydroxymethyltransferase 2 (mitochondrial) | Serine hydroxymethyltransferase 2 (mitochondrial) | 0.0053 | 0.4375 | 2.2857 |
| 15 vs. 25 | Dn | G3PKE0 | Galectin | #N/A | 0.0020 | 0.4382 | 2.2821 |
| 15 vs. 25 | Dn | G3PTV2 | Diphosphomevalonate decarboxylase | Diphosphomevalonate decarboxylase | 0.0045 | 0.4452 | 2.2462 |
| 15 vs. 25 | Dn | G3NLB9 | Uncharacterized protein | annotation not available | 0.0055 | 0.4480 | 2.2321 |
| 15 vs. 25 | Dn | G3PHA5 | Uncharacterized protein | Uncharacterized protein; Eukaryotic translation elongation factor 2a, tandem duplicate 2 | 0.0018 | 0.4487 | 2.2287 |
| 15 vs. 25 | Dn | G3Q3C6 | UDP-N-acetylglucosamine pyrophosphorylase 1, like 1 | #N/A | 0.0143 | 0.4545 | 2.2002 |
| 15 vs. 25 | Dn | G3PA08 | Uncharacterized protein (Fragment) | Uncharacterized protein; CD5 molecule-like | 0.0002 | 0.4571 | 2.1877 |
| 15 vs. 25 | Dn | G3N7N7 | Allantoicase | Allantoicase | 0.0130 | 0.4588 | 2.1796 |
| 15 vs. 25 | Dn | G3NRP8 | Uncharacterized protein | Uncharacterized protein; Involved in the regulation of homocysteine metabolism | 0.0014 | 0.4599 | 2.1744 |
| 15 vs. 25 | Dn | G3NLD8 | High density lipoprotein binding protein a | High density lipoprotein-binding protein a | 0.0004 | 0.4723 | 2.1173 |
| 15 vs. 25 | Dn | G3N6W4 | Uncharacterized protein | #N/A | 0.0163 | 0.4724 | 2.1169 |
| 15 vs. 25 | Dn | G3NCR2 | Serine and arginine rich splicing factor 4 | Serine/arginine-rich splicing factor 4 | 0.0000 | 0.4866 | 2.0551 |
| 15 vs. 25 | Dn | G3NW60 | Peptidyl-prolyl cis-trans isomerase | Peptidyl-prolyl cis-trans isomerase | 0.0398 | 0.4869 | 2.0538 |
| 15 vs. 25 | Dn | G3PJI1 | Cathepsin K | #N/A | 0.0078 | 0.4879 | 2.0496 |
| 15 vs. 25 | Dn | G3PPW2 | Serine and arginine rich splicing factor 2b | Uncharacterized protein; Serine/arginine-rich splicing factor 2b | 0.0210 | 0.4943 | 2.0231 |
| 15 vs. 25 | Dn | G3NVV6 | TAR DNA binding protein, like | TAR DNA binding protein, like | 0.0054 | 0.4956 | 2.0178 |
| 15 vs. 25 | Dn | G3PT87 | Betaine-homocysteine methyltransferase | Betaine-homocysteine methyltransferase | 0.0003 | 0.4974 | 2.0105 |
| KL15 vs. KL25 | Up | G3PUF6 | Uncharacterized protein | annotation not available | 0.0482 | 3.0813 | |
| KL15 vs. KL25 | Up | G3PSU0 | Heterogeneous nuclear ribonucleoprotein D | #N/A | 0.0140 | 3.0214 | |
| KL15 vs. KL25 | Up | G3N992 | Uncharacterized protein | ATP synthase, H+ transporting, mitochondrial Fo complex, subunit F6 | 0.0045 | 3.0177 | |
| KL15 vs. KL25 | Up | G3PTW7 | Uncharacterized protein | OCIA domain containing 1 | 0.0140 | 2.2701 | |
| KL15 vs. KL25 | Up | G3PG45 | Uncharacterized protein | annotation not available | 0.0211 | 2.1587 | |
| KL15 vs. KL25 | Dn | G3P7H4 | Leukocyte cell-derived chemotaxin 2 like | #N/A | 0.0211 | 0.2547 | 3.9262 |
| KL15 vs. KL25 | Dn | G3Q615 | Phytanoyl-CoA 2-hydroxylase | phytanoyl-CoA 2-hydroxylase | 0.0482 | 0.2663 | 3.7552 |
| KL15 vs. KL25 | Dn | G3PH88 | Peptidylprolyl isomerase | Peptidylprolyl isomerase; FK506 binding protein 3 | 0.0021 | 0.3130 | 3.1949 |
| KL15 vs. KL25 | Dn | G3NA94 | Mitochondrial ribosomal protein S16 | Mitochondrial ribosomal protein S16 | 0.0045 | 0.3220 | 3.1056 |
| KL15 vs. KL25 | Dn | G3PU83 | Ribonuclease T2 | Ribonuclease T2; Belongs to the RNase T2 family | 0.0354 | 0.3605 | 2.7739 |
| BL15 vs. BL25 | Up | G3PL95 | Uncharacterized protein | Uncharacterized protein; Histone H1 like | 0.0117 | 15.8483 | |
| BL15 vs. BL25 | Up | G3N8L3 | Uncharacterized protein | Uncharacterized protein; Histone H1 like | 0.0133 | 15.6498 | |
| BL15 vs. BL25 | Up | G3Q568 | Uncharacterized protein | Uncharacterized protein; Caldesmon 1 like | 0.0370 | 5.0109 | |
| BL15 vs. BL25 | Up | G3Q1M1 | Uncharacterized protein | annotation not available | 0.0230 | 4.5232 | |
| BL15 vs. BL25 | Up | G3N654 | Uncharacterized protein | #N/A | 0.0159 | 3.1409 | |
| BL15 vs. BL25 | Up | G3PCP4 | SAP domain containing ribonucleoprotein | SAP domain containing ribonucleoprotein | 0.0230 | 2.9919 | |
| BL15 vs. BL25 | Up | G3Q9H7 | Zgc:194209 | Zgc:194209 | 0.0257 | 2.8798 | |
| BL15 vs. BL25 | Up | G3N992 | Uncharacterized protein | ATP synthase, H+ transporting, mitochondrial Fo complex, subunit F6 | 0.0101 | 2.6236 | |
| BL15 vs. BL25 | Up | G3PW79 | Endothelial differentiation-related factor 1 | Endothelial differentiation-related factor 1 | 0.0255 | 2.6182 | |
| BL15 vs. BL25 | Up | G3PUL5 | SERPINE1 mRNA binding protein 1b | SERPINE1 mRNA binding protein 1 | 0.0255 | 2.6106 | |
| BL15 vs. BL25 | Up | G3PSU0 | Heterogeneous nuclear ribonucleoprotein D | #N/A | 0.0246 | 2.5279 | |
| BL15 vs. BL25 | Up | G3PSF9 | Tight junction protein 1a | Tight junction protein 1a; Belongs to the MAGUK family | 0.0246 | 2.4945 | |
| BL15 vs. BL25 | Up | G3QA55 | Centromere protein V | Centromere protein V | 0.0459 | 2.3557 | |
| BL15 vs. BL25 | Up | G3P521 | Histone H2A | Histone H2A; Polyhomeotic-like 2b | 0.0061 | 2.2897 | |
| BL15 vs. BL25 | Up | G3NII0 | SUB1 homolog, transcriptional regulator b | #N/A | 0.0117 | 2.1313 | |
| BL15 vs. BL25 | Up | G3PTW7 | Uncharacterized protein | OCIA domain containing 1 | 0.0159 | 2.0989 | |
| BL15 vs. BL25 | Up | G3PCT8 | Pleckstrin homology domain containing, family A member 6 | Pleckstrin homology domain containing, family A member 6 | 0.0489 | 2.0137 | |
| BL15 vs. BL25 | Dn | G3NX96 | Uncharacterized protein | annotation not available | 0.0210 | 0.2157 | 4.6361 |
| BL15 vs. BL25 | Dn | G3PUT5 | Sterol carrier protein 2a | Sterol carrier protein 2a; Belongs to the thiolase family | 0.0159 | 0.2165 | 4.6189 |
| BL15 vs. BL25 | Dn | G3Q615 | Phytanoyl-CoA 2-hydroxylase | phytanoyl-CoA 2-hydroxylase | 0.0061 | 0.2410 | 4.1494 |
| BL15 vs. BL25 | Dn | G3PBZ8 | Uncharacterized protein | #N/A | 0.0246 | 0.2436 | 4.1051 |
| BL15 vs. BL25 | Dn | G3PRF7 | Eukaryotic translation elongation factor 2b | Eukaryotic translation elongation factor 2b | 0.0219 | 0.2698 | 3.7064 |
| BL15 vs. BL25 | Dn | G3PJ37 | ELAV-like protein | #N/A | 0.0134 | 0.2737 | 3.6536 |
| BL15 vs. BL25 | Dn | G3NC33 | Fatty acid synthase | Fatty acid synthase | 0.0219 | 0.2832 | 3.5311 |
| BL15 vs. BL25 | Dn | G3NZ73 | Sulfurtransferase | #N/A | 0.0285 | 0.2913 | 3.4329 |
| BL15 vs. BL25 | Dn | G3P7H4 | Leukocyte cell-derived chemotaxin 2 like | #N/A | 0.0225 | 0.2916 | 3.4294 |

| Comparison | Change | Protein Accession | Skyline Description | STRING Description | Adjusted p-value | Fold Change | Inverse Dn Fold Change |
|---|---|---|---|---|---|---|---|
| BL15 vs. BL25 | Dn | G3Q8K8 | UHRF1 binding protein 1-like | UHRF1 (ICBP90) binding protein 1-like | 0.0030 | 0.3039 | 3.2906 |
| BL15 vs. BL25 | Dn | G3PG24 | Elongation factor like GTPase 1 | Elongation factor Tu GTP binding domain containing 1 | 0.0245 | 0.3159 | 3.1656 |
| BL15 vs. BL25 | Dn | G3NLB9 | Uncharacterized protein | annotation not available | 0.0159 | 0.3398 | 2.9429 |
| BL15 vs. BL25 | Dn | G3P6H1 | Lipase | Lipase, gastric; Belongs to the AB hydrolase superfamily. Lipase family | 0.0363 | 0.3407 | 2.9351 |
| BL15 vs. BL25 | Dn | G3PBB1 | RNA binding protein S1, serine-rich domain | RNA binding protein S1, serine-rich domain | 0.0117 | 0.3476 | 2.8769 |
| BL15 vs. BL25 | Dn | G3PA08 | Uncharacterized protein (Fragment) | Uncharacterized protein; CD5 molecule-like | 0.0117 | 0.3568 | 2.8027 |
| BL15 vs. BL25 | Dn | G3NVV6 | TAR DNA binding protein, like | TAR DNA binding protein, like | 0.0266 | 0.3606 | 2.7732 |
| BL15 vs. BL25 | Dn | G3PM16 | Acid phosphatase 2, lysosomal | #N/A | 0.0139 | 0.3617 | 2.7647 |
| BL15 vs. BL25 | Dn | G3PJR0 | Cathepsin S, ortholog2, tandem duplicate 1 | #N/A | 0.0134 | 0.3626 | 2.7579 |
| BL15 vs. BL25 | Dn | G3PJI1 | Cathepsin K | #N/A | 0.0225 | 0.3646 | 2.7427 |
| BL15 vs. BL25 | Dn | G3PY06 | Peptidylprolyl isomerase | #N/A | 0.0117 | 0.3655 | 2.7360 |
| BL15 vs. BL25 | Dn | G3PH88 | Peptidylprolyl isomerase | Peptidylprolyl isomerase; FK506 binding protein 3 | 0.0117 | 0.3717 | 2.6903 |
| BL15 vs. BL25 | Dn | G3PKE0 | Galectin | #N/A | 0.0266 | 0.3733 | 2.6788 |
| BL15 vs. BL25 | Dn | G3PCW5 | Fras1 related extracellular matrix protein 2b | Fras1 related extracellular matrix protein 2b | 0.0413 | 0.3741 | 2.6731 |
| BL15 vs. BL25 | Dn | G3PCV6 | Uncharacterized protein (Fragment) | annotation not available | 0.0134 | 0.3775 | 2.6490 |
| BL15 vs. BL25 | Dn | G3PET7 | Legumain | Legumain | 0.0030 | 0.3845 | 2.6008 |
| BL15 vs. BL25 | Dn | G3PR69 | Nascent polypeptide associated complex subunit alpha | Uncharacterized protein; Nascent polypeptide-associated complex alpha subunit | 0.0117 | 0.3942 | 2.5368 |
| BL15 vs. BL25 | Dn | G3PCG0 | Ribosomal protein S27a | #N/A | 0.0427 | 0.3948 | 2.5329 |
| BL15 vs. BL25 | Dn | G3Q313 | Heterogeneous nuclear ribonucleoprotein H1 | #N/A | 0.0407 | 0.3950 | 2.5316 |
| BL15 vs. BL25 | Dn | G3PT26 | Ubiquitin specific peptidase 47 | Ubiquitin specific peptidase 47; Belongs to the peptidase C19 family | 0.0278 | 0.3951 | 2.5310 |
| BL15 vs. BL25 | Dn | G3P2N9 | Nucleolin | Nucleolin | 0.0182 | 0.3967 | 2.5208 |
| BL15 vs. BL25 | Dn | G3PT87 | Betaine-homocysteine methyltransferase | Betaine-homocysteine methyltransferase | 0.0117 | 0.3997 | 2.5019 |
| BL15 vs. BL25 | Dn | G3PUI3 | Ribosomal protein L37 | Ribosomal protein L37; Binds to the 23S rRNA | 0.0285 | 0.4020 | 2.4876 |
| BL15 vs. BL25 | Dn | G3PCI1 | Tubulin alpha chain | Tubulin alpha chain | 0.0101 | 0.4022 | 2.4863 |
| BL15 vs. BL25 | Dn | G3PFH7 | Uncharacterized protein (Fragment) | annotation not available | 0.0255 | 0.4039 | 2.4759 |
| BL15 vs. BL25 | Dn | G3PLP5 | Ubiquitin family domain containing 1 | Ubiquitin family domain containing 1 | 0.0245 | 0.4067 | 2.4588 |
| BL15 vs. BL25 | Dn | G3PKM0 | Eukaryotic translation initiation factor 3 subunit G | Eukaryotic translation initiation factor 3 subunit G | 0.0117 | 0.4153 | 2.4079 |
| BL15 vs. BL25 | Dn | G3N810 | Peptidyl-prolyl cis-trans isomerase | #N/A | 0.0101 | 0.4235 | 2.3613 |
| BL15 vs. BL25 | Dn | G3PRS7 | Eukaryotic translation elongation factor 1 beta 2 | Eukaryotic translation elongation factor 1 beta 2 | 0.0350 | 0.4435 | 2.2548 |
| BL15 vs. BL25 | Dn | G3P4B9 | Uncharacterized protein | Heterogeneous nuclear ribonucleoprotein A1a | 0.0278 | 0.4488 | 2.2282 |
| BL15 vs. BL25 | Dn | G3NQE8 | Uncharacterized protein | Uncharacterized protein; RAD23 homolog Aa (S. cerevisiae) | 0.0255 | 0.4604 | 2.1720 |
| BL15 vs. BL25 | Dn | G3PA75 | Thioredoxin domain containing 17 | Thioredoxin domain containing 17 | 0.0255 | 0.4612 | 2.1683 |
| BL15 vs. BL25 | Dn | G3PIR4 | Ubiquilin 4 | annotation not available | 0.0486 | 0.4620 | 2.1645 |
| BL15 vs. BL25 | Dn | G3NQ97 | Fetuin B | Fetuin B | 0.0117 | 0.4683 | 2.1354 |
| BL15 vs. BL25 | Dn | G3N7F6 | Uncharacterized protein | Far upstream element (FUSE) binding protein 3 | 0.0230 | 0.4698 | 2.1286 |
| BL15 vs. BL25 | Dn | G3PU83 | Ribonuclease T2 | Ribonuclease T2; Belongs to the RNase T2 family | 0.0304 | 0.4809 | 2.0794 |
| BL15 vs. BL25 | Dn | G3NI02 | Filamin B | Filamin B, like | 0.0245 | 0.4819 | 2.0751 |
| BL15 vs. BL25 | Dn | G3NCR2 | Serine and arginine rich splicing factor 4 | Serine/arginine-rich splicing factor 4 | 0.0139 | 0.4820 | 2.0747 |
| BL15 vs. BL25 | Dn | G3NU73 | Poly(rC) binding protein 2 | #N/A | 0.0255 | 0.4860 | 2.0576 |
| BL15 vs. BL25 | Dn | G3NGF0 | Natural killer cell triggering receptor | Natural killer cell triggering receptor | 0.0266 | 0.4877 | 2.0504 |
| BL15 vs. BL25 | Dn | G3NVX4 | Peptidyl-prolyl cis-trans isomerase E | Peptidyl-prolyl cis-trans isomerase E | 0.0314 | 0.4903 | 2.0396 |
| BL15 vs. BL25 | Dn | G3PZS2 | Ribosomal protein L12 | #N/A | 0.0182 | 0.4993 | 2.0028 |
| 7 vs. 25 | Up | G3N8L3 | Uncharacterized protein | Uncharacterized protein; Histone H1 like | 0.0004 | 10.5298 | |
| 7 vs. 25 | Up | G3PL95 | Uncharacterized protein | Uncharacterized protein; Histone H1 like | 0.0008 | 8.0420 | |
| 7 vs. 25 | Up | G3P7C9 | Host cell factor C1a | Host cell factor C1b | 0.0092 | 7.5975 | |
| 7 vs. 25 | Up | G3NY82 | PDZ and LIM domain 5a | PDZ and LIM domain 5a | 0.0004 | 6.7042 | |
| 7 vs. 25 | Up | G3Q568 | Uncharacterized protein | Uncharacterized protein; Caldesmon 1 like | 0.0000 | 5.3293 | |
| 7 vs. 25 | Up | G3N5J6 | Uncharacterized protein | Uncharacterized protein; Histone H1 like | 0.0001 | 4.6973 | |
| 7 vs. 25 | Up | G3NTZ7 | Uncharacterized protein | annotation not available | 0.0001 | 4.5613 | |
| 7 vs. 25 | Up | G3PCP4 | SAP domain containing ribonucleoprotein | SAP domain containing ribonucleoprotein | 0.0000 | 4.2752 | |
| 7 vs. 25 | Up | G3P8Z9 | Tropomyosin 1 | Zgc:171719; Tropomyosin 1 (alpha) | 0.0008 | 4.2598 | |
| 7 vs. 25 | Up | G3N4A5 | Calponin | Calponin | 0.0000 | 4.2000 | |
| 7 vs. 25 | Up | G3PGC4 | Uncharacterized protein | Uncharacterized protein; Periaxin | 0.0003 | 4.1195 | |
| 7 vs. 25 | Up | G3N8J7 | Histone H2A | annotation not available | 0.0005 | 4.0665 | |
| 7 vs. 25 | Up | G3Q0J5 | Uncharacterized protein (Fragment) | #N/A | 0.0000 | 3.9307 | |
| 7 vs. 25 | Up | G3NZ55 | Eukaryotic translation initiation factor 4Bb | #N/A | 0.0013 | 3.7549 | |
| 7 vs. 25 | Up | G3NWG9 | Si:ch211-103n10.5 | Si:ch211-103n10.5 | 0.0098 | 3.7260 | |
| 7 vs. 25 | Up | G3PPE0 | Glutathione S-transferase theta 1a | #N/A | 0.0216 | 3.6715 | |
| 7 vs. 25 | Up | G3PSU0 | Heterogeneous nuclear ribonucleoprotein D | #N/A | 0.0000 | 3.6586 | |

| Comparison | Change | Protein Accession | Skyline Description | STRING Description | Adjusted p-value | Fold Change | Inverse Dn Fold Change |
|---|---|---|---|---|---|---|---|
| 7 vs. 25 | Up | G3P5E3 | Uncharacterized protein | Collagen, type XIV, alpha 1 | 0.0007 | 3.6432 | |
| 7 vs. 25 | Up | G3PLM8 | Histone H2A | annotation not available | 0.0169 | 3.5797 | |
| 7 vs. 25 | Up | G3NIA3 | Succinate dehydrogenase complex assembly factor 4 | Succinate dehydrogenase complex assembly factor 4; Chromosome 6 open reading frame 57 | 0.0007 | 3.4991 | |
| 7 vs. 25 | Up | G3N654 | Uncharacterized protein | #N/A | 0.0000 | 3.4165 | |
| 7 vs. 25 | Up | I7LRE8 | HN1-like protein | Jupiter microtubule associated homolog 2; Hematological and neurological expressed 1-like | 0.0491 | 3.3908 | |
| 7 vs. 25 | Up | G3N829 | Histone H3 | H3 histone, family 3C | 0.0080 | 3.3533 | |
| 7 vs. 25 | Up | G3N8J1 | Histone H4 | Histone H4; Core component of nucleosome. | 0.0003 | 3.2876 | |
| 7 vs. 25 | Up | G3PTW7 | Uncharacterized protein | OCIA domain containing 1 | 0.0000 | 3.1804 | |
| 7 vs. 25 | Up | G3Q990 | Ependymin-like 1 | Ependymin-like 1 | 0.0001 | 3.1706 | |
| 7 vs. 25 | Up | G3Q1M1 | Uncharacterized protein | annotation not available | 0.0015 | 3.1531 | |
| 7 vs. 25 | Up | G3Q3Z9 | Tropomyosin 2 (beta) | Tropomyosin 2 (beta); Belongs to the tropomyosin family | 0.0013 | 3.1102 | |
| 7 vs. 25 | Up | G3N8L5 | Histone H3 | annotation not available | 0.0013 | 3.0796 | |
| 7 vs. 25 | Up | G3NDG3 | Plectin a | Plectin a | 0.0001 | 3.0654 | |
| 7 vs. 25 | Up | G3ND30 | Peptide-methionine (R)-S-oxide reductase | #N/A | 0.0002 | 3.0298 | |
| 7 vs. 25 | Up | G3P8Z5 | Tropomyosin 1 | #N/A | 0.0014 | 3.0225 | |
| 7 vs. 25 | Up | G3NIM8 | Uncharacterized protein | Uncharacterized protein; Calcium binding and coiled-coil domain 2 | 0.0002 | 2.9239 | |
| 7 vs. 25 | Up | G3N992 | Uncharacterized protein | ATP synthase, H+ transporting, mitochondrial Fo complex, subunit F6 | 0.0004 | 2.9001 | |
| 7 vs. 25 | Up | G3N752 | Histone H2A | H2A histone family, member Z | 0.0072 | 2.8596 | |
| 7 vs. 25 | Up | G3PZB6 | Uncharacterized protein (Fragment) | annotation not available | 0.0007 | 2.8308 | |
| 7 vs. 25 | Up | G3N831 | Histone H2A | annotation not available | 0.0000 | 2.8112 | |
| 7 vs. 25 | Up | G3Q0J6 | Uncharacterized protein (Fragment) | AHNAK nucleoprotein | 0.0000 | 2.8043 | |
| 7 vs. 25 | Up | G3PUL5 | SERPINE1 mRNA binding protein 1b | SERPINE1 mRNA binding protein 1 | 0.0004 | 2.7050 | |
| 7 vs. 25 | Up | G3NMR4 | Si:dkey-165n16.1 | Si:dkey-165n16.1 | 0.0003 | 2.6653 | |
| 7 vs. 25 | Up | G3PSF9 | Tight junction protein 1a | Tight junction protein 1a; Belongs to the MAGUK family | 0.0001 | 2.6431 | |
| 7 vs. 25 | Up | G3NKI7 | Glyoxylate reductase 1 homolog (Arabidopsis) | Glyoxylate reductase 1 homolog (Arabidopsis) | 0.0036 | 2.6000 | |
| 7 vs. 25 | Up | G3PLA9 | Uncharacterized protein | Uncharacterized protein; Beta globin (LOC100174873), mRNA | 0.0020 | 2.5994 | |
| 7 vs. 25 | Up | G3Q3K8 | Eukaryotic translation initiation factor 4E binding protein 3, like | Eukaryotic translation initiation factor 4E binding protein 3, like | 0.0178 | 2.5637 | |
| 7 vs. 25 | Up | G3PBA6 | Cysteine-rich protein 2 | annotation not available | 0.0137 | 2.5326 | |
| 7 vs. 25 | Up | G3NCR7 | Death-associated protein | Death associated protein | 0.0124 | 2.5275 | |
| 7 vs. 25 | Up | G3NBK5 | PITH (C-terminal proteasome-interacting domain of thioredoxin-like) domain containing 1 | #N/A | 0.0000 | 2.5119 | |
| 7 vs. 25 | Up | G3NXD1 | Glutathione S-transferase rho | Glutathione S-transferase rho; Zgc:162356 | 0.0019 | 2.5005 | |
| 7 vs. 25 | Up | G3P455 | LIM and SH3 protein 1 | #N/A | 0.0007 | 2.4609 | |
| 7 vs. 25 | Up | G3PW79 | Endothelial differentiation-related factor 1 | Endothelial differentiation-related factor 1 | 0.0001 | 2.4396 | |
| 7 vs. 25 | Up | G3P834 | Translocase of inner mitochondrial membrane 13 homolog (yeast) | #N/A | 0.0005 | 2.4202 | |
| 7 vs. 25 | Up | G3P1Q8 | Coiled-coil domain containing 124 | Coiled-coil domain containing 124 | 0.0020 | 2.4181 | |
| 7 vs. 25 | Up | G3P0A9 | Uncharacterized protein | Uncharacterized protein; TRAF-type zinc finger domain containing 1 | 0.0128 | 2.4168 | |
| 7 vs. 25 | Up | G3P2U9 | H1 histone family, member 0 | H1 histone family, member 0 | 0.0066 | 2.4147 | |
| 7 vs. 25 | Up | G3P1F8 | Uncharacterized protein | annotation not available | 0.0030 | 2.3885 | |
| 7 vs. 25 | Up | G3Q1V8 | Uncharacterized protein | KIAA1191 | 0.0003 | 2.3793 | |
| 7 vs. 25 | Up | G3N8I6 | Uncharacterized protein | Uncharacterized protein; Histone H1 like | 0.0294 | 2.3730 | |
| 7 vs. 25 | Up | G3PPI0 | Uncharacterized protein | Complement factor properdin | 0.0008 | 2.3722 | |
| 7 vs. 25 | Up | G3PWS1 | Nucleophosmin 1b | Nucleophosmin 1b (nucleolar phosphoprotein B23, numatrin) | 0.0006 | 2.3520 | |
| 7 vs. 25 | Up | G3Q933 | RNA binding motif protein 4.3 | #N/A | 0.0015 | 2.3420 | |
| 7 vs. 25 | Up | G3NJB7 | Voltage-dependent anion channel 3 | Voltage-dependent anion channel 3 | 0.0088 | 2.3382 | |
| 7 vs. 25 | Up | G3PG45 | Uncharacterized protein | annotation not available | 0.0077 | 2.3052 | |
| 7 vs. 25 | Up | G3NII0 | SUB1 homolog, transcriptional regulator b | #N/A | 0.0000 | 2.2773 | |
| 7 vs. 25 | Up | G3P6K2 | Ezrin b | Ezrin b | 0.0051 | 2.2762 | |
| 7 vs. 25 | Up | G3P7U2 | Tpd52 like 2b | Tumor protein D52-like 2b | 0.0005 | 2.2612 | |
| 7 vs. 25 | Up | G3P1C3 | NADH:ubiquinone oxidoreductase subunit A7 | NADH dehydrogenase (ubiquinone) 1 alpha subcomplex, 7 | 0.0122 | 2.2062 | |
| 7 vs. 25 | Up | G3P3G0 | Protein phosphatase 1, regulatory (inhibitor) subunit 2 | Protein phosphatase 1, regulatory (inhibitor) subunit 2 | 0.0020 | 2.1825 | |
| 7 vs. 25 | Up | G3PUF6 | Uncharacterized protein | annotation not available | 0.0059 | 2.1587 | |
| 7 vs. 25 | Up | G3NXB8 | Glutathione S-transferase rho | Glutathione S-transferase rho; Zgc:162356 | 0.0271 | 2.1527 | |
| 7 vs. 25 | Up | G3NDJ4 | Multiple coagulation factor deficiency 2 | Multiple coagulation factor deficiency 2 | 0.0002 | 2.1490 | |
| 7 vs. 25 | Up | G3NG31 | Coiled-coil domain containing 58 | #N/A | 0.0020 | 2.1310 | |
| 7 vs. 25 | Up | G3NR25 | Uncharacterized protein | annotation not available | 0.0154 | 2.1304 | |
| 7 vs. 25 | Up | G3PYY3 | Phosphotriesterase related | Phosphotriesterase related | 0.0179 | 2.1181 | |

| Comparison | Change | Protein Accession | Skyline Description | STRING Description | Adjusted p-value | Fold Change | Inverse Dn Fold Change |
|---|---|---|---|---|---|---|---|
| 7 vs. 25 | Up | G3P3U6 | ATP synthase inhibitory factor subunit 1b | ATPase inhibitory factor 1b | 0.0074 | 2.0852 | |
| 7 vs. 25 | Up | G3PS27 | Coagulation factor VIIi | Coagulation factor VIIi | 0.0075 | 2.0714 | |
| 7 vs. 25 | Up | G3PAJ7 | Calreticulin | Calreticulin, like 2 | 0.0199 | 2.0477 | |
| 7 vs. 25 | Up | G3PJ54 | Vacuolar protein sorting 4b homolog B (S. cerevisiae) | Vacuolar protein sorting 4b (yeast); Belongs to the AAA ATPase family | 0.0037 | 2.0310 | |
| 7 vs. 25 | Dn | G3P7H4 | Leukocyte cell-derived chemotaxin 2 like | #N/A | 0.0000 | 0.1002 | 9.9800 |
| 7 vs. 25 | Dn | G3NA94 | Mitochondrial ribosomal protein S16 | Mitochondrial ribosomal protein S16 | 0.0091 | 0.1304 | 7.6687 |
| 7 vs. 25 | Dn | G3PIZ9 | TIA1 cytotoxic granule associated RNA binding protein | annotation not available | 0.0002 | 0.1896 | 5.2743 |
| 7 vs. 25 | Dn | G3NWV4 | Calcium-transporting ATPase | Calcium-transporting ATPase | 0.0005 | 0.2248 | 4.4484 |
| 7 vs. 25 | Dn | G3NGD4 | Podocan | Podocan | 0.0036 | 0.2301 | 4.3459 |
| 7 vs. 25 | Dn | G3Q1E3 | Uncharacterized protein | Ubiquitin-conjugating enzyme E2 variant 2 | 0.0092 | 0.2405 | 4.1580 |
| 7 vs. 25 | Dn | G3PG24 | Elongation factor like GTPase 1 | Elongation factor Tu GTP binding domain containing 1 | 0.0004 | 0.2642 | 3.7850 |
| 7 vs. 25 | Dn | G3PBZ8 | Uncharacterized protein | #N/A | 0.0013 | 0.2734 | 3.6576 |
| 7 vs. 25 | Dn | G3P6H1 | Lipase | Lipase, gastric; Belongs to the AB hydrolase superfamily. Lipase family | 0.0000 | 0.2811 | 3.5575 |
| 7 vs. 25 | Dn | G3PH88 | Peptidylprolyl isomerase | Peptidylprolyl isomerase; FK506 binding protein 3 | 0.0000 | 0.2930 | 3.4130 |
| 7 vs. 25 | Dn | G3Q3W7 | ATP-binding cassette, sub-family A (ABC1), member 1A | ATP-binding cassette, sub-family A (ABC1), member 1A | 0.0093 | 0.3122 | 3.2031 |
| 7 vs. 25 | Dn | G3NYH2 | Serine and arginine rich splicing factor 5b | Serine/arginine-rich splicing factor 5b | 0.0236 | 0.3147 | 3.1776 |
| 7 vs. 25 | Dn | G3PCW5 | Fras1 related extracellular matrix protein 2b | Fras1 related extracellular matrix protein 2b | 0.0011 | 0.3153 | 3.1716 |
| 7 vs. 25 | Dn | G3PJ37 | ELAV-like protein | #N/A | 0.0007 | 0.3170 | 3.1546 |
| 7 vs. 25 | Dn | G3PRF7 | Eukaryotic translation elongation factor 2b | Eukaryotic translation elongation factor 2b | 0.0001 | 0.3233 | 3.0931 |
| 7 vs. 25 | Dn | G3PUI3 | Ribosomal protein L37 | Ribosomal protein L37; Binds to the 23S rRNA | 0.0001 | 0.3317 | 3.0148 |
| 7 vs. 25 | Dn | G3Q3W0 | 3-hydroxy-3-methylglutaryl coenzyme A synthase | 3-hydroxy-3-methylglutaryl coenzyme A synthase | 0.0000 | 0.3382 | 2.9568 |
| 7 vs. 25 | Dn | G3NB91 | Acetylserotonin O-methyltransferase-like | #N/A | 0.0013 | 0.3415 | 2.9283 |
| 7 vs. 25 | Dn | G3PHB5 | Ribosomal protein S29 | #N/A | 0.0335 | 0.3421 | 2.9231 |
| 7 vs. 25 | Dn | G3NC94 | Uncharacterized protein | poly(rC) binding protein 3 | 0.0019 | 0.3530 | 2.8329 |
| 7 vs. 25 | Dn | G3PT26 | Ubiquitin specific peptidase 47 | Ubiquitin specific peptidase 47; Belongs to the peptidase C19 family | 0.0004 | 0.3606 | 2.7732 |
| 7 vs. 25 | Dn | G3Q8K8 | UHRF1 binding protein 1-like | UHRF1 (ICBP90) binding protein 1-like | 0.0024 | 0.3634 | 2.7518 |
| 7 vs. 25 | Dn | G3PVW5 | Isocitrate dehydrogenase [NADP] | Isocitrate dehydrogenase 2 (NADP+), mitochondrial | 0.0092 | 0.3689 | 2.7108 |
| 7 vs. 25 | Dn | G3Q615 | Phytanoyl-CoA 2-hydroxylase | phytanoyl-CoA 2-hydroxylase | 0.0007 | 0.3727 | 2.6831 |
| 7 vs. 25 | Dn | G3Q313 | Heterogeneous nuclear ribonucleoprotein H1 | #N/A | 0.0001 | 0.3741 | 2.6731 |
| 7 vs. 25 | Dn | G3PBB1 | RNA binding protein S1, serine-rich domain | RNA binding protein S1, serine-rich domain | 0.0013 | 0.3823 | 2.6157 |
| 7 vs. 25 | Dn | G3PIR4 | Ubiquilin 4 | annotation not available | 0.0000 | 0.3830 | 2.6110 |
| 7 vs. 25 | Dn | G3NVV6 | TAR DNA binding protein, like | TAR DNA binding protein, like | 0.0002 | 0.3854 | 2.5947 |
| 7 vs. 25 | Dn | G3NLM7 | Uncharacterized protein | Adaptor-related protein complex 2, mu 1 subunit | 0.0021 | 0.3884 | 2.5747 |
| 7 vs. 25 | Dn | G3N9N6 | Nucleolar protein interacting with the FHA domain of MKI67 | Nucleolar protein interacting with the FHA domain of MKI67 | 0.0066 | 0.3963 | 2.5233 |
| 7 vs. 25 | Dn | G3PVR3 | DIS3-like exonuclease 2 | DIS3-like exonuclease 2; 3'-5'-exoribonuclease that specifically recognizes RNAs polyuridylated at their 3' end and mediates their degradation. | 0.0136 | 0.3965 | 2.5221 |
| 7 vs. 25 | Dn | G3NU73 | Poly(rC) binding protein 2 | #N/A | 0.0000 | 0.4028 | 2.4826 |
| 7 vs. 25 | Dn | G3NZ73 | Sulfurtransferase | #N/A | 0.0154 | 0.4042 | 2.4740 |
| 7 vs. 25 | Dn | G3Q0H4 | Phosphoethanolamine methyltransferase | #N/A | 0.0049 | 0.4046 | 2.4716 |
| 7 vs. 25 | Dn | G3N6W4 | Uncharacterized protein | #N/A | 0.0014 | 0.4048 | 2.4704 |
| 7 vs. 25 | Dn | G3P2Y2 | Acetyl-CoA acetyltransferase 2 | acetyl-CoA acetyltransferase 2; Belongs to the thiolase family | 0.0491 | 0.4053 | 2.4673 |
| 7 vs. 25 | Dn | G3Q522 | Aldo-keto reductase family 1, member B1 (aldose reductase) | Aldo-keto reductase family 1, member B1 (aldose reductase) | 0.0447 | 0.4062 | 2.4618 |
| 7 vs. 25 | Dn | G3PHA5 | Uncharacterized protein | Uncharacterized protein; Eukaryotic translation elongation factor 2a, tandem duplicate 2 | 0.0025 | 0.4064 | 2.4606 |
| 7 vs. 25 | Dn | G3P9T5 | L-threonine dehydrogenase | L-threonine dehydrogenase | 0.0016 | 0.4070 | 2.4570 |
| 7 vs. 25 | Dn | G3PVS.6 | Heterogeneous nuclear ribonucleoprotein A0b | Heterogeneous nuclear ribonucleoprotein A0b | 0.0013 | 0.4098 | 2.4402 |
| 7 vs. 25 | Dn | G3PLP5 | Ubiquitin family domain containing 1 | Ubiquitin family domain containing 1 | 0.0028 | 0.4156 | 2.4062 |
| 7 vs. 25 | Dn | G3NLD8 | High density lipoprotein binding protein a | High density lipoprotein-binding protein a | 0.0000 | 0.4167 | 2.3998 |
| 7 vs. 25 | Dn | G3PUT5 | Sterol carrier protein 2a | Sterol carrier protein 2a; Belongs to the thiolase family | 0.0083 | 0.4214 | 2.3730 |
| 7 vs. 25 | Dn | G3N738 | Peptidyl-prolyl cis-trans isomerase | Peptidyl-prolyl cis-trans isomerase | 0.0019 | 0.4227 | 2.3657 |
| 7 vs. 25 | Dn | G3NDN6 | Uncharacterized protein | #N/A | 0.0058 | 0.4247 | 2.3546 |
| 7 vs. 25 | Dn | G3PA08 | Uncharacterized protein (Fragment) | Uncharacterized protein; CD5 molecule-like | 0.0036 | 0.4261 | 2.3469 |
| 7 vs. 25 | Dn | G3NPS5 | Eukaryotic translation initiation factor 4eb | Eukaryotic translation initiation factor 4eb | 0.0319 | 0.4279 | 2.3370 |

| Comparison | Change | Protein Accession | Skyline Description | STRING Description | Adjusted p-value | Fold Change | Inverse Dn Fold Change |
|---|---|---|---|---|---|---|---|
| 7 vs. 25 | Dn | G3PU83 | Ribonuclease T2 | Ribonuclease T2; Belongs to the RNase T2 family | 0.0002 | 0.4323 | 2.3132 |
| 7 vs. 25 | Dn | G3PRS7 | Eukaryotic translation elongation factor 1 beta 2 | Eukaryotic translation elongation factor 1 beta 2; Belongs to the EF-1-beta/EF-1-delta family | 0.0001 | 0.4397 | 2.2743 |
| 7 vs. 25 | Dn | G3NC33 | Fatty acid synthase | Fatty acid synthase | 0.0405 | 0.4461 | 2.2416 |
| 7 vs. 25 | Dn | G3PS00 | Coatomer subunit beta' | Coatomer subunit beta' | 0.0090 | 0.4474 | 2.2351 |
| 7 vs. 25 | Dn | G3P216 | ATP-citrate synthase | ATP-citrate synthase | 0.0004 | 0.4483 | 2.2306 |
| 7 vs. 25 | Dn | G3PG61 | Spectrin beta chain | Spectrin, beta, non-erythrocytic 4 | 0.0361 | 0.4485 | 2.2297 |
| 7 vs. 25 | Dn | G3NI04 | Polyadenylate-binding protein | #N/A | 0.0000 | 0.4591 | 2.1782 |
| 7 vs. 25 | Dn | G3PTV2 | Diphosphomevalonate decarboxylase | Diphosphomevalonate decarboxylase | 0.0013 | 0.4605 | 2.1716 |
| 7 vs. 25 | Dn | G3NYK9 | Uncharacterized protein | annotation not available | 0.0101 | 0.4620 | 2.1645 |
| 7 vs. 25 | Dn | G3NMN0 | Threonyl-tRNA synthetase | #N/A | 0.0004 | 0.4629 | 2.1603 |
| 7 vs. 25 | Dn | G3PQ71 | Uncharacterized protein | annotation not available | 0.0037 | 0.4653 | 2.1492 |
| 7 vs. 25 | Dn | G3PKE0 | Galectin | #N/A | 0.0060 | 0.4688 | 2.1331 |
| 7 vs. 25 | Dn | G3PY06 | Peptidylprolyl isomerase | #N/A | 0.0007 | 0.4696 | 2.1295 |
| 7 vs. 25 | Dn | G3PEV0 | Uncharacterized protein | Ubiquitin-conjugating enzyme E2, J1 | 0.0020 | 0.4714 | 2.1213 |
| 7 vs. 25 | Dn | G3N810 | Peptidyl-prolyl cis-trans isomerase | #N/A | 0.0004 | 0.4736 | 2.1115 |
| 7 vs. 25 | Dn | G3PX14 | Uncharacterized protein | Fibrillin 1 | 0.0014 | 0.4751 | 2.1048 |
| 7 vs. 25 | Dn | G3P506 | Valyl-tRNA synthetase | valyl-tRNA synthetase; Belongs to the class-I aminoacyl-tRNA synthetase family | 0.0161 | 0.4756 | 2.1026 |
| 7 vs. 25 | Dn | G3PXB5 | GTPase activating protein (SH3 domain) binding protein 1 | #N/A | 0.0037 | 0.4761 | 2.1004 |
| 7 vs. 25 | Dn | G3NJ90 | Signal recognition particle 9 kDa protein | Signal recognition particle 9 kDa protein | 0.0101 | 0.4802 | 2.0825 |
| 7 vs. 25 | Dn | G3PKM0 | Eukaryotic translation initiation factor 3 subunit G | Eukaryotic translation initiation factor 3 subunit G | 0.0001 | 0.4843 | 2.0648 |
| 7 vs. 25 | Dn | G3NXH2 | Uncharacterized protein | Basic leucine zipper and W2 domains 1a | 0.0156 | 0.4869 | 2.0538 |
| 7 vs. 25 | Dn | G3PCG0 | Ribosomal protein S27a | #N/A | 0.0193 | 0.4900 | 2.0408 |
| 7 vs. 25 | Dn | G3NK02 | Transcription factor BTF3 | Basic transcription factor 3; Belongs to the NAC-beta family | 0.0000 | 0.4941 | 2.0239 |
| 7 vs. 25 | Dn | G3PR63 | Mitochondrial ribosomal protein L27 | Mitochondrial ribosomal protein L27 | 0.0007 | 0.4988 | 2.0048 |
| 7 vs. 25 | Dn | G3PPW2 | Serine and arginine rich splicing factor 2b | Uncharacterized protein; Serine/arginine-rich splicing factor 2b | 0.0156 | 0.4994 | 2.0024 |
| KL7 vs. KL25 | Up | G3PLM8 | Histone H2A | annotation not available | 0.0279 | 7.9529 | |
| KL7 vs. KL25 | Up | G3N8J7 | Histone H2A | annotation not available | 0.0114 | 7.3250 | |
| KL7 vs. KL25 | Up | G3PT85 | Dimethylglycine dehydrogenase | Dimethylglycine dehydrogenase | 0.0384 | 5.5879 | |
| KL7 vs. KL25 | Up | G3Q568 | Uncharacterized protein | Uncharacterized protein; Caldesmon 1 like | 0.0114 | 5.3271 | |
| KL7 vs. KL25 | Up | G3Q0J5 | Uncharacterized protein (Fragment) | #N/A | 0.0113 | 4.5543 | |
| KL7 vs. KL25 | Up | G3PLA9 | Uncharacterized protein | Uncharacterized protein; Beta globin (LOC100174873), mRNA | 0.0109 | 4.5363 | |
| KL7 vs. KL25 | Up | G3P8Z9 | Tropomyosin 1 | Zgc:171719; Tropomyosin 1 (alpha) | 0.0266 | 4.2899 | |
| KL7 vs. KL25 | Up | G3N8S9 | Glutamate dehydrogenase 1a | Glutamate dehydrogenase 1a | 0.0278 | 4.2653 | |
| KL7 vs. KL25 | Up | G3NXH8 | Heat shock cognate 70 | #N/A | 0.0060 | 3.9640 | |
| KL7 vs. KL25 | Up | G3PTW7 | Uncharacterized protein | OCIA domain containing 1 | 0.0016 | 3.8666 | |
| KL7 vs. KL25 | Up | G3Q0L3 | Uncharacterized protein | Purine nucleoside phosphorylase 5b | 0.0421 | 3.8491 | |
| KL7 vs. KL25 | Up | G3NDG3 | Plectin a | Plectin a | 0.0190 | 3.8414 | |
| KL7 vs. KL25 | Up | G3Q990 | Ependymin-like 1 | Ependymin-like 1 | 0.0114 | 3.7124 | |
| KL7 vs. KL25 | Up | G3NJB7 | Voltage-dependent anion channel 3 | Voltage-dependent anion channel 3 | 0.0190 | 3.7118 | |
| KL7 vs. KL25 | Up | G3PYU1 | Cathepsin D | Cathepsin D; Belongs to the peptidase A1 family | 0.0292 | 3.6742 | |
| KL7 vs. KL25 | Up | G3NJ86 | Aldehyde dehydrogenase 2 family member, tandem duplicate 2 | #N/A | 0.0255 | 3.5198 | |
| KL7 vs. KL25 | Up | G3PYY3 | Phosphotriesterase related | Phosphotriesterase related | 0.0190 | 3.5167 | |
| KL7 vs. KL25 | Up | G3N7K9 | UTP--glucose-1-phosphate uridylyltransferase | #N/A | 0.0307 | 3.4046 | |
| KL7 vs. KL25 | Up | G3P7C9 | Host cell factor C1a | Host cell factor C1b | 0.0497 | 3.3672 | |
| KL7 vs. KL25 | Up | G3PGC4 | Uncharacterized protein | Uncharacterized protein; Periaxin | 0.0315 | 3.2905 | |
| KL7 vs. KL25 | Up | G3N831 | Histone H2A | annotation not available | 0.0060 | 3.2777 | |
| KL7 vs. KL25 | Up | G3P6A1 | Uncharacterized protein (Fragment) | annotation not available | 0.0016 | 3.1428 | |
| KL7 vs. KL25 | Up | G3P2N4 | Heat shock 60 protein 1 | #N/A | 0.0068 | 3.1086 | |
| KL7 vs. KL25 | Up | G3Q0J6 | Uncharacterized protein (Fragment) | AHNAK nucleoprotein | 0.0083 | 3.0854 | |
| KL7 vs. KL25 | Up | G3N4A5 | Calponin | Calponin | 0.0109 | 3.0513 | |
| KL7 vs. KL25 | Up | G3PCP4 | SAP domain containing ribonucleoprotein | SAP domain containing ribonucleoprotein | 0.0190 | 3.0506 | |
| KL7 vs. KL25 | Up | G3Q3Z9 | Tropomyosin 2 (beta) | Tropomyosin 2 (beta); Belongs to the tropomyosin family | 0.0455 | 2.9770 | |
| KL7 vs. KL25 | Up | G3NBK5 | PITH (C-terminal proteasome-interacting domain of thioredoxin-like) domain containing 1 | #N/A | 0.0191 | 2.9679 | |
| KL7 vs. KL25 | Up | G3N710 | Alpha-1,4 glucan phosphorylase | Alpha-1,4 glucan phosphorylase | 0.0060 | 2.9630 | |
| KL7 vs. KL25 | Up | G3N816 | Enolase 3, (beta, muscle) | Enolase 3, (beta, muscle) | 0.0428 | 2.9208 | |
| KL7 vs. KL25 | Up | G3N5J6 | Uncharacterized protein | Uncharacterized protein; Histone H1 like | 0.0442 | 2.8712 | |
| KL7 vs. KL25 | Up | G3N577 | Uncharacterized protein | annotation not available | 0.0406 | 2.8695 | |
| KL7 vs. KL25 | Up | G3PSU0 | Heterogeneous nuclear ribonucleoprotein D | #N/A | 0.0271 | 2.8691 | |
| KL7 vs. KL25 | Up | G3PUE4 | Glyoxylate reductase/hydroxypyruvate reductase b | Glyoxylate reductase/hydroxypyruvate reductase b | 0.0266 | 2.8552 | |

| Comparison | Change | Protein Accession | Skyline Description | STRING Description | Adjusted p-value | Fold Change | Inverse Dn Fold Change |
|---|---|---|---|---|---|---|---|
| KL7 vs. KL25 | Up | G3PAG5 | Aldehyde dehydrogenase 8 family, member A1 | Aldehyde dehydrogenase 8 family, member A1 | 0.0428 | 2.8504 | |
| KL7 vs. KL25 | Up | G3NT91 | Sialic acid acetylesterase | Sialic acid acetylesterase | 0.0368 | 2.8392 | |
| KL7 vs. KL25 | Up | G3NRQ4 | Uncharacterized protein | #N/A | 0.0292 | 2.7790 | |
| KL7 vs. KL25 | Up | G3Q9G8 | Single-stranded DNA binding protein 1 | Single-stranded DNA binding protein 1 | 0.0190 | 2.5444 | |
| KL7 vs. KL25 | Up | G3NXY4 | Phosphoglycerate mutase | Phosphoglycerate mutase 1a | 0.0301 | 2.5247 | |
| KL7 vs. KL25 | Up | G3NGT2 | Multifunctional fusion protein | #N/A | 0.0407 | 2.4611 | |
| KL7 vs. KL25 | Up | G3QA55 | Centromere protein V | Centromere protein V | 0.0439 | 2.4569 | |
| KL7 vs. KL25 | Up | G3N9H1 | Enolase 1b, (alpha) | Enolase 1b, (alpha) | 0.0315 | 2.4341 | |
| KL7 vs. KL25 | Up | G3Q1V8 | Uncharacterized protein | KIAA1191 | 0.0428 | 2.2851 | |
| KL7 vs. KL25 | Up | G3NG31 | Coiled-coil domain containing 58 | #N/A | 0.0428 | 2.2064 | |
| KL7 vs. KL25 | Up | G3PYR1 | Transaldolase | Transaldolase | 0.0138 | 2.1664 | |
| KL7 vs. KL25 | Up | G3P7U2 | Tpd52 like 2b | Tumor protein D52-like 2b | 0.0406 | 2.1640 | |
| KL7 vs. KL25 | Up | G3P8K7 | Histone H2A | annotation not available | 0.0407 | 2.1450 | |
| KL7 vs. KL25 | Up | G3N654 | Uncharacterized protein | #N/A | 0.0098 | 2.0954 | |
| KL7 vs. KL25 | Up | G3PD28 | Early endosome antigen 1 | Early endosome antigen 1 | 0.0455 | 2.0733 | |
| KL7 vs. KL25 | Dn | G3P7H4 | Leukocyte cell-derived chemotaxin 2 like | #N/A | 0.0016 | 0.1199 | 8.3403 |
| KL7 vs. KL25 | Dn | G3PHB3 | Ribosomal protein S29 | #N/A | 0.0234 | 0.1346 | 7.4294 |
| KL7 vs. KL25 | Dn | G3NYH2 | Serine and arginine rich splicing factor 5b | Serine/arginine-rich splicing factor 5b | 0.0060 | 0.1565 | 6.3898 |
| KL7 vs. KL25 | Dn | G3PUI3 | Ribosomal protein L37 | Ribosomal protein L37; Binds to the 23S rRNA | 0.0005 | 0.2059 | 4.8567 |
| KL7 vs. KL25 | Dn | G3PH88 | Peptidylprolyl isomerase | Peptidylprolyl isomerase; FK506 binding protein 3 | 0.0000 | 0.2161 | 4.6275 |
| KL7 vs. KL25 | Dn | G3Q313 | Heterogeneous nuclear ribonucleoprotein H1 | #N/A | 0.0074 | 0.2772 | 3.6075 |
| KL7 vs. KL25 | Dn | G3PIR4 | Ubiquilin 4 | annotation not available | 0.0016 | 0.2899 | 3.4495 |
| KL7 vs. KL25 | Dn | G3NVV6 | TAR DNA binding protein, like | TAR DNA binding protein, like | 0.0190 | 0.3357 | 2.9789 |
| KL7 vs. KL25 | Dn | G3PR63 | Mitochondrial ribosomal protein L27 | Mitochondrial ribosomal protein L27 | 0.0053 | 0.3509 | 2.8498 |
| KL7 vs. KL25 | Dn | G3Q3W0 | 3-hydroxy-3-methylglutaryl coenzyme A synthase | 3-hydroxy-3-methylglutaryl coenzyme A synthase | 0.0251 | 0.3540 | 2.8249 |
| KL7 vs. KL25 | Dn | G3NU73 | Poly(rC) binding protein 2 | #N/A | 0.0023 | 0.3553 | 2.8145 |
| KL7 vs. KL25 | Dn | G3NLD8 | High density lipoprotein binding protein a | High density lipoprotein-binding protein a | 0.0083 | 0.3590 | 2.7855 |
| KL7 vs. KL25 | Dn | G3PET7 | Legumain | Legumain | 0.0060 | 0.3756 | 2.6624 |
| KL7 vs. KL25 | Dn | G3PQ71 | Uncharacterized protein | annotation not available | 0.0455 | 0.3843 | 2.6021 |
| KL7 vs. KL25 | Dn | G3PWR7 | Far upstream element (FUSE) binding protein 3 | #N/A | 0.0148 | 0.3856 | 2.5934 |
| KL7 vs. KL25 | Dn | G3NMM0 | Mitochondrial ribosomal protein L14 | Mitochondrial ribosomal protein L14 | 0.0166 | 0.3881 | 2.5767 |
| KL7 vs. KL25 | Dn | G3Q9F3 | Eukaryotic translation initiation factor 4A1A | #N/A | 0.0315 | 0.4127 | 2.4231 |
| KL7 vs. KL25 | Dn | G3PT87 | Betaine-homocysteine methyltransferase | Betaine-homocysteine methyltransferase | 0.0060 | 0.4129 | 2.4219 |
| KL7 vs. KL25 | Dn | G3NSU1 | COX assembly mitochondrial protein | COX assembly mitochondrial protein 1 homolog (S. cerevisiae) | 0.0387 | 0.4158 | 2.4050 |
| KL7 vs. KL25 | Dn | G3PFB4 | Uncharacterized protein | Heterogeneous nuclear ribonucleoprotein L | 0.0109 | 0.4170 | 2.3981 |
| KL7 vs. KL25 | Dn | G3NHX9 | Translocase of outer mitochondrial membrane 34 | Translocase of outer mitochondrial membrane 34 | 0.0016 | 0.4177 | 2.3941 |
| KL7 vs. KL25 | Dn | G3NHG6 | Mitochondrial ribosomal protein L41 | Mitochondrial ribosomal protein L41 | 0.0231 | 0.4261 | 2.3469 |
| KL7 vs. KL25 | Dn | G3PJ89 | Mitochondrial ribosomal protein S18A | Mitochondrial ribosomal protein S18A | 0.0475 | 0.4283 | 2.3348 |
| KL7 vs. KL25 | Dn | G3PH61 | 40S ribosomal protein S30 | #N/A | 0.0492 | 0.4384 | 2.2810 |
| KL7 vs. KL25 | Dn | G3NCR2 | Serine and arginine rich splicing factor 4 | Serine/arginine-rich splicing factor 4 | 0.0060 | 0.4549 | 2.1983 |
| KL7 vs. KL25 | Dn | G3NK02 | Transcription factor BTF3 | Basic transcription factor 3; Belongs to the NAC-beta family | 0.0060 | 0.4605 | 2.1716 |
| KL7 vs. KL25 | Dn | G3P3P1 | Uncharacterized protein | annotation not available | 0.0323 | 0.4671 | 2.1409 |
| KL7 vs. KL25 | Dn | G3NS60 | DExD-box helicase 39A | #N/A | 0.0148 | 0.4698 | 2.1286 |
| KL7 vs. KL25 | Dn | G3NNX3 | Insulin-like growth factor 2 mRNA binding protein 1 | Insulin-like growth factor 2 mRNA binding protein 1 | 0.0114 | 0.4958 | 2.0169 |
| BL7 vs. BL25 | Up | G3N8L3 | Uncharacterized protein | Uncharacterized protein; Histone H1 like | 0.0015 | 35.4330 | |
| BL7 vs. BL25 | Up | G3PL95 | Uncharacterized protein | Uncharacterized protein; Histone H1 like | 0.0138 | 16.2084 | |
| BL7 vs. BL25 | Up | G3NY82 | PDZ and LIM domain 5a | PDZ and LIM domain 5a | 0.0051 | 10.7273 | |
| BL7 vs. BL25 | Up | G3Q568 | Uncharacterized protein | Uncharacterized protein; Caldesmon 1 like | 0.0052 | 8.5117 | |
| BL7 vs. BL25 | Up | G3N5J6 | Uncharacterized protein | Uncharacterized protein; Histone H1 like | 0.0085 | 7.6275 | |
| BL7 vs. BL25 | Up | G3PCP4 | SAP domain containing ribonucleoprotein | SAP domain containing ribonucleoprotein | 0.0015 | 7.5484 | |
| BL7 vs. BL25 | Up | G3NIA3 | Succinate dehydrogenase complex assembly factor 4 | Succinate dehydrogenase complex assembly factor 4; Chromosome 6 open reading frame 57 | 0.0052 | 7.1361 | |
| BL7 vs. BL25 | Up | G3PGC4 | Uncharacterized protein | Uncharacterized protein; Periaxin | 0.0070 | 6.8951 | |
| BL7 vs. BL25 | Up | G3NWG9 | Si:ch211-103n10.5 | Si:ch211-103n10.5 | 0.0331 | 6.6329 | |
| BL7 vs. BL25 | Up | G3N4A5 | Calponin | Calponin | 0.0017 | 5.8903 | |
| BL7 vs. BL25 | Up | G3NZ55 | Eukaryotic translation initiation factor 4Bb | #N/A | 0.0158 | 5.6812 | |
| BL7 vs. BL25 | Up | G3Q3K8 | Eukaryotic translation initiation factor 4E binding protein 3, like | Eukaryotic translation initiation factor 4E binding protein 3, like | 0.0166 | 5.6509 | |

| Comparison | Change | Protein Accession | Skyline Description | STRING Description | Adjusted p-value | Fold Change | Inverse Dn Fold Change |
|---|---|---|---|---|---|---|---|
| BL7 vs. BL25 | Up | G3NTZ7 | Uncharacterized protein | annotation not available | 0.0035 | 5.5612 | |
| BL7 vs. BL25 | Up | G3Q1M1 | Uncharacterized protein | annotation not available | 0.0052 | 5.2472 | |
| BL7 vs. BL25 | Up | G3PSI1 | Signal transducer and activator of transcription | Signal transduction and activation of transcription 1a | 0.0356 | 4.9234 | |
| BL7 vs. BL25 | Up | G3Q0J5 | Uncharacterized protein (Fragment) | #N/A | 0.0019 | 4.6076 | |
| BL7 vs. BL25 | Up | G3PBA6 | Cysteine-rich protein 2 | annotation not available | 0.0097 | 4.5132 | |
| BL7 vs. BL25 | Up | G3PSU0 | Heterogeneous nuclear ribonucleoprotein D | #N/A | 0.0018 | 4.2657 | |
| BL7 vs. BL25 | Up | G3P971 | Eukaryotic translation initiation factor 2B, subunit 4 delta | Eukaryotic translation initiation factor 2B, subunit 4 delta | 0.0148 | 4.0873 | |
| BL7 vs. BL25 | Up | G3PUL5 | SERPINE1 mRNA binding protein 1b | SERPINE1 mRNA binding protein 1 | 0.0022 | 4.0825 | |
| BL7 vs. BL25 | Up | G3N654 | Uncharacterized protein | #N/A | 0.0015 | 4.0460 | |
| BL7 vs. BL25 | Up | G3NHA0 | Metadherin a | Metadherin a | 0.0446 | 3.9025 | |
| BL7 vs. BL25 | Up | G3P1C3 | NADH:ubiquinone oxidoreductase subunit A7 | NADH dehydrogenase (ubiquinone) 1 alpha subcomplex, 7 | 0.0037 | 3.8269 | |
| BL7 vs. BL25 | Up | G3NSL0 | Eukaryotic translation initiation factor 3 subunit H | #N/A | 0.0457 | 3.7070 | |
| BL7 vs. BL25 | Up | G3P1Q8 | Coiled-coil domain containing 124 | Coiled-coil domain containing 124 | 0.0052 | 3.6857 | |
| BL7 vs. BL25 | Up | G3PSF9 | Tight junction protein 1a | Tight junction protein 1a; Belongs to the MAGUK family | 0.0022 | 3.6479 | |
| BL7 vs. BL25 | Up | G3ND30 | Peptide-methionine (R)-S-oxide reductase | #N/A | 0.0052 | 3.6396 | |
| BL7 vs. BL25 | Up | G3PW79 | Endothelial differentiation-related factor 1 | Endothelial differentiation-related factor 1 | 0.0015 | 3.3807 | |
| BL7 vs. BL25 | Up | G3P2U9 | H1 histone family, member 0 | H1 histone family, member 0 | 0.0359 | 3.3030 | |
| BL7 vs. BL25 | Up | G3Q933 | RNA binding motif protein 4.3 | #N/A | 0.0217 | 3.2716 | |
| BL7 vs. BL25 | Up | G3P455 | LIM and SH3 protein 1 | #N/A | 0.0073 | 3.2512 | |
| BL7 vs. BL25 | Up | G3PZB6 | Uncharacterized protein (Fragment) | annotation not available | 0.0403 | 3.1903 | |
| BL7 vs. BL25 | Up | G3PFC9 | Coiled-coil domain containing 9 | Coiled-coil domain containing 9 | 0.0166 | 3.1424 | |
| BL7 vs. BL25 | Up | G3Q0J6 | Uncharacterized protein (Fragment) | AHNAK nucleoprotein | 0.0022 | 3.1410 | |
| BL7 vs. BL25 | Up | G3P3U6 | ATP synthase inhibitory factor subunit 1b | ATPase inhibitory factor 1b | 0.0135 | 3.1389 | |
| BL7 vs. BL25 | Up | G3P1F8 | Uncharacterized protein | annotation not available | 0.0257 | 2.9531 | |
| BL7 vs. BL25 | Up | G3PWS1 | Nucleophosmin 1b | Nucleophosmin 1b (nucleolar phosphoprotein B23, numatrin); Nucleophosmin/nucleoplasmin, 1b | 0.0128 | 2.9506 | |
| BL7 vs. BL25 | Up | G3Q1V8 | Uncharacterized protein | KIAA1191 | 0.0073 | 2.9432 | |
| BL7 vs. BL25 | Up | G3P8F3 | Cytochrome c oxidase subunit | Cytochrome c oxidase subunit | 0.0357 | 2.8505 | |
| BL7 vs. BL25 | Up | G3NMR4 | Si:dkey-165n16.1 | Si:dkey-165n16.1 | 0.0085 | 2.7575 | |
| BL7 vs. BL25 | Up | G3Q829 | Zinc finger, C3HC-type containing 1 | Zinc finger, C3HC-type containing 1 | 0.0246 | 2.7408 | |
| BL7 vs. BL25 | Up | G3P3G0 | Protein phosphatase 1, regulatory (inhibitor) subunit 2 | Protein phosphatase 1, regulatory (inhibitor) subunit 2 | 0.0220 | 2.7398 | |
| BL7 vs. BL25 | Up | G3NIM8 | Uncharacterized protein | Uncharacterized protein; Calcium binding and coiled-coil domain 2 | 0.0140 | 2.6964 | |
| BL7 vs. BL25 | Up | G3PTW7 | Uncharacterized protein | OCIA domain containing 1 | 0.0015 | 2.6474 | |
| BL7 vs. BL25 | Up | G3P8Z5 | Tropomyosin 1 | #N/A | 0.0306 | 2.5998 | |
| BL7 vs. BL25 | Up | G3PVY2 | High mobility group box 2a | High-mobility group box 2a | 0.0443 | 2.5865 | |
| BL7 vs. BL25 | Up | G3N8J7 | Histone H2A | annotation not available | 0.0399 | 2.5847 | |
| BL7 vs. BL25 | Up | G3N992 | Uncharacterized protein | ATP synthase, H+ transporting, mitochondrial Fo complex, subunit F6 | 0.0052 | 2.5703 | |
| BL7 vs. BL25 | Up | G3Q6Z0 | Zinc finger protein 207, b | Zinc finger protein 207, b | 0.0170 | 2.5471 | |
| BL7 vs. BL25 | Up | G3N831 | Histone H2A | annotation not available | 0.0056 | 2.5381 | |
| BL7 vs. BL25 | Up | G3P819 | Adhesion regulating molecule 1 | Adhesion regulating molecule 1 | 0.0458 | 2.5251 | |
| BL7 vs. BL25 | Up | G3Q4G5 | Uncharacterized protein | Uncharacterized protein; Zgc:66433 | 0.0282 | 2.5186 | |
| BL7 vs. BL25 | Up | G3PAP4 | Synaptosomal-associated protein | Synaptosomal-associated protein, 23kDa; Belongs to the SNAP-25 family | 0.0094 | 2.5036 | |
| BL7 vs. BL25 | Up | G3PA37 | Uncharacterized protein | Haptoglobin | 0.0172 | 2.4770 | |
| BL7 vs. BL25 | Up | G3P7U2 | Tpd52 like 2b | Tumor protein D52-like 2b | 0.0290 | 2.4684 | |
| BL7 vs. BL25 | Up | G3P834 | Translocase of inner mitochondrial membrane 13 homolog (yeast) | #N/A | 0.0172 | 2.4628 | |
| BL7 vs. BL25 | Up | G3PCT8 | Pleckstrin homology domain containing, family A member 6 | Pleckstrin homology domain containing, family A member 6 | 0.0094 | 2.4517 | |
| BL7 vs. BL25 | Up | G3NY43 | LSM14A mRNA processing body assembly factor a | LSM14A mRNA processing body assembly factor a; LSM14 homolog Aa (SCD6, S. cerevisiae) | 0.0149 | 2.4497 | |
| BL7 vs. BL25 | Up | G3PX82 | RAN binding protein 3b | #N/A | 0.0491 | 2.4440 | |
| BL7 vs. BL25 | Up | G3NG31 | Coiled-coil domain containing 58 | #N/A | 0.0085 | 2.4177 | |
| BL7 vs. BL25 | Up | G3NDG3 | Plectin a | Plectin a | 0.0195 | 2.4002 | |
| BL7 vs. BL25 | Up | G3NZM5 | U6 snRNA-associated Sm-like protein LSm4 | LSM4 homolog, U6 small nuclear RNA associated (S. cerevisiae) | 0.0392 | 2.3736 | |
| BL7 vs. BL25 | Up | G3NII0 | SUB1 homolog, transcriptional regulator b | #N/A | 0.0022 | 2.3712 | |
| BL7 vs. BL25 | Up | G3P521 | Histone H2A | Histone H2A; Polyhomeotic-like 2b; Belongs to the histone H2A family | 0.0015 | 2.3644 | |
| BL7 vs. BL25 | Up | G3PCN8 | SAP domain containing ribonucleoprotein | #N/A | 0.0232 | 2.3144 | |
| BL7 vs. BL25 | Up | G3PJ42 | Aly/REF export factor | Aly/REF export factor | 0.0246 | 2.3094 | |

| Comparison | Change | Protein Accession | Skyline Description | STRING Description | Adjusted p-value | Fold Change | Inverse Dn Fold Change |
|---|---|---|---|---|---|---|---|
| BL7 vs. BL25 | Up | G3PSD1 | Eukaryotic translation initiation factor 3 subunit J | Eukaryotic translation initiation factor 3 subunit J | 0.0403 | 2.2882 | |
| BL7 vs. BL25 | Up | G3NL79 | La ribonucleoprotein domain family, member 1B | La ribonucleoprotein domain family, member 1B | 0.0290 | 2.2751 | |
| BL7 vs. BL25 | Up | G3Q9H7 | Zgc:194209 | Zgc:194209 | 0.0431 | 2.2707 | |
| BL7 vs. BL25 | Up | G3P199 | EWS RNA-binding protein 1b | #N/A | 0.0219 | 2.2698 | |
| BL7 vs. BL25 | Up | G3PXG1 | PDZ and LIM domain 5b | PDZ and LIM domain 5b | 0.0111 | 2.2544 | |
| BL7 vs. BL25 | Up | G3PJ54 | Vacuolar protein sorting 4b homolog B (S. cerevisiae) | Vacuolar protein sorting 4b (yeast); Belongs to the AAA ATPase family | 0.0418 | 2.2162 | |
| BL7 vs. BL25 | Up | G3PUD6 | Protein transport protein sec16 | Protein transport protein sec16 | 0.0107 | 2.1952 | |
| BL7 vs. BL25 | Up | G3PWB1 | Peptidyl-prolyl cis-trans isomerase | Protein (peptidyl-prolyl cis/trans isomerase) NIMA-interacting 1 | 0.0345 | 2.1947 | |
| BL7 vs. BL25 | Up | G3PPI0 | Uncharacterized protein | Complement factor properdin | 0.0345 | 2.1945 | |
| BL7 vs. BL25 | Up | G3PLU1 | Apoptotic chromatin condensation inducer 1a | Apoptotic chromatin condensation inducer 1b | 0.0195 | 2.1937 | |
| BL7 vs. BL25 | Up | G3P6Y2 | Bromodomain containing 4 | Bromodomain containing 4 | 0.0171 | 2.1804 | |
| BL7 vs. BL25 | Up | G3PG45 | Uncharacterized protein | annotation not available | 0.0397 | 2.1721 | |
| BL7 vs. BL25 | Up | G3NH63 | Uncharacterized protein | Translational machinery associated 7 homolog (S. cerevisiae) | 0.0380 | 2.1655 | |
| BL7 vs. BL25 | Up | G3NBK5 | PITH (C-terminal proteasome-interacting domain of thioredoxin-like) domain containing 1 | #N/A | 0.0107 | 2.1392 | |
| BL7 vs. BL25 | Up | G3NPM9 | ATP-dependent Clp protease proteolytic subunit | ClpP caseinolytic peptidase, ATP-dependent, proteolytic subunit homolog (E. coli) | 0.0345 | 2.0761 | |
| BL7 vs. BL25 | Up | G3P2I2 | Uncharacterized protein | Uncharacterized protein; Calpastatin | 0.0486 | 2.0065 | |
| BL7 vs. BL25 | Dn | G3P7H4 | Leukocyte cell-derived chemotaxin 2 like | #N/A | 0.0017 | 0.0861 | 11.6144 |
| BL7 vs. BL25 | Dn | G3PBZ8 | Uncharacterized protein | #N/A | 0.0022 | 0.1264 | 7.9114 |
| BL7 vs. BL25 | Dn | G3PIZ9 | TIA1 cytotoxic granule associated RNA binding protein | annotation not available | 0.0073 | 0.1525 | 6.5574 |
| BL7 vs. BL25 | Dn | G3NWV4 | Calcium-transporting ATPase | Calcium-transporting ATPase | 0.0085 | 0.1798 | 5.5617 |
| BL7 vs. BL25 | Dn | G3PG24 | Elongation factor like GTPase 1 | Elongation factor Tu GTP binding domain containing 1 | 0.0111 | 0.1940 | 5.1546 |
| BL7 vs. BL25 | Dn | G3P6H1 | Lipase | Lipase, gastric | 0.0022 | 0.1960 | 5.1020 |
| BL7 vs. BL25 | Dn | G3PRF7 | Eukaryotic translation elongation factor 2b | Eukaryotic translation elongation factor 2b | 0.0022 | 0.2002 | 4.9950 |
| BL7 vs. BL25 | Dn | G3NLM7 | Uncharacterized protein | Adaptor-related protein complex 2, mu 1 subunit; Belongs to the adaptor complexes medium subunit family | 0.0056 | 0.2089 | 4.7870 |
| BL7 vs. BL25 | Dn | G3PJ37 | ELAV-like protein | #N/A | 0.0081 | 0.2156 | 4.6382 |
| BL7 vs. BL25 | Dn | G3PT26 | Ubiquitin specific peptidase 47 | Ubiquitin specific peptidase 47; Belongs to the peptidase C19 family | 0.0022 | 0.2212 | 4.5208 |
| BL7 vs. BL25 | Dn | G3PCW5 | Fras1 related extracellular matrix protein 2b | Fras1 related extracellular matrix protein 2b | 0.0234 | 0.2479 | 4.0339 |
| BL7 vs. BL25 | Dn | G3NZ73 | Sulfurtransferase | #N/A | 0.0111 | 0.2503 | 3.9952 |
| BL7 vs. BL25 | Dn | G3PA08 | Uncharacterized protein (Fragment) | Uncharacterized protein; CD5 molecule-like | 0.0023 | 0.2609 | 3.8329 |
| BL7 vs. BL25 | Dn | G3NB91 | Acetylserotonin O-methyltransferase-like | #N/A | 0.0022 | 0.2677 | 3.7355 |
| BL7 vs. BL25 | Dn | G3Q3W0 | 3-hydroxy-3-methylglutaryl coenzyme A synthase | 3-hydroxy-3-methylglutaryl coenzyme A synthase | 0.0015 | 0.2679 | 3.7327 |
| BL7 vs. BL25 | Dn | G3Q8K8 | UHRF1 binding protein 1-like | UHRF1 (ICBP90) binding protein 1-like | 0.0052 | 0.2685 | 3.7244 |
| BL7 vs. BL25 | Dn | G3PVW5 | Isocitrate dehydrogenase [NADP] | Isocitrate dehydrogenase 2 (NADP+), mitochondrial | 0.0088 | 0.2692 | 3.7147 |
| BL7 vs. BL25 | Dn | G3N6W4 | Uncharacterized protein | #N/A | 0.0101 | 0.2715 | 3.6832 |
| BL7 vs. BL25 | Dn | G3Q615 | Phytanoyl-CoA 2-hydroxylase | phytanoyl-CoA 2-hydroxylase | 0.0111 | 0.2810 | 3.5587 |
| BL7 vs. BL25 | Dn | G3P4B9 | Uncharacterized protein | Heterogeneous nuclear ribonucleoprotein A1a | 0.0015 | 0.2824 | 3.5411 |
| BL7 vs. BL25 | Dn | G3PUT5 | Sterol carrier protein 2a | Sterol carrier protein 2a; Belongs to the thiolase family | 0.0232 | 0.2877 | 3.4758 |
| BL7 vs. BL25 | Dn | G3NC94 | Uncharacterized protein | poly(rC) binding protein 3 | 0.0197 | 0.2913 | 3.4329 |
| BL7 vs. BL25 | Dn | G3PHA5 | Uncharacterized protein | Uncharacterized protein; Eukaryotic translation elongation factor 2a, tandem duplicate 2 | 0.0254 | 0.2936 | 3.4060 |
| BL7 vs. BL25 | Dn | G3PJI1 | Cathepsin K | #N/A | 0.0384 | 0.2937 | 3.4048 |
| BL7 vs. BL25 | Dn | G3NKR5 | Uncharacterized protein | G1 to S phase transition 1 | 0.0015 | 0.2959 | 3.3795 |
| BL7 vs. BL25 | Dn | G3P9T5 | L-threonine dehydrogenase | L-threonine dehydrogenase | 0.0357 | 0.2978 | 3.3580 |
| BL7 vs. BL25 | Dn | G3PCV6 | Uncharacterized protein (Fragment) | annotation not available | 0.0015 | 0.2996 | 3.3378 |
| BL7 vs. BL25 | Dn | G3Q313 | Heterogeneous nuclear ribonucleoprotein H1 | #N/A | 0.0052 | 0.3056 | 3.2723 |
| BL7 vs. BL25 | Dn | G3NVV6 | TAR DNA binding protein, like | TAR DNA binding protein, like | 0.0106 | 0.3065 | 3.2626 |
| BL7 vs. BL25 | Dn | G3Q0H4 | Phosphoethanolamine methyltransferase | #N/A | 0.0292 | 0.3080 | 3.2468 |
| BL7 vs. BL25 | Dn | G3P2N9 | Nucleolin | Nucleolin | 0.0140 | 0.3130 | 3.1949 |
| BL7 vs. BL25 | Dn | G3NI35 | Uncharacterized protein | annotation not available | 0.0123 | 0.3187 | 3.1377 |
| BL7 vs. BL25 | Dn | G3NI41 | Myosin 1D | Si:ch211-94l19.4; Myosin ID | 0.0056 | 0.3212 | 3.1133 |
| BL7 vs. BL25 | Dn | G3PRS7 | Eukaryotic translation elongation factor 1 beta 2 | Eukaryotic translation elongation factor 1 beta 2 | 0.0018 | 0.3274 | 3.0544 |
| BL7 vs. BL25 | Dn | G3PWX3 | Eukaryotic translation initiation factor 3 subunit B | Eukaryotic translation initiation factor 3 subunit B | 0.0388 | 0.3290 | 3.0395 |
| BL7 vs. BL25 | Dn | G3PLP5 | Ubiquitin family domain containing 1 | Ubiquitin family domain containing 1 | 0.0345 | 0.3327 | 3.0057 |
| BL7 vs. BL25 | Dn | G3PG61 | Spectrin beta chain | Spectrin, beta, non-erythrocytic 4 | 0.0105 | 0.3350 | 2.9851 |

| Comparison | Change | Protein Accession | Skyline Description | STRING Description | Adjusted p-value | Fold Change | Inverse Dn Fold Change |
|---|---|---|---|---|---|---|---|
| BL7 vs. BL25 | Dn | G3PBB1 | RNA binding protein S1, serine-rich domain | RNA binding protein S1, serine-rich domain | 0.0111 | 0.3415 | 2.9283 |
| BL7 vs. BL25 | Dn | G3PS00 | Coatomer subunit beta' | Coatomer subunit beta' | 0.0106 | 0.3427 | 2.9180 |
| BL7 vs. BL25 | Dn | G3PMF2 | Gamma-glutamylamine cyclotransferase, tandem duplicate 3 | Gamma-glutamylamine cyclotransferase, tandem duplicate 2 | 0.0474 | 0.3474 | 2.8785 |
| BL7 vs. BL25 | Dn | G3N738 | Peptidyl-prolyl cis-trans isomerase | Peptidyl-prolyl cis-trans isomerase | 0.0132 | 0.3483 | 2.8711 |
| BL7 vs. BL25 | Dn | G3PEV0 | Uncharacterized protein | Ubiquitin-conjugating enzyme E2, J1 | 0.0187 | 0.3495 | 2.8612 |
| BL7 vs. BL25 | Dn | G3P0I6 | S-adenosylmethionine synthase | S-adenosylmethionine synthase | 0.0286 | 0.3540 | 2.8249 |
| BL7 vs. BL25 | Dn | G3PR69 | Nascent polypeptide associated complex subunit alpha | Uncharacterized protein; Nascent polypeptide-associated complex alpha subunit | 0.0094 | 0.3541 | 2.8241 |
| BL7 vs. BL25 | Dn | G3Q9V8 | STT3A, subunit of the oligosaccharyltransferase complex (catalytic) | STT3A, subunit of the oligosaccharyltransferase complex (catalytic); Integral membrane protein 1 | 0.0015 | 0.3590 | 2.7855 |
| BL7 vs. BL25 | Dn | G3PFH7 | Uncharacterized protein (Fragment) | annotation not available | 0.0246 | 0.3677 | 2.7196 |
| BL7 vs. BL25 | Dn | G3N6B1 | Asparaginyl-tRNA synthetase | asparaginyl-tRNA synthetase | 0.0399 | 0.3685 | 2.7137 |
| BL7 vs. BL25 | Dn | G3PU83 | Ribonuclease T2 | Ribonuclease T2; Belongs to the RNase T2 family | 0.0022 | 0.3706 | 2.6983 |
| BL7 vs. BL25 | Dn | G3PX14 | Uncharacterized protein | Fibrillin 1 | 0.0159 | 0.3719 | 2.6889 |
| BL7 vs. BL25 | Dn | G3PKE0 | Galectin | #N/A | 0.0110 | 0.3720 | 2.6882 |
| BL7 vs. BL25 | Dn | G3PKM0 | Eukaryotic translation initiation factor 3 subunit G | Eukaryotic translation initiation factor 3 subunit G | 0.0017 | 0.3731 | 2.6802 |
| BL7 vs. BL25 | Dn | G3PUI3 | Ribosomal protein L37 | Ribosomal protein L37; Binds to the 23S rRNA | 0.0286 | 0.3750 | 2.6667 |
| BL7 vs. BL25 | Dn | G3PTV2 | Diphosphomevalonate decarboxylase | Diphosphomevalonate decarboxylase; Performs the first committed step in the biosynthesis of isoprenes | 0.0216 | 0.3774 | 2.6497 |
| BL7 vs. BL25 | Dn | G3PUA5 | Eukaryotic translation initiation factor 4A, isoform 2 | Eukaryotic translation initiation factor 4A, isoform 2 | 0.0140 | 0.3789 | 2.6392 |
| BL7 vs. BL25 | Dn | G3NYK9 | Uncharacterized protein | annotation not available | 0.0286 | 0.3791 | 2.6378 |
| BL7 vs. BL25 | Dn | G3P3A2 | Synaptotagmin binding, cytoplasmic RNA interacting protein, like | Synaptotagmin binding, cytoplasmic RNA interacting protein, like | 0.0211 | 0.3795 | 2.6350 |
| BL7 vs. BL25 | Dn | G3QAZ2 | Transcription elongation regulator 1 | Transcription elongation regulator 1a (CA150) | 0.0192 | 0.3834 | 2.6082 |
| BL7 vs. BL25 | Dn | G3NB86 | ARP1 actin related protein 1, centractin | #N/A | 0.0232 | 0.3926 | 2.5471 |
| BL7 vs. BL25 | Dn | G3NI02 | Filamin B | Filamin B, like | 0.0115 | 0.4015 | 2.4907 |
| BL7 vs. BL25 | Dn | G3PC73 | Small nuclear ribonucleoprotein 200 (U5) | Small nuclear ribonucleoprotein 200 (U5) | 0.0232 | 0.4015 | 2.4907 |
| BL7 vs. BL25 | Dn | G3PVS.6 | Heterogeneous nuclear ribonucleoprotein A0b | Heterogeneous nuclear ribonucleoprotein A0b | 0.0150 | 0.4016 | 2.4900 |
| BL7 vs. BL25 | Dn | G3PY06 | Peptidylprolyl isomerase | #N/A | 0.0232 | 0.4029 | 2.4820 |
| BL7 vs. BL25 | Dn | G3PA13 | Uncharacterized protein | annotation not available | 0.0022 | 0.4046 | 2.4716 |
| BL7 vs. BL25 | Dn | G3N5L3 | Protein lin-7 homolog | Lin-7 homolog B (C. elegans) | 0.0388 | 0.4057 | 2.4649 |
| BL7 vs. BL25 | Dn | G3NGF8 | TIA1 cytotoxic granule-associated RNA binding protein-like 1 | TIA1 cytotoxic granule-associated RNA binding protein-like 1 | 0.0037 | 0.4064 | 2.4606 |
| BL7 vs. BL25 | Dn | G3Q708 | DnaJ (Hsp40) homolog, subfamily C, member 2 | DnaJ (Hsp40) homolog, subfamily C, member 2 | 0.0091 | 0.4075 | 2.4540 |
| BL7 vs. BL25 | Dn | G3PH88 | Peptidylprolyl isomerase | Peptidylprolyl isomerase; FK506 binding protein 3 | 0.0082 | 0.4118 | 2.4284 |
| BL7 vs. BL25 | Dn | G3NU73 | Poly(rC) binding protein 2 | #N/A | 0.0070 | 0.4119 | 2.4278 |
| BL7 vs. BL25 | Dn | G3N7N7 | Allantoicase | Allantoicase | 0.0141 | 0.4178 | 2.3935 |
| BL7 vs. BL25 | Dn | G3Q2F6 | Heat shock protein 4b | Heat shock protein 4b; Belongs to the heat shock protein 70 family | 0.0500 | 0.4178 | 2.3935 |
| BL7 vs. BL25 | Dn | G3Q9F3 | Eukaryotic translation initiation factor 4A1A | #N/A | 0.0094 | 0.4256 | 2.3496 |
| BL7 vs. BL25 | Dn | G3NRT5 | Malate dehydrogenase | Malate dehydrogenase 2, NAD (mitochondrial) | 0.0284 | 0.4303 | 2.3240 |
| BL7 vs. BL25 | Dn | G3NMN0 | Threonyl-tRNA synthetase | #N/A | 0.0026 | 0.4327 | 2.3111 |
| BL7 vs. BL25 | Dn | G3PET7 | Legumain | Legumain | 0.0023 | 0.4357 | 2.2952 |
| BL7 vs. BL25 | Dn | G3N810 | Peptidyl-prolyl cis-trans isomerase | #N/A | 0.0175 | 0.4377 | 2.2847 |
| BL7 vs. BL25 | Dn | G3N9N9 | Nucleolar protein interacting with the FHA domain of MKI67 | #N/A | 0.0034 | 0.4386 | 2.2800 |
| BL7 vs. BL25 | Dn | G3NHE9 | Ribosomal protein L30 | Ribosomal protein L30 | 0.0343 | 0.4394 | 2.2758 |
| BL7 vs. BL25 | Dn | G3NHQ7 | Tubulin alpha chain | Tubulin alpha chain | 0.0015 | 0.4403 | 2.2712 |
| BL7 vs. BL25 | Dn | G3NIZ6 | Tubulin alpha chain | Tubulin alpha chain | 0.0144 | 0.4410 | 2.2676 |
| BL7 vs. BL25 | Dn | G3NLD8 | High density lipoprotein binding protein a | High density lipoprotein-binding protein a | 0.0022 | 0.4427 | 2.2589 |
| BL7 vs. BL25 | Dn | G3N980 | Uncharacterized protein | #N/A | 0.0111 | 0.4436 | 2.2543 |
| BL7 vs. BL25 | Dn | G3NI04 | Polyadenylate-binding protein | #N/A | 0.0140 | 0.4447 | 2.2487 |
| BL7 vs. BL25 | Dn | G3PLD1 | Translocase of outer mitochondrial membrane 70 homolog A (S. cerevisiae) | Translocase of outer mitochondrial membrane 70 homolog A (yeast) | 0.0217 | 0.4451 | 2.2467 |
| BL7 vs. BL25 | Dn | G3PM16 | Acid phosphatase 2, lysosomal | #N/A | 0.0115 | 0.4481 | 2.2316 |
| BL7 vs. BL25 | Dn | G3PCI1 | Tubulin alpha chain | Tubulin alpha chain | 0.0217 | 0.4502 | 2.2212 |
| BL7 vs. BL25 | Dn | G3N7F6 | Uncharacterized protein | Far upstream element (FUSE) binding protein 3 | 0.0085 | 0.4521 | 2.2119 |
| BL7 vs. BL25 | Dn | G3NYK5 | Uncharacterized protein | #N/A | 0.0181 | 0.4561 | 2.1925 |
| BL7 vs. BL25 | Dn | G3P530 | Ubiquinol-cytochrome c reductase core protein 2b | #N/A | 0.0266 | 0.4596 | 2.1758 |
| BL7 vs. BL25 | Dn | G3P140 | Tyrosine--tRNA ligase | Tyrosine--tRNA ligase; tyrosyl-tRNA synthetase | 0.0183 | 0.4665 | 2.1436 |
| BL7 vs. BL25 | Dn | G3NT23 | Tubulin alpha chain | Tubulin alpha chain | 0.0034 | 0.4722 | 2.1177 |

| Comparison | Change | Protein Accession | Skyline Description | STRING Description | Adjusted p-value | Fold Change | Inverse Dn Fold Change |
|---|---|---|---|---|---|---|---|
| BL7 vs. BL25 | Dn | G3PHC6 | DnaJ heat shock protein family (Hsp40) member A2b | DnaJ (Hsp40) homolog, subfamily A, member 2, like | 0.0246 | 0.4826 | 2.0721 |
| BL7 vs. BL25 | Dn | G3P216 | ATP-citrate synthase | ATP-citrate synthase | 0.0357 | 0.4860 | 2.0576 |
| BL7 vs. BL25 | Dn | G3NVH8 | DEAD (Asp-Glu-Ala-Asp) box helicase 5 | DEAD (Asp-Glu-Ala-Asp) box polypeptide 5 | 0.0183 | 0.4881 | 2.0488 |
| BL7 vs. BL25 | Dn | G3PJR0 | Cathepsin S, ortholog2, tandem duplicate 1 | #N/A | 0.0219 | 0.4883 | 2.0479 |
| BL7 vs. BL25 | Dn | G3Q5E9 | KH-type splicing regulatory protein | KH-type splicing regulatory protein | 0.0037 | 0.4957 | 2.0173 |
| BL7 vs. BL25 | Dn | G3PFB4 | Uncharacterized protein | Heterogeneous nuclear ribonucleoprotein L | 0.0216 | 0.4970 | 2.0121 |

**Supplemental Table 2.2.** Functional enrichments (STRING network clusters, Uniprot keywords, PFAM protein domains, INTERPRO protein domains and features, and SMART protein domains) by comparison. Major comparisons (KL vs. BL, 15°C vs. 7°C, 15°C vs. 25°C, and 7°C vs. 25°C) were analyzed for functional enrichments with the entire liver proteome ranked by FC and include term ID, term description, genes mapped, direction of enrichment, and false discovery rate (FDR). Smaller comparisons (all others) were analyzed for functional enrichments by using only significantly different proteins (higher or lower abundance separated), and include term ID, term description, observed gene count, background gene count, and FDR.

| Comparison | Functional enrichment | #term ID | term description | genes mapped | direction | FDR |
|---|---|---|---|---|---|---|
| KL vs. BL | STRING | CL:21365 | Glycolysis, and Thiamin diphosphate-binding fold | 54 | BL > KL | 2.43E-07 |
| KL vs. BL | STRING | CL:21363 | Glycolysis, and Carbohydrate metabolism | 58 | BL > KL | 2.43E-07 |
| KL vs. BL | STRING | CL:21368 | Glycolysis, and L-lactate/malate dehydrogenase | 30 | BL > KL | 2.88E-07 |
| KL vs. BL | STRING | CL:21367 | Glycolysis, and L-lactate/malate dehydrogenase | 31 | BL > KL | 5.49E-07 |
| KL vs. BL | STRING | CL:21366 | Glycolysis, and Thiamin diphosphate-binding fold | 48 | BL > KL | 5.49E-07 |
| KL vs. BL | STRING | CL:22008 | AMP-binding, conserved site, and Aldehyde dehydrogenase domain | 42 | BL > KL | 3.50E-04 |
| KL vs. BL | STRING | CL:22009 | AMP-binding, conserved site, and Aldehyde dehydrogenase domain | 31 | BL > KL | 1.40E-03 |
| KL vs. BL | Uniprot | KW-0560 | Oxidoreductase | 42 | BL > KL | 7.30E-03 |
| KL vs. BL | PFAM | PF00538 | linker histone H1 and H5 family | 7 | KL > BL | 1.30E-03 |
| KL vs. BL | INTERPRO | IPR036388 | Winged helix-like DNA-binding domain superfamily | 20 | KL > BL | 2.70E-04 |
| KL vs. BL | INTERPRO | IPR036291 | NAD(P)-binding domain superfamily | 41 | BL > KL | 2.70E-04 |
| KL vs. BL | INTERPRO | IPR005819 | Histone H5 | 6 | KL > BL | 4.50E-04 |
| KL vs. BL | INTERPRO | IPR005818 | Linker histone H1/H5, domain H15 | 7 | KL > BL | 6.50E-04 |
| KL vs. BL | INTERPRO | IPR036390 | Winged helix DNA-binding domain superfamily | 19 | KL > BL | 2.10E-03 |
| KL vs. BL | SMART | SM00526 | Domain in histone families 1 and 5 | 7 | KL > BL | 5.50E-04 |
| **Comparison** | **Functional enrichment** | **#term ID** | **term description** | **observed gene count** | **background gene count** | **FDR** |
| KL7<BL7 | STRING | CL:7162 | mostly uncharacterized, incl. Low-density lipoprotein (LDL) receptor class A repeat, and Terpenoid cyclases/protein prenyltransferase alpha-alpha toroid | 5 | 170 | 2.20E-04 |
| KL7<BL7 | STRING | CL:7348 | LDLR class B repeat, and Lipid transport protein, beta-sheet shell | 3 | 39 | 7.50E-04 |
| KL7<BL7 | STRING | CL:7355 | Apolipoprotein A/E, and Lipoprotein N-terminal Domain | 2 | 11 | 2.90E-03 |
| KL7<BL7 | STRING | CL:22009 | AMP-binding, conserved site, and Aldehyde dehydrogenase domain | 3 | 103 | 4.50E-03 |
| KL7<BL7 | STRING | CL:26312 | Amidohydrolase family, and Purine metabolism | 2 | 25 | 7.30E-03 |
| KL7<BL7 | Uniprot | KW-0560 | Oxidoreductase | 4 | 214 | 4.50E-03 |
| KL7<BL7 | PFAM | PF07703 | Alpha-2-macroglobulin family N-terminal region | 2 | 12 | 4.80E-03 |
| KL7<BL7 | INTERPRO | IPR008927 | 6-phosphogluconate dehydrogenase-like, C-terminal domain superfamily | 2 | 15 | 7.40E-03 |
| KL7<BL7 | INTERPRO | IPR011625 | Alpha-2-macroglobulin, bait region domain | 2 | 12 | 7.40E-03 |
| KL7<BL7 | INTERPRO | IPR013328 | 6-phosphogluconate dehydrogenase, domain 2 | 2 | 9 | 7.40E-03 |
| KL7<BL7 | SMART | SM01359 | Alpha-2-Macroglobulin | 2 | 12 | 1.40E-03 |
| **Comparison** | **Functional enrichment** | **#term ID** | **term description** | **genes mapped** | **direction** | **FDR** |
| 15°C vs. 7°C | STRING | CL:21367 | Glycolysis, and L-lactate/malate dehydrogenase | 31 | 15°C > 7°C | 8.90E-04 |
| 15°C vs. 7°C | STRING | CL:21368 | Glycolysis, and L-lactate/malate dehydrogenase | 30 | 15°C > 7°C | 1.20E-03 |

| | | | | | | |
|---|---|---|---|---|---|---|
| 15°C vs. 7°C | STRING | CL:16360 | Ribosome biogenesis, and DEAD/DEAH box helicase | 24 | 7°C > 15°C | 3.70E-03 |
| 15°C vs. 7°C | STRING | CL:21791 | Tetrahydrofolate dehydrogenase/cyclohydrolase, and Pyridoxal phosphate-dependent transferase domain 1 | 23 | 15°C > 7°C | 3.90E-03 |
| 15°C vs. 7°C | STRING | CL:21363 | Glycolysis, and Carbohydrate metabolism | 58 | 15°C > 7°C | 3.90E-03 |
| 15°C vs. 7°C | STRING | CL:21371 | Glycolysis, and Enolase | 17 | 15°C > 7°C | 4.40E-03 |
| 15°C vs. 7°C | STRING | CL:16355 | mostly uncharacterized, incl. DEAD/DEAH box helicase, and Ribosome biogenesis | 25 | 7°C > 15°C | 4.40E-03 |
| 15°C vs. 7°C | STRING | CL:16363 | Ribosome biogenesis, and DEAD/DEAH box helicase | 23 | 7°C > 15°C | 4.40E-03 |
| 15°C vs. 7°C | STRING | CL:21790 | Pyridoxal phosphate-dependent transferase domain 1, and NAD(P)-binding domain | 24 | 15°C > 7°C | 5.40E-03 |
| 15°C vs. 7°C | Uniprot | KW-0324 | Glycolysis | 9 | 15°C > 7°C | 4.70E-03 |
| 15°C vs. 7°C | Uniprot | KW-0663 | Pyridoxal phosphate | 12 | 15°C > 7°C | 4.70E-03 |
| **Comparison** | **Functional enrichment** | **#term ID** | **term description** | **genes mapped** | **direction** | **FDR** |
| 15°C vs. 25°C | STRING | CL:11311 | Core histone H2A/H2B/H3/H4, and Histone H4 | 23 | 25°C > 15°C | 8.88E-09 |
| 15°C vs. 25°C | STRING | CL:11308 | Core histone H2A/H2B/H3/H4, and Histone H4 | 25 | 25°C > 15°C | 8.56E-08 |
| 15°C vs. 25°C | STRING | CL:11316 | Core histone H2A/H2B/H3/H4, and Histone H4 | 19 | 25°C > 15°C | 2.90E-05 |
| 15°C vs. 25°C | STRING | CL:11321 | Core histone H2A/H2B/H3/H4, and Histone H4 | 17 | 25°C > 15°C | 2.30E-03 |
| 15°C vs. 25°C | STRING | CL:16051 | mostly uncharacterized, incl. Ribosomal protein, and Ribosomal protein S18 | 12 | 15°C > 25°C | 2.30E-03 |
| 15°C vs. 25°C | STRING | CL:16058 | mostly uncharacterized, incl. Ribosomal protein, and Ribosomal protein S18 | 11 | 15°C > 25°C | 2.60E-03 |
| 15°C vs. 25°C | STRING | CL:16061 | Ribosomal protein, and Ribosomal protein S18 | 10 | 15°C > 25°C | 2.70E-03 |
| 15°C vs. 25°C | STRING | CL:22217 | Acyltransferase ChoActase/COT/CPT, and SCP2 sterol-binding domain | 9 | 15°C > 25°C | 2.70E-03 |
| 15°C vs. 25°C | STRING | CL:16065 | Ribosomal protein, and Translation protein SH3-like domain superfamily | 4 | 15°C > 25°C | 6.90E-03 |
| 15°C vs. 25°C | STRING | CL:16063 | Ribosomal protein, and Ribosomal protein L37/S30 | 6 | 15°C > 25°C | 8.20E-03 |
| 15°C vs. 25°C | Uniprot | KW-0158 | Chromosome | 19 | 25°C > 15°C | 2.25E-08 |
| 15°C vs. 25°C | Uniprot | KW-0238 | DNA-binding | 34 | 25°C > 15°C | 1.93E-05 |
| 15°C vs. 25°C | PFAM | PF00538 | linker histone H1 and H5 family | 7 | 25°C > 15°C | 8.43E-05 |
| 15°C vs. 25°C | INTERPRO | IPR005819 | Histone H5 | 6 | 25°C > 15°C | 4.80E-05 |
| 15°C vs. 25°C | INTERPRO | IPR005818 | Linker histone H1/H5, domain H15 | 7 | 25°C > 15°C | 8.16E-05 |
| 15°C vs. 25°C | INTERPRO | IPR036388 | Winged helix-like DNA-binding domain superfamily | 20 | 25°C > 15°C | 3.00E-03 |
| 15°C vs. 25°C | INTERPRO | IPR016039 | Thiolase-like | 4 | 15°C > 25°C | 4.10E-03 |
| 15°C vs. 25°C | INTERPRO | IPR014721 | Ribosomal protein S5 domain 2-type fold, subgroup | 5 | 15°C > 25°C | 6.10E-03 |
| 15°C vs. 25°C | SMART | SM00526 | Domain in histone families 1 and 5 | 7 | 25°C > 15°C | 3.47E-05 |
| **Comparison** | **Functional enrichment** | **#term ID** | **term description** | **observed gene count** | **background gene count** | **FDR** |
| BL25>BL15 | STRING | CL:11316 | Core histone H2A/H2B/H3/H4, and Histone H4 | 3 | 126 | 3.60E-03 |
| BL25>BL15 | Uniprot | KW-0158 | Chromosome | 3 | 79 | 1.50E-04 |
| BL25>BL15 | PFAM | PF00538 | linker histone H1 and H5 family | 2 | 17 | 1.20E-03 |
| BL25>BL15 | INTERPRO | IPR005818 | Linker histone H1/H5, domain H15 | 2 | 19 | 2.20E-03 |
| BL25>BL15 | INTERPRO | IPR005819 | Histone H5 | 2 | 15 | 2.20E-03 |
| BL25>BL15 | SMART | SM00526 | Domain in histone families 1 and 5 | 2 | 19 | 8.80E-04 |
| **Comparison** | **Functional enrichment** | **#term ID** | **term description** | **observed gene count** | **background gene count** | **FDR** |
| BL15>BL25 | STRING | CL:15673 | Ribosomal protein, and Protein biosynthesis | 6 | 188 | 1.60E-04 |
| BL15>BL25 | STRING | CL:15688 | Ribosomal protein, and Protein biosynthesis | 5 | 130 | 2.90E-04 |
| BL15>BL25 | STRING | CL:15691 | Ribosomal protein, and Protein biosynthesis | 4 | 122 | 1.30E-03 |
| BL15>BL25 | STRING | CL:7169 | SERine Proteinase INhibitors, and Peptidase S1A, coagulation factor VII/IX/X/C/Z | 3 | 43 | 1.30E-03 |
| BL15>BL25 | STRING | CL:8230 | Proteinase inhibitor I25, cystatin, conserved site, and Cathepsin D | 2 | 5 | 1.30E-03 |

| | | | | | | |
|---|---|---|---|---|---|---|
| BL15>BL25 | STRING | CL:7175 | Fibrinogen alpha/beta chain family, and PAN domain | 2 | 21 | 8.00E-03 |
| BL15>BL25 | STRING | CL:15692 | Ribosomal protein, and Translation protein, beta-barrel domain superfamily | 3 | 104 | 8.30E-03 |
| BL15>BL25 | Uniprot | KW-0694 | RNA-binding | 8 | 314 | 2.59E-06 |
| BL15>BL25 | PFAM | PF00076 | RNA recognition motif. (a.k.a. RRM, RBD, or RNP domain) | 7 | 208 | 4.40E-06 |
| BL15>BL25 | PFAM | PF00240 | Ubiquitin family | 3 | 43 | 1.80E-03 |
| BL15>BL25 | PFAM | PF00679 | Elongation factor G C-terminus | 2 | 7 | 1.80E-03 |
| BL15>BL25 | PFAM | PF14492 | Elongation Factor G, domain II | 2 | 6 | 1.80E-03 |
| BL15>BL25 | PFAM | PF00031 | Cystatin domain | 2 | 11 | 2.30E-03 |
| BL15>BL25 | PFAM | PF03144 | Elongation factor Tu domain 2 | 2 | 14 | 3.00E-03 |
| BL15>BL25 | PFAM | PF00160 | Cyclophilin type peptidyl-prolyl cis-trans isomerase/CLD | 2 | 18 | 4.00E-03 |
| BL15>BL25 | PFAM | PF11976 | Ubiquitin-2 like Rad60 SUMO-like | 2 | 18 | 4.00E-03 |
| BL15>BL25 | PFAM | PF00009 | Elongation factor Tu GTP binding domain | 2 | 30 | 8.00E-03 |
| BL15>BL25 | INTERPRO | IPR000504 | RNA recognition motif domain | 7 | 231 | 2.15E-05 |
| BL15>BL25 | INTERPRO | IPR012677 | Nucleotide-binding alpha-beta plait domain superfamily | 7 | 248 | 2.15E-05 |
| BL15>BL25 | INTERPRO | IPR035979 | RNA-binding domain superfamily | 7 | 251 | 2.15E-05 |
| BL15>BL25 | INTERPRO | IPR000640 | Elongation factor EFG, domain V-like | 2 | 7 | 2.60E-03 |
| BL15>BL25 | INTERPRO | IPR035647 | EF-G domain III/V-like | 2 | 7 | 2.60E-03 |
| BL15>BL25 | INTERPRO | IPR041095 | Elongation Factor G, domain II | 2 | 6 | 2.60E-03 |
| BL15>BL25 | INTERPRO | IPR000626 | Ubiquitin domain | 3 | 59 | 3.10E-03 |
| BL15>BL25 | INTERPRO | IPR000010 | Cystatin domain | 2 | 11 | 3.60E-03 |
| BL15>BL25 | INTERPRO | IPR016039 | Thiolase-like | 2 | 11 | 3.60E-03 |
| BL15>BL25 | INTERPRO | IPR004161 | Translation elongation factor EFTu-like, domain 2 | 2 | 14 | 4.40E-03 |
| BL15>BL25 | INTERPRO | IPR020892 | Cyclophilin-type peptidyl-prolyl cis-trans isomerase, conserved site | 2 | 14 | 4.40E-03 |
| BL15>BL25 | INTERPRO | IPR024936 | Cyclophilin-type peptidyl-prolyl cis-trans isomerase | 2 | 17 | 5.20E-03 |
| BL15>BL25 | INTERPRO | IPR002130 | Cyclophilin-type peptidyl-prolyl cis-trans isomerase domain | 2 | 18 | 5.30E-03 |
| BL15>BL25 | INTERPRO | IPR029000 | Cyclophilin-like domain superfamily | 2 | 18 | 5.30E-03 |
| BL15>BL25 | INTERPRO | IPR014721 | Ribosomal protein S5 domain 2-type fold, subgroup | 2 | 21 | 6.10E-03 |
| BL15>BL25 | INTERPRO | IPR000795 | Transcription factor, GTP-binding domain | 2 | 23 | 6.70E-03 |
| BL15>BL25 | INTERPRO | IPR003954 | RNA recognition motif domain, eukaryote | 2 | 25 | 7.40E-03 |
| BL15>BL25 | SMART | SM00360 | RNA recognition motif | 7 | 224 | 3.08E-06 |
| BL15>BL25 | SMART | SM00213 | Ubiquitin homologues | 3 | 43 | 7.80E-04 |
| BL15>BL25 | SMART | SM00838 | Elongation factor G C-terminus | 2 | 6 | 7.80E-04 |
| BL15>BL25 | SMART | SM00043 | Cystatin-like domain | 2 | 11 | 1.20E-03 |
| **Comparison** | **Functional enrichment** | **#term ID** | **term description** | **genes mapped** | **direction** | **FDR** |
| 7°C vs. 25°C | STRING | CL:11311 | Core histone H2A/H2B/H3/H4, and Histone H4 | 23 | 25°C > 7°C | 2.93E-08 |
| 7°C vs. 25°C | STRING | CL:11316 | Core histone H2A/H2B/H3/H4, and Histone H4 | 19 | 25°C > 7°C | 1.28E-07 |
| 7°C vs. 25°C | STRING | CL:11308 | Core histone H2A/H2B/H3/H4, and Histone H4 | 25 | 25°C > 7°C | 1.28E-07 |
| 7°C vs. 25°C | STRING | CL:11321 | Core histone H2A/H2B/H3/H4, and Histone H4 | 17 | 25°C > 7°C | 1.28E-07 |
| 7°C vs. 25°C | STRING | CL:16063 | Ribosomal protein, and Ribosomal protein L37/S30 | 6 | 7°C > 25°C | 5.40E-03 |
| 7°C vs. 25°C | STRING | CL:11325 | Core histone H2A/H2B/H3/H4, and Histone H4 | 15 | 25°C > 7°C | 5.50E-03 |
| 7°C vs. 25°C | Uniprot | KW-0158 | Chromosome | 19 | 25°C > 7°C | 4.69E-09 |
| 7°C vs. 25°C | Uniprot | KW-0238 | DNA-binding | 34 | 25°C > 7°C | 1.30E-04 |
| 7°C vs. 25°C | Uniprot | KW-0694 | RNA-binding | 85 | 7°C > 25°C | 9.30E-04 |
| 7°C vs. 25°C | Uniprot | KW-0544 | Nucleosome core | 13 | 25°C > 7°C | 3.40E-03 |
| 7°C vs. 25°C | PFAM | PF00538 | linker histone H1 and H5 family | 7 | 25°C > 7°C | 6.45E-05 |
| 7°C vs. 25°C | PFAM | PF14492 | Elongation Factor G, domain II | 3 | 7°C > 25°C | 5.30E-03 |
| 7°C vs. 25°C | PFAM | PF00679 | Elongation factor G C-terminus | 3 | 7°C > 25°C | 5.30E-03 |
| 7°C vs. 25°C | PFAM | PF00076 | RNA recognition motif. (a.k.a. RRM, RBD, or RNP domain) | 64 | 7°C > 25°C | 5.30E-03 |
| 7°C vs. 25°C | INTERPRO | IPR005819 | Histone H5 | 6 | 25°C > 7°C | 5.75E-05 |

| | | | | | | |
|---|---|---|---|---|---|---|
| 7°C vs. 25°C | INTERPRO | IPR005818 | Linker histone H1/H5, domain H15 | 7 | 25°C > 7°C | 6.23E-05 |
| 7°C vs. 25°C | INTERPRO | IPR035979 | RNA-binding domain superfamily | 67 | 7°C > 25°C | 4.80E-03 |
| 7°C vs. 25°C | INTERPRO | IPR000504 | RNA recognition motif domain | 67 | 7°C > 25°C | 4.80E-03 |
| 7°C vs. 25°C | INTERPRO | IPR012677 | Nucleotide-binding alpha-beta plait domain superfamily | 68 | 7°C > 25°C | 4.80E-03 |
| 7°C vs. 25°C | INTERPRO | IPR016039 | Thiolase-like | 4 | 7°C > 25°C | 4.90E-03 |
| 7°C vs. 25°C | INTERPRO | IPR035647 | EF-G domain III/V-like | 3 | 7°C > 25°C | 5.10E-03 |
| 7°C vs. 25°C | INTERPRO | IPR000640 | Elongation factor EFG, domain V-like | 3 | 7°C > 25°C | 5.10E-03 |
| 7°C vs. 25°C | INTERPRO | IPR014721 | Ribosomal protein S5 domain 2-type fold, subgroup | 5 | 7°C > 25°C | 5.60E-03 |
| 7°C vs. 25°C | INTERPRO | IPR009072 | Histone-fold | 13 | 25°C > 7°C | 5.70E-03 |
| 7°C vs. 25°C | INTERPRO | IPR007125 | Histone H2A/H2B/H3 | 12 | 25°C > 7°C | 9.60E-03 |
| 7°C vs. 25°C | SMART | SM00526 | Domain in histone families 1 and 5 | 7 | 25°C > 7°C | 2.65E-05 |
| 7°C vs. 25°C | SMART | SM00360 | RNA recognition motif | 67 | 7°C > 25°C | 2.50E-03 |
| 7°C vs. 25°C | SMART | SM00838 | Elongation factor G C-terminus | 3 | 7°C > 25°C | 2.90E-03 |
| **Comparison** | **Functional enrichment** | **#term ID** | **term description** | **observed gene count** | **background gene count** | **FDR** |
| KL25 > KL7 | STRING | CL:21372 | Glycolysis, and Enolase | 4 | 29 | 4.90E-05 |
| KL25 > KL7 | STRING | CL:21390 | Phosphoglycerate mutase 1, and Enolase, conserved site | 3 | 5 | 4.90E-05 |
| KL25 > KL7 | STRING | CL:11311 | Core histone H2A/H2B/H3/H4, and Histone H4 | 5 | 136 | 1.70E-04 |
| KL25 > KL7 | STRING | CL:21363 | Glycolysis, and Carbohydrate metabolism | 5 | 180 | 4.10E-04 |
| KL25 > KL7 | STRING | CL:11325 | Core histone H2A/H2B/H3/H4, and Histone H4 | 4 | 112 | 9.20E-04 |
| KL25 > KL7 | STRING | CL:10054 | Calponin repeat, and Caldesmon | 2 | 5 | 9.70E-04 |
| KL25 > KL7 | STRING | CL:28025 | Annexin A2, and Annexin A11 | 2 | 7 | 1.20E-03 |
| KL25 > KL7 | STRING | CL:21855 | FAD dependent oxidoreductase, and D-isomer specific 2-hydroxyacid dehydrogenase, catalytic domain | 2 | 19 | 5.20E-03 |
| KL25 > KL7 | STRING | CL:11331 | Core histone H2A/H2B/H3/H4, and Histone H4 | 3 | 99 | 6.10E-03 |
| KL25 > KL7 | Uniprot | KW-0158 | Chromosome | 5 | 79 | 1.41E-05 |
| KL25 > KL7 | Uniprot | KW-0544 | Nucleosome core | 4 | 47 | 3.65E-05 |
| KL25 > KL7 | PFAM | PF16211 | C-terminus of histone H2A | 4 | 27 | 1.26E-05 |
| KL25 > KL7 | PFAM | PF00125 | Core histone H2A/H2B/H3/H4 | 4 | 80 | 3.60E-04 |
| KL25 > KL7 | PFAM | PF00113 | Enolase, C-terminal TIM barrel domain | 2 | 6 | 9.90E-04 |
| KL25 > KL7 | PFAM | PF00261 | Tropomyosin | 2 | 7 | 9.90E-04 |
| KL25 > KL7 | PFAM | PF03952 | Enolase, N-terminal domain | 2 | 5 | 9.90E-04 |
| KL25 > KL7 | PFAM | PF12718 | Tropomyosin like | 2 | 7 | 9.90E-04 |
| KL25 > KL7 | PFAM | PF13378 | Enolase C-terminal domain-like | 2 | 6 | 9.90E-04 |
| KL25 > KL7 | INTERPRO | IPR002119 | Histone H2A | 4 | 23 | 1.24E-05 |
| KL25 > KL7 | INTERPRO | IPR032454 | Histone H2A, C-terminal domain | 4 | 22 | 1.24E-05 |
| KL25 > KL7 | INTERPRO | IPR032458 | Histone H2A conserved site | 4 | 21 | 1.24E-05 |
| KL25 > KL7 | INTERPRO | IPR007125 | Histone H2A/H2B/H3 | 4 | 50 | 7.47E-05 |
| KL25 > KL7 | INTERPRO | IPR009072 | Histone-fold | 4 | 77 | 3.00E-04 |
| KL25 > KL7 | INTERPRO | IPR020809 | Enolase, conserved site | 2 | 4 | 8.60E-04 |
| KL25 > KL7 | INTERPRO | IPR000533 | Tropomyosin | 2 | 7 | 1.40E-03 |
| KL25 > KL7 | INTERPRO | IPR000941 | Enolase | 2 | 6 | 1.40E-03 |
| KL25 > KL7 | INTERPRO | IPR020810 | Enolase, C-terminal TIM barrel domain | 2 | 6 | 1.40E-03 |
| KL25 > KL7 | INTERPRO | IPR020811 | Enolase, N-terminal | 2 | 6 | 1.40E-03 |
| KL25 > KL7 | INTERPRO | IPR029017 | Enolase-like, N-terminal | 2 | 7 | 1.40E-03 |
| KL25 > KL7 | INTERPRO | IPR029065 | Enolase C-terminal domain-like | 2 | 7 | 1.40E-03 |
| KL25 > KL7 | INTERPRO | IPR036849 | Enolase-like, C-terminal domain superfamily | 2 | 7 | 1.40E-03 |
| KL25 > KL7 | SMART | SM00414 | Histone 2A | 4 | 28 | 4.90E-06 |
| KL25 > KL7 | SMART | SM01192 | Enolase, C-terminal TIM barrel domain | 2 | 6 | 5.10E-04 |
| KL25 > KL7 | SMART | SM01193 | Enolase, N-terminal domain | 2 | 5 | 5.10E-04 |
| **Comparison** | **Functional enrichment** | **#term ID** | **term description** | **observed gene count** | **background gene count** | **FDR** |
| KL7 > KL25 | STRING | CL:16061 | Ribosomal protein, and Ribosomal protein S18 | 4 | 57 | 3.35E-05 |
| KL7 > KL25 | STRING | CL:17392 | RNA recognition motif. (a.k.a. RRM, RBD, or RNP domain) | 3 | 34 | 8.37E-05 |
| KL7 > KL25 | STRING | CL:16063 | Ribosomal protein, and Ribosomal protein L37/S30 | 3 | 43 | 1.30E-04 |

| | | | | | | |
|---|---|---|---|---|---|---|
| KL7 > KL25 | STRING | CL:17211 | RNA recognition motif. (a.k.a. RRM, RBD, or RNP domain), and mRNA processing | 4 | 184 | 3.00E-04 |
| KL7 > KL25 | STRING | CL:16066 | Translation protein SH3-like domain superfamily, and Ribosomal protein | 2 | 23 | 1.90E-03 |
| KL7 > KL25 | STRING | CL:17394 | RNA recognition motif. (a.k.a. RRM, RBD, or RNP domain) | 2 | 28 | 2.40E-03 |
| KL7 > KL25 | STRING | CL:15688 | Ribosomal protein, and Protein biosynthesis | 2 | 130 | 3.07E-02 |
| KL7 > KL25 | Uniprot | KW-0694 | RNA-binding | 7 | 314 | 3.76E-07 |
| KL7 > KL25 | PFAM | PF00076 | RNA recognition motif. (a.k.a. RRM, RBD, or RNP domain) | 6 | 208 | 7.37E-07 |
| KL7 > KL25 | PFAM | PF00013 | KH domain | 2 | 43 | 6.50E-03 |
| KL7 > KL25 | INTERPRO | IPR000504 | RNA recognition motif domain | 6 | 231 | 3.37E-06 |
| KL7 > KL25 | INTERPRO | IPR012677 | Nucleotide-binding alpha-beta plait domain superfamily | 6 | 248 | 3.37E-06 |
| KL7 > KL25 | INTERPRO | IPR035979 | RNA-binding domain superfamily | 6 | 251 | 3.37E-06 |
| KL7 > KL25 | INTERPRO | IPR004087 | K Homology domain | 2 | 48 | 8.60E-03 |
| KL7 > KL25 | INTERPRO | IPR004088 | K Homology domain, type 1 | 2 | 44 | 8.60E-03 |
| KL7 > KL25 | INTERPRO | IPR036612 | K Homology domain, type 1 superfamily | 2 | 50 | 8.60E-03 |
| KL7 > KL25 | SMART | SM00360 | RNA recognition motif | 6 | 224 | 5.65E-07 |
| KL7 > KL25 | SMART | SM00322 | K homology RNA-binding domain | 2 | 45 | 3.60E-03 |
| KL7 > KL25 | SMART | | | | | |

| **Comparison** | **Functional enrichment** | **#term ID** | **term description** | **observed gene count** | **background gene count** | **FDR** |
|---|---|---|---|---|---|---|
| BL25 > BL7 | STRING | CL:11311 | Core histone H2A/H2B/H3/H4, and Histone H4 | 9 | 136 | 1.69E-07 |
| BL25 > BL7 | STRING | CL:11572 | HMG box A DNA-binding domain, conserved site, and Histone H5 | 3 | 5 | 1.20E-04 |
| BL25 > BL7 | STRING | CL:11316 | Core histone H2A/H2B/H3/H4, and Histone H4 | 6 | 126 | 2.10E-04 |
| BL25 > BL7 | STRING | CL:11321 | Core histone H2A/H2B/H3/H4, and Histone H4 | 5 | 117 | 1.80E-03 |
| BL25 > BL7 | STRING | CL:10054 | Calponin repeat, and Caldesmon | 2 | 5 | 7.40E-03 |
| BL25 > BL7 | Uniprot | KW-0158 | Chromosome | 8 | 79 | 1.37E-08 |
| BL25 > BL7 | Uniprot | KW-0238 | DNA-binding | 10 | 740 | 2.60E-03 |
| BL25 > BL7 | Uniprot | KW-0544 | Nucleosome core | 3 | 47 | 7.80E-03 |
| BL25 > BL7 | Uniprot | KW-0539 | Nucleus | 11 | 1137 | 9.70E-03 |
| BL25 > BL7 | PFAM | PF00538 | linker histone H1 and H5 family | 5 | 17 | 4.13E-07 |
| BL25 > BL7 | PFAM | PF16211 | C-terminus of histone H2A | 3 | 27 | 3.50E-03 |
| BL25 > BL7 | PFAM | PF15936 | Domain of unknown function (DUF4749) | 2 | 8 | 8.70E-03 |
| BL25 > BL7 | INTERPRO | IPR005819 | Histone H5 | 5 | 15 | 4.92E-07 |
| BL25 > BL7 | INTERPRO | IPR005818 | Linker histone H1/H5, domain H15 | 5 | 19 | 6.68E-07 |
| BL25 > BL7 | INTERPRO | IPR002119 | Histone H2A | 3 | 23 | 2.40E-03 |
| BL25 > BL7 | INTERPRO | IPR032454 | Histone H2A, C-terminal domain | 3 | 22 | 2.40E-03 |
| BL25 > BL7 | INTERPRO | IPR032458 | Histone H2A conserved site | 3 | 21 | 2.40E-03 |
| BL25 > BL7 | INTERPRO | IPR036388 | Winged helix-like DNA-binding domain superfamily | 6 | 237 | 2.40E-03 |
| BL25 > BL7 | INTERPRO | IPR036390 | Winged helix DNA-binding domain superfamily | 6 | 225 | 2.40E-03 |
| BL25 > BL7 | INTERPRO | IPR031847 | Domain of unknown function DUF4749 | 2 | 8 | 6.60E-03 |
| BL25 > BL7 | INTERPRO | IPR007125 | Histone H2A/H2B/H3 | 3 | 50 | 8.50E-03 |
| BL25 > BL7 | SMART | SM00526 | Domain in histone families 1 and 5 | 5 | 19 | 3.53E-07 |
| BL25 > BL7 | SMART | SM00414 | Histone 2A | 3 | 28 | 2.00E-03 |

| **Comparison** | **Functional enrichment** | **#term ID** | **term description** | **observed gene count** | **background gene count** | **FDR** |
|---|---|---|---|---|---|---|
| BL7 > BL25 | STRING | CL:15673 | Ribosomal protein, and Protein biosynthesis | 10 | 188 | 5.31E-07 |
| BL7 > BL25 | STRING | CL:15688 | Ribosomal protein, and Protein biosynthesis | 8 | 130 | 4.26E-06 |
| BL7 > BL25 | STRING | CL:15691 | Ribosomal protein, and Protein biosynthesis | 7 | 122 | 1.48E-05 |
| BL7 > BL25 | STRING | CL:17422 | Heterogeneous nuclear ribonucleoprotein C, and HnRNP-L/PTB | 3 | 14 | 1.00E-03 |
| BL7 > BL25 | STRING | CL:15692 | Ribosomal protein, and Translation protein, beta-barrel domain superfamily | 5 | 104 | 1.40E-03 |
| BL7 > BL25 | STRING | CL:18123 | Hsp70 protein, and DnaJ C terminal domain | 3 | 26 | 4.30E-03 |
| BL7 > BL25 | STRING | CL:17440 | hnRNP A0, RNA recognition motif 1, and HnRNP-L/PTB | 2 | 5 | 5.90E-03 |

| | | | | | | |
|---|---|---|---|---|---|---|
| BL7 > BL25 | STRING | CL:15697 | Ribosomal protein, and Translation protein SH3-like domain superfamily | 4 | 93 | 7.50E-03 |
| BL7 > BL25 | STRING | CL:23657 | Fatty acid hydroxylase, and Sterol biosynthesis | 3 | 37 | 7.50E-03 |
| BL7 > BL25 | STRING | CL:17211 | RNA recognition motif. (a.k.a. RRM, RBD, or RNP domain), and mRNA processing | 5 | 184 | 8.50E-03 |
| BL7 > BL25 | Uniprot | KW-0694 | RNA-binding | 13 | 314 | 7.07E-09 |
| BL7 > BL25 | Uniprot | KW-0963 | Cytoplasm | 9 | 320 | 7.58E-05 |
| BL7 > BL25 | Uniprot | KW-0206 | Cytoskeleton | 5 | 74 | 2.00E-04 |
| BL7 > BL25 | Uniprot | KW-0547 | Nucleotide-binding | 14 | 1142 | 7.10E-04 |
| BL7 > BL25 | Uniprot | KW-0648 | Protein biosynthesis | 4 | 64 | 1.30E-03 |
| BL7 > BL25 | Uniprot | KW-0756 | Sterol biosynthesis | 2 | 4 | 2.10E-03 |
| BL7 > BL25 | Uniprot | KW-0493 | Microtubule | 4 | 84 | 2.30E-03 |
| BL7 > BL25 | Uniprot | KW-0443 | Lipid metabolism | 4 | 99 | 3.70E-03 |
| BL7 > BL25 | Uniprot | KW-0444 | Lipid biosynthesis | 3 | 42 | 3.70E-03 |
| BL7 > BL25 | Uniprot | KW-0067 | ATP-binding | 10 | 879 | 5.50E-03 |
| BL7 > BL25 | Uniprot | KW-0816 | Tricarboxylic acid cycle | 2 | 14 | 7.00E-03 |
| BL7 > BL25 | PFAM | PF00076 | RNA recognition motif. (a.k.a. RRM, RBD, or RNP domain) | 11 | 208 | 2.73E-08 |
| BL7 > BL25 | PFAM | PF00009 | Elongation factor Tu GTP binding domain | 4 | 30 | 1.60E-04 |
| BL7 > BL25 | PFAM | PF00091 | Tubulin/FtsZ family, GTPase domain | 4 | 26 | 1.60E-04 |
| BL7 > BL25 | PFAM | PF00679 | Elongation factor G C-terminus | 3 | 7 | 1.60E-04 |
| BL7 > BL25 | PFAM | PF03953 | Tubulin C-terminal domain | 4 | 25 | 1.60E-04 |
| BL7 > BL25 | PFAM | PF14492 | Elongation Factor G, domain II | 3 | 6 | 1.60E-04 |
| BL7 > BL25 | PFAM | PF00013 | KH domain | 4 | 43 | 3.20E-04 |
| BL7 > BL25 | PFAM | PF03144 | Elongation factor Tu domain 2 | 3 | 14 | 3.40E-04 |
| BL7 > BL25 | PFAM | PF03764 | Elongation factor G, domain IV | 2 | 5 | 2.80E-03 |
| BL7 > BL25 | INTERPRO | IPR000504 | RNA recognition motif domain | 11 | 231 | 1.78E-07 |
| BL7 > BL25 | INTERPRO | IPR012677 | Nucleotide-binding alpha-beta plait domain superfamily | 11 | 248 | 1.82E-07 |
| BL7 > BL25 | INTERPRO | IPR035979 | RNA-binding domain superfamily | 11 | 251 | 1.82E-07 |
| BL7 > BL25 | INTERPRO | IPR002452 | Alpha tubulin | 4 | 15 | 2.97E-05 |
| BL7 > BL25 | INTERPRO | IPR014721 | Ribosomal protein S5 domain 2-type fold, subgroup | 4 | 21 | 7.63E-05 |
| BL7 > BL25 | INTERPRO | IPR000795 | Transcription factor, GTP-binding domain | 4 | 23 | 8.78E-05 |
| BL7 > BL25 | INTERPRO | IPR037103 | Tubulin/FtsZ, C-terminal domain superfamily | 4 | 24 | 8.78E-05 |
| BL7 > BL25 | INTERPRO | IPR000217 | Tubulin | 4 | 26 | 8.86E-05 |
| BL7 > BL25 | INTERPRO | IPR000640 | Elongation factor EFG, domain V-like | 3 | 7 | 8.86E-05 |
| BL7 > BL25 | INTERPRO | IPR003008 | Tubulin/FtsZ, GTPase domain | 4 | 26 | 8.86E-05 |
| BL7 > BL25 | INTERPRO | IPR008280 | Tubulin/FtsZ, C-terminal | 4 | 26 | 8.86E-05 |
| BL7 > BL25 | INTERPRO | IPR009000 | Translation protein, beta-barrel domain superfamily | 4 | 31 | 8.86E-05 |
| BL7 > BL25 | INTERPRO | IPR017975 | Tubulin, conserved site | 4 | 26 | 8.86E-05 |
| BL7 > BL25 | INTERPRO | IPR018316 | Tubulin/FtsZ, 2-layer sandwich domain | 4 | 25 | 8.86E-05 |
| BL7 > BL25 | INTERPRO | IPR023123 | Tubulin, C-terminal | 4 | 25 | 8.86E-05 |
| BL7 > BL25 | INTERPRO | IPR035647 | EF-G domain III/V-like | 3 | 7 | 8.86E-05 |
| BL7 > BL25 | INTERPRO | IPR036525 | Tubulin/FtsZ, GTPase domain superfamily | 4 | 27 | 8.86E-05 |
| BL7 > BL25 | INTERPRO | IPR041095 | Elongation Factor G, domain II | 3 | 6 | 8.86E-05 |
| BL7 > BL25 | INTERPRO | IPR020568 | Ribosomal protein S5 domain 2-type fold | 4 | 34 | 1.10E-04 |
| BL7 > BL25 | INTERPRO | IPR004088 | K Homology domain, type 1 | 4 | 44 | 2.60E-04 |
| BL7 > BL25 | INTERPRO | IPR031157 | Tr-type G domain, conserved site | 3 | 13 | 2.60E-04 |
| BL7 > BL25 | INTERPRO | IPR004161 | Translation elongation factor EFTu-like, domain 2 | 3 | 14 | 2.80E-04 |
| BL7 > BL25 | INTERPRO | IPR004087 | K Homology domain | 4 | 48 | 3.30E-04 |
| BL7 > BL25 | INTERPRO | IPR036612 | K Homology domain, type 1 superfamily | 4 | 50 | 3.70E-04 |
| BL7 > BL25 | INTERPRO | IPR003954 | RNA recognition motif domain, eukaryote | 3 | 25 | 1.20E-03 |
| BL7 > BL25 | INTERPRO | IPR005517 | Translation elongation factor EFG/EF2, domain IV | 2 | 5 | 2.20E-03 |
| BL7 > BL25 | INTERPRO | IPR016039 | Thiolase-like | 2 | 11 | 7.90E-03 |
| BL7 > BL25 | SMART | SM00360 | RNA recognition motif | 11 | 224 | 2.15E-08 |
| BL7 > BL25 | SMART | SM00838 | Elongation factor G C-terminus | 3 | 6 | 5.83E-05 |
| BL7 > BL25 | SMART | SM00864 | Tubulin/FtsZ family, GTPase domain | 4 | 26 | 5.83E-05 |
| BL7 > BL25 | SMART | SM00865 | Tubulin/FtsZ family, C-terminal domain | 4 | 25 | 5.83E-05 |
| BL7 > BL25 | SMART | SM00322 | K homology RNA-binding domain | 4 | 45 | 2.00E-04 |
| BL7 > BL25 | SMART | SM00889 | Elongation factor G, domain IV | 2 | 5 | 1.60E-03 |

| Comparison | Functional enrichment | #term ID | term description | observed gene count | background gene count | FDR |
|---|---|---|---|---|---|---|
| KL7 vs. KL25 vs. BL7 vs. BL25 | STRING | CL:10054 | Calponin repeat, and Caldesmon | 2 | 5 | 1.50E-03 |
| KL7 vs. KL25 vs. BL7 vs. BL26 | STRING | CL:28025 | Annexin A2, and Annexin A11 | 2 | 7 | 1.50E-03 |
| KL7 vs. KL25 vs. BL7 vs. BL27 | STRING | CL:11311 | Core histone H2A/H2B/H3/H4, and Histone H4 | 3 | 136 | 4.10E-03 |
| KL7 vs. KL25 vs. BL7 vs. BL28 | Uniprot | KW-0158 | Chromosome | 3 | 79 | 1.50E-03 |
| KL7 vs. KL25 vs. BL7 vs. BL29 | PFAM | PF16211 | C-terminus of histone H2A | 2 | 27 | 4.70E-03 |
| KL7 vs. KL25 vs. BL7 vs. BL30 | INTERPRO | IPR002119 | Histone H2A | 2 | 23 | 8.50E-03 |
| KL7 vs. KL25 vs. BL7 vs. BL31 | INTERPRO | IPR032454 | Histone H2A, C-terminal domain | 2 | 22 | 8.50E-03 |
| KL7 vs. KL25 vs. BL7 vs. BL32 | INTERPRO | IPR032458 | Histone H2A conserved site | 2 | 21 | 8.50E-03 |
| KL7 vs. KL25 vs. BL7 vs. BL33 | SMART | SM00414 | Histone 2A | 2 | 28 | 3.00E-03 |
| KL7 vs. KL25 vs. BL7 vs. BL34 | SMART | SM00033 | Calponin homology domain | 2 | 75 | 1.00E-02 |

**Supplemental Table 2.3.** A list of all the proteins from the liver proteome set that are included in functionally enriched STRING network CL:21363 glycolysis, and carbohydrate metabolism (see Figure 2.4b) from the KL vs. BL comparison, including STRING labels and protein accession number, STRING description, FC, and adjusted-p value. The bolded entry, sorbitol dehydrogenase, had an adjusted p-value <0.05.

| STRING labels | Protein Accession | Description (STRING) | FC | Adjusted-p |
|---|---|---|---|---|
| ENO3 | G3N816 | Enolase 3, (beta, muscle) | 1.5055 | 0.1970 |
| ENSGACG00000000231 | G3N4S5 | Oxoglutarate (alpha-ketoglutarate) dehydrogenase b (lipoamide) | 1.1237 | 0.9065 |
| ENSGACG00000000473 | G3N5N3 | Zgc:56622 | 1.3066 | 0.3096 |
| ENSGACG00000000827 | G3N710 | Alpha-1,4 glucan phosphorylase | 1.6360 | 0.0782 |
| ENSGACG00000000973 | G3N7I7 | Malate dehydrogenase 1, NAD (soluble) | 1.7737 | 0.1617 |
| ENSGACG00000001103 | G3N7Z3 | Oxoglutarate (alpha-ketoglutarate) dehydrogenase b (lipoamide) | 1.1063 | 0.6927 |
| ENSGACG00000001505 | G3N9H1 | Enolase 1b, (alpha) | 1.6186 | 0.0922 |
| ENSGACG00000001637 | G3NA55 | Aconitase 1, soluble; Belongs to the aconitase/IPM isomerase family | 1.3197 | 0.4951 |
| ENSGACG00000002198 | G3NC51 | Phosphoenolpyruvate carboxykinase 2 (mitochondrial) | 1.6516 | 0.1703 |
| ENSGACG00000002519 | G3NDB1 | Si:ch211-217a12.1; Glutamic-pyruvate transaminase (alanine aminotransferase) | 1.3401 | 0.1327 |
| ENSGACG00000002813 | G3NEH8 | Glutamate dehydrogenase 1b | 1.4131 | 0.2806 |
| ENSGACG00000003103 | G3NFG7 | Ketohexokinase | 1.1968 | 0.7403 |
| ENSGACG00000004178 | G3NJP8 | Aldolase a, fructose-bisphosphate, a | 1.5497 | 0.2098 |
| ENSGACG00000005040 | G3NN43 | Malic enzyme 1, NADP(+)-dependent, cytosolic | 0.3791 | 0.4881 |
| ENSGACG00000006005 | G3NRH9 | Transketolase | 2.1045 | 0.0750 |
| ENSGACG00000006087 | G3NRT5 | Malate dehydrogenase 2, NAD (mitochondrial) | 1.3349 | 0.3294 |
| ENSGACG00000006964 | G3NVH9 | Phosphoglucomutase 1; Belongs to the phosphohexose mutase family | 1.4266 | 0.1562 |
| ENSGACG00000007164 | G3NW14 | 6-phosphogluconate dehydrogenase, decarboxylating | 1.5812 | 0.0736 |
| ENSGACG00000007509 | G3NXC0 | Dihydrolipoamide S-succinyltransferase | 1.1098 | 0.7880 |
| ENSGACG00000007534 | G3NXE2 | Aspartate aminotransferase; Glutamic-oxaloacetic transaminase 1, soluble | 1.3203 | 0.4223 |
| ENSGACG00000007567 | G3NXM9 | Aconitate hydratase, mitochondrial; Aconitase 2, mitochondrial | 1.3966 | 0.1182 |
| ENSGACG00000007692 | G3NXY4 | Phosphoglycerate mutase 1a; Belongs to the phosphoglycerate mutase family. BPG- dependent PGAM subfamily | 1.4535 | 0.1970 |
| ENSGACG00000007727 | G3NY35 | Aldolase A, fructose-bisphosphate | 1.4932 | 0.4040 |
| ENSGACG00000007744 | G3NY86 | Glucose phosphate isomerase a; Belongs to the GPI family | 1.5252 | 0.1443 |
| ENSGACG00000008240 | G3P046 | Dihydrolipoamide dehydrogenase | 1.3662 | 0.1192 |
| ENSGACG00000009687 | G3P5F2 | Aldo-keto reductase family 1, member A1a (aldehyde reductase) | 1.8266 | 0.0782 |
| ENSGACG00000009950 | G3P6I9 | Triosephosphate isomerase 1b | 1.5636 | 0.2090 |
| ENSGACG00000009964 | G3P6R2 | Transketolase b | 1.7287 | 0.0736 |
| ENSGACG00000010016 | G3P6N3 | Enolase 2 (gamma, neuronal) | 0.9790 | 0.9766 |
| ENSGACG00000010219 | G3P7L3 | Glyceraldehyde-3-phosphate dehydrogenase | 1.9087 | 0.1562 |
| ENSGACG00000010529 | G3P8K8 | Dihydrolipoamide S-succinyltransferase | 0.9300 | 0.8794 |
| ENSGACG00000010827 | G3P9S4 | Isocitrate dehydrogenase 2 (NADP+), mitochondrial | 4.5955 | 0.6986 |
| ENSGACG00000010851 | G3P9W8 | Citrate synthase; Belongs to the citrate synthase family | 1.0192 | 0.9618 |
| ENSGACG00000011403 | G3PBU7 | Fumarate hydratase | 1.2450 | 0.4317 |
| ENSGACG00000012197 | G3PEY0 | Hexose-6-phosphate dehydrogenase (glucose 1-dehydrogenase) | 1.4000 | 0.4133 |
| ENSGACG00000012936 | G3PHM0 | Glycogen [starch] synthase | 1.2768 | 0.4814 |
| ENSGACG00000012993 | G3PHX0 | Branched chain keto acid dehydrogenase E1, alpha polypeptide | 1.1670 | 0.5879 |
| ENSGACG00000013457 | G3PJP7 | Dihydrolipoamide acetyltransferase component of pyruvate dehydrogenase complex; Dihydrolipoamide branched chain transacylase E2 | 0.9399 | 0.7607 |
| ENSGACG00000014614 | G3PNW0 | Amylo-1, 6-glucosidase, 4-alpha-glucanotransferase a | 1.2207 | 0.4798 |
| ENSGACG00000015394 | G3PRR1 | dicarbonyl/L-xylulose reductase | 0.8890 | 0.6903 |
| **ENSGACG00000015578** | **G3PSH5** | **Sorbitol dehydrogenase** | **1.8798** | **0.0037** |
| ENSGACG00000015857 | G3PTJ4 | Fructose-1,6-bisphosphatase 1b; Belongs to the FBPase class 1 family | 1.4759 | 0.3207 |
| ENSGACG00000016476 | G3PVW5 | Isocitrate dehydrogenase 2 (NADP+), mitochondrial | 0.6710 | 0.4371 |
| ENSGACG00000017200 | G3PYR1 | Transaldolase | 1.4725 | 0.0782 |
| ENSGACG00000017272 | G3PYW9 | Glutamic pyruvate transaminase (alanine aminotransferase) 2, like | 1.1302 | 0.5792 |
| ENSGACG00000017982 | G3Q1L3 | Aldolase b, fructose-bisphosphate | 1.4453 | 0.2466 |
| ENSGACG00000018891 | G3Q522 | Aldo-keto reductase family 1, member B1 (aldose reductase) | 1.6721 | 0.2596 |
| ENSGACG00000019269 | G3Q6G2 | Deoxyribose-phosphate aldolase (putative); 2-deoxyribose-5-phosphate aldolase homolog (C. elegans) | 0.8177 | 0.2385 |
| ENSGACG00000019606 | G3Q7Q5 | Malate dehydrogenase 1Aa, NAD (soluble) | 1.8177 | 0.1608 |
| ENSGACG00000019607 | G3Q7R4 | UDP-glucose pyrophosphorylase 2a | 1.4210 | 0.2489 |

| STRING labels | Protein Accession | Description (STRING) | FC | Adjusted-p |
|---|---|---|---|---|
| ENSGACG00000019710 | G3Q870 | Pyruvate carboxylase | 1.8557 | 0.1616 |
| ENSGACG00000019770 | G3Q8D5 | annotation not available | 1.0486 | 0.8540 |
| ENSGACG00000020619 | G3QBK7 | Aldolase C, fructose-bisphosphate, b | 1.4562 | 0.1703 |
| ENSGACG00000020647 | G3QBP3 | Acetyltransferase component of pyruvate dehydrogenase complex | 0.7211 | 0.4442 |
| ENSGACG00000020677 | G3QBS8 | Pyruvate dehydrogenase E1 component subunit alpha | 1.5672 | 0.1443 |
| ENSGACG00000020795 | G3QC79 | Phosphoglycerate kinase 1 | 0.8715 | 0.5633 |
| IDH3A | G3PZV8 | Uncharacterized protein; Isocitrate dehydrogenase 3 (NAD+) alpha | 1.3218 | 0.2224 |
| PKLR | G3PCS9 | Pyruvate kinase, liver and RBC; Belongs to the pyruvate kinase family | 1.7992 | 0.1098 |

**Supplemental Table 2.4.** A list of all the proteins from the liver proteome set that are included in functionally enriched STRING network CL:22008 AMP-binding, conserved site, and aldehyde dehydrogenase domain (see Figure 2.4c) from the KL vs. BL comparison, including STRING labels and protein accession number, STRING description, FC, and adjusted-p value.

| STRING labels | Protein Accession | Description (STRING) | FC | Adjusted-p |
|---|---|---|---|---|
| ENSGACG00000002204 | G3NC33 | Fatty acid synthase | 1.2192 | 0.6695 |
| ENSGACG00000002342 | G3NCK6 | propionyl-Coenzyme A carboxylase, alpha polypeptide | 1.1739 | 0.5792 |
| ENSGACG00000002609 | G3NDN8 | 3-hydroxyisobutyryl-CoA hydrolase, mitochondrial | 1.2066 | 0.6594 |
| ENSGACG00000003347 | G3NGD4 | Podocan | 1.0145 | 0.9870 |
| ENSGACG00000003386 | G3NH06 | Aldo-keto reductase family 1, member A1b (aldehyde reductase) | 1.2528 | 0.5334 |
| ENSGACG00000003614 | G3NHC5 | 3-hydroxybutyrate dehydrogenase, type 1 | 1.6764 | 0.1437 |
| ENSGACG00000003908 | G3NIK0 | Aldehyde dehydrogenase 9 family, member A1a, tandem duplicate 2 | 0.8307 | 0.4776 |
| ENSGACG00000004710 | G3NLL5 | 4-aminobutyrate aminotransferase | 1.5666 | 0.2208 |
| ENSGACG00000005451 | G3NPI1 | annotation not available | 1.1043 | 0.7415 |
| ENSGACG00000005952 | G3NRB2 | Aldehyde dehydrogenase 16 family, member A1 | 1.3709 | 0.3219 |
| ENSGACG00000005956 | G3NRD3 | Choline dehydrogenase; Belongs to the GMC oxidoreductase family | 1.2112 | 0.2978 |
| ENSGACG00000006057 | G3NRP6 | enoyl-Coenzyme A, hydratase/3-hydroxyacyl Coenzyme A dehydrogenase | 1.3183 | 0.6544 |
| ENSGACG00000006125 | G3NRZ8 | methylcrotonoyl-Coenzyme A carboxylase 1 (alpha) | 1.2503 | 0.3751 |
| ENSGACG00000006219 | G3NSA8 | Solute carrier family 27 (fatty acid transporter), member 2 | 1.2881 | 0.1776 |
| ENSGACG00000006242 | G3NSH6 | Hydroxysteroid (17-beta) dehydrogenase 4 | 1.7281 | 0.2691 |
| ENSGACG00000006876 | G3NUV8 | Succinyl-CoA:3-ketoacid-coenzyme A transferase | 1.1786 | 0.5879 |
| ENSGACG00000007098 | G3NVU9 | 3-hydroxymethyl-3-methylglutaryl-Coenzyme A lyase (hydroxymethylglutaricaciduria) | 1.3108 | 0.2166 |
| ENSGACG00000008096 | G3NZG1 | S-formylglutathione hydrolase; Serine hydrolase involved in the detoxification of formaldehyde | 1.3001 | 0.4300 |
| ENSGACG00000008229 | G3P038 | 3-hydroxyisobutyrate dehydrogenase b | 1.3116 | 0.3491 |
| ENSGACG00000008812 | G3P216 | ATP-citrate synthase | 1.0823 | 0.8046 |
| ENSGACG00000009052 | G3P2Y2 | acetyl-CoA acetyltransferase 2; Belongs to the thiolase family | 1.5821 | 0.3002 |
| ENSGACG00000009260 | G3P3Q9 | Carnitine O-octanoyltransferase | 0.9284 | 0.6689 |
| ENSGACG00000010847 | G3P9Y0 | Propionyl Coenzyme A carboxylase, beta polypeptide | 1.1791 | 0.6464 |
| ENSGACG00000011008 | G3PAG5 | Aldehyde dehydrogenase 8 family, member A1 | 1.8580 | 0.0736 |
| ENSGACG00000012482 | G3PFX9 | Electron-transfer-flavoprotein, beta polypeptide | 1.1469 | 0.4535 |
| ENSGACG00000012603 | G3PGD9 | Aldehyde dehydrogenase 6 family, member A1 | 1.5511 | 0.0897 |
| ENSGACG00000014569 | G3PNP5 | Enoyl CoA hydratase domain containing 2 | 1.1497 | 0.7326 |
| ENSGACG00000014754 | G3PPG0 | acyl-Coenzyme A dehydrogenase, long chain | 1.7563 | 0.1443 |
| ENSGACG00000015021 | G3PQD2 | Solute carrier family 27 (fatty acid transporter), member 2a | 1.4266 | 0.6544 |
| ENSGACG00000015440 | G3PRY3 | Hydroxysteroid dehydrogenase like 2 | 1.5789 | 0.0782 |
| ENSGACG00000015516 | G3PS84 | Epoxide hydrolase 2, cytoplasmic | 1.2114 | 0.6298 |
| ENSGACG00000015778 | G3PT87 | Betaine-homocysteine methyltransferase | 0.9680 | 0.9184 |
| ENSGACG00000016189 | G3PUT5 | Sterol carrier protein 2a; Belongs to the thiolase family | 1.2581 | 0.5811 |
| ENSGACG00000016474 | G3PVW1 | Alcohol dehydrogenase 5 | 1.3772 | 0.2447 |
| ENSGACG00000016587 | G3PWD3 | Electron-transferring-flavoprotein dehydrogenase | 1.1036 | 0.6458 |
| ENSGACG00000017650 | G3Q0D3 | annotation not available | 0.9606 | 0.9870 |
| ENSGACG00000017655 | G3Q0D8 | annotation not available | 1.2522 | 0.7668 |
| ENSGACG00000018549 | G3Q3R5 | Carnitine O-acetyltransferase a | 1.3618 | 0.1473 |
| ENSGACG00000019268 | G3Q6G3 | acyl-Coenzyme A oxidase 1, palmitoyl | 1.1526 | 0.6393 |
| ENSGACG00000020308 | G3QAB5 | acetyl-Coenzyme A carboxylase alpha | 0.9135 | 0.7992 |
| ENSGACG00000020472 | G3QB05 | Aldehyde dehydrogenase 3 family, member A2b | 1.2130 | 0.5202 |
| SUCLG2 | G3P457 | Succinate--CoA ligase [GDP-forming] subunit beta, mitochondrial | 1.2238 | 0.3511 |

**Supplemental Table 2.5.** A list of all the proteins from the liver proteome set that are included in functionally enriched STRING network CL:21363 glycolysis, and carbohydrate metabolism (see Figure 2.5b) from the 15°C vs. 7°C comparison, including STRING labels and protein accession number, STRING description, FC, and adjusted-p value.

| STRING labels | Protein Accession | Description (STRING) | FC | Adjusted-p |
|---|---|---|---|---|
| ENO3 | G3N816 | Enolase 3, (beta, muscle) | 0.5981 | 0.3967 |
| ENSGACG00000000231 | G3N4S5 | Oxoglutarate (alpha-ketoglutarate) dehydrogenase b (lipoamide) | 0.7106 | 0.7882 |
| ENSGACG00000000473 | G3N5N3 | Zgc:56622 | 0.8137 | 0.7200 |
| ENSGACG00000000827 | G3N710 | Alpha-1,4 glucan phosphorylase | 0.6126 | 0.4091 |
| ENSGACG00000000973 | G3N7I7 | Malate dehydrogenase 1, NAD (soluble) | 0.7396 | 0.7356 |
| ENSGACG00000001103 | G3N7Z3 | Oxoglutarate (alpha-ketoglutarate) dehydrogenase b (lipoamide) | 0.9392 | 0.8950 |
| ENSGACG00000001505 | G3N9H1 | Enolase 1b, (alpha) | 0.5470 | 0.3188 |
| ENSGACG00000001637 | G3NA55 | Aconitase 1, soluble; Belongs to the aconitase/IPM isomerase family | 0.8246 | 0.8466 |
| ENSGACG00000002198 | G3NC51 | Phosphoenolpyruvate carboxykinase 2 (mitochondrial) | 0.6186 | 0.5243 |
| ENSGACG00000002519 | G3NDB1 | Si:ch211-217a12.1; Glutamic-pyruvate transaminase (alanine aminotransferase) | 0.8763 | 0.7799 |
| ENSGACG00000002813 | G3NEH8 | Glutamate dehydrogenase 1b; Belongs to the Glu/Leu/Phe/Val dehydrogenases family | 0.6464 | 0.4755 |
| ENSGACG00000003103 | G3NFG7 | Ketohexokinase | 0.6445 | 0.6857 |
| ENSGACG00000004178 | G3NJP8 | Aldolase a, fructose-bisphosphate, a | 0.5873 | 0.4973 |
| ENSGACG00000005040 | G3NN43 | Malic enzyme 1, NADP(+)-dependent, cytosolic | 0.3133 | 0.7249 |
| ENSGACG00000006005 | G3NRH9 | Transketolase | 1.1688 | 0.8742 |
| ENSGACG00000006087 | G3NRT5 | Malate dehydrogenase 2, NAD (mitochondrial) | 0.8676 | 0.8485 |
| ENSGACG00000006964 | G3NVH9 | Phosphoglucomutase 1; Belongs to the phosphohexose mutase family | 0.7175 | 0.5124 |
| ENSGACG00000007164 | G3NW14 | 6-phosphogluconate dehydrogenase, decarboxylating | 0.9248 | 0.8944 |
| ENSGACG00000007509 | G3NXC0 | Dihydrolipoamide S-succinyltransferase | 0.8125 | 0.8122 |
| ENSGACG00000007534 | G3NXE2 | Aspartate aminotransferase; Glutamic-oxaloacetic transaminase 1, soluble | 0.5878 | 0.3960 |
| ENSGACG00000007567 | G3NXM9 | Aconitate hydratase, mitochondrial; Aconitase 2, mitochondrial; Belongs to the aconitase/IPM isomerase family | 0.9018 | 0.8465 |
| ENSGACG00000007692 | G3NXY4 | Phosphoglycerate mutase 1a; Belongs to the phosphoglycerate mutase family. BPG- dependent PGAM subfamily | 0.5705 | 0.3523 |
| ENSGACG00000007727 | G3NY35 | Aldolase A, fructose-bisphosphate | 0.4250 | 0.3523 |
| ENSGACG00000007744 | G3NY86 | Glucose phosphate isomerase a; Belongs to the GPI family | 0.6704 | 0.4779 |
| ENSGACG00000008240 | G3P046 | Dihydrolipoamide dehydrogenase | 0.9615 | 0.9383 |
| ENSGACG00000009687 | G3P5F2 | Aldo-keto reductase family 1, member A1a (aldehyde reductase) | 0.7857 | 0.7617 |
| ENSGACG00000009950 | G3P6I9 | Triosephosphate isomerase 1b | 0.7409 | 0.6931 |
| ENSGACG00000009964 | G3P6R2 | Transketolase b | 0.7900 | 0.7454 |
| ENSGACG00000010016 | G3P6N3 | Enolase 2 (gamma, neuronal) | 0.7508 | 0.8126 |
| ENSGACG00000010219 | G3P7L3 | Glyceraldehyde-3-phosphate dehydrogenase | 0.4499 | 0.3967 |
| ENSGACG00000010529 | G3P8K8 | Dihydrolipoamide S-succinyltransferase | 1.2534 | 0.8001 |
| ENSGACG00000010827 | G3P9S4 | Isocitrate dehydrogenase 2 (NADP+), mitochondrial; Belongs to the isocitrate and isopropylmalate dehydrogenases family | 1.5995 | 0.7617 |
| ENSGACG00000010851 | G3P9W8 | Citrate synthase; Belongs to the citrate synthase family | 1.2149 | 0.7212 |
| ENSGACG00000011403 | G3PBU7 | Fumarate hydratase | 0.6668 | 0.4616 |
| ENSGACG00000012197 | G3PEY0 | Hexose-6-phosphate dehydrogenase (glucose 1-dehydrogenase) | 0.5686 | 0.5124 |
| ENSGACG00000012936 | G3PHM0 | Glycogen [starch] synthase; Transfers the glycosyl residue from UDP-Glc to the non- reducing end of alpha-1,4-glucan | 0.7945 | 0.7361 |
| ENSGACG00000012993 | G3PHX0 | Branched chain keto acid dehydrogenase E1, alpha polypeptide | 0.7343 | 0.5732 |
| ENSGACG00000013457 | G3PJP7 | Dihydrolipoamide acetyltransferase component of pyruvate dehydrogenase complex | 0.8348 | 0.6112 |
| ENSGACG00000014614 | G3PNW0 | Amylo-1, 6-glucosidase, 4-alpha-glucanotransferase a | 0.7623 | 0.6508 |
| ENSGACG00000015394 | G3PRR1 | dicarbonyl/L-xylulose reductase | 0.8747 | 0.8593 |
| ENSGACG00000015578 | G3PSH5 | Sorbitol dehydrogenase | 0.9110 | 0.8895 |
| ENSGACG00000015857 | G3PTJ4 | Fructose-1,6-bisphosphatase 1b; Belongs to the FBPase class 1 family | 0.4751 | 0.3523 |
| ENSGACG00000016476 | G3PVW5 | Isocitrate dehydrogenase 2 (NADP+), mitochondrial | 2.1154 | 0.3523 |
| ENSGACG00000017200 | G3PYR1 | Transaldolase | 0.8365 | 0.7356 |
| ENSGACG00000017272 | G3PYW9 | Glutamic pyruvate transaminase (alanine aminotransferase) 2, like | 0.8265 | 0.6857 |
| ENSGACG00000017982 | G3Q1L3 | Aldolase b, fructose-bisphosphate | 0.6053 | 0.4419 |
| ENSGACG00000018891 | G3Q522 | Aldo-keto reductase family 1, member B1 (aldose reductase) | 0.9790 | 0.9803 |
| ENSGACG00000019269 | G3Q6G2 | Deoxyribose-phosphate aldolase (putative); 2-deoxyribose-5-phosphate aldolase homolog (C. elegans) | 0.8269 | 0.5243 |
| ENSGACG00000019606 | G3Q7Q5 | Malate dehydrogenase 1Aa, NAD (soluble) | 0.5268 | 0.4677 |

| STRING labels | Protein Accession | Description (STRING) | FC | Adjusted-p |
|---|---|---|---|---|
| ENSGACG00000019607 | G3Q7R4 | UDP-glucose pyrophosphorylase 2a | 0.6403 | 0.4575 |
| ENSGACG00000019710 | G3Q870 | Pyruvate carboxylase | 0.5565 | 0.5165 |
| ENSGACG00000019770 | G3Q8D5 | annotation not available | 0.8052 | 0.6394 |
| ENSGACG00000020619 | G3QBK7 | Aldolase C, fructose-bisphosphate, b | 0.8676 | 0.8465 |
| ENSGACG00000020647 | G3QBP3 | Acetyltransferase component of pyruvate dehydrogenase complex | 1.2117 | 0.8499 |
| ENSGACG00000020677 | G3QBS8 | Pyruvate dehydrogenase E1 component subunit alpha | 1.1882 | 0.7928 |
| ENSGACG00000020795 | G3QC79 | Phosphoglycerate kinase 1 | 1.1330 | 0.8214 |
| IDH3A | G3PZV8 | Uncharacterized protein; Isocitrate dehydrogenase 3 (NAD+) alpha | 0.9735 | 0.9689 |
| PKLR | G3PCS9 | Pyruvate kinase, liver and RBC | 0.7584 | 0.7619 |

**Supplemental Table 2.6.** A list of all the proteins from the liver proteome set that are included in functionally enriched STRING network CL:16360 ribosome biogenesis, and DEAD/DEAH box helicase (see Figure 2.5c) from the 15°C vs. 7°C comparison, including STRING labels and protein accession number, STRING description, FC, and adjusted-p value.

| STRING labels | Protein Accession | Description (STRING) | FC | Adjusted-p |
|---|---|---|---|---|
| BOP1 | G3P849 | Ribosome biogenesis protein BOP1 | 1.1461 | 0.8551 |
| ENSGACG00000000309 | G3N523 | Guanine nucleotide binding protein-like 3 (nucleolar) | 1.0200 | 0.9721 |
| ENSGACG00000001551 | G3N9N6 | Nucleolar protein interacting with the FHA domain of MKI67 | 1.6400 | 0.3991 |
| ENSGACG00000002969 | G3NEY2 | Ribosome biogenesis regulatory protein | 1.1153 | 0.8346 |
| ENSGACG00000003882 | G3NID2 | Apoptosis antagonizing transcription factor | 1.0897 | 0.8633 |
| ENSGACG00000004373 | G3NKC3 | Dyskeratosis congenita 1, dyskerin | 1.2253 | 0.6995 |
| ENSGACG00000005150 | G3NN85 | Nucleolar and coiled-body phosphoprotein 1 | 1.0518 | 0.9389 |
| ENSGACG00000006802 | G3NUK0 | EBNA1 binding protein 2 | 1.0850 | 0.8899 |
| ENSGACG00000007026 | G3NVH8 | DEAD (Asp-Glu-Ala-Asp) box polypeptide 5 | 1.1294 | 0.8238 |
| ENSGACG00000007175 | G3NVZ3 | Ribosomal RNA processing 12 homolog (S. cerevisiae) | 1.9122 | 0.7834 |
| ENSGACG00000008087 | G3NZD3 | DEAD (Asp-Glu-Ala-Asp) box polypeptide 24 | 1.2979 | 0.6931 |
| ENSGACG00000008815 | G3P227 | NOP56 ribonucleoprotein homolog | 1.0879 | 0.8466 |
| ENSGACG00000009161 | G3P3J6 | Proliferation-associated 2G4, b | 1.6761 | 0.4755 |
| ENSGACG00000009462 | G3P4I2 | RNA binding motif protein 19 | 0.7715 | 0.7356 |
| ENSGACG00000009568 | G3P4V7 | SNU13 homolog, small nuclear ribonucleoprotein b (U4/U6.U5); NHP2 non-histone chromosome protein 2-like 1b (S. cerevisiae) | 0.9812 | 0.9785 |
| ENSGACG00000011176 | G3PB04 | Uncharacterized protein; Deoxynucleotidyltransferase, terminal, interacting protein 2 | 1.1111 | 0.8444 |
| ENSGACG00000013723 | G3PKK2 | Peter pan homolog (Drosophila) | 0.9545 | 0.9565 |
| ENSGACG00000013746 | G3PKR4 | NOP58 ribonucleoprotein homolog (yeast) | 1.0718 | 0.8980 |
| ENSGACG00000016491 | G3PVZ2 | Brix domain containing 2 | 1.1846 | 0.8349 |
| ENSGACG00000018892 | G3Q520 | NOP10 ribonucleoprotein homolog (yeast) | 1.2731 | 0.6931 |
| ENSGACG00000020754 | G3QC25 | MYB binding protein (P160) 1a | 1.6349 | 0.7457 |
| ENSGACG00000020889 | G3QCK6 | NHP2 ribonucleoprotein homolog (yeast) | 0.6890 | 0.5994 |
| RSL1D1 | G3NKP9 | Ribosomal L1 domain containing 1 | 1.1335 | 0.7454 |
| UTP14A | G3N9E0 | Si:dkey-251i10.3; UTP14, U3 small nucleolar ribonucleoprotein, homolog A (yeast) | 1.1714 | 0.7710 |

**Supplemental Table 2.7.** A list of all the proteins from the liver proteome set that are included in functionally enriched STRING network CL:21790 pyridoxal phosphate-dependent transferase domain 1, and NAD(P)-binding domain (see Figure 2.5d) from the 15°C vs. 7°C comparison, including STRING labels and protein accession number, STRING description, FC, and adjusted-p value. The bolded entry, L-threonine dehydrogenase, had an adjusted p-value <0.05.

| STRING labels | Protein Accession | Description (STRING) | FC | Adjusted-p |
|---|---|---|---|---|
| AMDHD1 | G3Q9D1 | Si:ch73-71d17.1; Amidohydrolase domain containing 1 | 0.6751 | 0.6931 |
| DDAH1 | G3NU76 | Dimethylarginine dimethylaminohydrolase 1 | 0.9085 | 0.9383 |
| ENSGACG00000000824 | G3N6Z5 | Urocanate hydratase 1 | 0.4704 | 0.4755 |
| ENSGACG00000001248 | G3N8J3 | Glycerate kinase | 0.7259 | 0.5822 |
| ENSGACG00000004497 | G3NKR2 | Alanine-glyoxylate aminotransferase a | 0.6886 | 0.4616 |
| ENSGACG00000004528 | G3NKY0 | Histidine ammonia-lyase; Belongs to the PAL/histidase family | 0.6150 | 0.4616 |
| ENSGACG00000004960 | G3NMJ1 | Hydroxyacid oxidase (glycolate oxidase) 1 | 0.6211 | 0.5165 |
| ENSGACG00000005149 | G3NN91 | Phosphoglycerate dehydrogenase; Belongs to the D-isomer specific 2-hydroxyacid dehydrogenase family | 0.7643 | 0.6112 |
| ENSGACG00000005698 | G3NQA8 | Glycine N-methyltransferase | 0.6985 | 0.3523 |
| ENSGACG00000005808 | G3NQQ2 | Aminomethyltransferase; The glycine cleavage system catalyzes the degradation of glycine; Belongs to the GcvT family | 1.0496 | 0.9365 |
| ENSGACG00000006410 | G3NT37 | Serine hydroxymethyltransferase 2 (mitochondrial) | 0.4502 | 0.5165 |
| ENSGACG00000006428 | G3NTC1 | Methylenetetrahydrofolate dehydrogenase (NADP+ dependent) 1b | 0.7655 | 0.6931 |
| ENSGACG00000007764 | G3NYA3 | Serine hydroxymethyltransferase; Interconversion of serine and glycine; Belongs to the SHMT family | 0.6321 | 0.3967 |
| **ENSGACG00000010817** | **G3P9T5** | **L-threonine dehydrogenase** | **1.7904** | **0.0013** |
| ENSGACG00000011258 | G3PBH8 | Aldehyde dehydrogenase 1 family, member L1; In the C-terminal section; belongs to the aldehyde dehydrogenase family. ALDH1L subfamily | 0.7057 | 0.3960 |
| ENSGACG00000013666 | G3PKG4 | Alanine-glyoxylate aminotransferase b | 0.4873 | 0.3960 |
| ENSGACG00000013689 | G3PKG8 | Pipecolic acid oxidase | 0.8794 | 0.8770 |
| ENSGACG00000014244 | G3PMH8 | Trifunctional purine biosynthetic protein adenosine-3; Phosphoribosylglycinamide formyltransferase; In the C-terminal section; belongs to the GART family | 1.1452 | 0.8444 |
| ENSGACG00000015161 | G3PQW2 | 5-aminoimidazole-4-carboxamide ribonucleotide formyltransferase/IMP cyclohydrolase | 1.0559 | 0.8899 |
| ENSGACG00000015411 | G3PRU6 | Formiminotransferase cyclodeaminase | 0.7486 | 0.3523 |
| ENSGACG00000015777 | G3PT85 | Dimethylglycine dehydrogenase | 0.4804 | 0.4419 |
| ENSGACG00000015955 | G3PTW8 | Methenyltetrahydrofolate synthetase domain containing | 1.0231 | 0.9790 |
| ENSGACG00000016093 | G3PUE4 | Glyoxylate reductase/hydroxypyruvate reductase b; Belongs to the D-isomer specific 2-hydroxyacid dehydrogenase family | 0.6072 | 0.3967 |
| ENSGACG00000017396 | G3PZF6 | Sarcosine dehydrogenase | 0.6747 | 0.5436 |

**Supplemental Table 2.8.** A list of all the proteins from the liver proteome set that are included in functionally enriched STRING network CL:11311 core histone H2A/H2B/H3/H4, and histone H4 (see Figure 2.6d) from the 15°C vs. 25°C comparison, including STRING labels and protein accession number, STRING description, FC, and adjusted-p value. The bolded entries indicate proteins with adjusted p-values <0.05.

| STRING labels | Protein Accession | Description (STRING) | FC | Adjusted-p |
|---|---|---|---|---|
| **ENSGACG00000000444** | **G3N5J6** | **Uncharacterized protein; Histone H1 like** | **2.7456** | **0.0061** |
| **ENSGACG00000001130** | **G3N831** | **annotation not available** | **2.0630** | **0.0001** |
| ENSGACG00000001249 | G3N8I6 | Uncharacterized protein; Histone H1 like | 1.5621 | 0.0923 |
| ENSGACG00000001250 | G3N8I9 | Histone H2B; Zgc:171759; Belongs to the histone H2B family | 1.1659 | 0.4838 |
| **ENSGACG00000001256** | **G3N8J7** | **annotation not available** | **2.4495** | **0.0051** |
| **ENSGACG00000001268** | **G3N8L3** | **Uncharacterized protein; Histone H1 like** | **9.0108** | **0.0004** |
| ENSGACG00000001273 | G3N8M2 | Histone H2B; Zgc:171759; Belongs to the histone H2B family | 1.3666 | 0.1976 |
| ENSGACG00000005637 | G3NQ31 | Uncharacterized protein; Chromobox homolog 1 | 0.9685 | 0.8929 |
| ENSGACG00000007312 | G3NWG9 | Si:ch211-103n10.5 | 2.9733 | 0.0604 |
| **ENSGACG00000009033** | **G3P2U9** | **H1 histone family, member 0** | **2.3601** | **0.0171** |
| ENSGACG00000010538 | G3P8K1 | annotation not available | 1.4446 | 0.4061 |
| **ENSGACG00000010540** | **G3P8K7** | **annotation not available** | **1.6401** | **0.0358** |
| **ENSGACG00000013915** | **G3PL95** | **Uncharacterized protein; Histone H1 like** | **9.9169** | **0.0004** |
| ENSGACG00000014018 | G3PLM8 | annotation not available | 2.2504 | 0.0978 |
| **ENSGACG00000014597** | **G3PNT4** | **Core histone macro-H2A; Variant histone H2A which replaces conventional H2A in a subset of nucleosomes** | **1.4720** | **0.0442** |
| **ENSGACG00000014877** | **G3N8J1** | **Histone H4** | **1.7582** | **0.0273** |
| ENSGACG00000016482 | G3PVY2 | High-mobility group box 2a | 1.5475 | 0.1111 |
| ENSGACG00000018032 | G3N8L5 | annotation not available | 1.6401 | 0.1203 |
| ENSGACG00000020545 | G3QB97 | High-mobility group box 1a | 1.4543 | 0.1864 |
| **H2AFB1** | **G3P521** | **Histone H2A; Polyhomeotic-like 2b; Belongs to the histone H2A family** | **1.9153** | **0.0001** |
| **H2AFZ** | **G3N752** | **H2A histone family, member Z** | **1.8056** | **0.0202** |
| H3F3C | G3N829 | H3 histone, family 3C | 1.4309 | 0.2882 |
| KDM5A | G3Q5D6 | Lysine (K)-specific demethylase 5A | 1.6180 | 0.2520 |

**Supplemental Table 2.9.** A list of all the proteins from the liver proteome set that are included in functionally enriched STRING network CL:22217 acyltransferase choactase/COT/CPT, and SCP2 sterol-binding domain (see Figure 2.6e) from the 15°C vs. 25°C comparison, including STRING labels and protein accession number, STRING description, FC, and Adjusted-p value. The bolded entries indicate proteins with adjusted p-values <0.05.

| STRING labels | Protein Accession | Description (STRING) | FC | Adjusted-p |
|---|---|---|---|---|
| **ENSGACG00000003347** | **G3NGD4** | **Podocan** | **0.2300** | **0.0097** |
| ENSGACG00000006242 | G3NSH6 | Hydroxysteroid (17-beta) dehydrogenase 4 | 0.6084 | 0.0784 |
| ENSGACG00000009260 | G3P3Q9 | Carnitine O-octanoyltransferase | 0.8620 | 0.4434 |
| ENSGACG00000014569 | G3PNP5 | Enoyl CoA hydratase domain containing 2; Belongs to the enoyl-CoA hydratase/isomerase family | 0.6039 | 0.1630 |
| ENSGACG00000015440 | G3PRY3 | Hydroxysteroid dehydrogenase like 2 | 0.7419 | 0.2486 |
| ENSGACG00000015516 | G3PS84 | Epoxide hydrolase 2, cytoplasmic | 1.1534 | 0.7660 |
| **ENSGACG00000016189** | **G3PUT5** | **Sterol carrier protein 2a; Belongs to the thiolase family** | **0.3460** | **0.0017** |
| ENSGACG00000017650 | G3Q0D3 | annotation not available | 0.2773 | 0.3945 |
| ENSGACG00000017655 | G3Q0D8 | annotation not available | 0.4036 | 0.0567 |

**Supplemental Table 2.10.** A list of all the proteins from the liver proteome set that are included in functionally enriched STRING network CL:16051 mostly uncharacterized, incl. ribosomal protein, and ribosomal protein S18 (see Figure 2.6f) from the 15°C vs. 25°C comparison, including STRING labels and protein accession number, STRING description, FC, and Adjusted-p value. The bolded entries indicate proteins with adjusted p-values <0.05.

| STRING labels | Protein Accession | Description (STRING) | FC | Adjusted-p |
|---|---|---|---|---|
| ENSGACG00000001379 | G3N902 | Mitochondrial ribosomal protein S18B | 0.5222 | 0.2543 |
| **ENSGACG00000001715** | **G3NA94** | **Mitochondrial ribosomal protein S16** | **0.1471** | **0.0163** |
| **ENSGACG00000003642** | **G3NHG6** | **Mitochondrial ribosomal protein L41** | **0.5869** | **0.0163** |
| **ENSGACG00000004206** | **G3NJN3** | **Mitochondrial ribosomal protein L24; Belongs to the universal ribosomal protein uL24 family** | **0.5613** | **0.0218** |
| **ENSGACG00000004984** | **G3NMM0** | **Mitochondrial ribosomal protein L14** | **0.5949** | **0.0177** |
| ENSGACG00000010541 | G3P8K9 | Mitochondrial ribosomal protein L12 | 0.7705 | 0.5733 |
| ENSGACG00000011130 | G3PAU9 | Mitochondrial ribosomal protein L23 | 0.6371 | 0.1092 |
| **ENSGACG00000013370** | **G3PJ89** | **Mitochondrial ribosomal protein S18A** | **0.5747** | **0.0022** |
| ENSGACG00000014227 | G3PMG0 | Phosphatidylethanolamine binding protein 1 | 0.7729 | 0.4853 |
| **ENSGACG00000015241** | **G3PR63** | **Mitochondrial ribosomal protein L27** | **0.5557** | **0.0029** |
| ENSGACG00000020425 | G3QAU0 | Mitochondrial ribosomal protein S31 | 1.0779 | 0.9014 |
| MRPL55 | G3NBS4 | Zgc:171480; Mitochondrial ribosomal protein L55 | 0.6538 | 0.1265 |

**Supplemental Figure 2.1.** Volcano plot for smaller comparisons with significant differences (adjusted p-value < 0.05) showing proteins depicted as 1) red diamonds: significantly higher in abundance (FC > 2) and significantly different (adjusted p-value < 0.05), 2) blue diamonds: significantly lower in abundance (FC < 0.5) and significantly different, and 3) grey diamonds: did not meet cut off for both FC and significance requirements. The comparisons represented in the figure are as follows: a) KL7°C vs. BL7°C, b) KL15°C vs. KL25°C, c) BL15°C vs. BL25°C, d) KL7°C vs. KL25°C, e) BL7°C vs. BL25°C.

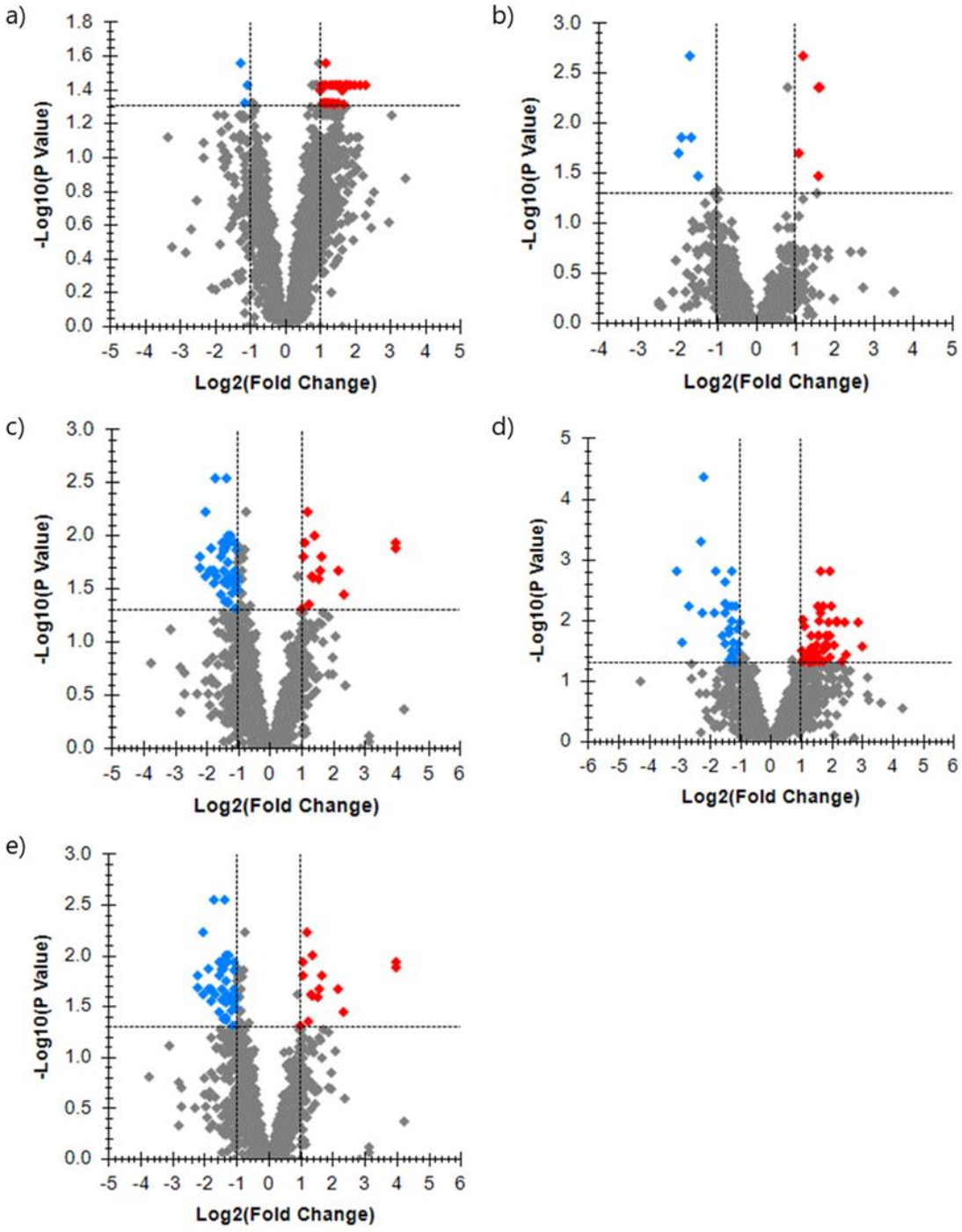

**Supplemental Figure 2.2.** Heat maps depicting significantly (adjusted p-value < 0.05) up and down regulated proteins for all biological replicates for smaller comparisons with significant differences. Yellow to red coloring represents proteins with a higher abundance, with red having the highest abundance. Dark blue to light blue represents proteins with a lower abundance, with light blue having the lowest abundance. The comparisons represented in the figure are as follows: a) KL7°C vs. BL7°C, b) KL15°C vs. KL25°C, c) BL15°C vs. BL25°C, d) KL7°C vs. KL25°C, e) BL7°C vs. BL25°C.

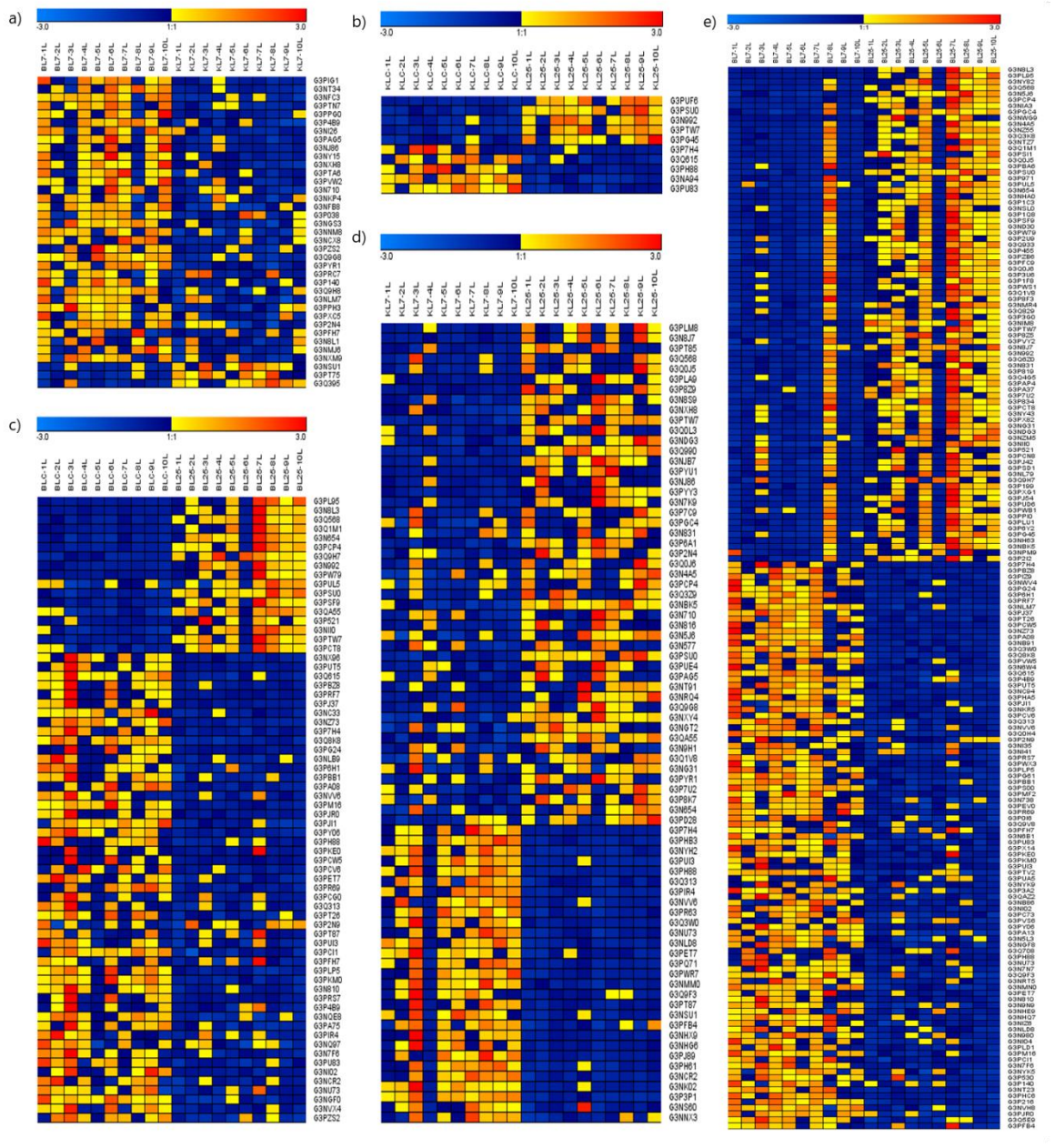

## CHAPTER 3

## Acute heat stress has different effects on the liver proteome of two populations of threespine sticklebacks (*Gasterosteus aculeatus*)


## ABSTRACT

A data-independent acquisition (DIA) assay library was used to examine thermal stress-induced, proteome-wide changes to the liver of Big lagoon (BL) and Klamath river (KL) populations of the threespine stickleback (*Gasterosteus aculeatus*). Lab-raised F1 progeny from each population were exposed to 28°C heat stress for two hours and allowed to recover at the original acclimation temperature of 15°C for either six or 24 hours, while controls remained at 15°C. BL fish displayed large changes in the liver proteome at six hours but had mostly regained protein homeostasis at 24 hours after the heat stress. In contrast, KL fish showed very little change in the liver proteome in response to acute heat stress at either time point, highlighting major differences in how the two populations respond to acute heat stress. HSP40-B1b was the only protein that was significantly elevated for both populations at both time points, suggesting a key role for this protein in regulating and orchestrating the response to acute heat stress for this species. Functional enrichment analyses using STRING identified larger networks and functional domains that were significantly enriched in the liver proteome of heat-stressed fish. STRING functional enrichment was complemented with KEGG pathway analyses of the large number of liver proteins that were significantly altered in BL fish at 6h after heat stress relative to controls (15°C). These analyses identified RNA processing, reactive oxygen species (ROS) homeostasis, and cellular and molecular structure as the main processes that were strongly altered in livers of BL fish but not in KL fish. We conclude that *G. aculeatus* response to heat stress differs

substantially between populations that have colonized different habitats. The different responses may indicate that divergent strategies for coping with heat stress have evolved rapidly in threespine sticklebacks.

## INTRODUCTION

Temperature is of the upmost importance for life, especially for ectothermic organisms, and has broad-ranging implications on the molecular, cellular, reproductive, and developmental success of individuals (Loarie et al., 2009; Menge & Olson, 1990; Seebacher, 2005; Zinn et al., 2010). Fish, being mostly ectothermic, are particularly impacted by changes in temperature (Beitinger & Fitzpatrick, 1979). As global temperatures are expected to rise throughout the 21$^{st}$ century along with the duration, intensity, and spatial extent of acute heat waves (IPCC, 2014), an increasing burden will be placed on the ability of fish to survive and recover from heat stress. Organisms are uniquely adapted to their environment, and their proteins have evolved to function most efficiently under the typical temperature regimes faced in their environment (Crawford et al., 1999). Temperature (thermal stress) is likely a strong driving force behind natural selection (Seebacher, 2005). Important factors such as coastal ecosystem biodiversity and ecosystem functioning and services have already been impacted by intensified heatwaves, in addition to acidification, sea level rise and changes in oxygen and salinity levels (IPCC, 2019). These environmental impacts have also lead to changes in the biogeographic patterns of numerous organisms (Nicolas et al., 2011; Somero, 2011). Populations from different parts of a species' biogeographic range respond to temperature changes differently (Genner et al., 2004). Therefore, it is important to understand the mechanisms behind the variety of responses to thermal challenge. Estuaries represent habitat that is especially susceptible to warming, with lagoons and

rivers facing the highest levels of warming due to their shallow depths, limited exchange with the ocean, and limited opportunities for behavioral avoidance such as escape to cooler areas (Scanes et al., 2020). Given differences in genetics and specific adaptations to various environments, it will become increasingly important to understand the molecular underpinnings of organismal responses to thermal stress.

Threespine sticklebacks (*Gasterosteus aculeatus*) are widely distributed throughout the northern hemisphere, including throughout California, and are comprised of many phenotypically diverse populations along both a longitudinal (North America, Europe, Asia) and latitudinal (Mexico to Alaska) gradient (Bell & Foster, 1994). There are three main morphotypes: completely plated (fully plated along the sides), partially plated (anterior plates and plates on the caudal keel), and low plated (anterior plates only) (Hagen & Gilbertson, 1972). Plating, especially in freshwater habitats, has been associated with many different factors such as predator presence, calcium availability, water flow, and climate (Östlund-Nilsson et al., 2007). Threespine sticklebacks are euryhaline fish that live in a variety of habitats including freshwater, brackish water, and coastal marine habitat, as well as populating some of the most susceptible habitats to warming from climate change—rivers and lagoons (Scanes et al., 2020). The genome sequence and a high-quality annotated reference proteome are available for this species, which empowers quantitative proteomics approaches. Furthermore, sticklebacks are abundant, easy to capture, survive well in captivity, can be bred in the laboratory, are easily externally fertilized, and have relatively short life cycles.

The proteome is more directly related to an organism's phenotype and more likely to be acted upon by natural selection than either the genome or transcriptome (Diz et al., 2012). Relationships between the abundances of transcript and corresponding protein is often nonlinear

and proteomics studies are necessary to reveal these relationships (Anderson & Seilhamer, 1997; Diz et al., 2012; Feder & Walser, 2005). Data-independent acquisition (DIA) mass spectrometry is a recently developed proteomics method that is well-suited for ecological proteomics studies (Gillet et al., 2012; J. Li et al., 2018). DIA fragments all of the precursor ions within a specified m/z window allowing for more reliable and consistent identification and quantification of multiple peptides for more than a thousand proteins in each sample (Fernández-Costa et al., 2020; J. Li et al., 2018; K. W. Li et al., 2020). Co-expression patterns of multiple proteins can then be evaluated by network analyses to identify molecular pathways that are regulated by heat and other stresses (Hall et al., 2020; Kültz et al., 2016; Tomanek, 2010).

In this study, we focus on the liver proteome because liver function reflects the overall physiological status of an organism (Liu et al., 2016; Qian & Xue, 2016; Trefts et al., 2017). To address the question as to how different genotypes and evolutionary histories represented by different populations of the same species influence the response to acute heat stress in fish, we examined the liver proteome of two *G. aculeatus* populations representing different morphotypes that occur in different estuarine habitats (river versus lagoon).

## MATERIALS AND METHODS

### Breeding of wild-caught fish, rearing of F1 progeny and range finding experiment

Fish were collected from the Klamath river (Klamath, CA) and Big lagoon (Trinidad, CA), externally fertilized, and F1 progeny were reared as previously described (Chapter 1). The critical thermal maximum (CTMax) was determined for both the Big lagoon (BL) and Klamath river (KL) populations as previously described (Chapter 1) and the results of this range finding experiment were used as the basis for selecting an appropriate temperature (28°C) for an acute

heat stress experiment. Experimental work was approved by and conducted according to UC Davis Institutional Animal Care and Use Committee (IACUC) rules and regulations (IACUC number 18010, AAALAC number 127 A3433-01).

**Exposure of fish to acute heat stress**

Lab-raised F1 offspring from BL and KL populations were kept at 15°C and 9 g/kg for three weeks prior to experimentation. Fish were fed *ad libitum* but withheld food 24 hours prior to the acute heat stress. For the two-hour acute heat stress, fish were transferred from 15°C to 28°C, which represents a survivable temperature that is lower than the CTMax (to ensure that the fish remain alive and do not lose equilibrium), but high enough (~90% CTMax) to represent a heat stress as indicated by fish becoming more active and agitated at 28°C. Fish were randomly assigned to experimental groups. Clear one-liter lidded containers were used to contain and separate fish and allowed for quick transfer and identification. The containers had mesh windows on either side to allow for rapid water circulation and aeration. Fish were observed throughout the two-hour acute heat stress to monitor behavior. All fish recovered at 15°C post heat stress. Control fish experienced the same handling as experimental fish but were kept at 15°C. Controls and heat stressed fish were sampled at either six or 24 hours after the end of the heat stress. Fish were sacrificed via spinal transection to not introduce drugs or chemicals into the tissues prior to proteomic analysis. At the time of dissection, fish were weighed, measured, photographed (left side), and sexed. Livers were dissected, flash-frozen in liquid nitrogen and stored at -80°C. Experimental groups are denoted as follows: BL15-6h, BL control fish kept at 15°C and sampled six hours after heat stress; BL28-6h, BL fish acutely heat-stressed at 28°C and sampled six hours after heat stress; BL15-24h, BL control fish kept at 15°C and sampled 24 hours after heat stress;

BL28-24h, BL fish acutely heat-stressed at 28°C and sampled 24 hours after heat stress. The same abbreviations are used for the experiment with KL fish except that the prefix BL is substituted with KL. Due to some mortality and removal of samples that did not meet QC criteria (mProphet q-values < 0.05 for the majority of transitions in the DIA assay library), the number of replicates in the experimental and control groups varies slightly as follows: BL15-6h, n=10; BL28-6h, n=10; BL15-24h, n=9; BL28-24h, n=10; KL15-6h, n=9; KL28-6h, n=10; KL15-24h, n=6; KL28-24h, n=9.

**Sample preparation, data-dependent acquisition (DDA), and data-independent acquisition (DIA)**

Sample preparation for quantitative, label-free, liquid chromatography tandem mass spectrometry (LCMS2) proteomics, DDA acquisition, and DIA acquisition were conducted exactly as previously described (Chapter 2). All DDA data are available at ProteomeXchange (PXD024677). The final DIA assay library, all DIA data and relevant metadata are available at Panorama Public (https://panoramaweb.org/bbl03.url).

**Statistical analysis and figure generation**

Heat maps were generated using Genesis 1.8.1 (Thallinger Lab, Graz University of Technology). Functional enrichment networks were analyzed and created in STRING 11.0 (Szklarczyk et al., 2019). STRING settings were as follows: Network edges were set to confidence (line thickness indicates strength of data support), all active interaction sources were included (text mining, experiments, databases, co-expression, neighborhood, gene fusion, and co-occurrence), the minimum required interaction score was medium confidence (0.400). Volcano plots, mass error

histograms, mProphet q-value distributions, and retention time reproducibility graphs were generated in Skyline 20.1.0.76 (Pino et al., 2017). Venny 2.1 (Oliveros, 2007) was used to create the Venn diagram. Skyline 20.1.0.76 was used for quantitative analyses and visualization of DIA data, and slight variations in retention time across runs were corrected using 14 manually selected iRT standards (Pino et al., 2017). The mass accuracy was set at 20 ppm for transitions. For group comparisons, the normalization method employed was equalize medians, the confidence level was 95% at the protein level, the summary method was Tukey's median polish, and the q-value cutoff was 0.05.

**Functional enrichment analysis**

Functional enrichment analysis was conducted with STRING 11.0 (Szklarczyk et al., 2019). For all four comparisons (BL15-6h vs. BL28-6h, BL15-24h vs. BL28-24h, KL15-6h vs. KL28-6h, KL15-24h vs. KL28-24h) the STRING "Proteins with Values/Ranks" function was used, with fold change serving as the rank used for the analysis. This list included the entire protein set with their corresponding fold changes based on the particular comparison for the liver tissue after both automated and manual curation of the assay library. Manual DIA assay library curation was conducted as the final step for each Skyline document to remove proteins that cannot be reliably quantified for a given set of samples. For proteins significantly 1) higher or 2) lower in abundance in the BL15-6h vs. BL28-6h comparison, the STRING "Multiple Proteins" function was used to functionally interpret these differences since the corresponding proteins were so numerous. For all comparisons, functional enrichments in STRING network clusters, Uniprot keywords, PFAM protein domains, INTERPRO protein domains and features, and SMART protein domains were analyzed and considered significant for FDR < 0.01. Additionally, for the

BL15-6h vs. BL28-6h comparison, KEGG Mapper v4.3 (Kanehisa & Sato, 2020) was used to map significantly different proteins to KEGG (Kyoto Encyclopedia of Genes and Genomes) pathways for further biological interpretation. *G. aculeatus* protein accession numbers were assigned to the corresponding K number for input into KEGG Mapper using Ghost Koala v2.2 (Kanehisa et al., 2016). All KEGG pathway graphics were created using KEGG Mapper v4.3 (Kanehisa Laboratories).

## RESULTS

### Liver spectral library and DIA assay library

The spectral library used was the same as that described in Chapter 2. The DIA assay library curated in Chapter 2 was also used for analysis in this study. Due to the larger number of samples in this study (N=73), separate Skyline files were created for each comparison. First, the corresponding DIA raw data were imported for all scans within ten minutes of the predicted retention time (RT). Peaks for the 14 previously selected internal retention time standards were manually checked for correct peak selection for the newly imported scans and the retention time calculator was updated for each comparison. mProphet was used to train a peak scoring model to optimize selection of the correct peaks and the retention time calculator was again updated to reflect any slight adjustments. All scans were then reimported within five minutes of the predicted RT, the mProphet peak picking model was retrained, all peaks were reintegrated to the new model, and the retention time calculator was adjusted again. The above steps were completed for each of the four comparisons, and all significantly different proteins were manually validated. Mass error, q-value distributions after the final mProphet model training and

peak reintegration, and the retention time reproducibility serve as quality control validation and are visualized for all four comparisons (Figure 3.1).

**Large effects of acute heat stress on BL after 6h recovery**

The response of the liver proteome was most elaborate for this population and time point. The volcano plot and heat map are shown in Figure 3.2. More than 200 proteins were significantly different in abundance at a fold change (FC) cut off of 2 or 0.5, respectively, 104 proteins were significantly elevated, and 101 proteins were significantly reduced in BL28-6h vs. BL15-6h (Supplemental Table 3.1). STRING analysis, which was based on FCs of all proteins in the DIA assay library, identified only STRING network clusters that were significantly (FDR <0.01) functionally depleted in BL28-6h vs. BL15-6h (Supplemental Table 3.2). They included ribosomal proteins, protein biosynthesis, and translation protein SH3 as well as disulphide isomerase, heat shock protein 70kD at the C-terminal domain, thioredoxin, calreticulin, and endoplasmic reticulum proteins. Uniprot keywords and PFAM, INTERPRO, and SMART entries were also functionally depleted in BL28-6h vs. BL15-6h. They included ribosomal protein, signal, ribonucleoprotein, and immunoglobulin E while histone H1and H5 were functionally enriched (Supplemental Table 3.2).

Another STRING functional enrichment analysis was conducted on only the proteins that were 1) significantly (adjusted p-value < 0.05) more abundant in BL28-6h vs. BL15-6h and 2) significantly less abundant in BL28-6h vs. BL15-6h since the number of these proteins was so numerous (Supplemental Table 3.3). From the group of proteins significantly higher in BL28-6h than BL15-6h, there were seven main significantly enriched STRING network clusters (Figure 3.3, Table 3.1): HSP20/alpha crystallin family and BAG domains, histones, RNA recognition

motif. and LSM domains, initiation factor 4E and MIF4G domains, ribosomal protein and protein biosynthesis, BolA protein and NFU1-like, and mitochondrion and eukaryotic porin. Some of the additional functional enrichments included RNA-binding, DNA-binding, peptidyl-prolyl cis-trans isomerase domain, high mobility group (HMG) box domains, zinc knuckle, LIM domains, and nucleotide-binding alpha-beta plait domains (Supplemental Table 3.3).

From the group of proteins significantly lower in BL28-6h than BL15-6h, there were ten main significantly enriched STRING network clusters (Figure 3.4, Table 3.2): filamin B and C, low-density lipoprotein (LDL) receptors, calreticulin family and disulphide isomerases, glycolysis and rhiamin diphosphate-binding fold, ribosomal protein and protein biosynthesis, respiratory chain and hydrogen ion transport, ribosomal protein L25/Gln-tRNA synthetase and lysine-tRNA ligase, RNA recognition motif. and mRNA processing, myosin tail, and actin and F-actin-capping protein subunit alpha/beta. Some of the additional functional enrichments included thioredoxins and redox-active center proteins, and heat shock protein 70 family (Supplemental Table 3.3).

Kyoto Encyclopedia of Genes and Genomes (KEGG) Mapper Search Results were also conducted on proteins that were significantly different in abundance between BL28-6h and BL15-6h. Four KEGG pathways with four or more proteins were elevated post heat stress (Table 3.3): RNA transport (Supplemental Figure 3.1), spliceosome (Supplemental Figure 3.2), oxidative phosphorylation (Figure 3.5), and mRNA surveillance pathway (Supplemental Figure 3.3). Six KEGG pathways with four or more proteins were depleted in heat stressed BL fish versus the control six hours after heat stress (Table 3.4): lysosome (six proteins), peroxisome (five proteins), phagosome (five proteins), apoptosis (five proteins), cholesterol metabolism (four proteins), and oxidative phosphorylation (Figure 3.5). Note that several proteins involved in

oxidative phosphorylation are elevated while others in the same pathway are reduced after 6h recovery from heat stress (see discussion below).

**Reduced effects of acute heat stress on the BL liver proteome after 24h recovery**

Two proteins, DnaJ heat shock protein family (HSP40) member B1b (G3Q4Q5) and an uncharacterized protein (G3Q568) were significantly higher in abundance (BL28-24h > BL15-24h) and met the fold change cut off of greater than two (Figure 3.6, Supplemental Table 3.1). Six proteins, eukaryotic translation elongation factor 2b (G3PRF7), phosphoethanolamine methyltransferase (G3Q0H4), leukocyte cell-derived chemotaxin 2 like (G3P7H4), angiotensinogen (G3P5J3), acetyl-CoA acyltransferase 2 (G3NIZ1), and fibrinogen gamma chain (G3PXC5) were significantly lower in abundance in BL28-24h and met the fold change cut off of less than 0.5 (Figure 3.6, Supplemental Table 3.1). STRING network analysis with all proteins in the set included and with fold change as the rank yielded only STRING network cluster functional enrichments that were lower in the acute heat stressed group (BL28-24h) (Supplemental Table 3.2). The main significantly (FDR < 0.01) functionally enriched STRING network clusters pertained to ribosomal proteins, protein biosynthesis and translation protein SH3-like domain superfamily (Supplemental Table 3.2). Significantly functionally enriched Uniprot keywords (BL15-24h > BL28-24h) included signal and ribosomal protein. SMART protein domains that were significantly functionally enriched in BL15 included elongation factor G C-terminus and actin, while significant functional enrichments for BL28 from the SMART protein domains included domains in histone families 1 and 5.

**Small effects of acute heat stress on KL**

In contrast to the large effect of heat stress on the liver proteome of BL fish, only a single protein was significantly different in KL fish at six hours post heat stress (Figure 3.7, Supplemental Table 3.1). DnaJ heat shock protein 40 family member B1b (HSP40-B1b, G3Q4Q5) was significantly elevated in KL28-6h vs. KL15-6h by over 13-fold (adjusted p-value: 3.55E-05). STRING analysis of all proteins in DIA assay library with FC as the rank yielded only significant (FDR < 0.01) STRING network clusters that were functionally depleted in KL28-6h vs. KL15-6h, including glycolysis, L-lactate/malate dehydrogenase, thiamin diphosphate-binding fold, carbohydrate metabolism, and glycolysis (Supplemental Table 3.2).

Three proteins were significantly altered in abundance after 24h recovery from heat stress in KL fish (Figure 8, Supplemental Table 3.1). HSP40-B1b (G3Q4Q5) was significantly elevated by over 8-fold (adjusted p-value: 0.037) while sulfurtransferase (G3NZ73) and an uncharacterized protein (G3Q4H0) were significantly reduced in KL28-24h vs. KL15-24h. Despite having few individual proteins reach significance, numerous STRING network clusters were significantly functionally enriched after analysis of all proteins in the DIA assay library with FC as the ranking, including ribosomal proteins, protein biosynthesis, translation, ribosomal biogenesis, RNA-binding and zinc-finger, RNA recognition motifs, and DEAD/DEAH box helicase (Supplemental Table 3.2).

STRING network clusters that were significantly functionally depleted in KL28-24h vs. KL15-24h included glycolysis, L-lactate/malate dehydrogenase, carbohydrate metabolism, oxidoreductase, thiamin diphosphate-binding fold, tyrosine 3-monoxygenase-like and pyridoxal phosphate-dependent transferase, AMP-binding and aldehyde dehydrogenase, NAD(P)-binding domain superfamily, enolase, low-density lipoprotein receptors, tyrosine 3-monooxygenase-like and sepiapterin reductase, A-macroglobulins and complement C3, pyridoxal phosphate-

dependent transferase domain 1, ClpP/crotonase-like domain superfamily, and metal-dependent hydrolase and adenylate /UMP-CMP kinase (Supplemental Table 3.2).

## DISCUSSION

### HSP40-B1b is a key regulator after acute temperature stress in *G. aculeatus* liver

HSP40-B1b was the only protein that was significantly elevated in both populations at both recovery times suggesting that it is a key component in coordinating the heat stress response throughout the recovery period in this species (Figure 3.9). HSP40 (also known as DnaJ) is a molecular chaperone that is mainly located in the cytoplasm but moves into the nucleus and nucleolus during heat stress before returning to the cytoplasm during recovery (Hattori et al., 1992; Ohtsuka & Hata, 2000). HSP40 proteins work in conjunction with HSP70 and different HSP40 isoforms can convey specific functionality to HSP70 (Rassow et al., 1995). HSP40 proteins select substrates to bind to HSP70 and help to stabilize substrate binding by stimulating ATP hydrolysis in HSP70. What makes the B member HSP40 isoforms unique is that they possess another layer of regulation in the form of a glycine-phenylalanine rich section that blocks the HSP70 binding site (Faust et al., 2020). The blocked HSP70 binding site is only released after HSP40 interacts with a secondary site on the HSP70 C-terminal tail, allowing for precise targeting and clustering of HSP70 to a specific substrate and is hypothesized to be the reason for B member HSP40 proteins being vital for disaggregating amyloid fibers (Faust et al., 2020). Even a small increase in temperature can cause proteins to denature, creating the opportunity for unwanted protein-protein interactions and aggregates to form (Richter et al., 2010). Two other B member proteins are included in the liver proteome DIA assay library used for this study

(including another B1 protein), but it was specifically member B1b that was elevated across all four experiments, suggesting that this particular protein provides some specific function or advantage over the other B member variants during heat stress. A specialized function of HSP40-B1b in allowing HSP70 to target pertinent protein aggregates highlights one possible explanation for its widespread and sustained increase during heat stress.

The literature regarding HSP40 after acute temperature stress in fish mainly pertains to gene expression levels. Heat stressed (1°C/h increase from 24°C until 36°C, then held 30-100 minutes) catfish (hybrids between *Ictalurus punctatus* and *Ictalurus furcatus*) had enriched expression of three HSP40 members (A1, A4, B1) in gill and liver of fish with both high and low heat tolerance (Liu et al., 2013). More heat tolerant fish exhibited higher expression levels of HSP40-B1 than the low heat tolerant fish, which had higher levels of HSP40-A. This finding suggests that higher levels of the HSP40-B1 in conjunction with the very large increases in HSP70 expression levels in highly heat tolerant fish convey a higher heat tolerance (Liu et al., 2013). Liver transcriptomics of heat-stressed (22°C to 31°C) large yellow croakers (*Larimichthy crocea*) revealed a 4.7 fold increase in gene expression of HSP40 (Qian & Xue, 2016). However in gilthead sea bream (*Sparus aurata*), HSP40 expression levels (including HSP40-A3A and HscB) of hepatic mitochondria were not significantly altered after temperature stress (water temperature cycles of 2 days at 12 °C to 3 days at 20 °C), whereas HSP60 and HSP10 were consistently upregulated (Bermejo-Nogales et al., 2014). This finding suggests that HSP40 function during heat stress is not universal across all species and cell organelles.

**RNA processing his rapidly regulated during recovery from heat shock in BL fish**

Three KEGG pathways (RNA transport, spliceosome, and mRNA surveillance) were enriched in proteins that were significantly more abundant in livers of heat shocked BL fish after six hours recovery. This result clearly indicates an increase in RNA processing after heat stress. RNA splicing and protein synthesis appear to be inhibited during and for several hours after heat shock until enough heat shock proteins accumulate during recovery to alleviate this disruption and allow for recovery of cellular processes (Yost & Lindquist, 1986). Because of macromolecular damage that impairs cellular processes, responses to severe stress are often more pronounced during the recovery period than during actual exposure to stress (Kültz, 2005). For this reason, we have designed our experiments to allow for recovery from acute stress.

The mRNA surveillance pathway serves as a quality control pathway to ensure that erroneous mRNA templates are not translated (Fasken & Corbett, 2005). Of the four proteins in this pathway that were significantly elevated in BL fish, three are a part of the exon-junction complex (EJC) and the fourth is a polyadenylate-binding factor that is involved in both recognition of premature termination codons that leads to nonsense mediated decay (NMD) and in translational stalling. The EJC is also involved in splicing (Hir et al., 2016), and all four proteins are also involved in RNA transport as per the KEGG pathway analysis.

Additional overlap between the STRING clusters and KEGG pathways for the significantly more abundant proteins in BL fish after 6h recovery included three RNA recognition motif (RRM, RBD, RNP domain) and LSM domain proteins included in the KEGG spliceosome and RNA transport pathways and multiple ribosomal and translation proteins involved in the KEGG RNA transport pathway. The STRING analysis also showed significant functional enrichment in histones, especially histone 1 or histone 1-like proteins. Remodeling of the nucleosome, which is comprised of DNA wrapped around histone proteins, occurs after

stress to regulate gene expression by allowing access to stress-response genes so transcription can take place (de Nadal et al., 2011). The regulation of gene expression is highly stress and organism specific (de Nadal et al., 2011), and the changes in protein abundance involved in these processes have the potential to provide insight into the types and severity of stresses faced by species in the wild.

**ROS metabolism is rapidly regulated during recovery from heat shock in BL fish**

ROS levels increase as a result of many types of stress, including heat stress (Fedyaeva et al., 2014). STRING and KEGG pathway analyses consistently identified ROS homeostasis and metabolism functions to be highly enriched among proteins that were significantly elevated in BL28-6h. These proteins included eukaryotic porins and proteins in the oxidative phosphorylation pathway. Furthermore, oxidative phosphorylation was the only KEGG pathway with at least four significantly more and at least four significantly less abundant proteins in BL28-6h or any other condition tested (Figure 3.5). While proteins that make up complexes I, II, and III decreased, proteins that constitute complexes I and IV increased. Heat stress inhibits the electron transport chain and ATP synthesis by oxidizing protein thiols in complex I, II, IV, and V (Slimen et al., 2014). Complex I is especially susceptible to heat stress and is likely the reason why oxidative phosphorylation rates decrease overall during heat stress (Downs & Heckathorn, 1998). Small molecular weight HSPs may provide some protection to NADH:ubiquinone oxidoreductases in Complex I and allow for a return to function (Downs & Heckathorn, 1998), which could be one explanation for the increases in HSP40, HSP20, and four NADH:ubiquinone oxidoreductases in BL28-6h. High mobility group (HMG) box proteins, which were also

functionally enriched, may facilitate redox-sensitive signaling and DNA repair of oxidative damage (Ilmakunnas et al., 2008; Lotze & Tracey, 2005; Tang et al., 2010).

However, the regulation of ROS metabolism after heat stress is complex as depletion of ROS related functions at the network and pathway level was also observed in BL28-6h. Lysosome, peroxisome, phagosome, apoptosis, and cholesterol metabolism are KEGG pathways containing at least four proteins that were significantly decreased in abundance in the BL28-6h (Table 3.4). These pathways aid in protein degradation and other catabolism within the cell. They also produce ROS and their functional depletion further highlights the importance of reducing internal ROS production during recovery from heat stress. Lysosomes translocate protons into the interior in a redox chain that uses oxygen as the terminal electron acceptor and results in the release of hydroxyl radicals, a particularly powerful ROS (Nohl & Gille, 2005). Peroxisomes, which are susceptible to oxidation and damage from environmental stress, play a role in ROS homeostasis as they both produce and scavenge ROS and are capable of being inactivated if internal ROS production becomes too great (Schrader & Fahimi, 2006; Su et al., 2019; Walker et al., 2018). Increased hepatic cholesterol synthesis in aged rats has been shown to lead to an increase in superoxide ions and an increase in intracellular ROS levels (Trapani & Pallottini, 2010). Therefore, downregulation of these functions aids in the recovery from ROS accumulation during heat stress.

Functional depletion of structural proteins such as filamin, myosin, and actin was evident in BL28-6h suggesting that the cytoskeleton was reorganized. Actin remodeling aids in cell translocation, shape changes, and resistance to mechanical stress and filamin A is a cross-linking agent that forms three-dimensional networks with actin (Nakamura et al., 2007). Filamin B is also an actin binding protein that aids in reorganization of the actin cytoskeleton (Zhao et al.,

2015). ROS such as $H_2O_2$ can damage structural proteins (Slimen et al., 2014), and the cytoskeleton is also highly susceptible to heat stress (Tomanek, 2014). Our results support a key role of minimizing ROS production after heat stress in BL fish, but this evidence is not seen in KL fish indicating that different populations can differ in their strategies for coping with heat stress.

**Proteostasis mechanisms are rapidly regulated during recovery from heat shock in BL**

Proteostasis processes, including protein stability and synthesis regulation, were functionally enriched in STRING network clusters of significantly regulated proteins in BL28-6h. As mentioned previously, HSP20 was among those besides HSP40-B1b. Peptidyl-proline isomerases (PPIases) help accelerate the folding of nascent polypeptide chains (Fischer & Schmid, 1990). Ribosomal proteins and translation were among the processes most affected by heat stress. Like oxidative phosphorylation, ribosomal proteins and translation were also significantly functionally enriched (six proteins, Table 3.1) and depleted (eight proteins, Table 3.2) in BL28-6h. Given the need to increase translation of certain proteins in response to stress to enable recovery while suppressing energetically costly translation of other less vital proteins, i.e. to change translational preference, it is not surprising that there were both increases and decreases in ribosomal proteins responsible for translation. Translation inhibition can occur during heat stress, when handling misfolded and aggregated proteins takes priority, but is later reinstated in an effort to efficiently return to protein homeostasis after attempting to salvage existing proteins (Cherkasov et al., 2013). The RNA recognition motif is a highly versatile way to regulate translational preference through high binding affinity and sequence specificity that is recognized by the translation machinery (Maris et al., 2005). This function was also both

functionally enriched and depleted suggesting that a shift in translational preference is highly prevalent in BL28-6h.

**Induction of low rather than higher molecular weight HSPs in BL**

Unlike most genes, HSP genes typically do not contain introns and are, therefore, less affected by the inhibition of RNA processing during stress and immediate recovery from stress allowing them to be translated more rapidly than most other proteins (Basu et al., 2002). By six hours after the acute heat stress, HSP40-B1b and HSP-b8 (from the HSP20 family) were the only heat shock proteins elevated in BL fish. Even though HSP110, HSP90, and HSP70 are all thought to be potential biomarkers of acute heat stress (Mahanty et al., 2016), none of them was elevated under any condition tested in our study despite 28°C clearly being a challenging temperature (90% CTMax). This finding supports the argument that induction of a classical heat shock response in fish typically occurs at the critical lethal temperature (100% CTMax) (Currie, 2011). HSP transcript levels may have spiked before the six hour timepoint, but protein abundance lags behind and several studies have shown that HSP proteins remain elevated for up to several days after heat stress (Lewis et al., 2016; Purohit et al., 2014).

The lack of high molecular weight HSP induction is likely not a result of a lack of protein unfolding. Ubiquitin associated protein 2-like (G3NKL2) and ubiquitin like 4A (G3P9X2) were both significantly elevated in BL28-6h, while ubiquitin specific peptidase 47, which catalyzes the removal of ubiquitin and aids in cell proliferation and survival (Piao et al., 2015), and ubiquitin carboxyl-terminal hydrolase (G3P5Z2), which is also involved in cell survival (Shen et al., 2006) were both significantly decreased. In a DNA microarray study on *Gillichthys mirabilias* gill tissue, the authors found that regardless of acclimation temperature a mild

temperature stress strongly upregulated the HSP70 gene, slightly higher temperatures upregulated the gene encoding ubiquitin, and extreme temperature stress upregulated the gene encoding cyclin-dependent kinase inhibitor 1B (Logan & Somero, 2011). These results indicate that functions aiding in the removal of unfolded proteins are clearly promoted.

**The KL population responds much less to acute heat stress than the BL population**

A striking finding of this study is the large difference in the response to acute heat stress in KL versus BL populations, despite having an almost identical CTMax (Chapter 1). Unlike the elaborate response of BL fish discussed above, the KL population showed a very limited response to acute temperature stress, at least for the two timepoints analyzed. Only a single KL liver protein (HSP40-B1b) was significantly different after six hours post-heat stress and only three after 24 hours post-heat stress. BL fish also had only eight significant differences in protein abundance compared to controls after 24h recovery from heat stress, suggesting that after 24 hours protein homeostasis had essentially returned to normal. However, the dramatic difference between the two populations at the 6h recovery time arises from differences in the timing of the response, i.e. highly transient protein changes may have been missed in the KL population because only two timepoints (six and 24 hours) were analyzed. In an acute heat shock experiment (15°C to 22°C for 30 minutes) with arctic char, liver mRNA transcript levels for HSP70 were significantly elevated one, two, and four hours post heat shock, while protein levels of HSP70 were significantly elevated at two, four, eight, 16, and 24 hours post heat shock (Lewis et al., 2016). While it seems unlikely that transcription, translation, and degradation of a large number of proteins would all occur within six hours of recovery, it is slightly more feasible that protein changes peaked and then returned to homeostasis in between the six hour and 24-hour

time point for the KL population. Even if that were the case, the difference between these populations is still very intriguing. Significantly functionally enriched STRING network clusters in livers of heat stressed KL fish at 24 hours support the notion that KL fish may have a delayed response relative to BL fish. These functional clusters were similar to those observed in BL fish at 6h post heat-stress. Their enrichment implies increased ribosomal function, presumably to replenish damaged proteins after the heat stress. Moreover, ribosomes in prokaryotes play a key role as sensors of temperature stress that induces the universal cellular stress response and they are a potential biomarker for cellular stress in eukaryotes (Cheng-Guang & Gualerzi, 2021; Quinn et al., 2011b; VanBogelen & Neidhardt, 1990). In heat stressed arctic char (15°C to 19°C for 72h), ribosome biogenesis began shortly after returning to the control temperature in the gill, but stayed elevated and even increased 72h thereafter (Quinn et al., 2011b). A delayed response to heat stress in KL vs. BL fish could be caused by a more severe inhibition of normal functioning during and after the acute temperature stress in KL than in BL, which is able to mount a much more robust response within six hours after acute heat stress. Alternatively, there may be greater diversity in the acute temperature stress response in the Klamath population that prevented significance in both the one-on-one protein abundance comparisons and the network-based approach. Given that both populations have very similar CTMax (Chapter 1), it seems unlikely that the KL population was simply not challenged by the acute heat stress. Studies on *Drosphila melanogaster* and a close relative, *Drosophila simulans,* found evidence for major selective sweeps in both populations occupying the same hot and dry canyon habitat, but little adaptive convergence, suggesting multiple solutions to dealing with environmental challenge (Kang et al., 2019). Future experiments informed by our work include studies that dissect the temporal scale of the response at greater resolution and compare it in other tissues.

## DATA ACCESSIBILITY

All proteomics data and metadata are accessible at the following repositories: ProteomeXchange (ID=PXD024677) for all DDA data and Panorama Public (https://panoramaweb.org/bbl03.url) for the DIA assay library and all DIA data.

## ACKNOWLEDGMENTS

Part of this work was funded by NSF grant IOS-1656371. Permission was granted from Kanehisa Laboratories to publish the KEGG pathway images in Figure 3.5 and Supplemental Figures 3.1, 3.2, and 3.3.

## REFERENCES


Anderson, L., & Seilhamer, J. (1997). A comparison of selected mRNA and protein abundances in human liver. *ELECTROPHORESIS*, *18*(3–4), 533–537. https://doi.org/10.1002/elps.1150180333

Basu, N., Todgham, A. E., Ackerman, P. A., Bibeau, M. R., Nakano, K., Schulte, P. M., & Iwama, G. K. (2002). Heat shock protein genes and their functional significance in fish. *Gene*, *295*(2), 173–183. https://doi.org/10.1016/S0378-1119(02)00687-X

Beitinger, T. L., & Fitzpatrick, L. C. (1979). Physiological and Ecological Correlates of Preferred Temperature in Fish. *American Zoologist*, *19*(1), 319–329. https://doi.org/10.1093/icb/19.1.319

Bell, M. A., & Foster, S. A. (Eds.). (1994). *The evolutionary biology of the threespine stickleback*. Oxford University Press.

Bermejo-Nogales, A., Nederlof, M., Benedito-Palos, L., Ballester-Lozano, G. F., Folkedal, O., Olsen, R. E., Sitjà-Bobadilla, A., & Pérez-Sánchez, J. (2014). Metabolic and transcriptional responses of gilthead sea bream (Sparus aurata L.) to environmental stress: New insights in fish mitochondrial phenotyping. *General and Comparative Endocrinology*, *205*, 305–315. https://doi.org/10.1016/j.ygcen.2014.04.016

Cheng-Guang, H., & Gualerzi, C. O. (2021). The Ribosome as a Switchboard for Bacterial Stress Response. *Frontiers in Microbiology*, *11*, 619038. https://doi.org/10.3389/fmicb.2020.619038

Cherkasov, V., Hofmann, S., Druffel-Augustin, S., Mogk, A., Tyedmers, J., Stoecklin, G., & Bukau, B. (2013). Coordination of Translational Control and Protein Homeostasis during

Severe Heat Stress. *Current Biology*, *23*(24), 2452–2462. https://doi.org/10.1016/j.cub.2013.09.058

Crawford, D. L., Pierce, V. A., & Segal, J. A. (1999). Evolutionary Physiology of Closely Related Taxa: Analyses of Enzyme Expression. *American Zoologist*, *39*(2), 389–400.

Currie, S. (2011). TEMPERATURE | Heat Shock Proteins and Temperature. In A. P. Farrell (Ed.), *Encyclopedia of Fish Physiology* (pp. 1732–1737). Academic Press. https://doi.org/10.1016/B978-0-12-374553-8.00196-9

de Nadal, E., Ammerer, G., & Posas, F. (2011). Controlling gene expression in response to stress. *Nature Reviews Genetics*, *12*(12), 833–845. https://doi.org/10.1038/nrg3055

Diz, A. P., Martínez-Fernández, M., & Rolán-Alvarez, E. (2012). Proteomics in evolutionary ecology: Linking the genotype with the phenotype. *Molecular Ecology*, *21*(5), 1060–1080. https://doi.org/10.1111/j.1365-294X.2011.05426.x

Downs, C. A., & Heckathorn, S. A. (1998). The mitochondrial small heat-shock protein protects NADH:ubiquinone oxidoreductase of the electron transport chain during heat stress in plants. *FEBS Letters*, *430*(3), 246–250. https://doi.org/10.1016/s0014-5793(98)00669-3

Fasken, M. B., & Corbett, A. H. (2005). Process or perish: Quality control in mRNA biogenesis. *Nature Structural & Molecular Biology*, *12*(6), 482–488. https://doi.org/10.1038/nsmb945

Faust, O., Abayev-Avraham, M., Wentink, A. S., Maurer, M., Nillegoda, N. B., London, N., Bukau, B., & Rosenzweig, R. (2020). HSP40 proteins use class-specific regulation to drive HSP70 functional diversity. *Nature*, *587*(7834), 489–494. https://doi.org/10.1038/s41586-020-2906-4

Feder, M. E., & Walser, J.-C. (2005). The biological limitations of transcriptomics in elucidating stress and stress responses. *Journal of Evolutionary Biology*, *18*(4), 901–910. https://doi.org/10.1111/j.1420-9101.2005.00921.x

Fedyaeva, A. V., Stepanov, A. V., Lyubushkina, I. V., Pobezhimova, T. P., & Rikhvanov, E. G. (2014). Heat shock induces production of reactive oxygen species and increases inner mitochondrial membrane potential in winter wheat cells. *Biochemistry. Biokhimiia*, *79*(11), 1202–1210. https://doi.org/10.1134/S0006297914110078

Fernández-Costa, C., Martínez-Bartolomé, S., McClatchy, D. B., Saviola, A. J., Yu, N.-K., & Yates, J. R. (2020). Impact of the Identification Strategy on the Reproducibility of the DDA and DIA Results. *Journal of Proteome Research*, *19*(8), 3153–3161. https://doi.org/10.1021/acs.jproteome.0c00153

Fischer, G., & Schmid, F. X. (1990). The mechanism of protein folding. Implications of in vitro refolding models for de novo protein folding and translocation in the cell. *Biochemistry*, *29*(9), 2205–2212. https://doi.org/10.1021/bi00461a001

Genner, M. J., Sims, D. W., Wearmouth, V. J., Southall, E. J., Southward, A. J., Henderson, P. A., & Hawkins, S. J. (2004). Regional climatic warming drives long–term community changes of British marine fish. *Proceedings of the Royal Society of London. Series B: Biological Sciences*, *271*(1539), 655–661. https://doi.org/10.1098/rspb.2003.2651

Gillet, L. C., Navarro, P., Tate, S., Rost, H., Selevsek, N., Reiter, L., Bonner, R., & Aebersold, R. (2012). Targeted data extraction of the MS/MS spectra generated by data-independent acquisition: A new concept for consistent and accurate proteome analysis. *Mol Cell Proteomics*, *11*(6), O111 016717. https://doi.org/10.1074/mcp.O111.016717

Hagen, D. W., & Gilbertson, L. G. (1972). Geographic variation and environmental selection in Gasterosteus aculeatus L. in the Pacific Northwest, America. *Evolution*, *26*(1), 32–51. https://doi.org/10.1111/j.1558-5646.1972.tb00172.x

Hall, M., Kültz, D., & Almaas, E. (2020). Identification of key proteins involved in stickleback environmental adaptation with system-level analysis. *Physiol. Genomics*, *52*(11), 531–548. https://doi.org/10.1101/2020.02.11.943522

Hattori, H., Liu, Y. C., Tohnai, I., Ueda, M., Kaneda, T., Kobayashi, T., Tanabe, K., & Ohtsuka, K. (1992). Intracellular localization and partial amino acid sequence of a stress-inducible 40-kDa protein in HeLa cells. *Cell Structure and Function*, *17*(1), 77–86. https://doi.org/10.1247/csf.17.77

Hir, H. L., Saulière, J., & Wang, Z. (2016). The exon junction complex as a node of post-transcriptional networks. *Nature Reviews Molecular Cell Biology*, *17*(1), 41–54. https://doi.org/10.1038/nrm.2015.7

Ilmakunnas, M., Tukiainen, E. M., Rouhiainen, A., Rauvala, H., Arola, J., Nordin, A., Mäkisalo, H., Höckerstedt, K., & Isoniemi, H. (2008). High mobility group box 1 protein as a marker of hepatocellular injury in human liver transplantation. *Liver Transplantation*, *14*(10), 1517–1525. https://doi.org/10.1002/lt.21573

IPCC. (2014). *Climate Change 2014: Synthesis Report. Contribution of Working Groups I, II and III to the Fifth Assessment Report of the Intergovernmental Panel on Climate Change* (p. 151). Intergovernmental Panel on Climate Change. https://www.ipcc.ch/site/assets/uploads/2018/02/SYR_AR5_FINAL_full.pdf

IPCC. (2019). *Summary for Policymakers. In: IPCC Special Report on the Ocean and Cryosphere in a Changing Climate* (p. In press). Intergovernmental Panel on Climate Change. https://www.ipcc.ch/srocc/chapter/summary-for-policymakers/

Kanehisa, M., & Sato, Y. (2020). KEGG Mapper for inferring cellular functions from protein sequences. *Protein Science: A Publication of the Protein Society*, *29*(1), 28–35. https://doi.org/10.1002/pro.3711

Kanehisa, M., Sato, Y., & Morishima, K. (2016). BlastKOALA and GhostKOALA: KEGG Tools for Functional Characterization of Genome and Metagenome Sequences. *Journal of Molecular Biology*, *428*(4), 726–731. https://doi.org/10.1016/j.jmb.2015.11.006

Kang, L., Rashkovetsky, E., Michalak, K., Garner, H. R., Mahaney, J. E., Rzigalinski, B. A., Korol, A., Nevo, E., & Michalak, P. (2019). Genomic divergence and adaptive convergence in Drosophila simulans from Evolution Canyon, Israel. *Proceedings of the National Academy of Sciences*, *116*(24), 11839–11844. https://doi.org/10.1073/pnas.1720938116

Kültz, D. (2005). Molecular and evolutionary basis of the cellular stress response. *Annual Review of Physiology*, *67*, 225–257. https://doi.org/10.1146/annurev.physiol.67.040403.103635

Kültz, D., Li, J., Paguio, D., Pham, T., Eidsaa, M., & Almaas, E. (2016). Population-specific renal proteomes of marine and freshwater three-spined sticklebacks. *Journal of Proteomics*, *135*, 112–131. https://doi.org/10.1016/j.jprot.2015.10.002

Lewis, M., Götting, M., Anttila, K., Kanerva, M., Prokkola, J. M., Seppänen, E., Kolari, I., & Nikinmaa, M. (2016). Different Relationship between hsp70 mRNA and hsp70 Levels in

the Heat Shock Response of Two Salmonids with Dissimilar Temperature Preference. *Frontiers in Physiology*, *7*, 511. https://doi.org/10.3389/fphys.2016.00511

Li, J., Levitan, B., Gomez-Jimenez, S., & Kültz, D. (2018). Development of a Gill Assay Library for Ecological Proteomics of Threespine Sticklebacks (Gasterosteus aculeatus). *Molecular & Cellular Proteomics*, *17*(11), 2146–2163. https://doi.org/10.1074/mcp.RA118.000973

Li, K. W., Gonzalez-Lozano, M. A., Koopmans, F., & Smit, A. B. (2020). Recent Developments in Data Independent Acquisition (DIA) Mass Spectrometry: Application of Quantitative Analysis of the Brain Proteome. *Frontiers in Molecular Neuroscience*, *13*, 564446. https://doi.org/10.3389/fnmol.2020.564446

Liu, B., Xu, P., Brown, P. B., Xie, J., Ge, X., Miao, L., Zhou, Q., Ren, M., & Pan, L. (2016). The effect of hyperthermia on liver histology, oxidative stress and disease resistance of the Wuchang bream, Megalobrama amblycephala. *Fish & Shellfish Immunology*, *52*, 317–324. https://doi.org/10.1016/j.fsi.2016.03.018

Liu, S., Wang, X., Sun, F., Zhang, J., Feng, J., Liu, H., Rajendran, K. V., Sun, L., Zhang, Y., Jiang, Y., Peatman, E., Kaltenboeck, L., Kucuktas, H., & Liu, Z. (2013). RNA-Seq reveals expression signatures of genes involved in oxygen transport, protein synthesis, folding, and degradation in response to heat stress in catfish. *Physiological Genomics*, *45*(12), 462–476. https://doi.org/10.1152/physiolgenomics.00026.2013

Loarie, S. R., Duffy, P. B., Hamilton, H., Asner, G. P., Field, C. B., & Ackerly, D. D. (2009). The velocity of climate change. *Nature*, *462*(7276), 1052–1055. https://doi.org/10.1038/nature08649

Logan, C. A., & Somero, G. N. (2011). Effects of thermal acclimation on transcriptional responses to acute heat stress in the eurythermal fish Gillichthys mirabilis (Cooper). *American Journal of Physiology-Regulatory, Integrative and Comparative Physiology*, *300*(6), R1373–R1383. https://doi.org/10.1152/ajpregu.00689.2010

Lotze, M. T., & Tracey, K. J. (2005). High-mobility group box 1 protein (HMGB1): Nuclear weapon in the immune arsenal. *Nature Reviews Immunology*, *5*(4), 331–342. https://doi.org/10.1038/nri1594

Mahanty, A., Purohit, G. K., Banerjee, S., Karunakaran, D., Mohanty, S., & Mohanty, B. P. (2016). Proteomic changes in the liver of Channa striatus in response to high temperature stress. *ELECTROPHORESIS*, *37*(12), 1704–1717. https://doi.org/10.1002/elps.201500393

Maris, C., Dominguez, C., & Allain, F. H.-T. (2005). The RNA recognition motif, a plastic RNA-binding platform to regulate post-transcriptional gene expression. *The FEBS Journal*, *272*(9), 2118–2131. https://doi.org/10.1111/j.1742-4658.2005.04653.x

Menge, B. A., & Olson, A. M. (1990). Role of scale and environmental factors in regulation of community structure. *Trends in Ecology & Evolution*, *5*(2), 52–57. https://doi.org/10.1016/0169-5347(90)90048-I

Nakamura, F., Osborn, T. M., Hartemink, C. A., Hartwig, J. H., & Stossel, T. P. (2007). Structural basis of filamin A functions. *Journal of Cell Biology*, *179*(5), 1011–1025. https://doi.org/10.1083/jcb.200707073

Nicolas, D., Chaalali, A., Drouineau, H., Lobry, J., Uriarte, A., Borja, A., & Boët, P. (2011). Impact of global warming on European tidal estuaries: Some evidence of northward

migration of estuarine fish species. *Regional Environmental Change*, *11*(3), 639–649. https://doi.org/10.1007/s10113-010-0196-3

Nohl, H., & Gille, L. (2005). Lysosomal ROS formation. *Redox Report: Communications in Free Radical Research*, *10*(4), 199–205. https://doi.org/10.1179/135100005X70170

Ohtsuka, K., & Hata, M. (2000). Molecular chaperone function of mammalian Hsp70 and Hsp40-a review. *International Journal of Hyperthermia*, *16*(3), 231–245. https://doi.org/10.1080/026567300285259

Oliveros, J. C. (2007). *Venny. An interactive tool for comparing lists with Venn's diagrams.* https://bioinfogp.cnb.csic.es/tools/venny/index.html

Östlund-Nilsson, S., Mayer, I., & Huntingford, F. A. (Eds.). (2007). *Biology of the Three-Spined Stickleback*. CRC Press. https://www.crcpress.com/Biology-of-the-Three-Spined-Stickleback/Ostlund-Nilsson-Mayer-Huntingford/p/book/9780849332197

Piao, J., Tashiro, A., Nishikawa, M., Aoki, Y., Moriyoshi, E., Hattori, A., & Kakeya, H. (2015). Expression, purification and enzymatic characterization of a recombinant human ubiquitin-specific protease 47. *The Journal of Biochemistry*, *158*(6), 477–484. https://doi.org/10.1093/jb/mvv063

Pino, L. K., Searle, B. C., Bollinger, J. G., Nunn, B., MacLean, B., & MacCoss, M. J. (2017). The Skyline ecosystem: Informatics for quantitative mass spectrometry proteomics. *Mass Spectrometry Reviews*, *39*(3), 229–244. https://doi.org/10.1002/mas.21540

Purohit, G. K., Mahanty, A., Suar, M., Sharma, A. P., Mohanty, B. P., & Mohanty, S. (2014). Investigating hsp Gene Expression in Liver of Channa striatus under Heat Stress for Understanding the Upper Thermal Acclimation. *BioMed Research International*, *2014*, 381719. https://doi.org/10.1155/2014/381719

Qian, B., & Xue, L. (2016). Liver transcriptome sequencing and de novo annotation of the large yellow croaker (Larimichthy crocea) under heat and cold stress. *Marine Genomics*, *25*, 95–102. https://doi.org/10.1016/j.margen.2015.12.001

Quinn, N. L., McGowan, C. R., Cooper, G. A., Koop, B. F., & Davidson, W. S. (2011). Ribosomal genes and heat shock proteins as putative markers for chronic, sublethal heat stress in Arctic charr: Applications for aquaculture and wild fish. *Physiological Genomics*, *43*(18), 1056–1064. https://doi.org/10.1152/physiolgenomics.00090.2011

Rassow, J., Voos, W., & Pfanner, N. (1995). Partner proteins determine multiple functions of Hsp70. *Trends in Cell Biology*, *5*(5), 207–212. https://doi.org/10.1016/0962-8924(95)80013-7

Richter, K., Haslbeck, M., & Buchner, J. (2010). The Heat Shock Response: Life on the Verge of Death. *Molecular Cell*, *40*(2), 253–266. https://doi.org/10.1016/j.molcel.2010.10.006

Scanes, E., Scanes, P. R., & Ross, P. M. (2020). Climate change rapidly warms and acidifies Australian estuaries. *Nature Communications*, *11*(1), 1803. https://doi.org/10.1038/s41467-020-15550-z

Schrader, M., & Fahimi, H. D. (2006). Peroxisomes and oxidative stress. *Biochimica et Biophysica Acta (BBA) - Molecular Cell Research*, *1763*(12), 1755–1766. https://doi.org/10.1016/j.bbamcr.2006.09.006

Seebacher, F. (2005). A review of thermoregulation and physiological performance in reptiles: What is the role of phenotypic flexibility? *Journal of Comparative Physiology B*, *175*(7), 453–461. https://doi.org/10.1007/s00360-005-0010-6

Shen, H., Sikorska, M., LeBlanc, J., Walker, P. R., & Liu, Q. Y. (2006). Oxidative stress regulated expression of Ubiquitin Carboxyl-terminal Hydrolase-L1: Role in cell survival. *Apoptosis*, *11*(6), 1049–1059. https://doi.org/10.1007/s10495-006-6303-8

Slimen, I. B., Najar, T., Ghram, A., Dabbebi, H., Ben Mrad, M., & Abdrabbah, M. (2014). Reactive oxygen species, heat stress and oxidative-induced mitochondrial damage. A review. *International Journal of Hyperthermia: The Official Journal of European Society for Hyperthermic Oncology, North American Hyperthermia Group*, *30*(7), 513–523. https://doi.org/10.3109/02656736.2014.971446

Somero, G. N. (2011). The Physiology of Global Change: Linking Patterns to Mechanisms. *Annual Review of Marine Science*, *4*(1), 39–61. https://doi.org/10.1146/annurev-marine-120710-100935

Su, T., Li, W., Wang, P., & Ma, C. (2019). Dynamics of Peroxisome Homeostasis and Its Role in Stress Response and Signaling in Plants. *Frontiers in Plant Science*, *10*, 705. https://doi.org/10.3389/fpls.2019.00705

Szklarczyk, D., Gable, A. L., Lyon, D., Junge, A., Wyder, S., Huerta-Cepas, J., Simonovic, M., Doncheva, N. T., Morris, J. H., Bork, P., Jensen, L. J., & Mering, C. von. (2019). STRING v11: Protein-protein association networks with increased coverage, supporting functional discovery in genome-wide experimental datasets. *Nucleic Acids Research*, *47*(D1), D607–D613. https://doi.org/10.1093/nar/gky1131

Tang, D., Kang, R., Zeh, H. J., & Lotze, M. T. (2010). High-Mobility Group Box 1, Oxidative Stress, and Disease. *Antioxidants & Redox Signaling*, *14*(7), 1315–1335. https://doi.org/10.1089/ars.2010.3356

Tomanek, L. (2010). Environmental Proteomics: Changes in the Proteome of Marine Organisms in Response to Environmental Stress, Pollutants, Infection, Symbiosis, and Development. *Annual Review of Marine Science*, *3*(1), 373–399. https://doi.org/10.1146/annurev-marine-120709-142729

Tomanek, L. (2014). Proteomics to study adaptations in marine organisms to environmental stress. *Journal of Proteomics*, *105*, 92–106. https://doi.org/10.1016/j.jprot.2014.04.009

Trapani, L., & Pallottini, V. (2010). Age-Related Hypercholesterolemia and HMG-CoA Reductase Dysregulation: Sex Does Matter (A Gender Perspective). *Current Gerontology and Geriatrics Research*, *2010*, Article ID 420139. https://doi.org/10.1155/2010/420139

Trefts, E., Gannon, M., & Wasserman, D. H. (2017). The liver. *Current Biology*, *27*(21), R1147–R1151. https://doi.org/10.1016/j.cub.2017.09.019

VanBogelen, R. A., & Neidhardt, F. C. (1990). Ribosomes as sensors of heat and cold shock in Escherichia coli. *Proceedings of the National Academy of Sciences of the United States of America*, *87*(15), 5589–5593.

Walker, C. L., Pomatto, L. C. D., Tripathi, D. N., & Davies, K. J. A. (2018). Redox Regulation of Homeostasis and Proteostasis in Peroxisomes. *Physiological Reviews*, *98*(1), 89–115. https://doi.org/10.1152/physrev.00033.2016

Yost, H. J., & Lindquist, S. (1986). RNA splicing is interrupted by heat shock and is rescued by heat shock protein synthesis. *Cell*, *45*(2), 185–193. https://doi.org/10.1016/0092-8674(86)90382-X

Zhao, Y., Shapiro, S. S., & Eto, M. (2015). F-actin clustering and cell dysmotility induced by the pathological W148R missense mutation of filamin B at the actin-binding domain.

*American Journal of Physiology-Cell Physiology*, *310*(1), C89–C98. https://doi.org/10.1152/ajpcell.00274.2015

Zinn, K. E., Tunc-Ozdemir, M., & Harper, J. F. (2010). Temperature stress and plant sexual reproduction: Uncovering the weakest links. *Journal of Experimental Botany*, *61*(7), 1959–1968. https://doi.org/10.1093/jxb/erq053

## TABLES AND FIGURES

**Table 3.1.** List of the main functionally enriched STRING network clusters after analysis of only the group of proteins that were significantly higher abundance in the BL28-6h vs. BL15-6h comparison with network cluster ID, network cluster description, observed gene count (number of genes that were significantly higher in BL28-6h that were found in the respective clusters), background gene count (total number of genes in the respective network cluster), and false discovery rate (FDR; clusters with an FDR < 0.01 were considered significantly functionally enriched). Below each network is a list of the significantly higher abundance proteins by description on the left and accession number on the right. See Figure 3.3 for the network interactions.

| network cluster ID | network cluster description | observed gene count | background gene count | false discovery rate (FDR) |
|---|---|---|---|---|
| **CL:11311** | **Core histone H2A/H2B/H3/H4, and Histone H4** | **8** | **136** | **1.24E-05** |
| 1 | Uncharacterized protein; Histone H1 like | G3N5J6 | | |
| 2 | Uncharacterized protein; Histone H1 like | G3N8I6 | | |
| 3 | Uncharacterized protein; Histone H1 like | G3N8L3 | | |
| 4 | Si:ch211-103n10.5 | G3NWG9 | | |
| 5 | H1 histone family, member 0 | G3P2U9 | | |
| 6 | Uncharacterized protein; Histone H1 like | G3PL95 | | |
| 7 | High-mobility group box 2a | G3PVY2 | | |
| 8 | High-mobility group box 1a | G3QB97 | | |
| **CL:17225** | **mixed, incl. RNA recognition motif. (a.k.a. RRM, RBD, or RNP domain), and LSM domain** | **7** | **122** | **6.48E-05** |
| 1 | Splicing factor 1 | G3N6Z3 | | |
| 2 | PRP6 pre-mRNA processing factor 6 homolog (S. cerevisiae) | G3NDK9 | | |
| 3 | Y box binding protein 1 | G3NT55 | | |
| 4 | Heterogeneous nuclear ribonucleoprotein M | G3P7K2 | | |
| 5 | Polypyrimidine tract binding protein 1a | G3PAI7 | | |
| 6 | Aly/REF export factor | G3PJ42 | | |
| 7 | Small nuclear ribonucleoprotein polypeptide A' | G3PLX6 | | |
| **CL:22897** | **mixed, incl. Mitochondrion, and Eukaryotic porin** | **7** | **197** | **0.00025** |
| 1 | Succinate dehydrogenase complex assembly factor 4; Chromosome 6 open reading frame 57 | G3NIA3 | | |
| 2 | NADH dehydrogenase (ubiquinone) Fe-S protein 5 | G3NBA2 | | |
| 3 | MICOS complex subunit | G3NZR5 | | |
| 4 | NADH dehydrogenase (ubiquinone) 1 alpha subcomplex, 7 | G3P1C3 | | |
| 5 | NADH dehydrogenase [ubiquinone] iron-sulfur protein 6, mitochondrial | G3P2T0 | | |
| 6 | Cytochrome c oxidase subunit | G3P8F3 | | |
| 7 | Expressed sequence CO360592; NADH dehydrogenase (ubiquinone) 1 beta subcomplex, 4, 15kDa | G3NDE4 | | |
| **CL:23489** | **mixed, incl. BolA protein, and NFU1-like** | **3** | **17** | **0.00089** |
| 1 | Uncharacterized protein; bolA family member 2B; Belongs to the BolA/IbaG family | G3N716 | | |
| 2 | Si:ch211-191d15.2 | G3P202 | | |
| 3 | bolA homolog 1 (E. coli); Belongs to the BolA/IbaG family | G3PIL0 | | |
| **CL:15673** | **mixed, incl. Ribosomal protein, and Protein biosynthesis** | **6** | **188** | **0.0013** |
| 1 | Apoptotic chromatin condensation inducer 1b | G3PLU1 | | |
| 2 | Eukaryotic translation initiation factor 3 subunit D | G3PNK2 | | |
| 3 | Polyadenylate-binding protein; Binds the poly(A) tail of mRNA | G3NI20 | | |
| 4 | Signal recognition particle receptor (docking protein) | G3NTJ5 | | |
| 5 | annotation not available | G3PAD7 | | |
| 6 | Density-regulated protein; Belongs to the DENR family | G3PSL6 | | |
| **CL:27778** | **HSP20/alpha crystallin family, and BAG domains, present in regulator of HSP70 proteins** | **2** | **6** | **0.0042** |
| 1 | BCL2-associated athanogene 3 | G3NGE0 | | |
| 2 | Heat shock protein, alpha-crystallin-related, b8; (HSP20) family | G3PMJ6 | | |
| **CL:16954** | **mixed, incl. Eukaryotic initiation factor 4E, and MIF4G domain** | **3** | **48** | **0.0095** |
| 1 | Eukaryotic translation initiation factor 4 gamma, 3 | G3NL77 | | |
| 2 | Ataxin 2-like | G3NX14 | | |
| 3 | Eukaryotic translation initiation factor 4E binding protein 3, like | G3Q3K8 | | |

**Table 3.2.** List of the main functionally enriched STRING network clusters after analysis of only the group of proteins that were significantly lower abundance in the BL28-6h vs. BL15-6h comparison with network cluster ID, network cluster description, observed gene count (number of genes that were significantly lower in BL28-6h that were found in the respective clusters), background gene count (total number of genes in the respective network cluster), and false discovery rate (FDR; clusters with an FDR < 0.01 were considered significantly functionally enriched). Below each network is a list of the significantly lower abundance proteins by description on the left and accession number on the right. See Figure 3.4 for the network interactions.

| network cluster ID | network cluster description | observed gene count | background gene count | false discovery rate (FDR) |
|---|---|---|---|---|
| **CL:18342** | **mixed, incl. Calreticulin family, and Disulphide isomerase** | **7** | **27** | **1.16E-08** |
| 1 | Calreticulin | G3NFC1 | | |
| 2 | Stromal cell-derived factor 2-like 1 | G3NI26 | | |
| 3 | Protein disulfide isomerase family A, member 3 | G3NVG1 | | |
| 4 | DnaJ (HSP40) homolog, subfamily B, member 11 | G3P2Z2 | | |
| 5 | Protein disulfide isomerase family A, member 6 | G3P4Y4 | | |
| 6 | Heat shock protein 5; Belongs to the heat shock protein 70 family | G3PWI0 | | |
| 7 | Hypoxia up-regulated 1; Belongs to the heat shock protein 70 family | G3Q9L0 | | |
| **CL:15673** | **mixed, incl. Ribosomal protein, and Protein biosynthesis** | **8** | **188** | **3.04E-05** |
| 1 | Eukaryotic translation initiation factor 3 subunit B | G3PWX3 | | |
| 2 | Signal recognition particle 9 kDa protein | G3NJ90 | | |
| 3 | G1 to S phase transition 1 | G3NKR5 | | |
| 4 | Ribosomal protein S18; Belongs to the universal ribosomal protein uS13 family | G3P5V0 | | |
| 5 | Uncharacterized protein; Eukaryotic translation elongation factor 2a, tandem duplicate 2 | G3PHA5 | | |
| 6 | Eukaryotic translation elongation factor 2b | G3PRF7 | | |
| 7 | Eukaryotic translation elongation factor 1 beta 2; Belongs to the EF-1-beta/EF-1-delta family | G3PRS7 | | |
| 8 | Uncharacterized protein; Nascent polypeptide-associated complex alpha subunit | G3PR69 | | |
| **CL:7162** | **mostly uncharacterized, incl. Low-density lipoprotein (LDL) receptor class A repeat, and Terpenoid cyclases/protein prenyltransferase alpha-alpha toroid** | **6** | **170** | **0.0012** |
| 1 | Alpha-2-macroglobulin-like 1 | G3NNM8 | | |
| 2 | Uncharacterized protein; Fetuin B | G3NQA7 | | |
| 3 | Serine (or cysteine) proteinase inhibitor, clade C (antithrombin), member 1; Belongs to the serpin family | G3PK17 | | |
| 4 | ATP-binding cassette, sub-family A (ABC1), member 1A | G3Q3W7 | | |
| 5 | Sex hormone binding globulin | G3Q6T4 | | |
| 6 | Inter-alpha-trypsin inhibitor heavy chain family, member 4 | G3N9S1 | | |
| **CL:16242** | **Ribosomal protein L25/Gln-tRNA synthetase, N-terminal, and Lysine-tRNA ligase, class II** | **2** | **5** | **0.0051** |
| 1 | Tyrosine--tRNA ligase; tyrosyl-tRNA synthetase | G3P140 | | |
| 2 | arginyl-tRNA synthetase; Belongs to the class-I aminoacyl-tRNA synthetase family | G3QCA0 | | |
| **CL:27789** | **mixed, incl. Filamin C, and Filamin-B** | **2** | **5** | **0.0051** |
| 1 | Filamin A, alpha (actin binding protein 280) | G3PIA8 | | |
| 2 | Filamin B, like | G3NI02 | | |
| **CL:17211** | **mixed, incl. RNA recognition motif. (a.k.a. RRM, RBD, or RNP domain), and mRNA processing** | **5** | **184** | **0.009** |
| 1 | poly(rC) binding protein 3 | G3NC94 | | |
| 2 | Heterogeneous nuclear ribonucleoprotein A1a | G3P4B9 | | |
| 3 | U2 snRNP auxiliary factor large subunit; Necessary for the splicing of pre-mRNA | G3P8Z0 | | |
| 4 | Heterogeneous nuclear ribonucleoprotein A0b | G3PVS.6 | | |
| 5 | Small nuclear ribonucleoprotein 200 (U5) | G3PC73 | | |
| **CL:22901** | **mixed, incl. Respiratory chain, and Hydrogen ion transport** | **4** | **109** | **0.0096** |
| 1 | NADH:ubiquinone oxidoreductase core subunit S1; NADH dehydrogenase (ubiquinone) Fe-S protein 1, 75kDa (NADH-coenzyme Q reductase) | G3NK47 | | |
| 2 | Succinate dehydrogenase [ubiquinone] flavoprotein subunit, mitochondrial | G3NQT9 | | |
| 3 | NADH dehydrogenase (ubiquinone) flavoprotein 2 | G3PWJ1 | | |
| 4 | Ubiquinol-cytochrome c reductase, complex III subunit X | G3PXN8 | | |
| **CL:1207** | **mixed, incl. Myosin tail, and Unconventional myosin-IXb** | **2** | **16** | **0.0171** |
| 1 | Actin, alpha, cardiac muscle 1a; Belongs to the actin family | G3NS10 | | |
| 2 | Myosin, heavy polypeptide 11, smooth muscle b | G3PQ56 | | |
| **CL:21365** | **mixed, incl. Glycolysis, and Thiamin diphosphate-binding fold** | **4** | **147** | **0.0198** |
| 1 | Malate dehydrogenase 2, NAD (mitochondrial) | G3NRT5 | | |
| 2 | Branched chain keto acid dehydrogenase E1, alpha polypeptide | G3PHX0 | | |
| 3 | Isocitrate dehydrogenase 2 (NADP+), mitochondrial | G3PVW5 | | |
| 4 | Aldo-keto reductase family 1, member B1 (aldose reductase) | G3Q522 | | |
| **CL:879** | **mixed, incl. Actin, conserved site, and F-actin-capping protein subunit alpha/beta** | **2** | **24** | **0.0291** |
| 1 | annotation not available | G3NYK9 | | |
| 2 | Uncharacterized protein; Actin, beta-like 2; Belongs to the actin family | G3N8W8 | | |

**Table 3.3.** KEGG Pathways with more than four proteins that were significantly (adjusted p-value < 0.05) more abundant in BL28 than control six hours post heat stress. The proteins that were significantly more abundant are listed for each KEGG pathway by accession number, KEGG identifier, name, and full name/description.

| KEGG Pathway (# significantly more abundant proteins in BL28-6h) | Accession Number | KEGG Identifier, name; full name/description |
|---|---|---|
| map03013 | G3PNK2 | K03251 EIF3D; translation initiation factor 3 subunit D |
| RNA transport (9) | G3NZ46 | K03258 EIF4B; translation initiation factor 4B |
| | G3P4P8 | K03260 EIF4G; translation initiation factor 4G |
| | G3PLU1 | K12875 ACIN1; apoptotic chromatin condensation inducer in the nucleus |
| | G3PJ42 | K12881 THOC4; THO complex subunit 4 |
| | G3PFS1 | K13114 PNN; pinin |
| | G3NW20 | K13126 PABPC; polyadenylate-binding protein |
| | G3NP66 | K14296 NUP153; nuclear pore complex protein Nup153 |
| | G3Q3K8 | K18645 EIF4EBP3; eukaryotic translation initiation factor 4E binding protein 3 |
| map03040 | G3PLX6 | K11092 SNRPA1; U2 small nuclear ribonucleoprotein A' |
| Spliceosome (7) | G3NDK9 | K12855 PRPF6; pre-mRNA-processing factor 6 |
| | G3PLU1 | K12875 ACIN1; apoptotic chromatin condensation inducer in the nucleus |
| | G3PJ42 | K12881 THOC4; THO complex subunit 4 |
| | G3NXK6 | K12886 HNRNPK; heterogeneous nuclear ribonucleoprotein K |
| | G3P7K9 | K12887 HNRNPM; heterogeneous nuclear ribonucleoprotein M |
| | G3N9B7 | K12892 SFRS3; splicing factor, arginine/serine-rich 3 |
| map00190 | G3P8F3 | K02267 COX6B; cytochrome c oxidase subunit 6b |
| Oxidative phosphorylation (5) | G3NBA2 | K03938 NDUFS5; NADH dehydrogenase (ubiquinone) Fe-S protein 5 |
| | G3P2T0 | K03939 NDUFS6; NADH dehydrogenase (ubiquinone) Fe-S protein 6 |
| | G3P1C3 | K03951 NDUFA7; NADH dehydrogenase (ubiquinone) 1 alpha subcomplex subunit 7 |
| | G3NDE4 | K03960 NDUFB4; NADH dehydrogenase (ubiquinone) 1 beta subcomplex subunit 4 |
| map03015 | G3PLU1 | K12875 ACIN1; apoptotic chromatin condensation inducer in the nucleus |
| mRNA surveillance pathway (4) | G3PJ42 | K12881 THOC4; THO complex subunit 4 |
| | G3PFS1 | K13114 PNN; pinin |
| | G3NVY7 | K13126 PABPC; polyadenylate-binding protein |

**Table 3.4.** KEGG Pathways with more than four proteins that were significantly (adjusted p-value < 0.05) less abundant in BL28 than control six hours post heat stress. The proteins that were significantly less abundant are listed for each KEGG pathway by accession number, KEGG identifier, name, and full name/description.

| KEGG Pathway (# significantly less abundant proteins in BL28-6h) | Accession Number | KEGG Identifier, name; full name/description |
|---|---|---|
| map04142 Lysosome (6) | G3P542 | K01365 CTSL; cathepsin L [EC:3.4.22.15] |
| | G3NID5 | K01368 CTSS; cathepsin S [EC:3.4.22.27] |
| | G3PJI1 | K01371 CTSK; cathepsin K [EC:3.4.22.38] |
| | G3PV80 | K12384 SCARB2; lysosome membrane protein 2 |
| | G3PMC9 | K12391 AP1G1; AP-1 complex subunit gamma-1 |
| | G3NY15 | K13443 NPC2; Niemann-Pick C2 protein |
| map04146 Peroxisome (5) | G3P9S4 | K00031 IDH1; isocitrate dehydrogenase [EC:1.1.1.42] |
| | G3Q615 | K00477 PHYH; phytanoyl-CoA hydroxylase [EC:1.14.11.18] |
| | G3PEP2 | K00624 E2.3.1.7; carnitine O-acetyltransferase [EC:2.3.1.7] |
| | G3Q823 | K07513 ACAA1; acetyl-CoA acyltransferase 1 [EC:2.3.1.16] |
| | G3PFW5 | K07753 PECR; peroxisomal trans-2-enoyl-CoA reductase [EC:1.3.1.38] |
| map04145 Phagosome (5) | G3P542 | K01365 CTSL; cathepsin L [EC:3.4.22.15] |
| | G3NID5 | K01368 CTSS; cathepsin S [EC:3.4.22.27] |
| | G3N8X9 | K05692 ACTB_G1; actin beta/gamma 1 |
| | G3N6W9 | K07897 RAB7A; Ras-related protein Rab-7A |
| | G3NFC1 | K08057 CALR; calreticulin |
| map04210 Apoptosis (5) | G3P542 | K01365 CTSL; cathepsin L [EC:3.4.22.15] |
| | G3NID5 | K01368 CTSS; cathepsin S [EC:3.4.22.27] |
| | G3PJI1 | K01371 CTSK; cathepsin K [EC:3.4.22.38] |
| | G3N8X9 | K05692 ACTB_G1; actin beta/gamma 1 |
| | G3NBQ0 | K07611 LMNB; lamin B |
| map04979 Cholesterol metabolism (4) | G3NCY2 | K04524 APOE; apolipoprotein E |
| | G3P0K8 | K05641 ABCA1; ATP-binding cassette, subfamily A (ABC1), member 1 |
| | G3PLC2 | K05664 ABCB11; ATP-binding cassette, subfamily B (MDR/TAP), member 11 |
| | G3NY15 | K13443 NPC2; Niemann-Pick C2 protein |
| map00190 Oxidative phosphorylation (4) | G3NQT9 | K00234 SDHA; succinate dehydrogenase (ubiquinone) flavoprotein subunit [EC:1.3.5.1] |
| | G3PXN8 | K00419 QCR9; ubiquinol-cytochrome c reductase subunit 9 |
| | G3NK47 | K03934 NDUFS1; NADH dehydrogenase (ubiquinone) Fe-S protein 1 [EC:7.1.1.2] |
| | G3PWJ1 | K03943 NDUFV2; NADH dehydrogenase (ubiquinone) flavoprotein 2 [EC:7.1.1.2] |

**Figure 3.1.** From left to right: mass error histogram for all transitions, mProphet q-value distribution for all peaks (q < 0.05 included in group comparison analyses), and retention time reproducibility of all peptides in the assay library for a) BL15-6h vs. BL28-6h, b) BL15-24h vs. BL28-24h, c) KL15-6h vs. KL28-6h, and d) KL15-24h vs. KL28-24h.

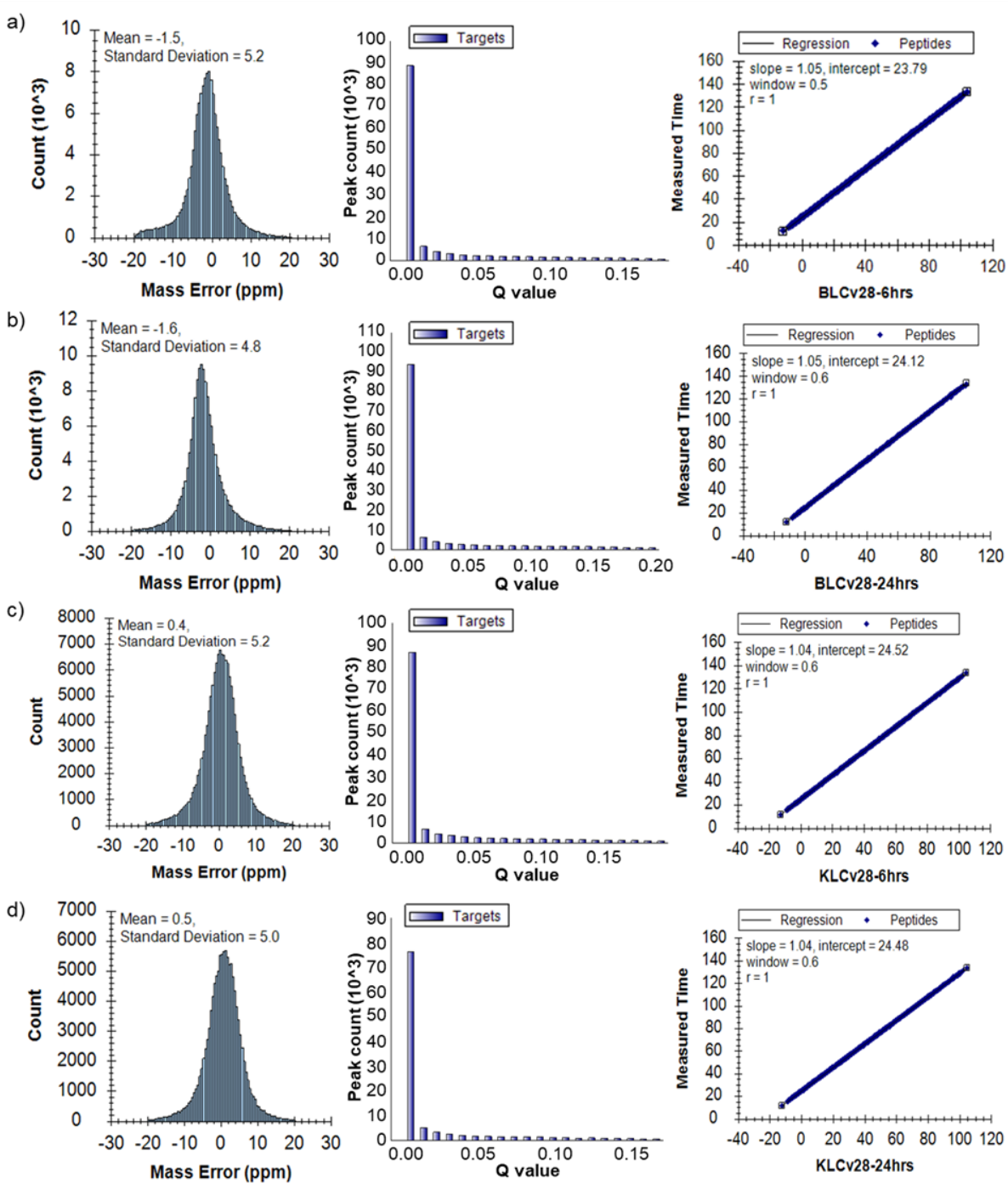

**Figure 3.2.** Figure 2. a) Heat map depicting significantly different abundances of proteins for all biological replicates (adjusted p-value < 0.05) in the BL15-6h vs. BL28-6h comparison. Proteins higher in BL28-6h are on the left panel and proteins lower in abundance in BL28-6h are on the right panel. Yellow to red coloring represents proteins with a higher abundance, with red having the highest abundance. Dark blue to light blue represents proteins with a lower abundance, with light blue having the lowest abundance. b) Volcano plot for BL15-6h vs. BL28-6h with significant differences (adjusted p-value < 0.05) showing proteins depicted as 1) red diamonds: significantly higher in abundance (FC > 2) and significantly different (adjusted p-value < 0.05), 2) blue diamonds: significantly lower in abundance (FC < 0.5) and significantly different, and 3) grey diamonds: did not meet cut off for both FC and significance requirements.

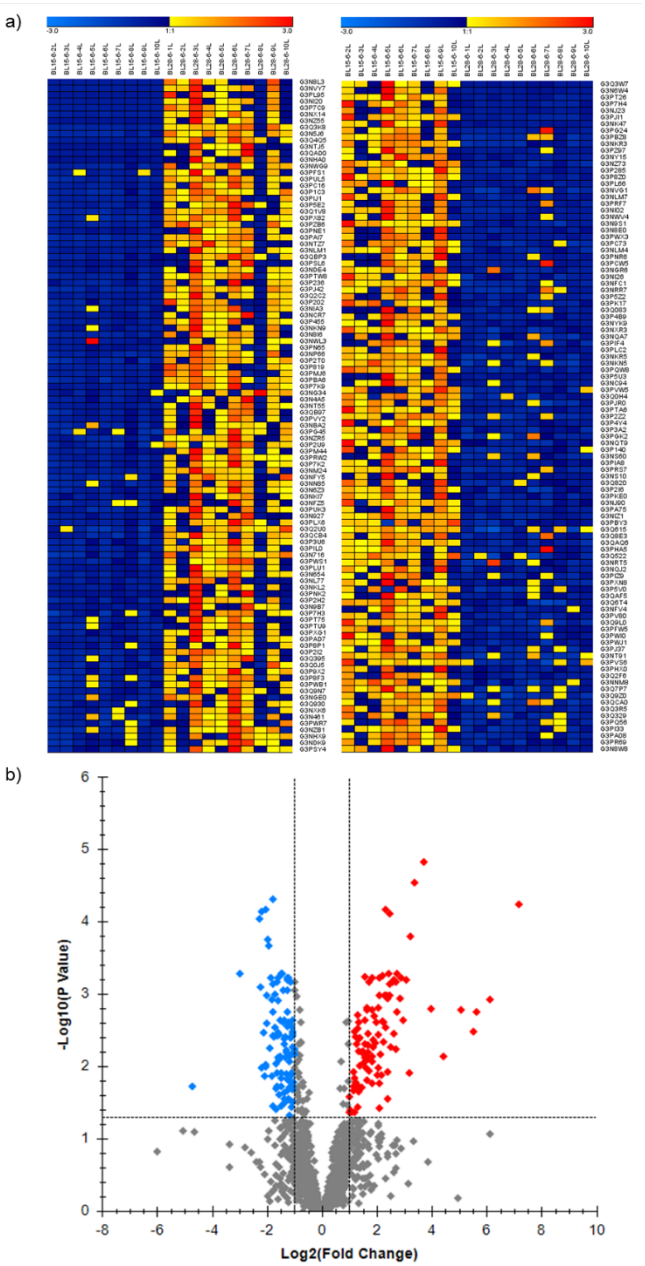

**Figure 3.3.** A network of STRING interactions for proteins that were significantly higher in BL28 over BL15 six hours post-acute temperature stress. Some of the main STRING network clusters that were functionally enriched (FDR < 0.01) are labeled and grouped by color including: CL:27778 HSP20/alpha crystallin family, and BAG domains, present in regulator of HSP70 proteins, CL:11311 core histone H2A/H2B/H3/H4, and histone H4, CL:17225 mixed, incl. RNA recognition motif. (a.k.a. RRR, RBD, or RNP domain), and LSM domain, CL:16954 mixed, incl. eukaryotic initiation factor 4E, and MIF4G domain, CL:15673 mixed, incl. ribosomal protein, and protein biosynthesis, CL:23489 mixed, incl. BolA protein, and NFU1-like, and CL:22897 mixed, incl. mitochondrion, and eukaryotic porin. Only significantly higher proteins with known connections to other proteins in the set are displayed, with the thickness of the line indicating the confidence of the connection. See Table 3.1 for protein descriptions.

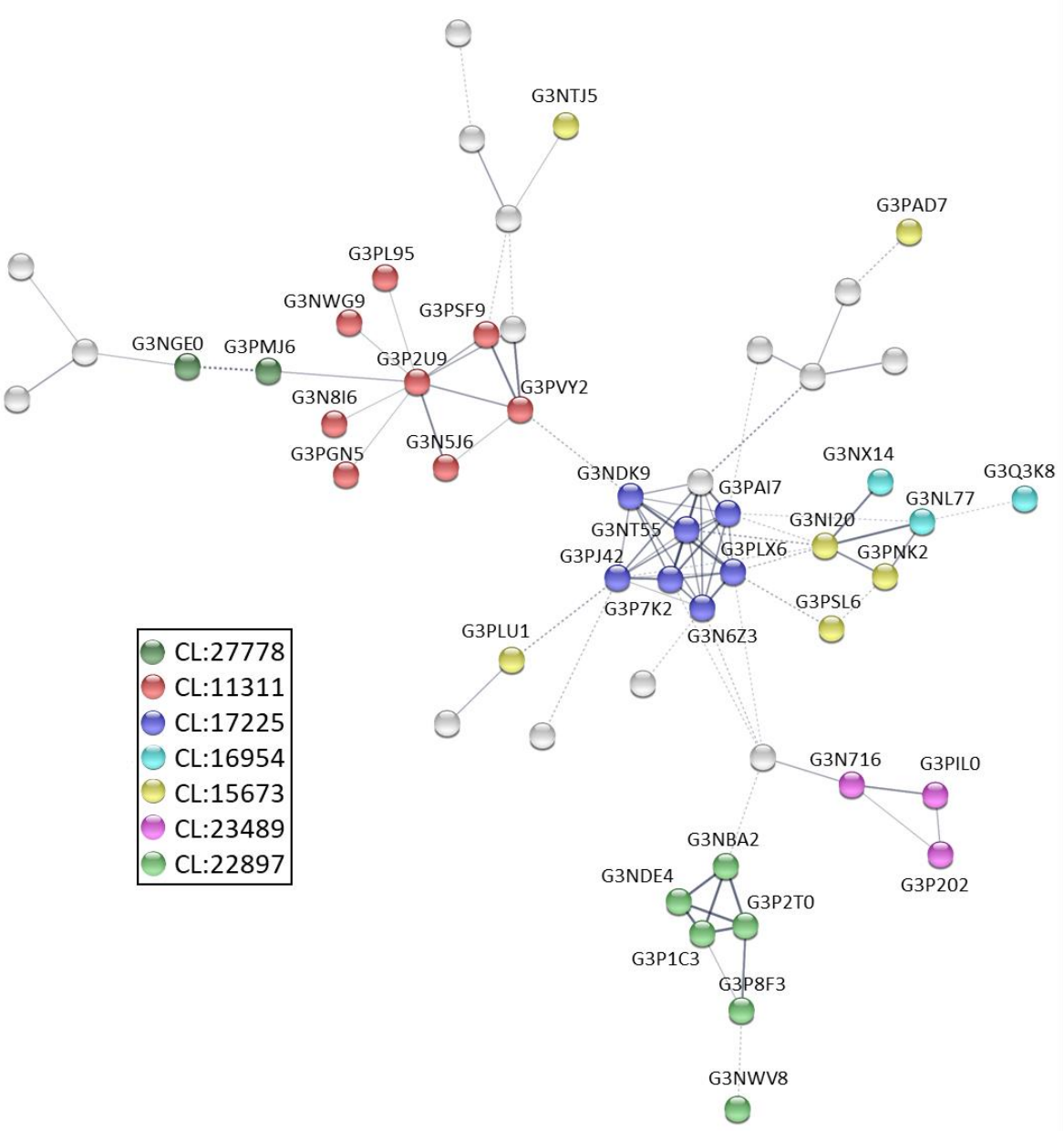

**Figure 3.4.** A network of STRING interactions for proteins that were significantly lower in BL28 versus BL15 six hours post-acute temperature stress. Some of the main STRING network clusters that were functionally enriched are labeled and grouped by color including: CL:27789 mixed, incl. filamin C, and filamin-B, CL:7162 mostly uncharacterized, incl. low-density lipoprotein (LDL) receptor class A repeat, and terpenoid cyclases/protein prenyltransferase alpha-alpha toroid, CL:18342 mixed, incl. calreticulin family, and disulphide isomerase, CL:21365 mixed, incl. glycolysis, and thiamin diphosphate-binding fold, CL:15673 mixed, incl. ribosomal protein, and protein biosynthesis, CL:22901 mixed, incl. respiratory chain, and hydrogen ion transport, CL:16242 ribosomal protein L25/Gln-tRNA synthetase, N-terminal, and lysine-tRNA ligase, class II, CL:17211 mixed, incl. RNA recognition motif. (a.k.a. RRM, RBD, or RNP domain), and mRNA processing, CL:1207 mixed, incl. myosin tail, and unconventional myosin-Ixb, CL:879 mixed, incl. actin, conserved site, and F-actin-capping protein subunit alpha/beta. Only significantly lower abundance proteins with known connections to other proteins in the set are displayed, with the thickness of the line indicating the confidence of the connection. See Table 3.2 for protein descriptions.

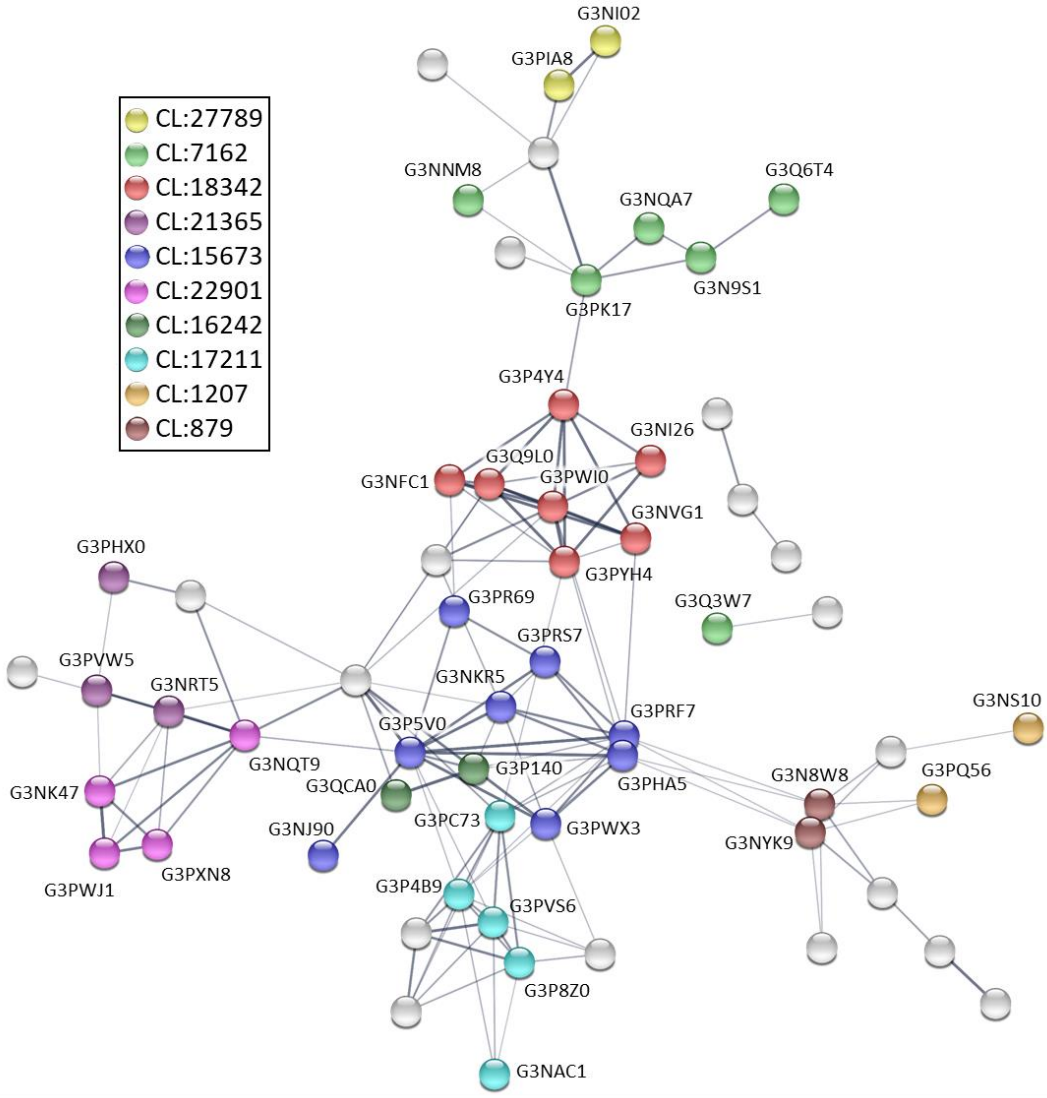

**Figure 3.5.** Oxidative phosphorylation (electron transport chain) KEGG pathway with significantly elevated proteins (BL28-6h > BL15-6h) colored in red and significantly less abundant proteins (BL28-6h < BL15-6h) colored in blue. Complex I (NADH dehydrogenase) contained various proteins that were both higher and lower in abundance. Complex II and III contained a significantly lower abundance protein, and Complex IV contained a significantly more abundant protein. See Table 3.3 and Table 3.4 for full names, protein accession numbers, and KEGG identifiers.

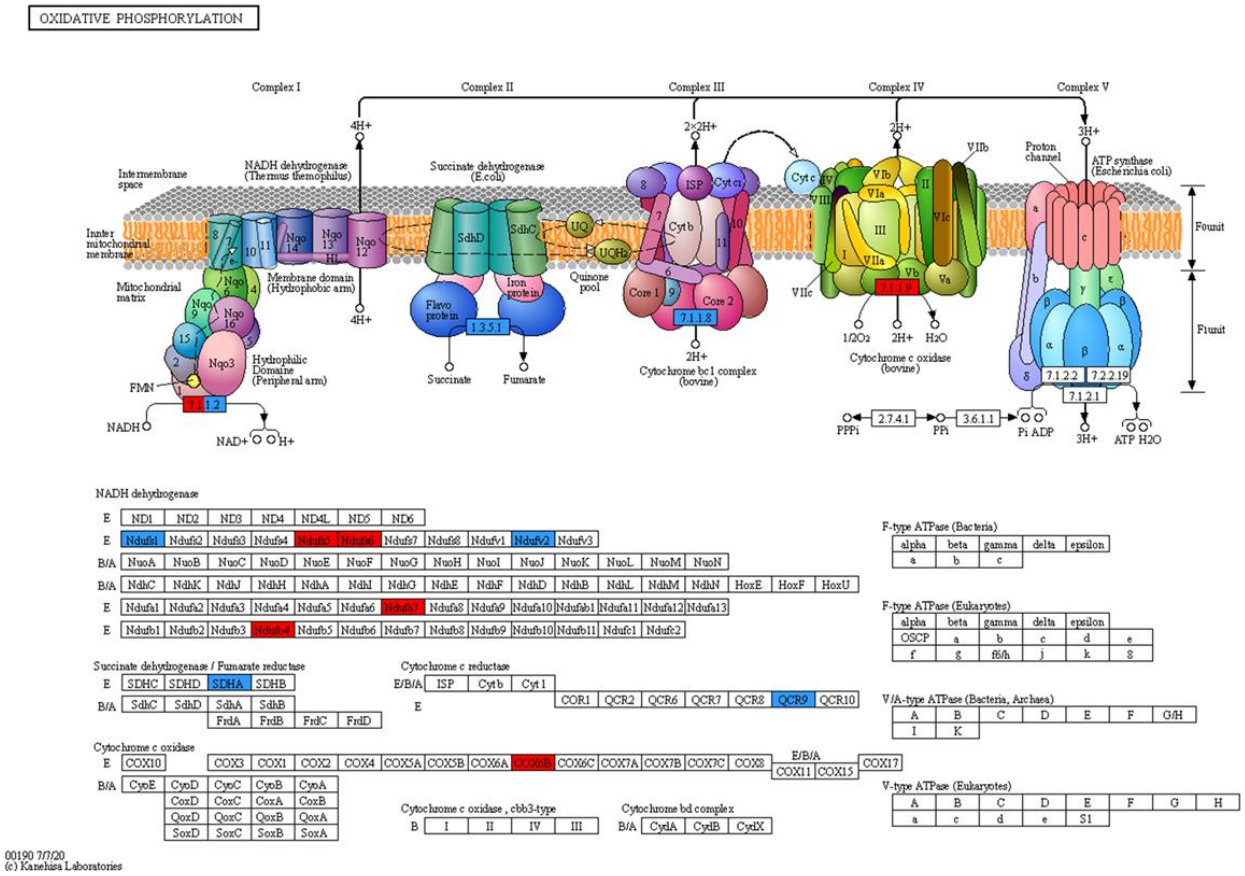

**Figure 3.6.** a) Heat map depicting significantly different abundances of proteins for all biological replicates (adjusted p-value < 0.05) in the BL15-24h vs. BL28-24h comparison. Yellow to red coloring represents proteins with a higher abundance, with red having the highest abundance. Dark blue to light blue represents proteins with a lower abundance, with light blue having the lowest abundance. b) Volcano plot for BL15-24h vs. BL28-24h with significant differences (adjusted p-value < 0.05) showing proteins depicted as 1) red diamonds: significantly higher in abundance (FC > 2) and significantly different (adjusted p-value < 0.05), 2) blue diamonds: significantly lower in abundance (FC < 0.5) and significantly different, and 3) grey diamonds: did not meet cut off for both FC and significance requirements.

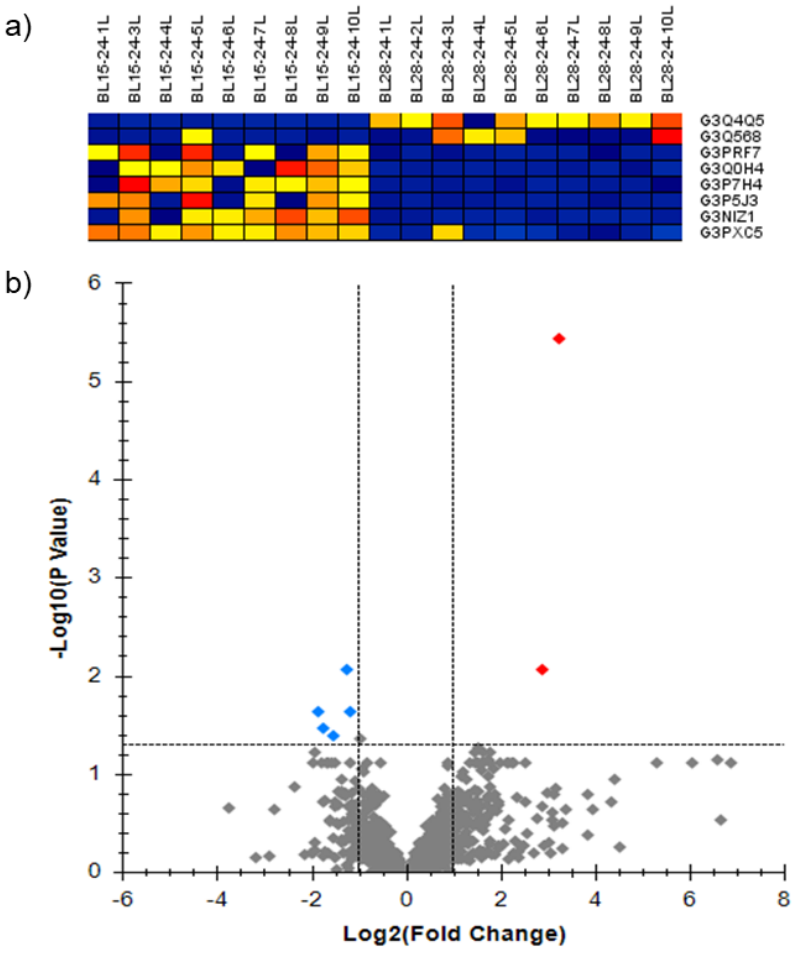

**Figure 3.7.** a) Heat map depicting significantly different abundances of proteins for all biological replicates (adjusted p-value < 0.05) in the KL15-6h vs. KL28-6h comparison. Yellow to red coloring represents proteins with a higher abundance, with red having the highest abundance. Dark blue to light blue represents proteins with a lower abundance, with light blue having the lowest abundance. b) Volcano plot for KL15-6h vs. KL28-6h with significant differences (adjusted p-value < 0.05) showing proteins depicted as 1) red diamonds: significantly higher in abundance (FC > 2) and significantly different (adjusted p-value < 0.05), 2) blue diamonds: significantly lower in abundance (FC < 0.5) and significantly different, and 3) grey diamonds: did not meet cut off for both FC and significance requirements.

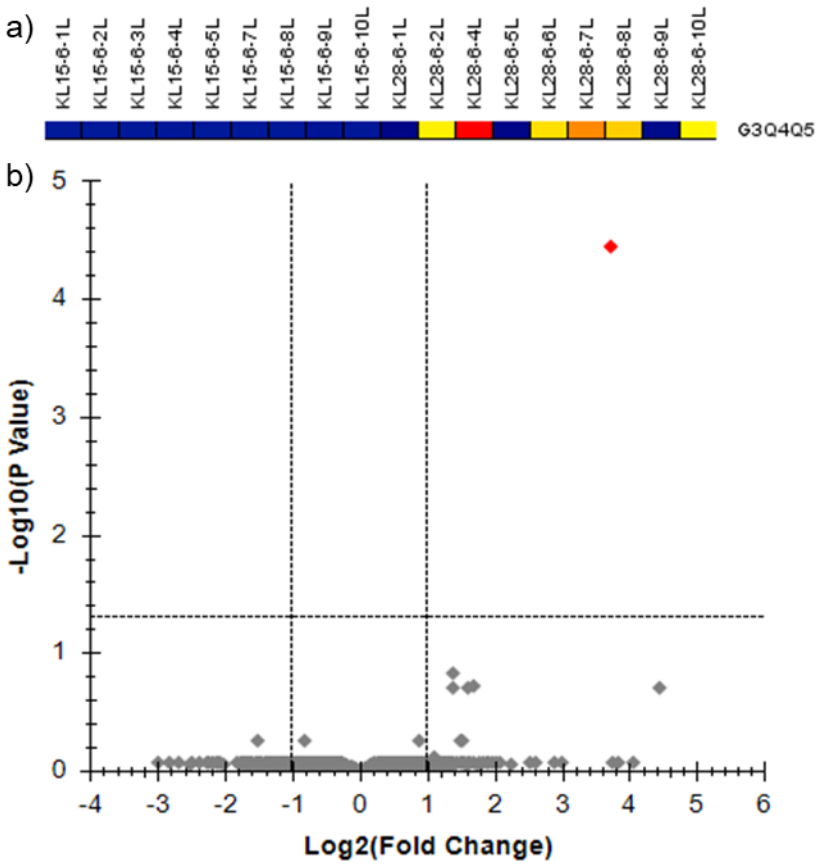

**Figure 3.8.** a) Heat map depicting significantly different abundances of proteins for all biological replicates (adjusted p-value < 0.05) in the KL15-24h vs. KL28-24h comparison. Yellow to red coloring represents proteins with a higher abundance, with red having the highest abundance. Dark blue to light blue represents proteins with a lower abundance, with light blue having the lowest abundance. b) Volcano plot for KL15-24h vs. KL28-24h with significant differences (adjusted p-value < 0.05) showing proteins depicted as 1) red diamonds: significantly higher in abundance (FC > 2) and significantly different (adjusted p-value < 0.05), 2) blue diamonds: significantly lower in abundance (FC < 0.5) and significantly different, and 3) grey diamonds: did not meet cut off for both FC and significance requirements.

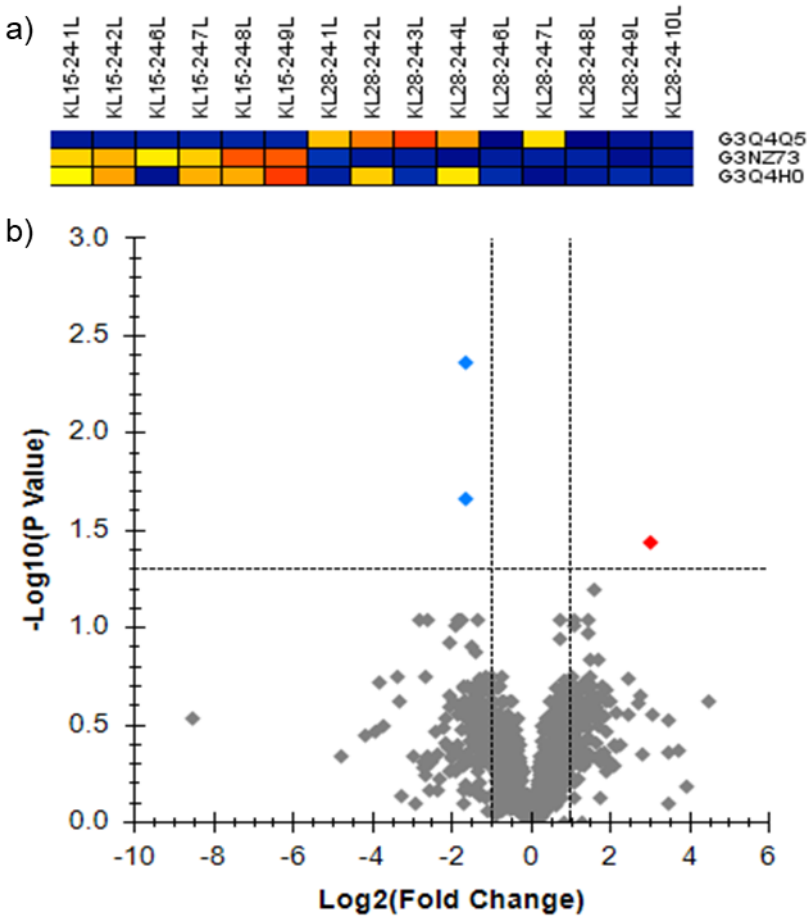

**Figure 3.9.** a) Ven diagram (produced using Venny 2.1) showing the overlap for significantly different proteins between and among the four group comparisons that were conducted. One protein, G3Q4Q5, DnaJ/HSP40-B1b was significantly more abundant for both populations after heat stress compared to control at both time points (6h and 24h), signifying its importance after acute heat stress. There were six proteins that were significantly different in abundance in heat stressed versus control groups for more than one comparison, including DnaJ/HSP40-B1b, sulfurtransferase, complement component C3, eukaryotic translation elongation factor, leukocyte cell-derived chemotaxin 2 like, and acetyl-CoA acyltransferase 2. b) Bar graph showing the average normalized (medians equalized) area for DnaJ/HSP40-B1b for each of the control and experimental groups. Although abundance levels dropped slightly in both populations from 6 to 24 hours post-heat stress, HSP40-B1b still remained significantly higher than control groups.

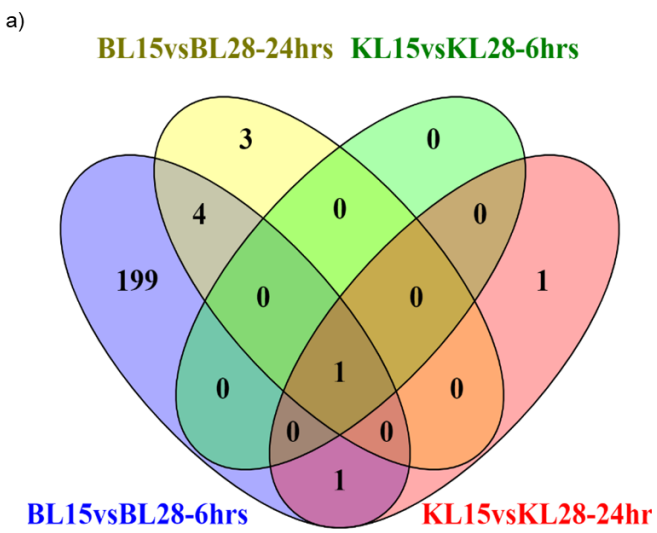


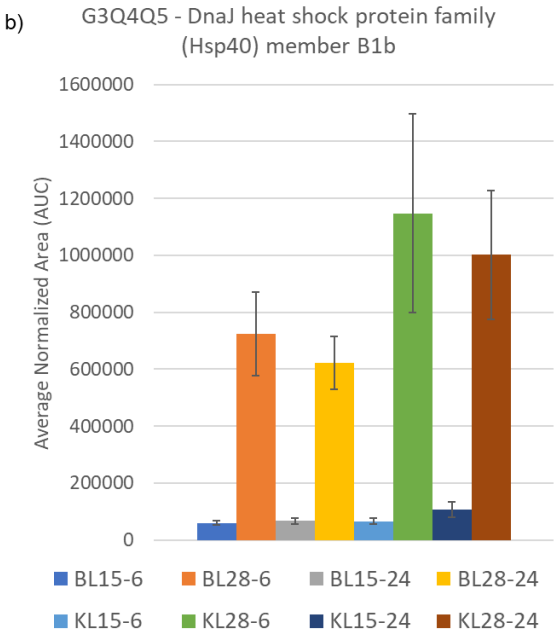

**Supplemental Table 3.1.** Skyline generated adjusted p-value and fold change with both Skyline and STRING descriptions for all the significantly higher or lower abundance proteins that also met fold change requirements (FC > 2 or < 0.5) for all four comparisons (BL15 vs. 28-6h, BL15 vs. BL28-24 h, KL15 vs. KL28-6h, and KL15 vs. KL28-24h). The “Inverse Dn Fold Change” column takes -1/FC to make lower abundance values more intuitive. For example, for A vs. B, a fold change of 0.127 is 7.87 times lower (-) in B than A. Direction of fold change can also be determined from the "Change" column, with "Up" having increased abundance in B relative to A and "Dn" having decreased abundance in B relative to A.

| Comparison | Change | Protein Accession | Skyline Description | STRING Description | Adjusted p-value | Fold Change | Inverse Dn Fold Change |
|---|---|---|---|---|---|---|---|
| BL15-6h vs. BL28-6h | Up | G3N8L3 | Uncharacterized protein | Uncharacterized protein; Histone H1 like | 5.736E-05 | 142.497 | |
| BL15-6h vs. BL28-6h | Up | G3NVY7 | Polyadenylate-binding protein | #N/A | 1.185E-03 | 68.969 | |
| BL15-6h vs. BL28-6h | Up | G3PL95 | Uncharacterized protein | Uncharacterized protein; Histone H1 like | 1.746E-03 | 49.910 | |
| BL15-6h vs. BL28-6h | Up | G3NI20 | Polyadenylate-binding protein | Polyadenylate-binding protein; Binds the poly(A) tail of mRNA | 3.320E-03 | 45.249 | |
| BL15-6h vs. BL28-6h | Up | G3P7C9 | Host cell factor C1a | Host cell factor C1b | 1.660E-03 | 33.565 | |
| BL15-6h vs. BL28-6h | Up | G3NX14 | Uncharacterized protein | Ataxin 2-like | 7.258E-03 | 21.433 | |
| BL15-6h vs. BL28-6h | Up | G3NZ55 | Eukaryotic translation initiation factor 4Bb | #N/A | 1.616E-03 | 15.578 | |
| BL15-6h vs. BL28-6h | Up | G3Q3K8 | Eukaryotic translation initiation factor 4E binding protein 3, like | Eukaryotic translation initiation factor 4E binding protein 3, like | 1.489E-05 | 13.222 | |
| BL15-6h vs. BL28-6h | Up | G3N5J6 | Uncharacterized protein | Uncharacterized protein; Histone H1 like | 2.910E-05 | 10.448 | |
| BL15-6h vs. BL28-6h | Up | G3Q4Q5 | DnaJ heat shock protein family (HSP40) member B1b | #N/A | 1.589E-04 | 9.433 | |
| BL15-6h vs. BL28-6h | Up | G3NTJ5 | SRP receptor subunit alpha | Signal recognition particle receptor (docking protein) | 1.230E-02 | 9.088 | |
| BL15-6h vs. BL28-6h | Up | G3QAD0 | Nucleophosmin 1a | #N/A | 6.384E-04 | 8.368 | |
| BL15-6h vs. BL28-6h | Up | G3NHA0 | Metadherin a | Metadherin a | 2.323E-03 | 7.708 | |
| BL15-6h vs. BL28-6h | Up | G3NWG9 | Si:ch211-103n10.5 | Si:ch211-103n10.5 | 5.914E-04 | 7.293 | |
| BL15-6h vs. BL28-6h | Up | G3PFS1 | Pinin, desmosome associated protein | Pinin, desmosome associated protein | 1.157E-03 | 7.152 | |
| BL15-6h vs. BL28-6h | Up | G3PUL5 | SERPINE1 mRNA binding protein 1b | SERPINE1 mRNA binding protein 1 | 5.286E-04 | 6.661 | |
| BL15-6h vs. BL28-6h | Up | G3PC16 | High mobility group box 1b | High-mobility group box 1b | 1.746E-03 | 6.598 | |
| BL15-6h vs. BL28-6h | Up | G3P1C3 | NADH:ubiquinone oxidoreductase subunit A7 | NADH dehydrogenase (ubiquinone) 1 alpha subcomplex, 7 | 6.739E-04 | 6.465 | |
| BL15-6h vs. BL28-6h | Up | G3PIJ1 | Gephyrin a | annotation not available | 5.803E-03 | 6.435 | |
| BL15-6h vs. BL28-6h | Up | G3P5E2 | Tubulin folding cofactor B | Tubulin folding cofactor B | 3.502E-03 | 6.206 | |
| BL15-6h vs. BL28-6h | Up | G3Q1V8 | Uncharacterized protein | KIAA1191 | 6.389E-04 | 6.073 | |
| BL15-6h vs. BL28-6h | Up | G3PX82 | RAN binding protein 3b | #N/A | 6.766E-04 | 5.931 | |
| BL15-6h vs. BL28-6h | Up | G3PZB6 | Uncharacterized protein (Fragment) | annotation not available | 5.420E-03 | 5.629 | |
| BL15-6h vs. BL28-6h | Up | G3PNE1 | SERPINE1 mRNA binding protein 1a | #N/A | 7.355E-04 | 5.601 | |
| BL15-6h vs. BL28-6h | Up | G3PAI7 | Polypyrimidine tract binding protein 1a | Polypyrimidine tract binding protein 1a | 7.729E-05 | 5.577 | |
| BL15-6h vs. BL28-6h | Up | G3NTZ7 | Uncharacterized protein | annotation not available | 1.026E-03 | 5.468 | |
| BL15-6h vs. BL28-6h | Up | G3NLM1 | Uncharacterized protein | #N/A | 5.286E-04 | 5.397 | |
| BL15-6h vs. BL28-6h | Up | G3QBP3 | Acetyltransferase component of pyruvate dehydrogenase complex | Acetyltransferase component of pyruvate dehydrogenase complex | 1.202E-02 | 5.255 | |
| BL15-6h vs. BL28-6h | Up | G3PSL6 | Density-regulated protein | Density-regulated protein; Belongs to the DENR family | 2.769E-02 | 5.234 | |
| BL15-6h vs. BL28-6h | Up | G3NDE4 | NADH:ubiquinone oxidoreductase subunit B4 | Expressed sequence CO360592; NADH dehydrogenase (ubiquinone) 1 beta subcomplex, 4, 15kDa | 1.153E-03 | 5.220 | |
| BL15-6h vs. BL28-6h | Up | G3PTW8 | Methenyltetrahydrofolate synthetase domain containing | Methenyltetrahydrofolate synthetase domain containing | 1.056E-03 | 5.088 | |
| BL15-6h vs. BL28-6h | Up | G3P236 | Coronin | #N/A | 2.926E-03 | 5.005 | |
| BL15-6h vs. BL28-6h | Up | G3PJ42 | Aly/REF export factor | Aly/REF export factor | 6.781E-05 | 4.957 | |

| Comparison | Change | Protein Accession | Skyline Description | STRING Description | Adjusted p-value | Fold Change | Inverse Dn Fold Change |
|---|---|---|---|---|---|---|---|
| BL15-6h vs. BL28-6h | Up | G3Q2C2 | Uncharacterized protein | #N/A | 1.026E-03 | 4.848 | |
| BL15-6h vs. BL28-6h | Up | G3P202 | Iron-sulfur cluster assembly enzyme | Si:ch211-191d15.2 | 4.537E-03 | 4.780 | |
| BL15-6h vs. BL28-6h | Up | G3NIA3 | Succinate dehydrogenase complex assembly factor 4 | Succinate dehydrogenase complex assembly factor 4; Chromosome 6 open reading frame 57 | 2.441E-03 | 4.726 | |
| BL15-6h vs. BL28-6h | Up | G3NCR7 | Death-associated protein | Death associated protein | 2.356E-03 | 4.587 | |
| BL15-6h vs. BL28-6h | Up | G3P455 | LIM and SH3 protein 1 | #N/A | 5.512E-04 | 4.583 | |
| BL15-6h vs. BL28-6h | Up | G3NKN9 | Dehydrogenase E1 and transketolase domain containing 1 | #N/A | 1.297E-02 | 4.447 | |
| BL15-6h vs. BL28-6h | Up | G3N8I6 | Uncharacterized protein | Uncharacterized protein; Histone H1 like | 6.739E-03 | 4.367 | |
| BL15-6h vs. BL28-6h | Up | G3NWL3 | Mitochondrial fission factor | #N/A | 1.026E-03 | 4.287 | |
| BL15-6h vs. BL28-6h | Up | G3PN65 | G protein-coupled receptor, class C, group 5, member C | G protein-coupled receptor, family C, group 5, member C | 3.761E-02 | 4.287 | |
| BL15-6h vs. BL28-6h | Up | G3NP66 | Nucleoporin 153 | Nucleoporin 153 | 1.709E-02 | 4.267 | |
| BL15-6h vs. BL28-6h | Up | G3P2T0 | NADH dehydrogenase [ubiquinone] iron-sulfur protein 6, mitochondrial | NADH dehydrogenase [ubiquinone] iron-sulfur protein 6, mitochondrial | 5.914E-04 | 4.246 | |
| BL15-6h vs. BL28-6h | Up | G3P819 | Adhesion regulating molecule 1 | Adhesion regulating molecule 1 | 1.040E-02 | 4.206 | |
| BL15-6h vs. BL28-6h | Up | G3PMJ6 | Heat shock protein b8 | Heat shock protein, alpha-crystallin-related, b8; Belongs to the small heat shock protein (HSP20) family | 1.547E-03 | 4.164 | |
| BL15-6h vs. BL28-6h | Up | G3PBA6 | Cysteine-rich protein 2 | annotation not available | 3.622E-03 | 4.139 | |
| BL15-6h vs. BL28-6h | Up | G3P7K9 | Heterogeneous nuclear ribonucleoprotein M | #N/A | 3.622E-03 | 4.137 | |
| BL15-6h vs. BL28-6h | Up | G3NG34 | Uncharacterized protein | #N/A | 1.331E-02 | 4.016 | |
| BL15-6h vs. BL28-6h | Up | G3N4A5 | Calponin | Calponin | 2.448E-03 | 3.929 | |
| BL15-6h vs. BL28-6h | Up | G3NT55 | Y box binding protein 1 | Y box binding protein 1 | 4.702E-03 | 3.835 | |
| BL15-6h vs. BL28-6h | Up | G3QB97 | High mobility group box 1 | High-mobility group box 1a | 2.042E-03 | 3.788 | |
| BL15-6h vs. BL28-6h | Up | G3PVY2 | High mobility group box 2a | High-mobility group box 2a | 4.273E-03 | 3.640 | |
| BL15-6h vs. BL28-6h | Up | G3NBA2 | NADH:ubiquinone oxidoreductase subunit S5 | NADH dehydrogenase (ubiquinone) Fe-S protein 5 | 5.467E-03 | 3.622 | |
| BL15-6h vs. BL28-6h | Up | G3PG45 | Uncharacterized protein | annotation not available | 8.527E-03 | 3.585 | |
| BL15-6h vs. BL28-6h | Up | G3NZR5 | MICOS complex subunit | MICOS complex subunit | 1.660E-03 | 3.570 | |
| BL15-6h vs. BL28-6h | Up | G3P2U9 | H1 histone family, member 0 | H1 histone family, member 0 | 7.258E-03 | 3.547 | |
| BL15-6h vs. BL28-6h | Up | G3PM44 | Uncharacterized protein | annotation not available | 1.711E-02 | 3.540 | |
| BL15-6h vs. BL28-6h | Up | G3PRW2 | Transcription factor A, mitochondrial | #N/A | 5.914E-04 | 3.529 | |
| BL15-6h vs. BL28-6h | Up | G3P7K2 | Heterogeneous nuclear ribonucleoprotein M | Heterogeneous nuclear ribonucleoprotein M | 6.766E-04 | 3.296 | |
| BL15-6h vs. BL28-6h | Up | G3NM24 | Protein phosphatase 1 regulatory subunit 9A-like A | Si:ch1073-219n12.1 | 1.154E-02 | 3.276 | |
| BL15-6h vs. BL28-6h | Up | G3NFY5 | 6-phosphofructo-2-kinase/fructose-2,6-biphosphatase 2a | 6-phosphofructo-2-kinase/fructose-2,6-biphosphatase 2a | 5.024E-03 | 3.223 | |
| BL15-6h vs. BL28-6h | Up | G3NN85 | Uncharacterized protein (Fragment) | Nucleolar and coiled-body phosphoprotein 1 | 6.314E-03 | 3.196 | |
| BL15-6h vs. BL28-6h | Up | G3N6Z3 | Splicing factor 1 | Splicing factor 1 | 3.536E-03 | 3.162 | |
| BL15-6h vs. BL28-6h | Up | G3NKI7 | Glyoxylate reductase 1 homolog (Arabidopsis) | Glyoxylate reductase 1 homolog (Arabidopsis) | 7.951E-03 | 3.139 | |
| BL15-6h vs. BL28-6h | Up | G3NFZ5 | PDZ and LIM domain 1 (elfin) | PDZ and LIM domain 1 (elfin) | 1.558E-02 | 3.132 | |
| BL15-6h vs. BL28-6h | Up | G3PUK3 | Family with sequence similarity 114 member A1 | Family with sequence similarity 114, member A1 | 7.258E-03 | 3.123 | |
| BL15-6h vs. BL28-6h | Up | G3N927 | ATP-binding cassette, sub-family F (GCN20), member 1 | #N/A | 1.660E-03 | 3.110 | |
| BL15-6h vs. BL28-6h | Up | G3PLX6 | Small nuclear ribonucleoprotein polypeptide A' | Small nuclear ribonucleoprotein polypeptide A' | 1.547E-03 | 3.090 | |
| BL15-6h vs. BL28-6h | Up | G3Q2U0 | Si:ch211-156l18.7 | Keratin 94; Zgc:92035; Belongs to the intermediate filament family | 1.031E-02 | 3.047 | |
| BL15-6h vs. BL28-6h | Up | G3QCB4 | Family with sequence similarity 114 member A2 | Family with sequence similarity 114, member A2 | 7.258E-03 | 3.015 | |
| BL15-6h vs. BL28-6h | Up | G3P3U6 | ATP synthase inhibitory factor subunit 1b | ATPase inhibitory factor 1b | 2.287E-03 | 2.971 | |
| BL15-6h vs. BL28-6h | Up | G3PIL0 | BolA family member 1 | bolA homolog 1 (E. coli); Belongs to the BolA/IbaG family | 4.888E-03 | 2.963 | |

| Comparison | Change | Protein Accession | Skyline Description | STRING Description | Adjusted p-value | Fold Change | Inverse Dn Fold Change |
|---|---|---|---|---|---|---|---|
| BL15-6h vs. BL28-6h | Up | G3N716 | BolA family member 2 | Uncharacterized protein; bolA family member 2B; Belongs to the BolA/IbaG family | 5.722E-04 | 2.949 | |
| BL15-6h vs. BL28-6h | Up | G3PWS1 | Nucleophosmin 1b | Nucleophosmin 1b (nucleolar phosphoprotein B23, numatrin); Nucleophosmin/nucleoplasmin, 1b | 7.570E-03 | 2.930 | |
| BL15-6h vs. BL28-6h | Up | G3PLU1 | Apoptotic chromatin condensation inducer 1a | Apoptotic chromatin condensation inducer 1b | 8.982E-03 | 2.891 | |
| BL15-6h vs. BL28-6h | Up | G3N654 | Uncharacterized protein | #N/A | 6.204E-03 | 2.800 | |
| BL15-6h vs. BL28-6h | Up | G3NL77 | Eukaryotic translation initiation factor 4 gamma, 3a | Eukaryotic translation initiation factor 4 gamma, 3 | 1.923E-02 | 2.769 | |
| BL15-6h vs. BL28-6h | Up | G3NKL2 | Ubiquitin associated protein 2-like | Ubiquitin associated protein 2-like | 6.302E-03 | 2.752 | |
| BL15-6h vs. BL28-6h | Up | G3PNK2 | Eukaryotic translation initiation factor 3 subunit D | Eukaryotic translation initiation factor 3 subunit D | 9.824E-03 | 2.626 | |
| BL15-6h vs. BL28-6h | Up | G3P2H2 | Uncharacterized protein | #N/A | 3.980E-03 | 2.595 | |
| BL15-6h vs. BL28-6h | Up | G3N9B7 | Uncharacterized protein | #N/A | 1.906E-02 | 2.563 | |
| BL15-6h vs. BL28-6h | Up | G3P7H3 | Muscleblind like splicing regulator 1 | Muscleblind like splicing regulator 1 | 2.054E-02 | 2.560 | |
| BL15-6h vs. BL28-6h | Up | G3PT75 | Tubulin-specific chaperone A | #N/A | 2.223E-02 | 2.537 | |
| BL15-6h vs. BL28-6h | Up | G3PTU9 | Programmed cell death 5 | Programmed cell death 5 | 4.139E-03 | 2.536 | |
| BL15-6h vs. BL28-6h | Up | G3PXG1 | PDZ and LIM domain 5b | PDZ and LIM domain 5b | 2.441E-03 | 2.523 | |
| BL15-6h vs. BL28-6h | Up | G3PAD7 | Eukaryotic translation initiation factor 5A | annotation not available | 6.081E-03 | 2.502 | |
| BL15-6h vs. BL28-6h | Up | G3P8P1 | Epsin 1 | Epsin 1 | 3.616E-02 | 2.476 | |
| BL15-6h vs. BL28-6h | Up | G3P2I2 | Uncharacterized protein | Uncharacterized protein; Calpastatin | 2.962E-03 | 2.470 | |
| BL15-6h vs. BL28-6h | Up | G3Q395 | Peptidyl-prolyl cis-trans isomerase | Peptidyl-prolyl cis-trans isomerase | 1.928E-03 | 2.439 | |
| BL15-6h vs. BL28-6h | Up | G3Q0J5 | Uncharacterized protein (Fragment) | #N/A | 4.846E-03 | 2.375 | |
| BL15-6h vs. BL28-6h | Up | G3P9X2 | Ubiquitin like 4A | Zgc:56596; Ubiquitin-like 4A | 3.916E-03 | 2.367 | |
| BL15-6h vs. BL28-6h | Up | G3P8F3 | Cytochrome c oxidase subunit | Cytochrome c oxidase subunit | 1.906E-02 | 2.355 | |
| BL15-6h vs. BL28-6h | Up | G3PWB1 | Peptidyl-prolyl cis-trans isomerase | Protein (peptidyl-prolyl cis/trans isomerase) NIMA-interacting 1 | 1.633E-02 | 2.338 | |
| BL15-6h vs. BL28-6h | Up | G3Q9N7 | SRA stem-loop interacting RNA binding protein | SRA stem-loop interacting RNA binding protein | 3.320E-03 | 2.304 | |
| BL15-6h vs. BL28-6h | Up | G3NGE0 | BCL2 associated athanogene 3 | BCL2-associated athanogene 3 | 1.435E-02 | 2.295 | |
| BL15-6h vs. BL28-6h | Up | G3Q930 | RNA binding motif protein 4.3 | RNA binding motif protein 4.3 | 4.368E-02 | 2.283 | |
| BL15-6h vs. BL28-6h | Up | G3NXK6 | Heterogeneous nuclear ribonucleoprotein K | Heterogeneous nuclear ribonucleoprotein K | 1.906E-02 | 2.245 | |
| BL15-6h vs. BL28-6h | Up | G3N461 | CCHC-type zinc finger, nucleic acid binding protein a | CCHC-type zinc finger, nucleic acid binding protein a | 1.202E-02 | 2.220 | |
| BL15-6h vs. BL28-6h | Up | G3PWR7 | Far upstream element (FUSE) binding protein 3 | #N/A | 2.188E-02 | 2.201 | |
| BL15-6h vs. BL28-6h | Up | G3NZB1 | Uncharacterized protein | #N/A | 4.294E-02 | 2.105 | |
| BL15-6h vs. BL28-6h | Up | G3NHX9 | Translocase of outer mitochondrial membrane 34 | Translocase of outer mitochondrial membrane 34 | 4.083E-02 | 2.070 | |
| BL15-6h vs. BL28-6h | Up | G3NDK9 | PRP6 pre-mRNA processing factor 6 homolog (S. cerevisiae) | PRP6 pre-mRNA processing factor 6 homolog (S. cerevisiae) | 2.621E-02 | 2.005 | |
| BL15-6h vs. BL28-6h | Up | G3PSY4 | General transcription factor IIB | General transcription factor IIB | 4.270E-02 | 2.005 | |
| BL15-6h vs. BL28-6h | Dn | G3Q3W7 | ATP-binding cassette, sub-family A (ABC1), member 1A | ATP-binding cassette, sub-family A (ABC1), member 1A | 1.902E-02 | 0.038 | 26.525 |
| BL15-6h vs. BL28-6h | Dn | G3N6W4 | Uncharacterized protein | #N/A | 5.286E-04 | 0.128 | 7.837 |
| BL15-6h vs. BL28-6h | Dn | G3PT26 | Ubiquitin specific peptidase 47 | Ubiquitin specific peptidase 47; Belongs to the peptidase C19 family | 9.178E-05 | 0.209 | 4.778 |
| BL15-6h vs. BL28-6h | Dn | G3P7H4 | Leukocyte cell-derived chemotaxin 2 like | #N/A | 8.059E-04 | 0.211 | 4.751 |
| BL15-6h vs. BL28-6h | Dn | G3NJ23 | Dynein light chain | #N/A | 1.040E-02 | 0.216 | 4.634 |
| BL15-6h vs. BL28-6h | Dn | G3PJI1 | Cathepsin K | #N/A | 7.156E-05 | 0.220 | 4.552 |
| BL15-6h vs. BL28-6h | Dn | G3NK47 | NADH:ubiquinone oxidoreductase core subunit S1 | NADH:ubiquinone oxidoreductase core subunit S1 | 3.367E-03 | 0.228 | 4.390 |

| Comparison | Change | Protein Accession | Skyline Description | STRING Description | Adjusted p-value | Fold Change | Inverse Dn Fold Change |
|---|---|---|---|---|---|---|---|
| BL15-6h vs. BL28-6h | Dn | G3PG24 | Elongation factor like GTPase 1 | Elongation factor Tu GTP binding domain containing 1 | 1.376E-02 | 0.238 | 4.195 |
| BL15-6h vs. BL28-6h | Dn | G3PBZ8 | Uncharacterized protein | #N/A | 1.001E-02 | 0.240 | 4.160 |
| BL15-6h vs. BL28-6h | Dn | G3NKR3 | Heterogeneous nuclear ribonucleoprotein A3 | #N/A | 6.781E-05 | 0.241 | 4.146 |
| BL15-6h vs. BL28-6h | Dn | G3PZ97 | USO1 vesicle transport factor | USO1 homolog, vesicle docking protein (yeast) | 9.365E-03 | 0.243 | 4.115 |
| BL15-6h vs. BL28-6h | Dn | G3NY15 | Niemann-Pick disease, type C2 | Niemann-Pick disease, type C2 | 2.527E-03 | 0.247 | 4.054 |
| BL15-6h vs. BL28-6h | Dn | G3NZ73 | Sulfurtransferase | #N/A | 1.028E-03 | 0.248 | 4.031 |
| BL15-6h vs. BL28-6h | Dn | G3P285 | STEAP family member 4 | #N/A | 1.778E-04 | 0.257 | 3.891 |
| BL15-6h vs. BL28-6h | Dn | G3P8Z0 | U2 snRNP auxiliary factor large subunit | U2 snRNP auxiliary factor large subunit; Necessary for the splicing of pre-mRNA | 2.170E-04 | 0.263 | 3.802 |
| BL15-6h vs. BL28-6h | Dn | G3PL66 | Uncharacterized protein | annotation not available | 5.572E-03 | 0.268 | 3.731 |
| BL15-6h vs. BL28-6h | Dn | G3NVG1 | Protein disulfide-isomerase | Protein disulfide isomerase family A, member 3 | 5.914E-04 | 0.273 | 3.667 |
| BL15-6h vs. BL28-6h | Dn | G3NLM7 | Uncharacterized protein | Adaptor-related protein complex 2, mu 1 subunit | 1.185E-03 | 0.280 | 3.577 |
| BL15-6h vs. BL28-6h | Dn | G3PRF7 | Eukaryotic translation elongation factor 2b | Eukaryotic translation elongation factor 2b | 1.371E-02 | 0.282 | 3.550 |
| BL15-6h vs. BL28-6h | Dn | G3NI02 | Filamin B | Filamin B, like | 4.898E-05 | 0.287 | 3.481 |
| BL15-6h vs. BL28-6h | Dn | G3NWV4 | Calcium-transporting ATPase | Calcium-transporting ATPase | 3.548E-02 | 0.289 | 3.455 |
| BL15-6h vs. BL28-6h | Dn | G3N9S1 | Uncharacterized protein | Inter-alpha-trypsin inhibitor heavy chain family, member 4 | 7.355E-04 | 0.290 | 3.446 |
| BL15-6h vs. BL28-6h | Dn | G3N8E0 | Purine rich element binding protein B | Purine-rich element binding protein Ba | 1.784E-03 | 0.291 | 3.434 |
| BL15-6h vs. BL28-6h | Dn | G3PWX3 | Eukaryotic translation initiation factor 3 subunit B | Eukaryotic translation initiation factor 3 subunit B | 3.796E-03 | 0.294 | 3.406 |
| BL15-6h vs. BL28-6h | Dn | G3PC73 | Small nuclear ribonucleoprotein 200 (U5) | Small nuclear ribonucleoprotein 200 (U5) | 3.900E-03 | 0.296 | 3.383 |
| BL15-6h vs. BL28-6h | Dn | G3NLM4 | Sorting nexin 5 | Sorting nexin 5 | 1.005E-03 | 0.304 | 3.292 |
| BL15-6h vs. BL28-6h | Dn | G3PNR6 | Si:dkey-26g8.5 | Si:dkey-26g8.5; Cathepsin La; Belongs to the peptidase C1 family | 2.863E-03 | 0.304 | 3.291 |
| BL15-6h vs. BL28-6h | Dn | G3PCW5 | Fras1 related extracellular matrix protein 2b | Fras1 related extracellular matrix protein 2b | 3.888E-02 | 0.311 | 3.216 |
| BL15-6h vs. BL28-6h | Dn | G3NGR6 | Apolipoprotein Eb | #N/A | 9.294E-03 | 0.314 | 3.181 |
| BL15-6h vs. BL28-6h | Dn | G3NI26 | Stromal cell-derived factor 2-like 1 | Stromal cell-derived factor 2-like 1 | 2.045E-02 | 0.316 | 3.169 |
| BL15-6h vs. BL28-6h | Dn | G3NFC1 | Uncharacterized protein | Calreticulin | 6.766E-04 | 0.322 | 3.110 |
| BL15-6h vs. BL28-6h | Dn | G3NRR7 | Myosin, heavy chain 9b, non-muscle | Myosin, heavy polypeptide 9b, non-muscle | 1.906E-02 | 0.322 | 3.107 |
| BL15-6h vs. BL28-6h | Dn | G3P5Z2 | Ubiquitin carboxyl-terminal hydrolase | #N/A | 1.216E-02 | 0.322 | 3.106 |
| BL15-6h vs. BL28-6h | Dn | G3PK17 | Serpin peptidase inhibitor, clade C (antithrombin), member 1 | Serine (or cysteine) proteinase inhibitor, clade C (antithrombin), member 1; Belongs to the serpin family | 3.794E-03 | 0.323 | 3.098 |
| BL15-6h vs. BL28-6h | Dn | G3Q083 | EH-domain containing 1a | EH-domain containing 1a | 7.552E-03 | 0.327 | 3.054 |
| BL15-6h vs. BL28-6h | Dn | G3P4B9 | Uncharacterized protein | Heterogeneous nuclear ribonucleoprotein A1a | 1.237E-03 | 0.328 | 3.053 |
| BL15-6h vs. BL28-6h | Dn | G3NYK9 | Uncharacterized protein | annotation not available | 3.367E-03 | 0.332 | 3.015 |
| BL15-6h vs. BL28-6h | Dn | G3NXR3 | Uncharacterized protein | Uncharacterized protein; Si:ch73-343l4.6 | 5.914E-04 | 0.334 | 2.994 |
| BL15-6h vs. BL28-6h | Dn | G3NQA7 | Uncharacterized protein | Uncharacterized protein; Fetuin B | 3.600E-03 | 0.336 | 2.981 |
| BL15-6h vs. BL28-6h | Dn | G3PIF4 | von Willebrand factor | Von Willebrand factor | 2.441E-02 | 0.336 | 2.979 |
| BL15-6h vs. BL28-6h | Dn | G3PLC2 | ATP-binding cassette, sub-family B (MDR/TAP), member 11b | ATP-binding cassette, sub-family B (MDR/TAP), member 11b | 8.111E-03 | 0.341 | 2.933 |
| BL15-6h vs. BL28-6h | Dn | G3NKR5 | Uncharacterized protein | G1 to S phase transition 1 | 2.323E-03 | 0.353 | 2.834 |
| BL15-6h vs. BL28-6h | Dn | G3NKN5 | Dehydrogenase E1 and transketolase domain containing 1 | Dehydrogenase E1 and transketolase domain containing 1 | 7.258E-03 | 0.353 | 2.832 |
| BL15-6h vs. BL28-6h | Dn | G3PQW8 | Uncharacterized protein | Uncharacterized protein; Fibronectin 1b | 5.286E-04 | 0.355 | 2.819 |
| BL15-6h vs. BL28-6h | Dn | G3P5U3 | Si:ch73-86n18.1 | #N/A | 1.471E-02 | 0.359 | 2.782 |
| BL15-6h vs. BL28-6h | Dn | G3NC94 | Uncharacterized protein | poly(rC) binding protein 3 | 1.899E-02 | 0.360 | 2.781 |
| BL15-6h vs. BL28-6h | Dn | G3PVW5 | Isocitrate dehydrogenase [NADP] | Isocitrate dehydrogenase 2 (NADP+), mitochondria | 1.216E-02 | 0.360 | 2.775 |
| BL15-6h vs. BL28-6h | Dn | G3Q0H4 | Phosphoethanolamine methyltransferase | #N/A | 3.585E-02 | 0.361 | 2.767 |
| BL15-6h vs. BL28-6h | Dn | G3PJR0 | Cathepsin S, ortholog2, tandem duplicate 1 | #N/A | 5.286E-04 | 0.369 | 2.707 |

| Comparison | Change | Protein Accession | Skyline Description | STRING Description | Adjusted p-value | Fold Change | Inverse Dn Fold Change |
|---|---|---|---|---|---|---|---|
| BL15-6h vs. BL28-6h | Dn | G3PTA6 | AP-1 complex subunit gamma | Adaptor-related protein complex 1, gamma 1 subunit | 8.914E-04 | 0.376 | 2.657 |
| BL15-6h vs. BL28-6h | Dn | G3P2Z2 | DnaJ heat shock protein family (HSP40) member B11 | DnaJ (HSP40) homolog, subfamily B, member 11 | 2.441E-03 | 0.380 | 2.634 |
| BL15-6h vs. BL28-6h | Dn | G3P4Y4 | Protein disulfide isomerase family A, member 6 | Protein disulfide isomerase family A, member 6 | 2.323E-03 | 0.385 | 2.595 |
| BL15-6h vs. BL28-6h | Dn | G3P3A2 | Synaptotagmin binding, cytoplasmic RNA interacting protein, like | Synaptotagmin binding, cytoplasmic RNA interacting protein, like | 4.846E-03 | 0.386 | 2.592 |
| BL15-6h vs. BL28-6h | Dn | G3PGK2 | Golgi reassembly stacking protein 1a | Golgi reassembly stacking protein 1 | 3.167E-02 | 0.387 | 2.585 |
| BL15-6h vs. BL28-6h | Dn | G3NQT9 | Succinate dehydrogenase [ubiquinone] flavoprotein subunit, mitochondrial | Succinate dehydrogenase [ubiquinone] flavoprotein subunit, mitochondrial | 2.294E-02 | 0.387 | 2.583 |
| BL15-6h vs. BL28-6h | Dn | G3P140 | Tyrosine--tRNA ligase | Tyrosine--tRNA ligase; tyrosyl-tRNA synthetase | 4.139E-03 | 0.388 | 2.576 |
| BL15-6h vs. BL28-6h | Dn | G3NS60 | DExD-box helicase 39A | #N/A | 2.844E-02 | 0.391 | 2.561 |
| BL15-6h vs. BL28-6h | Dn | G3PIA8 | Uncharacterized protein | Filamin A, alpha (actin binding protein 280) | 3.895E-03 | 0.395 | 2.534 |
| BL15-6h vs. BL28-6h | Dn | G3PRS7 | Eukaryotic translation elongation factor 1 beta 2 | Eukaryotic translation elongation factor 1 beta 2 | 7.494E-03 | 0.400 | 2.499 |
| BL15-6h vs. BL28-6h | Dn | G3NS10 | Actin, alpha 1, skeletal muscle | Actin, alpha, cardiac muscle 1a; Belongs to the actin family | 1.284E-02 | 0.404 | 2.477 |
| BL15-6h vs. BL28-6h | Dn | G3Q820 | Acetyl-CoA acyltransferase 1 | #N/A | 5.991E-03 | 0.404 | 2.473 |
| BL15-6h vs. BL28-6h | Dn | G3P2I6 | Uncharacterized protein | #N/A | 6.314E-03 | 0.406 | 2.466 |
| BL15-6h vs. BL28-6h | Dn | G3PKE0 | Galectin | #N/A | 8.914E-04 | 0.416 | 2.403 |
| BL15-6h vs. BL28-6h | Dn | G3NJ90 | Signal recognition particle 9 kDa protein | Signal recognition particle 9 kDa protein | 1.784E-03 | 0.417 | 2.399 |
| BL15-6h vs. BL28-6h | Dn | G3PA75 | Thioredoxin domain containing 17 | Thioredoxin domain containing 17 | 5.914E-04 | 0.418 | 2.392 |
| BL15-6h vs. BL28-6h | Dn | G3NIZ1 | Acetyl-CoA acyltransferase 2 | #N/A | 6.389E-04 | 0.419 | 2.389 |
| BL15-6h vs. BL28-6h | Dn | G3PBY3 | Ribosomal protein S9 | #N/A | 2.131E-02 | 0.419 | 2.387 |
| BL15-6h vs. BL28-6h | Dn | G3Q615 | Phytanoyl-CoA 2-hydroxylase | phytanoyl-CoA 2-hydroxylase | 2.784E-03 | 0.419 | 2.387 |
| BL15-6h vs. BL28-6h | Dn | G3Q8E3 | Staphylococcal nuclease domain-containing protein | Staphylococcal nuclease domain containing 1 | 1.485E-02 | 0.423 | 2.364 |
| BL15-6h vs. BL28-6h | Dn | G3QAQ6 | Spectrin beta chain | Spectrin, beta, non-erythrocytic 2 | 5.914E-04 | 0.426 | 2.346 |
| BL15-6h vs. BL28-6h | Dn | G3PHA5 | Uncharacterized protein | Uncharacterized protein; Eukaryotic translation elongation factor 2a, tandem duplicate 2 | 1.528E-02 | 0.430 | 2.326 |
| BL15-6h vs. BL28-6h | Dn | G3Q522 | Aldo-keto reductase family 1, member B1 (aldose reductase) | Aldo-keto reductase family 1, member B1 (aldose reductase) | 2.844E-02 | 0.430 | 2.324 |
| BL15-6h vs. BL28-6h | Dn | G3NRT5 | Malate dehydrogenase | Malate dehydrogenase 2, NAD (mitochondrial) | 2.437E-03 | 0.431 | 2.319 |
| BL15-6h vs. BL28-6h | Dn | G3NQJ2 | Proteasome 26S subunit, ATPase 6 | #N/A | 8.539E-03 | 0.440 | 2.272 |
| BL15-6h vs. BL28-6h | Dn | G3PIZ9 | TIA1 cytotoxic granule associated RNA binding protein | annotation not available | 2.918E-02 | 0.442 | 2.263 |
| BL15-6h vs. BL28-6h | Dn | G3PXN8 | Ubiquinol-cytochrome c reductase, complex III subunit X | Ubiquinol-cytochrome c reductase, complex III subunit X | 1.923E-02 | 0.442 | 2.262 |
| BL15-6h vs. BL28-6h | Dn | G3P5V0 | Ribosomal protein S18 | Ribosomal protein S18 | 4.743E-02 | 0.443 | 2.255 |
| BL15-6h vs. BL28-6h | Dn | G3QAF5 | Moesin a | Moesin a | 7.321E-03 | 0.446 | 2.243 |
| BL15-6h vs. BL28-6h | Dn | G3Q6T4 | Sex hormone-binding globulin | Sex hormone binding globulin | 1.614E-02 | 0.447 | 2.237 |
| BL15-6h vs. BL28-6h | Dn | G3NFV4 | Heterogeneous nuclear ribonucleoprotein R | Heterogeneous nuclear ribonucleoprotein R | 3.977E-03 | 0.451 | 2.216 |
| BL15-6h vs. BL28-6h | Dn | G3PV80 | Uncharacterized protein | annotation not available | 1.923E-02 | 0.452 | 2.213 |
| BL15-6h vs. BL28-6h | Dn | G3Q9L0 | Hypoxia up-regulated 1 | Hypoxia up-regulated 1 | 3.980E-03 | 0.454 | 2.202 |
| BL15-6h vs. BL28-6h | Dn | G3PFW5 | Peroxisomal trans-2-enoyl-CoA reductase | #N/A | 6.766E-04 | 0.457 | 2.190 |
| BL15-6h vs. BL28-6h | Dn | G3PWI0 | Heat shock protein 5 | Heat shock protein 5; Belongs to the heat shock protein 70 family | 3.655E-02 | 0.461 | 2.172 |
| BL15-6h vs. BL28-6h | Dn | G3PWJ1 | NADH:ubiquinone oxidoreductase core subunit V2 | NADH dehydrogenase (ubiquinone) flavoprotein 2 | 2.784E-03 | 0.461 | 2.170 |
| BL15-6h vs. BL28-6h | Dn | G3PJ37 | ELAV-like protein | #N/A | 1.284E-02 | 0.464 | 2.155 |
| BL15-6h vs. BL28-6h | Dn | G3NT91 | Sialic acid acetylesterase | Sialic acid acetylesterase | 3.826E-03 | 0.465 | 2.151 |
| BL15-6h vs. BL28-6h | Dn | G3PVS.6 | Heterogeneous nuclear ribonucleoprotein A0b | Heterogeneous nuclear ribonucleoprotein A0b | 1.297E-02 | 0.468 | 2.136 |

| Comparison | Change | Protein Accession | Skyline Description | STRING Description | Adjusted p-value | Fold Change | Inverse Dn Fold Change |
|---|---|---|---|---|---|---|---|
| BL15-6h vs. BL28-6h | Dn | G3PHX0 | 2-oxoisovalerate dehydrogenase subunit alpha | Branched chain keto acid dehydrogenase E1, alpha polypeptide | 1.233E-02 | 0.470 | 2.130 |
| BL15-6h vs. BL28-6h | Dn | G3Q2F6 | Heat shock protein 4b | Heat shock protein 4b | 6.696E-03 | 0.471 | 2.123 |
| BL15-6h vs. BL28-6h | Dn | G3NNM8 | Uncharacterized protein | Alpha-2-macroglobulin-like 1 | 2.059E-02 | 0.472 | 2.119 |
| BL15-6h vs. BL28-6h | Dn | G3Q7P7 | MICOS complex subunit MIC60 | #N/A | 3.492E-03 | 0.475 | 2.107 |
| BL15-6h vs. BL28-6h | Dn | G3Q9Z0 | FinTRIM family, member 82 | finTRIM family, member 82 | 2.323E-03 | 0.477 | 2.095 |
| BL15-6h vs. BL28-6h | Dn | G3QCA0 | Arginyl-tRNA synthetase | arginyl-tRNA synthetase | 1.906E-02 | 0.478 | 2.092 |
| BL15-6h vs. BL28-6h | Dn | G3Q3R5 | Carnitine O-acetyltransferase a | Carnitine O-acetyltransferase a | 3.318E-03 | 0.479 | 2.087 |
| BL15-6h vs. BL28-6h | Dn | G3Q329 | Lamin B1 | Lamin B1; Belongs to the intermediate filament family | 3.767E-03 | 0.480 | 2.083 |
| BL15-6h vs. BL28-6h | Dn | G3PQ56 | Uncharacterized protein | Myosin, heavy polypeptide 11, smooth muscle b | 3.058E-02 | 0.481 | 2.077 |
| BL15-6h vs. BL28-6h | Dn | G3PI33 | NAD-dependent protein deacylase sirtuin-5, mitochondrial | NAD-dependent protein deacylase sirtuin-5, mitochondrial | 5.420E-03 | 0.483 | 2.073 |
| BL15-6h vs. BL28-6h | Dn | G3PA08 | Uncharacterized protein (Fragment) | Uncharacterized protein; CD5 molecule-like | 1.630E-02 | 0.484 | 2.068 |
| BL15-6h vs. BL28-6h | Dn | G3PR69 | Nascent polypeptide associated complex subunit alpha | Uncharacterized protein; Nascent polypeptide-associated complex alpha subunit | 6.760E-03 | 0.497 | 2.011 |
| BL15-6h vs. BL28-6h | Dn | G3N8W8 | Uncharacterized protein | Uncharacterized protein; Actin, beta-like 2; Belongs to the actin family | 5.803E-03 | 0.499 | 2.005 |
| BL15-24h vs. BL28-24h | Up | G3Q4Q5 | DnaJ heat shock protein family (HSP40) member B1b | #N/A | 3.727E-06 | 9.336 | |
| BL15-24h vs. BL28-24h | Up | G3Q568 | Uncharacterized protein | Uncharacterized protein; Caldesmon 1 like | 8.619E-03 | 7.391 | |
| BL15-24h vs. BL28-24h | Dn | G3PRF7 | Eukaryotic translation elongation factor 2b | Eukaryotic translation elongation factor 2b | 2.317E-02 | 0.275 | 3.634 |
| BL15-24h vs. BL28-24h | Dn | G3Q0H4 | Phosphoethanolamine methyltransferase | #N/A | 3.470E-02 | 0.298 | 3.361 |
| BL15-24h vs. BL28-24h | Dn | G3P7H4 | Leukocyte cell-derived chemotaxin 2 like | #N/A | 4.099E-02 | 0.348 | 2.878 |
| BL15-24h vs. BL28-24h | Dn | G3P5J3 | Angiotensinogen | Angiotensinogen; Belongs to the serpin family | 8.619E-03 | 0.424 | 2.360 |
| BL15-24h vs. BL28-24h | Dn | G3NIZ1 | Acetyl-CoA acyltransferase 2 | #N/A | 2.317E-02 | 0.446 | 2.245 |
| BL15-24h vs. BL28-24h | Dn | G3PXC5 | Fibrinogen gamma chain | Fibrinogen, gamma polypeptide | 4.347E-02 | 0.509 | 1.966 |
| KL15-6h vs. KL28-6h | Up | G3Q4Q5 | DnaJ heat shock protein family (HSP40) member B1b | #N/A | 3.550E-05 | 13.212 | |
| KL15-24h vs. KL28-24h | Up | G3Q4Q5 | DnaJ heat shock protein family (HSP40) member B1b | #N/A | 3.671E-02 | 8.253 | |
| KL15-24h vs. KL28-24h | Dn | G3NZ73 | Sulfurtransferase | #N/A | 2.208E-02 | 0.325 | 3.079 |
| KL15-24h vs. KL28-24h | Dn | G3Q4H0 | Uncharacterized protein | Complement component 3 | 4.418E-03 | 0.326 | 3.065 |

**Supplemental Table 3.2.** Functional enrichments (STRING network clusters, Uniprot keywords, PFAM protein domains, INTERPRO protein domains and features, and SMART protein domains) by comparison. All four comparisons (BL15-6h vs. BL28-6h, BL15-24h vs. BL28-24h, KL15-6h vs. KL28-6h, and KL15-24h vs. KL28-24h) were analyzed for functional enrichments with the entire liver proteome ranked by FC. The table includes term ID, term description, genes mapped, direction, and false discovery rate (FDR).

| Comparison | Functional enrichment | #term ID | term description | genes mapped | direction | FDR |
|---|---|---|---|---|---|---|
| BL15-6h vs. BL28-6h | STRING | CL:15706 | Ribosomal protein, and Translation protein SH3-like domain superfamily | 66 | 15°C>28°C | 5.16E-05 |
| BL15-6h vs. BL28-6h | STRING | CL:15702 | mixed, incl. Ribosomal protein, and Translation protein SH3-like domain superfamily | 70 | 15°C>28°C | 5.16E-05 |
| BL15-6h vs. BL28-6h | STRING | CL:15694 | mixed, incl. Ribosomal protein, and Translation protein SH3-like domain superfamily | 74 | 15°C>28°C | 5.16E-05 |
| BL15-6h vs. BL28-6h | STRING | CL:15697 | mixed, incl. Ribosomal protein, and Translation protein SH3-like domain superfamily | 72 | 15°C>28°C | 5.16E-05 |
| BL15-6h vs. BL28-6h | STRING | CL:15715 | Ribosomal protein, and Translation protein SH3-like domain superfamily | 58 | 15°C>28°C | 5.94E-05 |
| BL15-6h vs. BL28-6h | STRING | CL:15692 | mixed, incl. Ribosomal protein, and Translation protein, beta-barrel domain superfamily | 80 | 15°C>28°C | 9.13E-05 |
| BL15-6h vs. BL28-6h | STRING | CL:15710 | Ribosomal protein, and Translation protein SH3-like domain superfamily | 63 | 15°C>28°C | 9.75E-05 |
| BL15-6h vs. BL28-6h | STRING | CL:15718 | Ribosomal protein, and Translation protein SH3-like domain superfamily | 54 | 15°C>28°C | 1.90E-04 |
| BL15-6h vs. BL28-6h | STRING | CL:15720 | Ribosomal protein, and Translation protein SH3-like domain superfamily | 29 | 15°C>28°C | 4.90E-04 |
| BL15-6h vs. BL28-6h | STRING | CL:15691 | mixed, incl. Ribosomal protein, and Protein biosynthesis | 91 | 15°C>28°C | 8.00E-04 |
| BL15-6h vs. BL28-6h | STRING | CL:18338 | mixed, incl. Thioredoxin, conserved site, and Calreticulin family | 17 | 15°C>28°C | 1.00E-03 |
| BL15-6h vs. BL28-6h | STRING | CL:18343 | mixed, incl. Disulphide isomerase, and Heat shock protein 70kD, C-terminal domain superfamily | 10 | 15°C>28°C | 1.00E-03 |
| BL15-6h vs. BL28-6h | STRING | CL:18342 | mixed, incl. Calreticulin family, and Disulphide isomerase | 16 | 15°C>28°C | 1.00E-03 |
| BL15-6h vs. BL28-6h | STRING | CL:18336 | mixed, incl. Thioredoxin, and Endoplasmic reticulum | 21 | 15°C>28°C | 1.10E-03 |
| BL15-6h vs. BL28-6h | STRING | CL:15688 | mixed, incl. Ribosomal protein, and Protein biosynthesis | 95 | 15°C>28°C | 1.10E-03 |
| BL15-6h vs. BL28-6h | STRING | CL:15687 | mixed, incl. Ribosomal protein, and Protein biosynthesis | 103 | 15°C>28°C | 1.20E-03 |
| BL15-6h vs. BL28-6h | STRING | CL:15722 | Ribosomal protein, and Translation protein SH3-like domain superfamily | 25 | 15°C>28°C | 1.50E-03 |
| BL15-6h vs. BL28-6h | STRING | CL:18335 | mixed, incl. Translocon-associated protein (TRAP), alpha subunit, and Thioredoxin | 24 | 15°C>28°C | 2.30E-03 |
| BL15-6h vs. BL28-6h | STRING | CL:15674 | mixed, incl. Ribosomal protein, and Protein biosynthesis | 105 | 15°C>28°C | 3.20E-03 |
| BL15-6h vs. BL28-6h | STRING | CL:15673 | mixed, incl. Ribosomal protein, and Protein biosynthesis | 111 | 15°C>28°C | 6.10E-03 |
| BL15-6h vs. BL28-6h | Uniprot | KW-0689 | Ribosomal protein | 39 | 15°C>28°C | 1.10E-03 |
| BL15-6h vs. BL28-6h | Uniprot | KW-0732 | Signal | 120 | 15°C>28°C | 1.10E-03 |
| BL15-6h vs. BL28-6h | Uniprot | KW-0687 | Ribonucleoprotein | 47 | 15°C>28°C | 7.50E-03 |
| BL15-6h vs. BL28-6h | PFAM | PF00538 | linker histone H1 and H5 family | 7 | 28°C>15°C | 8.40E-03 |
| BL15-6h vs. BL28-6h | INTERPRO | IPR005818 | Linker histone H1/H5, domain H15 | 7 | 28°C>15°C | 8.20E-03 |
| BL15-6h vs. BL28-6h | INTERPRO | IPR005819 | Histone H5 | 6 | 28°C>15°C | 8.20E-03 |
| BL15-6h vs. BL28-6h | INTERPRO | IPR014756 | Immunoglobulin E-set | 11 | 15°C>28°C | 8.80E-03 |
| BL15-6h vs. BL28-6h | SMART | SM00526 | Domain in histone families 1 and 5 | 7 | 28°C>15°C | 3.50E-03 |
| BL15-24h vs. BL28-24h | STRING | CL:15694 | mixed, incl. Ribosomal protein, and Translation protein SH3-like domain superfamily | 74 | 15°C>28°C | 3.15E-05 |
| BL15-24h vs. BL28-24h | STRING | CL:15702 | mixed, incl. Ribosomal protein, and Translation protein SH3-like domain superfamily | 70 | 15°C>28°C | 3.15E-05 |
| BL15-24h vs. BL28-24h | STRING | CL:15697 | mixed, incl. Ribosomal protein, and Translation protein SH3-like domain superfamily | 72 | 15°C>28°C | 3.15E-05 |
| BL15-24h vs. BL28-24h | STRING | CL:15692 | mixed, incl. Ribosomal protein, and Translation protein, beta-barrel domain superfamily | 80 | 15°C>28°C | 4.82E-05 |
| BL15-24h vs. BL28-24h | STRING | CL:15706 | Ribosomal protein, and Translation protein SH3-like domain superfamily | 66 | 15°C>28°C | 4.82E-05 |
| BL15-24h vs. BL28-24h | STRING | CL:15710 | Ribosomal protein, and Translation protein SH3-like domain superfamily | 63 | 15°C>28°C | 8.28E-05 |
| BL15-24h vs. BL28-24h | STRING | CL:15715 | Ribosomal protein, and Translation protein SH3-like domain superfamily | 58 | 15°C>28°C | 2.80E-04 |
| BL15-24h vs. BL28-24h | STRING | CL:15718 | Ribosomal protein, and Translation protein SH3-like domain superfamily | 54 | 15°C>28°C | 3.60E-04 |
| BL15-24h vs. BL28-24h | STRING | CL:15688 | mixed, incl. Ribosomal protein, and Protein biosynthesis | 95 | 15°C>28°C | 1.10E-03 |
| BL15-24h vs. BL28-24h | STRING | CL:15691 | mixed, incl. Ribosomal protein, and Protein biosynthesis | 91 | 15°C>28°C | 1.10E-03 |
| BL15-24h vs. BL28-24h | STRING | CL:15687 | mixed, incl. Ribosomal protein, and Protein biosynthesis | 103 | 15°C>28°C | 2.60E-03 |
| BL15-24h vs. BL28-24h | STRING | CL:15674 | mixed, incl. Ribosomal protein, and Protein biosynthesis | 105 | 15°C>28°C | 8.40E-03 |
| BL15-24h vs. BL28-24h | Uniprot | KW-0732 | Signal | 121 | 15°C>28°C | 4.50E-03 |
| BL15-24h vs. BL28-24h | Uniprot | KW-0689 | Ribosomal protein | 39 | 15°C>28°C | 6.20E-03 |
| BL15-24h vs. BL28-24h | SMART | SM00838 | Elongation factor G C-terminus | 3 | 15°C>28°C | 6.90E-03 |
| BL15-24h vs. BL28-24h | SMART | SM00526 | Domain in histone families 1 and 5 | 7 | 28°C>15°C | 6.90E-03 |
| BL15-24h vs. BL28-24h | SMART | SM00268 | Actin | 6 | 15°C>28°C | 6.90E-03 |
| KL15-6h vs. KL28-6h | STRING | CL:21367 | mixed, incl. Glycolysis, and L-lactate/malate dehydrogenase | 31 | 15°C>28°C | 4.20E-04 |
| KL15-6h vs. KL28-6h | STRING | CL:21368 | mixed, incl. Glycolysis, and L-lactate/malate dehydrogenase | 30 | 15°C>28°C | 5.00E-04 |
| KL15-6h vs. KL28-6h | STRING | CL:21366 | mixed, incl. Glycolysis, and Thiamin diphosphate-binding fold | 48 | 15°C>28°C | 4.30E-03 |
| KL15-6h vs. KL28-6h | STRING | CL:21365 | mixed, incl. Glycolysis, and Thiamin diphosphate-binding fold | 54 | 15°C>28°C | 4.30E-03 |
| KL15-6h vs. KL28-6h | STRING | CL:21363 | mixed, incl. Glycolysis, and Carbohydrate metabolism | 58 | 15°C>28°C | 4.30E-03 |
| KL15-6h vs. KL28-6h | Uniprot | KW-0324 | Glycolysis | 10 | 15°C>28°C | 3.30E-03 |

| Comparison | Functional enrichment | #term ID | term description | genes mapped | direction | FDR |
|---|---|---|---|---|---|---|
| KL15-24h vs. KL28-24h | STRING | CL:21368 | mixed, incl. Glycolysis, and L-lactate/malate dehydrogenase | 31 | 15°C>28°C | 1.99E-08 |
| KL15-24h vs. KL28-24h | STRING | CL:21367 | mixed, incl. Glycolysis, and L-lactate/malate dehydrogenase | 32 | 15°C>28°C | 3.86E-08 |
| KL15-24h vs. KL28-24h | STRING | CL:21363 | mixed, incl. Glycolysis, and Carbohydrate metabolism | 59 | 15°C>28°C | 1.82E-07 |
| KL15-24h vs. KL28-24h | STRING | CL:21365 | mixed, incl. Glycolysis, and Thiamin diphosphate-binding fold | 55 | 15°C>28°C | 3.55E-06 |
| KL15-24h vs. KL28-24h | STRING | CL:21366 | mixed, incl. Glycolysis, and Thiamin diphosphate-binding fold | 49 | 15°C>28°C | 3.66E-06 |
| KL15-24h vs. KL28-24h | STRING | CL:15673 | mixed, incl. Ribosomal protein, and Protein biosynthesis | 110 | 28°C>15°C | 2.10E-04 |
| KL15-24h vs. KL28-24h | STRING | CL:22400 | mixed, incl. Tyrosine 3-monooxygenase-like, and Pyridoxal phosphate-dependent transferase | 14 | 15°C>28°C | 2.40E-04 |
| KL15-24h vs. KL28-24h | STRING | CL:15674 | mixed, incl. Ribosomal protein, and Protein biosynthesis | 104 | 28°C>15°C | 6.90E-04 |
| KL15-24h vs. KL28-24h | STRING | CL:15687 | mixed, incl. Ribosomal protein, and Protein biosynthesis | 102 | 28°C>15°C | 8.90E-04 |
| KL15-24h vs. KL28-24h | STRING | CL:15688 | mixed, incl. Ribosomal protein, and Protein biosynthesis | 94 | 28°C>15°C | 9.60E-04 |
| KL15-24h vs. KL28-24h | STRING | CL:16355 | mostly uncharacterized, incl. DEAD/DEAH box helicase, and Ribosome biogenesis | 25 | 28°C>15°C | 1.90E-03 |
| KL15-24h vs. KL28-24h | STRING | CL:16363 | mixed, incl. Ribosome biogenesis, and DEAD/DEAH box helicase | 23 | 28°C>15°C | 2.00E-03 |
| KL15-24h vs. KL28-24h | STRING | CL:15691 | mixed, incl. Ribosomal protein, and Protein biosynthesis | 90 | 28°C>15°C | 2.00E-03 |
| KL15-24h vs. KL28-24h | STRING | CL:22009 | mixed, incl. AMP-binding, conserved site, and Aldehyde dehydrogenase domain | 31 | 15°C>28°C | 2.20E-03 |
| KL15-24h vs. KL28-24h | STRING | CL:22008 | mixed, incl. AMP-binding, conserved site, and Aldehyde dehydrogenase domain | 42 | 15°C>28°C | 2.30E-03 |
| KL15-24h vs. KL28-24h | STRING | CL:21371 | mixed, incl. Glycolysis, and Enolase | 19 | 15°C>28°C | 2.30E-03 |
| KL15-24h vs. KL28-24h | STRING | CL:21372 | Glycolysis, and Enolase | 16 | 15°C>28°C | 2.90E-03 |
| KL15-24h vs. KL28-24h | STRING | CL:16360 | mixed, incl. Ribosome biogenesis, and DEAD/DEAH box helicase | 24 | 28°C>15°C | 3.30E-03 |
| KL15-24h vs. KL28-24h | STRING | CL:22137 | mixed, incl. Aldehyde dehydrogenase domain, and Alcohol dehydrogenase, zinc-type, conserved site | 13 | 15°C>28°C | 4.00E-03 |
| KL15-24h vs. KL28-24h | STRING | CL:7161 | mostly uncharacterized, incl. Low-density lipoprotein (LDL) receptor class A repeat, and Terpenoid cyclases/protein prenyltransferase alpha-alpha toroid | 47 | 15°C>28°C | 4.70E-03 |
| KL15-24h vs. KL28-24h | STRING | CL:22135 | mixed, incl. Aldehyde dehydrogenase domain, and Alcohol dehydrogenase, zinc-type, conserved site | 16 | 15°C>28°C | 6.20E-03 |
| KL15-24h vs. KL28-24h | STRING | CL:22401 | mixed, incl. Tyrosine 3-monooxygenase-like, and Sepiapterin reductase | 6 | 15°C>28°C | 6.40E-03 |
| KL15-24h vs. KL28-24h | STRING | CL:15692 | mixed, incl. Ribosomal protein, and Translation protein, beta-barrel domain superfamily | 80 | 28°C>15°C | 8.90E-03 |
| KL15-24h vs. KL28-24h | STRING | CL:26110 | mostly uncharacterized, incl. Metal-dependent hydrolase, and Adenylate kinase/UMP-CMP kinase | 23 | 15°C>28°C | 9.80E-03 |
| KL15-24h vs. KL28-24h | Uniprot | KW-0694 | RNA-binding | 88 | 28°C>15°C | 7.60E-04 |
| KL15-24h vs. KL28-24h | Uniprot | KW-0560 | Oxidoreductase | 42 | 15°C>28°C | 7.60E-04 |
| KL15-24h vs. KL28-24h | Uniprot | KW-0863 | Zinc-finger | 38 | 28°C>15°C | 2.70E-03 |
| KL15-24h vs. KL28-24h | Uniprot | KW-0324 | Glycolysis | 10 | 15°C>28°C | 8.00E-03 |
| KL15-24h vs. KL28-24h | PFAM | PF07678 | A-macroglobulin complement component | 8 | 15°C>28°C | 1.90E-04 |
| KL15-24h vs. KL28-24h | PFAM | PF07677 | A-macroglobulin receptor | 7 | 15°C>28°C | 2.00E-04 |
| KL15-24h vs. KL28-24h | PFAM | PF10569 | Alpha-macro-globulin thiol-ester bond-forming region | 7 | 15°C>28°C | 2.00E-04 |
| KL15-24h vs. KL28-24h | PFAM | PF00207 | Alpha-2-macroglobulin family | 7 | 15°C>28°C | 2.00E-04 |
| KL15-24h vs. KL28-24h | PFAM | PF07703 | Alpha-2-macroglobulin family N-terminal region | 7 | 15°C>28°C | 6.20E-04 |
| KL15-24h vs. KL28-24h | PFAM | PF01835 | MG2 domain | 6 | 15°C>28°C | 1.70E-03 |
| KL15-24h vs. KL28-24h | PFAM | PF00076 | RNA recognition motif. (a.k.a. RRM, RBD, or RNP domain) | 66 | 28°C>15°C | 4.20E-03 |
| KL15-24h vs. KL28-24h | INTERPRO | IPR011626 | Alpha-macroglobulin, TED domain | 8 | 15°C>28°C | 1.90E-04 |
| KL15-24h vs. KL28-24h | INTERPRO | IPR008930 | Terpenoid cyclases/protein prenyltransferase alpha-alpha toroid | 8 | 15°C>28°C | 1.90E-04 |
| KL15-24h vs. KL28-24h | INTERPRO | IPR036595 | Alpha-macroglobulin, receptor-binding domain superfamily | 7 | 15°C>28°C | 2.60E-04 |
| KL15-24h vs. KL28-24h | INTERPRO | IPR009048 | Alpha-macroglobulin, receptor-binding | 7 | 15°C>28°C | 2.60E-04 |
| KL15-24h vs. KL28-24h | INTERPRO | IPR036291 | NAD(P)-binding domain superfamily | 41 | 15°C>28°C | 2.60E-04 |
| KL15-24h vs. KL28-24h | INTERPRO | IPR001599 | Alpha-2-macroglobulin | 7 | 15°C>28°C | 2.60E-04 |
| KL15-24h vs. KL28-24h | INTERPRO | IPR016040 | NAD(P)-binding domain | 22 | 15°C>28°C | 5.60E-04 |
| KL15-24h vs. KL28-24h | INTERPRO | IPR011625 | Alpha-2-macroglobulin, bait region domain | 7 | 15°C>28°C | 7.50E-04 |
| KL15-24h vs. KL28-24h | INTERPRO | IPR012677 | Nucleotide-binding alpha-beta plait domain superfamily | 70 | 28°C>15°C | 8.40E-04 |
| KL15-24h vs. KL28-24h | INTERPRO | IPR035711 | Complement C3-like | 7 | 15°C>28°C | 1.20E-03 |
| KL15-24h vs. KL28-24h | INTERPRO | IPR019742 | Alpha-2-macroglobulin, conserved site | 6 | 15°C>28°C | 1.20E-03 |
| KL15-24h vs. KL28-24h | INTERPRO | IPR015422 | Pyridoxal phosphate-dependent transferase domain 1 | 12 | 15°C>28°C | 1.40E-03 |
| KL15-24h vs. KL28-24h | INTERPRO | IPR002890 | Macroglobulin domain | 6 | 15°C>28°C | 1.50E-03 |
| KL15-24h vs. KL28-24h | INTERPRO | IPR036188 | FAD/NAD(P)-binding domain superfamily | 15 | 15°C>28°C | 2.50E-03 |
| KL15-24h vs. KL28-24h | INTERPRO | IPR035979 | RNA-binding domain superfamily | 69 | 28°C>15°C | 2.50E-03 |
| KL15-24h vs. KL28-24h | INTERPRO | IPR000504 | RNA recognition motif domain | 69 | 28°C>15°C | 2.50E-03 |
| KL15-24h vs. KL28-24h | INTERPRO | IPR029045 | ClpP/crotonase-like domain superfamily | 7 | 15°C>28°C | 8.50E-03 |
| KL15-24h vs. KL28-24h | SMART | SM01361 | A-macroglobulin receptor | 7 | 15°C>28°C | 1.60E-04 |
| KL15-24h vs. KL28-24h | SMART | SM01360 | Alpha-2-macroglobulin family | 7 | 15°C>28°C | 1.60E-04 |
| KL15-24h vs. KL28-24h | SMART | SM01359 | Alpha-2-Macroglobulin | 7 | 15°C>28°C | 4.30E-04 |
| KL15-24h vs. KL28-24h | SMART | SM00360 | RNA recognition motif | 69 | 28°C>15°C | 2.10E-03 |

**Supplemental Table 3.3.** Functional enrichments (STRING network clusters, Uniprot keywords, PFAM protein domains, INTERPRO protein domains and features, and SMART protein domains) for only the significantly higher or lower abundance proteins from the BL15-6h vs. BL28-6h comparison. Proteins significantly more abundant in BL28-6h are denoted as BL28-6h > BL15-6h in the table and proteins significantly less abundant in BL28-6h are denoted as BL15-6h > BL28-6h in the table. For these analyses, the table includes term ID, term description, observed gene count, background gene count, and FDR.

| Comparison | Functional enrichment | #term ID | term description | observed gene count | background gene count | FDR |
|---|---|---|---|---|---|---|
| BL28-6h > BL15-6h | STRING | CL:11572 | HMG box A DNA-binding domain, conserved site, and Histone H5 | 4 | 5 | 7.30E-06 |
| BL28-6h > BL15-6h | STRING | CL:11311 | Core histone H2A/H2B/H3/H4, and Histone H4 | 8 | 136 | 1.24E-05 |
| BL28-6h > BL15-6h | STRING | CL:17225 | mixed, incl. RNA recognition motif. (a.k.a. RRM, RBD, or RNP domain), and LSM domain | 7 | 122 | 6.48E-05 |
| BL28-6h > BL15-6h | STRING | CL:17391 | RNA recognition motif. (a.k.a. RRM, RBD, or RNP domain) | 5 | 39 | 6.48E-05 |
| BL28-6h > BL15-6h | STRING | CL:22901 | mixed, incl. Respiratory chain, and Hydrogen ion transport | 6 | 109 | 1.60E-04 |
| BL28-6h > BL15-6h | STRING | CL:17392 | RNA recognition motif. (a.k.a. RRM, RBD, or RNP domain) | 4 | 34 | 2.50E-04 |
| BL28-6h > BL15-6h | STRING | CL:22897 | mixed, incl. Mitochondrion, and Eukaryotic porin | 7 | 197 | 2.50E-04 |
| BL28-6h > BL15-6h | STRING | CL:22908 | mixed, incl. Respiratory chain, and NAD | 4 | 40 | 3.90E-04 |
| BL28-6h > BL15-6h | STRING | CL:22902 | mixed, incl. Respiratory chain, and Hydrogen ion transport | 5 | 102 | 8.90E-04 |
| BL28-6h > BL15-6h | STRING | CL:23489 | mixed, incl. BolA protein, and NFU1-like | 3 | 17 | 8.90E-04 |
| BL28-6h > BL15-6h | STRING | CL:22912 | mixed, incl. Respiratory chain, and UcrQ family | 3 | 19 | 1.00E-03 |
| BL28-6h > BL15-6h | STRING | CL:15673 | mixed, incl. Ribosomal protein, and Protein biosynthesis | 6 | 188 | 1.30E-03 |
| BL28-6h > BL15-6h | STRING | CL:17394 | RNA recognition motif. (a.k.a. RRM, RBD, or RNP domain) | 3 | 28 | 2.70E-03 |
| BL28-6h > BL15-6h | STRING | CL:27778 | HSP20/alpha crystallin family, and BAG domains, present in regulator of HSP70 proteins | 2 | 6 | 4.20E-03 |
| BL28-6h > BL15-6h | STRING | CL:30394 | Protein of unknown function DUF719, and Dpy-19/Dpy-19-like | 2 | 6 | 4.20E-03 |
| BL28-6h > BL15-6h | STRING | CL:16954 | mixed, incl. Eukaryotic initiation factor 4E, and MIF4G domain | 3 | 48 | 9.50E-03 |
| BL28-6h > BL15-6h | STRING | CL:11316 | Core histone H2A/H2B/H3/H4, and Histone H4 | 4 | 126 | 1.44E-02 |
| BL28-6h > BL15-6h | STRING | CL:17422 | mixed, incl. Heterogeneous nuclear ribonucleoprotein C, and HnRNP-L/PTB | 2 | 14 | 1.46E-02 |
| BL28-6h > BL15-6h | STRING | CL:15674 | mixed, incl. Ribosomal protein, and Protein biosynthesis | 4 | 165 | 3.36E-02 |
| BL28-6h > BL15-6h | STRING | CL:16003 | mixed, incl. Est1 DNA/RNA binding domain, and UPF3 domain | 2 | 23 | 3.36E-02 |
| BL28-6h > BL15-6h | STRING | CL:16956 | mixed, incl. Eukaryotic initiation factor 4E, and MIF4G domain | 2 | 24 | 3.43E-02 |
| BL28-6h > BL15-6h | STRING | CL:17232 | mixed, incl. LSM domain, and Dim1 family | 2 | 29 | 4.38E-02 |
| BL28-6h > BL15-6h | Uniprot | KW-0158 | Chromosome | 6 | 79 | 3.50E-05 |
| BL28-6h > BL15-6h | Uniprot | KW-0694 | RNA-binding | 9 | 314 | 8.06E-05 |
| BL28-6h > BL15-6h | Uniprot | KW-0238 | DNA-binding | 9 | 740 | 2.94E-02 |
| BL28-6h > BL15-6h | PFAM | PF00538 | linker histone H1 and H5 family | 6 | 17 | 2.39E-08 |
| BL28-6h > BL15-6h | PFAM | PF00076 | RNA recognition motif. (a.k.a. RRM, RBD, or RNP domain) | 6 | 208 | 3.90E-03 |
| BL28-6h > BL15-6h | PFAM | PF00639 | PPIC-type PPIASE domain | 2 | 2 | 3.90E-03 |
| BL28-6h > BL15-6h | PFAM | PF01722 | BolA-like protein | 2 | 3 | 3.90E-03 |
| BL28-6h > BL15-6h | PFAM | PF05334 | Protein of unknown function (DUF719) | 2 | 2 | 3.90E-03 |
| BL28-6h > BL15-6h | PFAM | PF13616 | PPIC-type PPIASE domain | 2 | 2 | 3.90E-03 |
| BL28-6h > BL15-6h | PFAM | PF13893 | RNA recognition motif. (a.k.a. RRM, RBD, or RNP domain) | 3 | 31 | 3.90E-03 |
| BL28-6h > BL15-6h | PFAM | PF15936 | Domain of unknown function (DUF4749) | 2 | 8 | 7.20E-03 |
| BL28-6h > BL15-6h | PFAM | PF00505 | HMG (high mobility group) box | 3 | 50 | 1.06E-02 |
| BL28-6h > BL15-6h | PFAM | PF09011 | HMG-box domain | 3 | 49 | 1.06E-02 |
| BL28-6h > BL15-6h | PFAM | PF00098 | Zinc knuckle | 2 | 27 | 4.52E-02 |
| BL28-6h > BL15-6h | PFAM | PF00412 | LIM domain | 3 | 95 | 4.82E-02 |
| BL28-6h > BL15-6h | INTERPRO | IPR005819 | Histone H5 | 6 | 15 | 2.48E-08 |
| BL28-6h > BL15-6h | INTERPRO | IPR005818 | Linker histone H1/H5, domain H15 | 6 | 19 | 4.00E-08 |
| BL28-6h > BL15-6h | INTERPRO | IPR017967 | HMG box A DNA-binding domain, conserved site | 3 | 3 | 6.30E-05 |
| BL28-6h > BL15-6h | INTERPRO | IPR000504 | RNA recognition motif domain | 8 | 231 | 1.70E-04 |
| BL28-6h > BL15-6h | INTERPRO | IPR012677 | Nucleotide-binding alpha-beta plait domain superfamily | 8 | 248 | 2.30E-04 |
| BL28-6h > BL15-6h | INTERPRO | IPR035979 | RNA-binding domain superfamily | 8 | 251 | 2.30E-04 |
| BL28-6h > BL15-6h | INTERPRO | IPR000297 | Peptidyl-prolyl cis-trans isomerase, PpiC-type | 2 | 2 | 2.10E-03 |
| BL28-6h > BL15-6h | INTERPRO | IPR007998 | Protein of unknown function DUF719 | 2 | 2 | 2.10E-03 |
| BL28-6h > BL15-6h | INTERPRO | IPR002634 | BolA protein | 2 | 3 | 2.80E-03 |
| BL28-6h > BL15-6h | INTERPRO | IPR036065 | BolA-like superfamily | 2 | 3 | 2.80E-03 |
| BL28-6h > BL15-6h | INTERPRO | IPR036390 | Winged helix DNA-binding domain superfamily | 6 | 225 | 4.30E-03 |
| BL28-6h > BL15-6h | INTERPRO | IPR036388 | Winged helix-like DNA-binding domain superfamily | 6 | 237 | 5.20E-03 |
| BL28-6h > BL15-6h | INTERPRO | IPR031847 | Domain of unknown function DUF4749 | 2 | 8 | 8.50E-03 |
| BL28-6h > BL15-6h | INTERPRO | IPR009071 | High mobility group box domain | 3 | 52 | 1.54E-02 |
| BL28-6h > BL15-6h | INTERPRO | IPR036910 | High mobility group box domain superfamily | 3 | 54 | 1.60E-02 |
| BL28-6h > BL15-6h | SMART | SM00526 | Domain in histone families 1 and 5 | 6 | 19 | 1.94E-08 |
| BL28-6h > BL15-6h | SMART | SM00360 | RNA recognition motif | 8 | 224 | 6.79E-05 |
| BL28-6h > BL15-6h | SMART | SM00398 | high mobility group | 3 | 52 | 1.75E-02 |
| BL15-6h > BL28-6h | STRING | CL:18342 | mixed, incl. Calreticulin family, and Disulphide isomerase | 7 | 27 | 1.16E-08 |
| BL15-6h > BL28-6h | STRING | CL:18343 | mixed, incl. Disulphide isomerase, and Heat shock protein 70kD, C-terminal domain superfamily | 5 | 17 | 9.74E-07 |

| Comparison | Functional enrichment | #term ID | term description | observed gene count | background gene count | FDR |
|---|---|---|---|---|---|---|
| BL15-6h > BL28-6h | STRING | CL:15673 | mixed, incl. Ribosomal protein, and Protein biosynthesis | 8 | 188 | 3.04E-05 |
| BL15-6h > BL28-6h | STRING | CL:15687 | mixed, incl. Ribosomal protein, and Protein biosynthesis | 7 | 146 | 6.43E-05 |
| BL15-6h > BL28-6h | STRING | CL:15688 | mixed, incl. Ribosomal protein, and Protein biosynthesis | 6 | 130 | 3.00E-04 |
| BL15-6h > BL28-6h | STRING | CL:7162 | mostly uncharacterized, incl. Low-density lipoprotein (LDL) receptor class A repeat, and Terpenoid cyclases/protein prenyltransferase alpha-alpha toroid | 6 | 170 | 1.20E-03 |
| BL15-6h > BL28-6h | STRING | CL:7167 | mixed, incl. SERine Proteinase INhibitors, and Peptidase S1A, coagulation factor VII/IX/X/C/Z | 4 | 50 | 1.20E-03 |
| BL15-6h > BL28-6h | STRING | CL:15691 | mixed, incl. Ribosomal protein, and Protein biosynthesis | 5 | 122 | 2.20E-03 |
| BL15-6h > BL28-6h | STRING | CL:16242 | Ribosomal protein L25/Gln-tRNA synthetase, N-terminal, and Lysine-tRNA ligase, class II | 2 | 5 | 5.10E-03 |
| BL15-6h > BL28-6h | STRING | CL:17392 | RNA recognition motif. (a.k.a. RRM, RBD, or RNP domain) | 3 | 34 | 5.10E-03 |
| BL15-6h > BL28-6h | STRING | CL:18346 | Heat shock protein HSP90, conserved site, and Heat shock protein 70, conserved site | 2 | 5 | 5.10E-03 |
| BL15-6h > BL28-6h | STRING | CL:18379 | Calreticulin family, and Beta-2-Microglobulin | 2 | 5 | 5.10E-03 |
| BL15-6h > BL28-6h | STRING | CL:27789 | mixed, incl. Filamin C, and Filamin-B | 2 | 5 | 5.10E-03 |
| BL15-6h > BL28-6h | STRING | CL:15692 | mixed, incl. Ribosomal protein, and Translation protein, beta-barrel domain superfamily | 4 | 104 | 9.00E-03 |
| BL15-6h > BL28-6h | STRING | CL:17211 | mixed, incl. RNA recognition motif. (a.k.a. RRM, RBD, or RNP domain), and mRNA processing | 5 | 184 | 9.00E-03 |
| BL15-6h > BL28-6h | STRING | CL:22901 | mixed, incl. Respiratory chain, and Hydrogen ion transport | 4 | 109 | 9.60E-03 |
| BL15-6h > BL28-6h | STRING | CL:17225 | mixed, incl. RNA recognition motif. (a.k.a. RRM, RBD, or RNP domain), and LSM domain | 4 | 122 | 1.25E-02 |
| BL15-6h > BL28-6h | STRING | CL:17422 | mixed, incl. Heterogeneous nuclear ribonucleoprotein C, and HnRNP-L/PTB | 2 | 14 | 1.43E-02 |
| BL15-6h > BL28-6h | STRING | CL:7177 | mixed, incl. Fibrinogen alpha/beta chain family, and Cystatin domain | 2 | 15 | 1.57E-02 |
| BL15-6h > BL28-6h | STRING | CL:1207 | mixed, incl. Myosin tail, and Unconventional myosin-IXb | 2 | 16 | 1.71E-02 |
| BL15-6h > BL28-6h | STRING | CL:21365 | mixed, incl. Glycolysis, and Thiamin diphosphate-binding fold | 4 | 147 | 1.98E-02 |
| BL15-6h > BL28-6h | STRING | CL:879 | mixed, incl. Actin, conserved site, and F-actin-capping protein subunit alpha/beta | 2 | 24 | 2.91E-02 |
| BL15-6h > BL28-6h | STRING | CL:15697 | mixed, incl. Ribosomal protein, and Translation protein SH3-like domain superfamily | 3 | 93 | 3.39E-02 |
| BL15-6h > BL28-6h | STRING | CL:22902 | mixed, incl. Respiratory chain, and Hydrogen ion transport | 3 | 102 | 3.95E-02 |
| BL15-6h > BL28-6h | Uniprot | KW-0694 | RNA-binding | 9 | 314 | 2.20E-04 |
| BL15-6h > BL28-6h | Uniprot | KW-0067 | ATP-binding | 13 | 879 | 8.30E-04 |
| BL15-6h > BL28-6h | Uniprot | KW-0816 | Tricarboxylic acid cycle | 3 | 14 | 8.30E-04 |
| BL15-6h > BL28-6h | Uniprot | KW-0648 | Protein biosynthesis | 4 | 64 | 2.10E-03 |
| BL15-6h > BL28-6h | Uniprot | KW-0009 | Actin-binding | 4 | 120 | 1.37E-02 |
| BL15-6h > BL28-6h | Uniprot | KW-0676 | Redox-active center | 2 | 15 | 1.76E-02 |
| BL15-6h > BL28-6h | Uniprot | KW-0030 | Aminoacyl-tRNA synthetase | 2 | 17 | 1.92E-02 |
| BL15-6h > BL28-6h | Uniprot | KW-0809 | Transit peptide | 2 | 20 | 2.29E-02 |
| BL15-6h > BL28-6h | PFAM | PF00009 | Elongation factor Tu GTP binding domain | 4 | 30 | 5.20E-04 |
| BL15-6h > BL28-6h | PFAM | PF00076 | RNA recognition motif. (a.k.a. RRM, RBD, or RNP domain) | 7 | 208 | 5.20E-04 |
| BL15-6h > BL28-6h | PFAM | PF00679 | Elongation factor G C-terminus | 3 | 7 | 5.20E-04 |
| BL15-6h > BL28-6h | PFAM | PF14492 | Elongation Factor G, domain II | 3 | 6 | 5.20E-04 |
| BL15-6h > BL28-6h | PFAM | PF03144 | Elongation factor Tu domain 2 | 3 | 14 | 8.20E-04 |
| BL15-6h > BL28-6h | PFAM | PF00012 | HSP70 protein | 3 | 16 | 9.60E-04 |
| BL15-6h > BL28-6h | PFAM | PF06723 | MreB/Mbl protein | 3 | 16 | 9.60E-04 |
| BL15-6h > BL28-6h | PFAM | PF00022 | Actin | 3 | 23 | 1.90E-03 |
| BL15-6h > BL28-6h | PFAM | PF03764 | Elongation factor G, domain IV | 2 | 5 | 3.90E-03 |
| BL15-6h > BL28-6h | PFAM | PF00676 | Dehydrogenase E1 component | 2 | 10 | 1.10E-02 |
| BL15-6h > BL28-6h | PFAM | PF00630 | Filamin/ABP280 repeat | 2 | 14 | 1.80E-02 |
| BL15-6h > BL28-6h | PFAM | PF02736 | Myosin N-terminal SH3-like domain | 2 | 21 | 3.43E-02 |
| BL15-6h > BL28-6h | INTERPRO | IPR000640 | Elongation factor EFG, domain V-like | 3 | 7 | 8.20E-04 |
| BL15-6h > BL28-6h | INTERPRO | IPR000795 | Transcription factor, GTP-binding domain | 4 | 23 | 8.20E-04 |
| BL15-6h > BL28-6h | INTERPRO | IPR009000 | Translation protein, beta-barrel domain superfamily | 4 | 31 | 8.20E-04 |
| BL15-6h > BL28-6h | INTERPRO | IPR035647 | EF-G domain III/V-like | 3 | 7 | 8.20E-04 |
| BL15-6h > BL28-6h | INTERPRO | IPR041095 | Elongation Factor G, domain II | 3 | 6 | 8.20E-04 |
| BL15-6h > BL28-6h | INTERPRO | IPR000504 | RNA recognition motif domain | 7 | 231 | 1.30E-03 |
| BL15-6h > BL28-6h | INTERPRO | IPR004001 | Actin, conserved site | 3 | 13 | 1.30E-03 |
| BL15-6h > BL28-6h | INTERPRO | IPR004161 | Translation elongation factor EFTu-like, domain 2 | 3 | 14 | 1.30E-03 |
| BL15-6h > BL28-6h | INTERPRO | IPR012677 | Nucleotide-binding alpha-beta plait domain superfamily | 7 | 248 | 1.30E-03 |
| BL15-6h > BL28-6h | INTERPRO | IPR013126 | Heat shock protein 70 family | 3 | 14 | 1.30E-03 |
| BL15-6h > BL28-6h | INTERPRO | IPR018181 | Heat shock protein 70, conserved site | 3 | 13 | 1.30E-03 |
| BL15-6h > BL28-6h | INTERPRO | IPR020902 | Actin/actin-like conserved site | 3 | 16 | 1.30E-03 |
| BL15-6h > BL28-6h | INTERPRO | IPR029047 | Heat shock protein 70kD, peptide-binding domain superfamily | 3 | 13 | 1.30E-03 |
| BL15-6h > BL28-6h | INTERPRO | IPR029048 | Heat shock protein 70kD, C-terminal domain superfamily | 3 | 14 | 1.30E-03 |
| BL15-6h > BL28-6h | INTERPRO | IPR031157 | Tr-type G domain, conserved site | 3 | 13 | 1.30E-03 |
| BL15-6h > BL28-6h | INTERPRO | IPR035979 | RNA-binding domain superfamily | 7 | 251 | 1.30E-03 |
| BL15-6h > BL28-6h | INTERPRO | IPR014721 | Ribosomal protein S5 domain 2-type fold, subgroup | 3 | 21 | 1.60E-03 |
| BL15-6h > BL28-6h | INTERPRO | IPR004000 | Actin family | 3 | 22 | 1.70E-03 |
| BL15-6h > BL28-6h | INTERPRO | IPR014756 | Immunoglobulin E-set | 5 | 125 | 1.90E-03 |
| BL15-6h > BL28-6h | INTERPRO | IPR041337 | Heterogeneous nuclear ribonucleoprotein Q acidic domain | 2 | 3 | 1.90E-03 |

| Comparison | Functional enrichment | #term ID | term description | observed gene count | background gene count | FDR |
|---|---|---|---|---|---|---|
| BL15-6h > BL28-6h | INTERPRO | IPR005517 | Translation elongation factor EFG/EF2, domain IV | 2 | 5 | 3.80E-03 |
| BL15-6h > BL28-6h | INTERPRO | IPR020568 | Ribosomal protein S5 domain 2-type fold | 3 | 34 | 4.50E-03 |
| BL15-6h > BL28-6h | INTERPRO | IPR006535 | HnRNP R/Q splicing factor | 2 | 6 | 4.60E-03 |
| BL15-6h > BL28-6h | INTERPRO | IPR001017 | Dehydrogenase, E1 component | 2 | 7 | 5.60E-03 |
| BL15-6h > BL28-6h | INTERPRO | IPR005788 | Disulphide isomerase | 2 | 7 | 5.60E-03 |
| BL15-6h > BL28-6h | INTERPRO | IPR036249 | Thioredoxin-like superfamily | 4 | 114 | 1.07E-02 |
| BL15-6h > BL28-6h | INTERPRO | IPR001298 | Filamin/ABP280 repeat | 2 | 13 | 1.43E-02 |
| BL15-6h > BL28-6h | INTERPRO | IPR029061 | Thiamin diphosphate-binding fold | 2 | 14 | 1.58E-02 |
| BL15-6h > BL28-6h | INTERPRO | IPR017868 | Filamin/ABP280 repeat-like | 2 | 15 | 1.72E-02 |
| BL15-6h > BL28-6h | INTERPRO | IPR017937 | Thioredoxin, conserved site | 2 | 15 | 1.72E-02 |
| BL15-6h > BL28-6h | INTERPRO | IPR027401 | Myosin IQ motif-containing domain superfamily | 2 | 23 | 3.49E-02 |
| BL15-6h > BL28-6h | INTERPRO | IPR027417 | P-loop containing nucleoside triphosphate hydrolase | 10 | 1000 | 3.70E-02 |
| BL15-6h > BL28-6h | INTERPRO | IPR004009 | Myosin, N-terminal, SH3-like | 2 | 25 | 3.81E-02 |
| BL15-6h > BL28-6h | INTERPRO | IPR001589 | Actinin-type actin-binding domain, conserved site | 2 | 26 | 3.98E-02 |
| BL15-6h > BL28-6h | SMART | SM00838 | Elongation factor G C-terminus | 3 | 6 | 2.30E-04 |
| BL15-6h > BL28-6h | SMART | SM00360 | RNA recognition motif | 7 | 224 | 6.90E-04 |
| BL15-6h > BL28-6h | SMART | SM00268 | Actin | 3 | 23 | 2.30E-03 |
| BL15-6h > BL28-6h | SMART | SM00889 | Elongation factor G, domain IV | 2 | 5 | 3.90E-03 |
| BL15-6h > BL28-6h | SMART | SM00557 | Filamin-type immunoglobulin domains | 2 | 14 | 1.76E-02 |

**Supplemental Figure 3.1.** RNA transport KEGG pathway with significantly elevated proteins (BL28-6h > BL15-6h) colored in red. See Table 3.3 for full names, protein accession numbers, and KEGG identifiers.

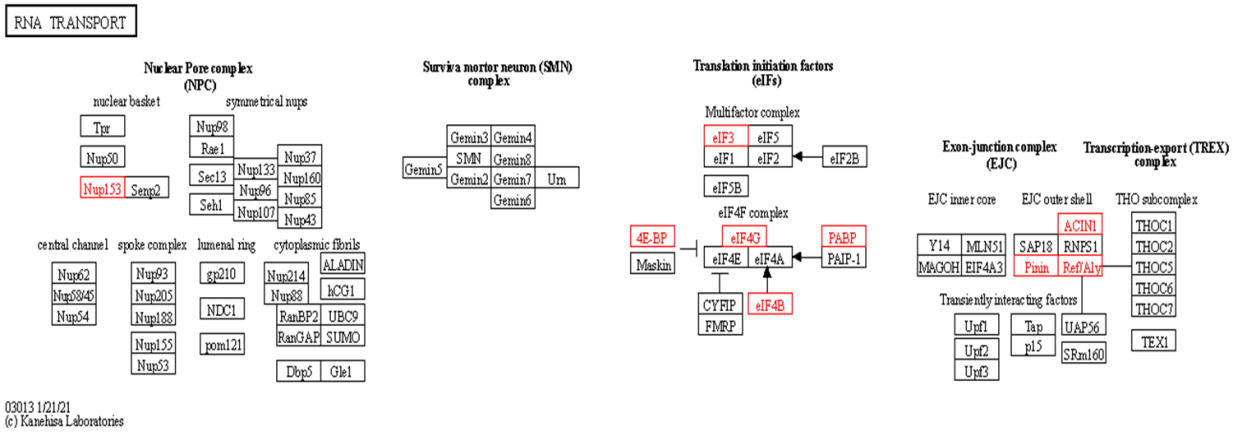

**Supplemental Figure 3.2.** Spliceosome KEGG pathway with significantly elevated proteins (BL28-6h > BL15-6h) colored in red. See Table 3.3 for full names, protein accession numbers, and KEGG identifiers.

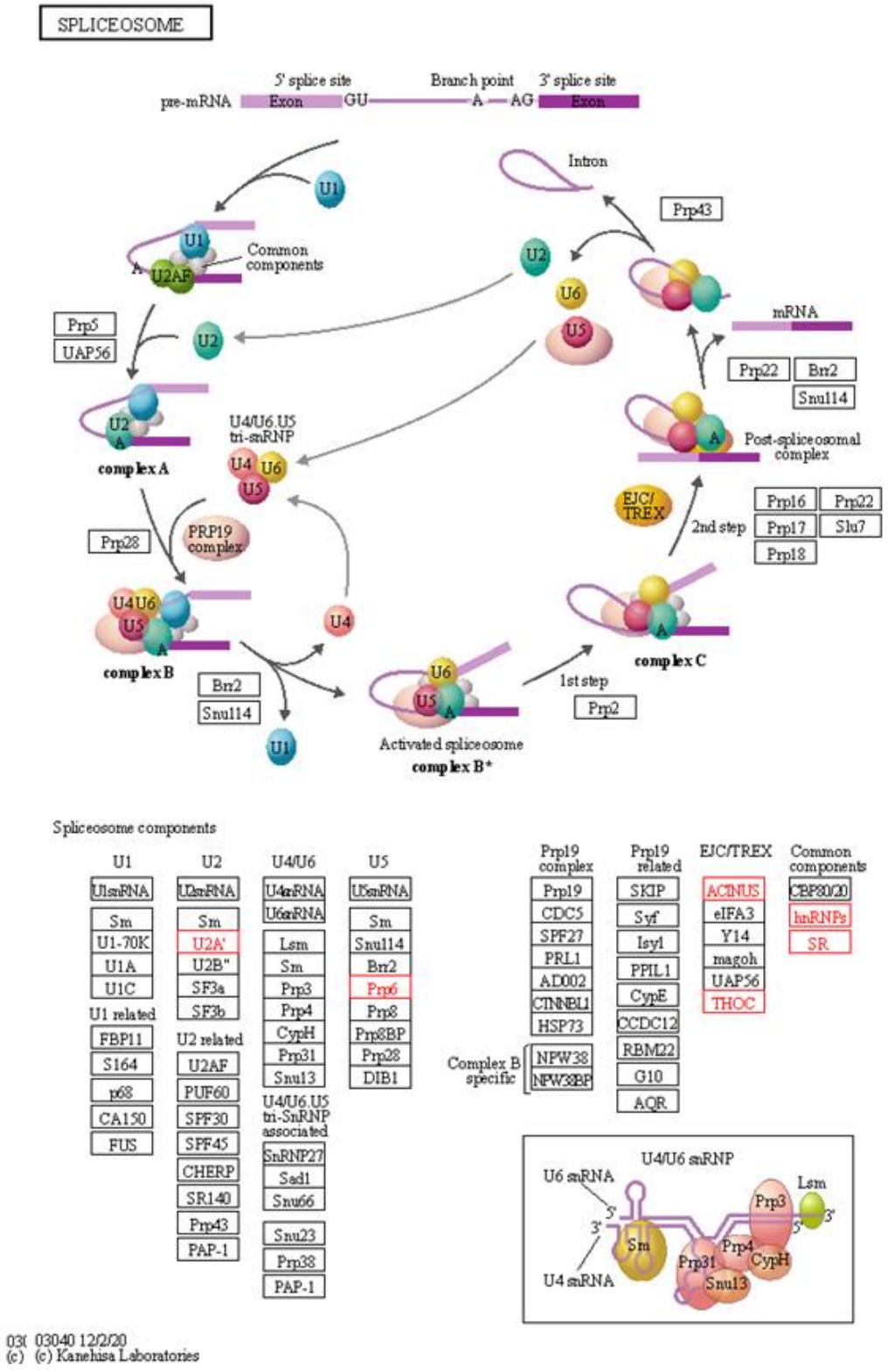

**Supplemental Figure 3.3.** mRNA surveillance KEGG pathway with significantly elevated proteins (BL28-6h > BL15-6h) colored in red. See Table 3.3 for full names, protein accession numbers, and KEGG identifiers.

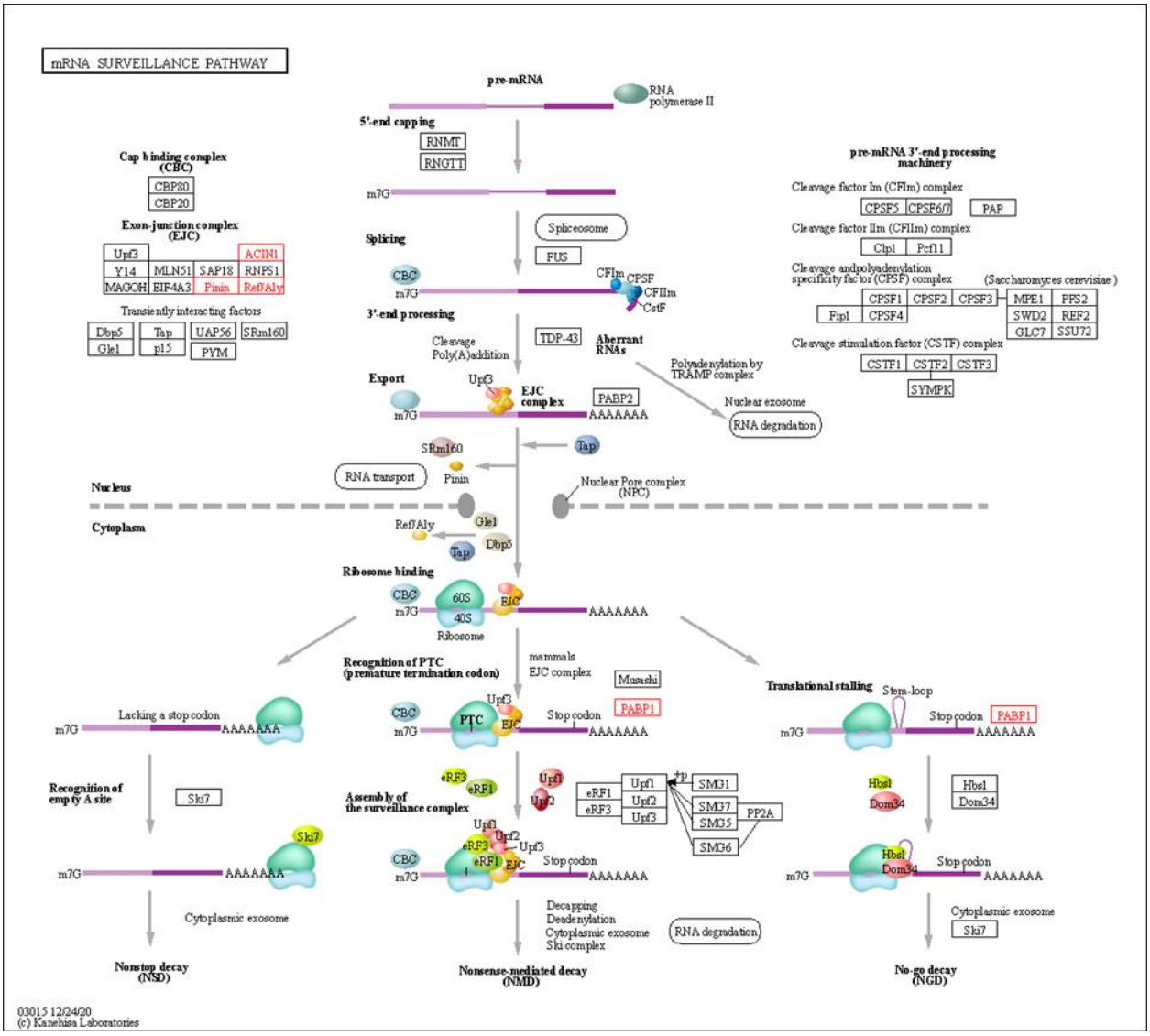

## SUMMARY

To investigate the molecular underpinnings of various types of temperature stress, two populations of threespine sticklebacks (*Gasterosteus aculeatus*) were bred and reared in the laboratory under identical conditions. This dissertation examined the stress response pathways and the functional molecular responses utilized to acclimate to and recover from various temperature stress challenges. Metabolite concentrations, body indices, protein abundance changes, and protein network alterations were examined to understand the impacts of temperature stress on these fish. Similarities between the two populations underscored important conserved responses while differences demonstrated functional variation in response to temperature stressors. A brief recapitulation of the chapters' main findings is below, followed by a more general discussion.

From Chapter 1, first generation progeny from the two populations had almost identical thermal tolerances. Glutamine/glutamate ratios were highly temperature dependent in white muscle tissue and gill glucose levels differed by population. There were also significant differences in body measurements between the two populations, which represent different morphotypes, but not among the different temperature conditions.

Chapters 2 and 3 focused on proteomic analysis of the liver, a tissue that provides a good overall representation of the condition of a fish and plays a vital role in a wide array of physiological processes such as the homeostasis, metabolism, and detoxification (Liu et al., 2016; Trefts et al., 2017). In Chapter 2, the Big Lagoon (BL) population had a stronger response to both warm and cold chronic temperature stress than the Klamath River (KL) population. At 7°C (cold condition), BL showed alterations in protein homeostasis that likely fueled higher energy demands, but both populations appeared to successfully acclimate to this temperature. The warm temperature acclimation revealed major increases in proteins involved in chromatin

structure and transcription, while there were decreases in proteins related to translation and fatty acid metabolism.

In Chapter 3, HSP40-B1b was significantly higher in abundance for both populations at both time points, suggesting a key role for this protein in regulating and orchestrating the response to acute temperature stress for this species. Six hours after acute heat stress, the BL population had significant changes in proteins related to the regulation of RNA processing, regulation of reactive oxygen species (ROS) homeostasis, and changes in liver cell molecular structure. The BL population exhibited a much stronger response to acute temperature stress than the KL population at the two timepoints examined. After 24 hours of recovery, both populations appeared to have regained homeostasis, with only a few key proteins remaining significantly elevated or decreased.

Despite having very similar thermal tolerances, there were clear differences in how the two populations responded to temperature stress. Overall, BL exhibited a much stronger response than KL for both chronic and acute temperature stress challenges at the timepoints observed. In the chronic temperature stress experiments, there were differences in cold acclimation between KL and BL at the individual protein level. For the chronic warm acclimation, however, the population differences were highlighted by the functional enrichment analysis. In the acute heat stress experiments, there were very large differences between the two populations six hours after heat stress. In BL livers, over 200 significant changes in protein abundance were observed compared to controls, while in KL there were only six. However, functional enrichment analyses detected numerous changes in KL at the 24 hour timepoint despite having only one significantly different protein at the individual abundance level. These experiments underscore the importance of looking at both individual protein and functional protein network level changes to understand

organismal and population responses to a given environmental condition. While large or consistent changes in individual proteins can point to key regulators and potential bioindicators, network level functional analysis can provide a more comprehensive look at functional responses and provide a much more robust and specific platform for predictive bioindication (Goh & Wong, 2016; Wu et al., 2014).

As more complete data sets are compiled, the opportunity to investigate the nuances of molecular changes will increase, providing specificity to the type and degree of a stressor. Established proteomic signatures could provide insight into the condition of organisms from the field (da Costa et al., 2015). Inclusion of more populations, species, and tissues in future analyses will simultaneously allow for investigations of similarities that point to essential, highly conserved mechanisms, while differences provide insight into the unique ways these different populations and species have evolved to handle specific challenges. Although beyond the scope of this dissertation, the data sets can be mined further to provide valuable insight into the types, locations, targets, and quantities of post-translational modifications, which provide a means of rapid communication, regulation, and functional alteration (Witze et al., 2007).

Proteins, the functional and structural results of a genome interacting with the environment, are a direct measure of gene expression plus posttranscriptional regulation and represent a largely underexamined arena for understanding evolutionary biology and ecology (Karr, 2008). Proteomics provides an important tool for understanding how molecular phenotypes contribute to evolutionary processes, since one gene can result in a diversity of proteins after post-transcriptional and post-translational modifications (Baer & Millar, 2016; Diz et al., 2012; Tomanek, 2014). Given the potential for selection to act on different proteomic networks, understanding core functional networks and how they relate to one another through

functional analyses is another important component to understanding evolutionary ecology (Baer & Millar, 2016). Although specific to one species exposed to a single abiotic factor, this dissertation contributes a small piece of the very large amount of data that will be needed to understand the complex and diverse ways in which organisms respond and adapt to a changing environment. Many more studies of this nature will be necessary to provide a more comprehensive understanding of the complex changes that occur within a proteome and how those changes ultimately contribute to the phenotypes on which selection acts.

References

Baer, B., & Millar, A. H. (2016). Proteomics in evolutionary ecology. *Journal of Proteomics*, *135*, 4–11. https://doi.org/10.1016/j.jprot.2015.09.031

da Costa, J. P., Carvalhais, V., Ferreira, R., Amado, F., Vilanova, M., Cerca, N., & Vitorino, R. (2015). Proteome signatures—How are they obtained and what do they teach us? *Applied Microbiology and Biotechnology*, *99*(18), 7417–7431. https://doi.org/10.1007/s00253-015-6795-7

Diz, A. P., Martínez-Fernández, M., & Rolán-Alvarez, E. (2012). Proteomics in evolutionary ecology: Linking the genotype with the phenotype. *Molecular Ecology*, *21*(5), 1060–1080. https://doi.org/10.1111/j.1365-294X.2011.05426.x

Goh, W. W. B., & Wong, L. (2016). Integrating Networks and Proteomics: Moving Forward. *Trends in Biotechnology*, *34*(12), 951–959. https://doi.org/10.1016/j.tibtech.2016.05.015

Karr, T. L. (2008). Application of proteomics to ecology and population biology. *Heredity*, *100*(2), 200–206. https://doi.org/10.1038/sj.hdy.6801008

Liu, B., Xu, P., Brown, P. B., Xie, J., Ge, X., Miao, L., Zhou, Q., Ren, M., & Pan, L. (2016). The effect of hyperthermia on liver histology, oxidative stress and disease resistance of the

Wuchang bream, Megalobrama amblycephala. *Fish & Shellfish Immunology*, *52*, 317–324. https://doi.org/10.1016/j.fsi.2016.03.018

Tomanek, L. (2014). Proteomics to study adaptations in marine organisms to environmental stress. *Journal of Proteomics*, *105*, 92–106. https://doi.org/10.1016/j.jprot.2014.04.009

Trefts, E., Gannon, M., & Wasserman, D. H. (2017). The liver. *Current Biology*, *27*(21), R1147–R1151. https://doi.org/10.1016/j.cub.2017.09.019

Witze, E. S., Old, W. M., Resing, K. A., & Ahn, N. G. (2007). Mapping protein post-translational modifications with mass spectrometry. *Nature Methods*, *4*(10), 798–806. https://doi.org/10.1038/nmeth1100

Wu, X., Hasan, M. A., & Chen, J. Y. (2014). Pathway and network analysis in proteomics. *Journal of Theoretical Biology*, *362*, 44–52. https://doi.org/10.1016/j.jtbi.2014.05.031